ARCHER: Analysis of the Radiation Challenge to Human ExploRation

Final Report

DSE Group S15

July 3, 2018
Revision 2.0

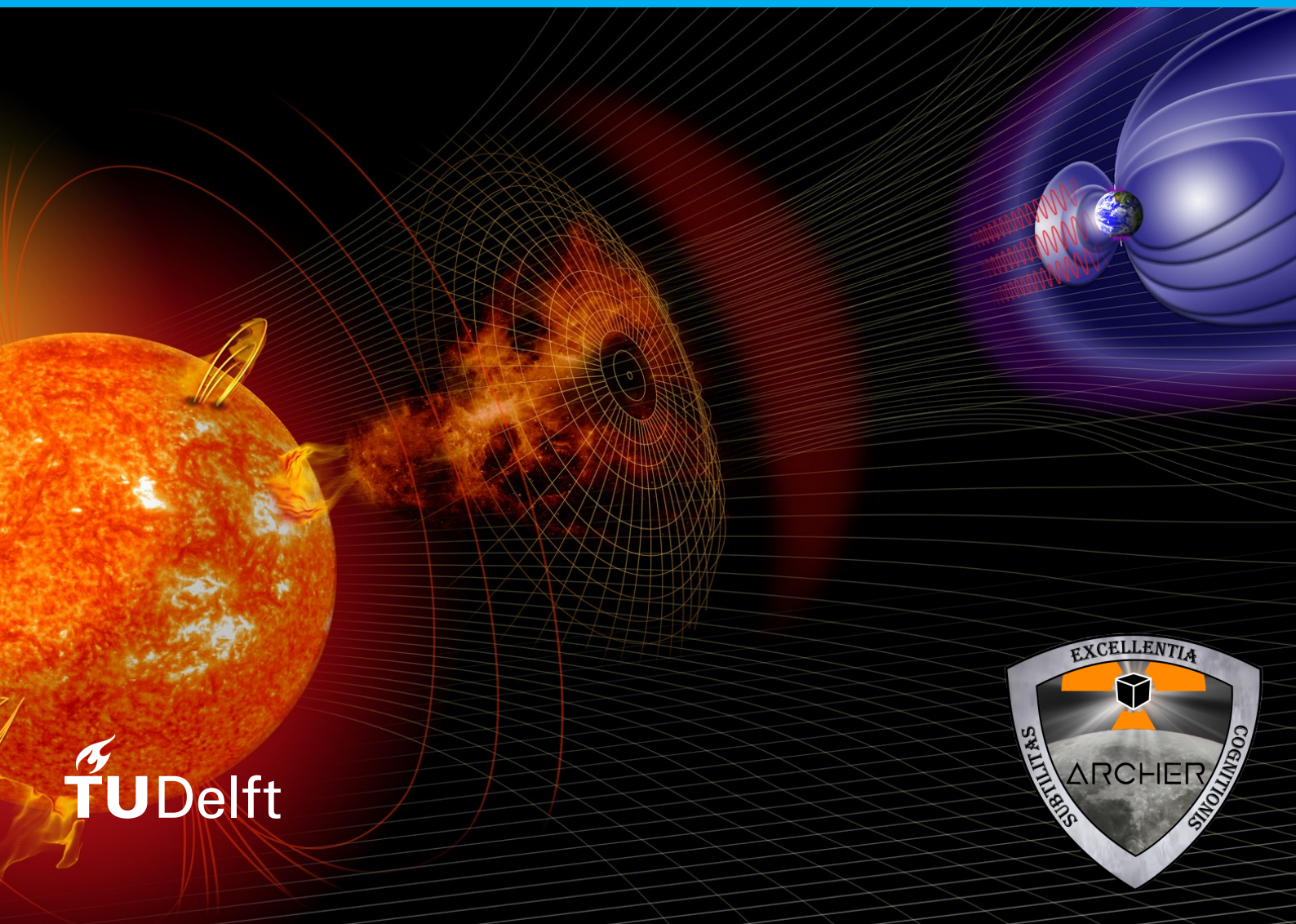

ARCHER: Analysis of the Radiation Challenge to Human ExploRation

Final Report

by

DSE Group S15

Team Members

Gianmarco Ferrari	4489314
Trevor Fradgley	4354613
Mateusz Glowacki	4431421
Jonas Hener	4430166
Nathan A. van 't Hof	4444469
Jack A. Kyle	4476492
David Rijlaarsdam	4307127
Rowan Vijverberg	4286820
Marti Vilella Ramisa	4447301

Cover Photo Source: www.nasa.gov/mission_pages/sunEarth/news/storms-on-sun.html
[Retrieved 24 April 2018]

TU Delft

Acknowledgements

We would like to express our special thanks to our supervisors:

Dr A. Menicucci, Dr J. Heiligers and Dr R. Hedayati.

Their experience and enthusiasm were contagious and their continuous support invaluable. Their patience and extensive feedback very much improved the quality of this report.

Furthermore, we would like to thank all other staff at the Technical University of Delft who have helped us throughout the design process. Specifically we would like to name:

- *Ir.* J. Bouwmeester – -Researcher, Space Systems Engineering
- Dr A. Cervone — Assistant Professor, Space Systems Engineering
- Dr S. Speretta — Researcher, Space Systems Engineering
- M.Ş. Uludağ — Electronic Engineer, Space Systems Engineering
- E. van den Bos — CAD Specialist, Aerospace Structures and Computational Mechanics
- T. van den Oever — MSc Student, Astrodynamics and Space Missions

Their fast responses and willingness to help allowed us to make design choices faster than we could ever have anticipated.

We would also like to thank our professors who have taught us everything we know over the course of the Bachelor curriculum. Only using all the skills we gathered throughout these courses have we been able to see this project to a good end.

Our gratitude also goes out to the engineers working in industry and at other scientific institutions who took the time to give us advice and information. Specifically we would like to thank:

- Nico Golembiewski — AZUR SPACE Solar Power GmbH
- J. Duncan — Blue Canyon Technologies
- Dr M. Tsay — Busek Co. Inc.
- Dr G. Furano — European Space Agency
- Dr T. Szewczyk — European Space Agency
- M.B. Jensen — GOMspace
- *Ir.* R. Florea — Hyperion Technologies B.V.
- *Ir.* H. Brouwer — Innovative Solutions In Space B.V.
- K. Goel — Innovative Solutions In Space B.V.
- Dr J. Reveles — Oxford Space Systems
- Dr A. Kalman — Pumpkin Space Systems Inc.
- Dr T. Dachev — Space Research and Technology Institute of the Bulgarian Academy of Sciences
- Dr M. Fernandez — Syrlinks
- M. Langer — Technische Universität München
- Dr D. Rafalskyi — ThrustMe
- Dr L. Pinsky — University of Houston
- Dr M. Holik — University of West Bohemia
- C. Samson — VACCO Industries

We'd like to thank TU Delft for supplying us with their student licenses for Catia and ANSYS. Furthermore, we would like to thank the following organisations who granted us access to their software:

- T. Bass from AGI and M. Smith from ANTYCIP simulation, supplied Systems Tool Kit (STK)
- National Aeronautics and Space Administration, supplied Project Cost Estimating Capability Version 2.2
- European Space Agency, supplied SPace ENVironment Information System (SPENVIS)
- Tableau Software: Business Intelligence and Analytics, supplied Tableau

Last but not least we would like to thank the PMSE team, and specifically our TA S. Singh. Without the tools they handed to us the organisation of the work would have been an impossible task, and without their feedback this project could not have been the success it was.

Contents

List of Abbreviations

∆DOR	delta-Differential One-way Ranging
ADCS	Attitude Determination and Control System
AGI	Analytical Graphics, Inc.
APCP	Ammonium Perchlorate Composite Propellant
ARCHER	Analysis of the Radiation Challenge to Human ExploRation
BCT	Blue Canyon Tech
BER	Bit Error Rate
BPSK	Binary Phase-Shift Keying
CCSDS	Consultative Committee for Space Data Systems
CD	Concurrent Design
CDF	Concurrent Design Facility
CDH	Command and Data Handling
CDR	Critical Design Review
CERN	European Organization for Nuclear Research
CO_2	Carbon Dioxide
COMMS	Communications
COSPAR	Committee on Space Research
COTS	Commercial Off-The-Shelf
CPU	Central Processing Unit
CRaTER	Cosmic Ray Telescope for the Effects of Radiation
CRTBP	Circular Restricted Three Body Problem
CUS	Customer
DOD	Depth of Discharge
DPRAM	Dual-Ported Random-Access Memory
DSA	Deep Space Antenna
DSE	Design Synthesis Exercise
ECHA	European Chemicals Agency
ECSS	European Cooperation for Space Standardization
EDAC	Error Detection and Correction
EIRP	Equivalent Isotropically Radiated Power
EM-1	Exploration Mission 1
EOL	End of Life
EPS	Electrical Power System
ESA	European Space Agency
ETU	Engineering Testing Unit
FDIR	Fault Detection, Isolation and Recovery
FEC	Forward Error Correcting
FPGA	Field-Programmable Gate Array
GA	Genetic Algorithm
GEO	Geosynchronous Orbit
GS	Ground Station
GTO	Geostationary Transfer Orbit
GWP	Global Warming Potential
HRBE	Hiscock Radiation Belt Explorer
I2C	Inter-Integrated Circuit
IMU	Inertial Measurement Unit
INFN	National Institute for Nuclear Physics
InSight	Interior Exploration using Seismic Investigations, Geodesy and Heat Transport
ISL	Innovative Space Logistics
ITAR	International Traffic in Arms Regulations
ITU	International Telecommunication Union
JAXA	Japan Aerospace Exploration Agency
JEMS	Jitter Environment Measurement System
JPL	Jet Propulsion Laboratory
LEG	Legal
LEO	Low Earth Orbit
LET	Linear Energy Transfer
LH_2	Liquid Hydrogen
LHC	Large Hadron Collider

LOP-G	Lunar Orbital Platform-Gateway
LOS	Loss of signal
LOX	Liquid Oxygen
LRO	Lunar Reconnaissance Orbiter
LTO	Lunar Transfer Orbit
MAI	Maintenance, Assembly and Integration plan
MarCO	Mars Cube One
MCOTS	Modified Commercial Off-The-Shelf
MSG	Maintenance Steering Group
NASA	National Aeronautics and Space Administration
OBC	On Board Computer
PBAN	Polybutadiene Acrylonitrile
PCU	Power Control Unit
PDR	Preliminary Design Review
PM	Project Management
PMSE	Project Management and Systems Engineering
PROP	Propulsion
RAD	Radiation Assessment Detector
RAMS	Reliability, Availability, Maintainability and Safety
RCS	Reaction Control System
S/C	Spacecraft
SADA	Solar Array Drive Assembly
SDRAM	Synchronous Cynamic Random-Access Memory
SE	Systems Engineering
SEE	Single Event Effect
SEL	Single Event Latchup
SET	Single Event Transient
SEU	Single Event Upset
SLOC	Source Lines of Code
SLS	Space Launch System
SNR	Signal-to-Noise Ratio
SPI	Serial Peripheral Interface
SSC	Swedish Space Corporation
STA	Stakeholder
STK	Systems Tool Kit
SWOT	Strengths, Weaknesses, Opportunities and Threats
SYS	System
TEC	Technical
TID	Total Ionising Dose
TRL	Technology Readiness Level
V&V	Verification and Validation
WDT	Watchdog Timer
XTRP	X-band TRansPonder

List of Symbols

α	Absorptivity	[-]
Δv	Delta-v	[m/s]
ϵ	Emissivity	[-]
μ_l	Lunar Gravitational Parameter	[m^3/s^2]
ω_t	Angular rate	[rad/s]
ρ	Density	[kg/m^3]
σ	Stefan-Boltzmann constant	[$W/(m^2 \cdot K^4)$]
θ	Angle of solar incidence	[°]
θ	Angular displacement	[rad]
θ	True anomaly	[°]
Ω	Argument of the right ascending node	[°]
ω	Argument of periapsis	[°]
$\widehat{N}$	Unit force vector	[-]
A	Area	[m^2]
a	Semi-major axis	[m]
c	Specific heat	[J/(kg·K)]
c	Speed of light	[m/s]
C/N_o	Carrier-to-Noise Ratio	[dB]
d	Distance	[m]
D_i	Inherent degradation	[-]
D_y	Yearly degradation	[-]
E	Young's Modulus	[Pa]
e	Eccentricity	[-]
E_b/N_o	Signal-to-Noise Ratio (SNR)	[dB]
E_e	Irradiance	[W/m^2]
F	Force	[N]
f	Frequency	[GHz]
F_R	Receiver Noise Figure	[K]
F_{req}	Required thrust	[N]
G/T	Gain-to-noise-temperature	[dB/K]
g_0	Standard acceleration due to gravity	[m/s^2]
G_{Rx}	Receiving Antenna Gain	[dBi]
G_{Tx}	Transmitter Antenna Gain	[dBi]
h_i	Angular momentum	[N·m·s]
I	Moment of inertia	[m^4]
i	Inclination	[°]
I_{sp}	Specific Impulse	[s]
I_{tot}	Total impulse	[N·s]
J_{ii}	Mass moment of inertia (pre deploy)	[$kg \cdot m^2$]
J_{jj}	Mass moment of inertia (post deploy)	[$kg \cdot m^2$]
K	Constant for frequency analysis	[-]
L	Mission Lifetime	[yrs]
l	Length	[m]
L_i	Thruster arm	[m]
L_s	Free Space Losses	[dB]
L_{atm}	Atmospheric Losses	[dB]
L_{comb}	Combined Link Losses	[dB]
L_{in}	Receiver Input Losses	[dB]
L_{out}	Transmitter Output Losses	[dB]
L_{path}	Net Path Losses	[dB]
L_{point}	Combined Pointing Losses	[dB]
L_{prec}	Precipitation Losses	[dB]
M_0	Initial wet mass	[kg]
m_l	Mass per length	[kg/m]
P	Power	[W]
p	Semi-latus rectum	[km]
P_{cell}	Power solar cell	[W]
P_{Tx}	Transmitter Power	[dBW]
q	Reflective factor	[-]
r	Moment arm	[m]
r	Radius	[m]
R_b	Bit Rate	[dB-Hz]
T	Temperature	[K]
t	Time	[s]
T_0	Reference Temperature of 290 K	[K]
T_1	Temperature radiating body	[K]
T_2	Temperature of the radiating environment	[K]
T_s	Effective System Noise Temperature	[K]
T_{GGT}	Gravity-gradient torque	[N·m]
T_{SRP}	Solar radiation pressure torque	[N·m]
T_{ant}	Antenna Noise Temperature	[K]
T_{slew}	Slew torque	[N·m]

Executive Overview

National space agencies and billionaire-backed companies such as SpaceX, Blue Origin and Virgin Galactic are racing to explore space, the Moon and beyond. One major obstacle is the radiation that astronauts are exposed to. A recent NASA experiment showed a 7% difference in gene expression between an astronaut who spent a year in low-Earth orbit and his ground-based twin brother[1]. Currently, there is ambiguity surrounding the effects of the radiation environment on astronaut's DNA and general health once they leave the protection of the Earth's magnetic field. However, it is clear that radiation can have lethal consequences. In order to design safe and ethical missions into deep space, data on radiation levels is imperative. Therefore, for the Analysis of the Radiation Challenge to Human space ExploRation, we present: Mission ARCHER.

ARCHER's mission objective is *"To characterise the interplanetary radiation environment to aid future human space exploration."* In order to satisfy this, accurate measurements are required, but the mission must deliver scientific data in a resource efficient manner. This will improve the market value of the project and thus its chances of being realised. For this purpose, a low-cost satellite platform has been selected: the CubeSat [1]. Throughout the Design Synthesis Exercise our goal has been to *"Develop an economically and technically feasible CubeSat mission design to be launched by 2022, capable of reliably characterising the interplanetary radiation environment, by 9 students in 10 weeks time."* This report outlines how we have fulfilled this goal.

Before any work could be done, the team had to get organised. This was done using multiple project management and system design tools. First, the main roles such as project manager, system engineer, secretary, sustainability and quality assurance officer, were split up amongst the team members. This was documented using an Organogram. The planning of the work to be done was analysed using a work flow diagram, which was further analysed using a work breakdown structure. Using the results from these a Gantt chart was developed which outlined the work to be done in the first half of the project.

There were two design cycles in this project, the mission profile design and the system hardware design. During the mission profile design phase, the stakeholder requirements had to be first analysed and from these the technical requirements were generated. This resulted in a list of well over 150 requirements long, ranging from requirements dictating the measuring capabilities of the payload to the structural integrity. With a preliminary idea of what the system required, the mission destination and science orbits had to be engineered. A design option tree was created with 4950 possible mission destinations and orbits [2]. These included orbits centred around the sun, around all solar system planets and around the Moon. Possible orbits included circular, elliptical, retrograde, Lagrange points and others. First, high level design choices were made to limit the total number of missions. The remaining missions were checked for feasibility of he concept. After cutting the total missions to a reasonable number, a trade-off was performed to establish which mission profiles would be examined in more detail. Thus, the entire design option tree was cut down to four missions. These missions were:

- M1: Multiple (phased) launches, single CubeSat per launch to an elliptical Moon orbit. Entire mission duration in the order of 10 years.
- M2: Single launch, 2 CubeSats to different highly eccentric polar orbits around Earth. Entire mission duration in the order of 2 years.
- M3: Single launch, 2 CubeSats to different targets. Targets are elliptical Moon orbit and Lagrangian point L5 in Earth-Moon system. Entire mission duration in the order of 2 years.
- M4: Single launch, 2 CubeSats to different orbits around Mars. Entire mission duration in the order of 2 years.

These four mission profiles were analysed in more depth. Both low and high-thrust options were considered as well as different sizes for each of the CubeSats. This was done using tools developed specifically to allow concurrent engineering to quickly and effectively be used to design a CubeSat up to a preliminary level. Using the results from this, a trade-off was done, clearly showing M3 to be the most suitable option to fulfil the mission objective.

[1] `www.nasa.gov/feature/nasa-twins-study-confirms-preliminary-findings` [Retrieved 19 June 2018]

The trade-off results were verified through a sensitivity analysis with a wide range of variable weighting factors. This validation approach clearly showed that the results of the trade-off were not a function of the weighting and that M3 was indeed the best option. As such it was decided to send two identical 12U low-thrust CubeSats to measure the radiation: Artemis would travel to the Moon, and Diana to the Earth-Moon L_5 point.

Now that a mission profile was chosen, design phase 2 could begin and the CubeSat system could be developed in detail. The starting point of this was the initial analysis of a potential design done previously. The preliminary resource budgets were based on these figures, allowing the next design step to be faster.

The subsystem driving the design, the payload, was designed almost completely independently from the rest of the system, with the other subsystems being designed to accommodate the needs of the payload and the final mission goal, to better characterise the radiation environment beyond Earth's magnetosphere. The payload selected for the ARCHER spacecraft is composed of two FITPixLite detectors for measuring the Linear Energy Transfer (LET) of charged particles, and one modified FITPixLite for uncharged (neutrons) particle detection [3]. Finally a magnetometer to measure the magnetic field is also used.

The reason why the FITPixLite was preferred over other radiation detectors is simply because of its incredible capabilities in measuring extensive 'dynamic ranges' as required for Mission ARCHER. This type of device, also referred to as a hybrid semiconductor pixel detector, was the only viable option in order to feasibly cover the demanding energetic range the customer wanted, while being compliant with the CubeSat platform. As an example, the only non-pixel based detector capable of fulfilling Mission ARCHER's requirements was the one currently orbiting the Moon on board of the Lunar Reconnaissance Orbiter (LRO), CRaTER. However, this device is almost 6 CubeSat units big and weighs more the 5 kg. Clearly, not a feasible option. Moreover, another argument in favour of the FITPixLite is its relatively flexible customisation possibilities. This means that by only applying some specific coatings on the sensor's head one can utilise the FITPixLite to also detect uncharged particles. The advantages of such configuration are multiple: reduction in subsystem complexity, decrease in cost and ease of system integration.

As for the magnetic field measurement, one design consideration should be addressed. In order to perform correct and reliable measurements the magnetometer should be isolated as much as possible from all the electromagnetic sources within that spacecraft which can possibly interfere with it. As a CubeSat has a very compact internal configuration, it follows that the only viable mounting solution is by means of a boom mechanism which will extend the magnetometer outside the CubeSat and away from electromagnetic interference. Fortunately, this is already a space-proven concept within CubeSat missions.

The selected boom mechanism is a composite retractable boom which has already been flown on board of the AlSat-Nano 3U CubeSat carrying a magnetometer sensor head very similar to the one to be flown by Mission ARCHER [4, 5]. This payload configuration is able to detect neutrons with energies between 0.1 and 200 MeV, measure the Linear Energy Transfer (LET) of charged particles in the range of $5 \cdot 10^{-4}$ to 10^6 eV cm^2/mg and determine the total ionising dose and dose rate as well as recording the local magnetic field with a sensitivity of ±100 μm.

In the detailed design, it became clear early on that there is only one propulsion system available capable of delivering the Δv required to reach the intended orbits. This is the BIT-3 from Busek [6], an ion engine fuelled with solid iodine. Not only is it able to deliver a Δv of 1564.9 m/s at a fuel mass of 1.5 kg, it is also capable of 1.15 mN of thrust at 75 W and it can gimble up to 10°. The fact that it is throttleable also means that the propulsion subsystem does not always need to work at constant maximum power, and thus the electrical power subsystem can be designed for a lower power requirement, which reduces its mass.

One consequence of this engine choice is that the total system mass could not exceed 20.5 kg, as then the initial manoeuvre to slow down before reaching the Moon would become infeasible. This hard constraint on the system mass would prove driving for the rest of the design. The resulting budget was extremely close to the maximum mass, but left quite some margin with respect to the maximum volume volume.

Using the maximum mass and the exact engine properties, the trajectories were modelled with custom made software and Systems Tool Kit was subsequently used to model the eclipse times. Accurate eclipse analysis is extremely important for sizing the electrical power subsystem and for the thermal analysis. The custom made software was used to reverse propagate the final science orbits. Using this approach two transfer orbits, one from L_2 to the Moon and another from L_2 to L_5, were found. The resulting transfer orbits required a Δv of 585 m/s and 256 m/s respectively and can be seen in Figs. 1 and 2.

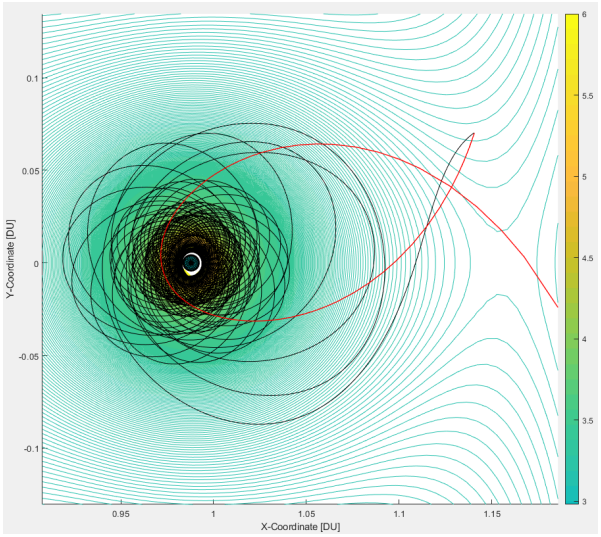

Figure 1: Insertion orbit for Artemis, from a point near L_2 to the science orbit around the Moon.

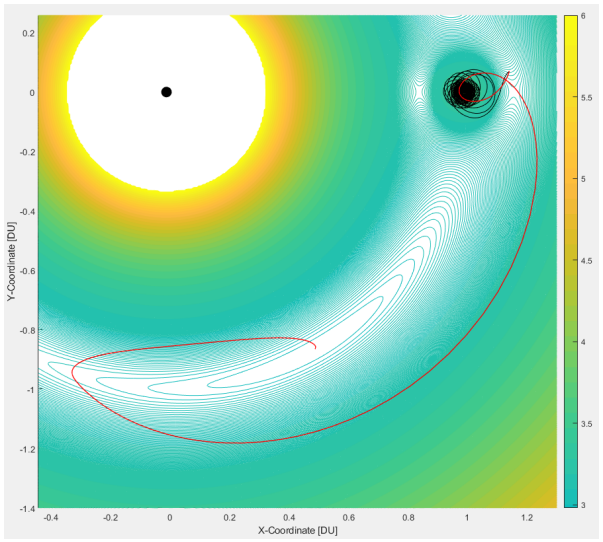

Figure 2: Insertion orbit for Diana, from a point near L_2 to L_5.

The system configuration was designed concurrently with the subsystems. One major issue was the location of the engine. The goal was to place it such that the thrust vector would align with the centre of mass of the system. Originally the engine was placed such that it would thrust along the longitudinal axis as is done in the majority of vehicles. However, this meant that the structure would require extensive redesign to allow the engine to be placed in the middle. This also created unused volume as the space beside the engine could not be effectively used. There was also surface area problems as the solar panels, solar array drive assembly, communications, payload and Attitude Determination and Control System all required surface area. This problem was solved by taking the unusual choice of placing the engine such that it thrusts along a lateral axis. As a result, it could fit exactly into the centre layer, volume was saved and the surface area problem became more manageable. It also solved a problem with regards to desaturating the reaction wheels. By moving the Attitude Determination and Control System thrusters to the long edge the arm of these thrusters increased, reducing the required thrust to achieve the same amount of momentum dumping. If the CubeSat was in low-Earth orbit, the additional drag in this configuration would be problematic but as Diana and Artemis will be travelling to the Moon they will not experience atmospheric drag. The configuration change can be seen in Fig. 3.

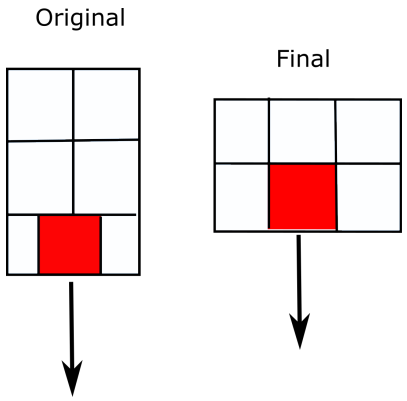

Figure 3: Location of the engine and the direction of thrust

Another major challenge is the data rate. The payload with multiple FITPixes, generated 4 Mb/s of data. Especially at large distances this would become problematic for the communications. This was tackled by using a reflect array, similar to the one used on the MarCO CubeSats. This was only possible due to the new configuration, as a patch antenna was required to allow the CubeSat to both transmit and receive data at the same time. In the original configuration there was no room for this patch antenna as it would have to be placed over the engine.

In addition, the CubeSats had to withstand the very radiation they were sent to measure. An analysis of the challenge was made and structural shielding was installed. In addition, the on board computer was designed to withstand the radiation environment by selecting a processor capable of immunity against single event effect and high total ionising dose resistance.

Not only did the engine require a large amount of power, the communications also had large power requirements. This was due to both these subsystems having a large power requirement when active, and the fact that they also needed to be powered on most of the time. The only way for the power requirements to be met would be to point the solar panels toward the sun continuously. This can be done using a solar array drive assembly. However, miniaturised solar array drive assembly's capable of fitting on CubeSats are a state-of-the-art technology with only one feasible option currently on the market. Furthermore, in order to fit the solar panels, they needed to be folded three times. As an extra margin 20 body mounted solar cells were added. This meant that by actively controlling the orientation of the CubeSats, the solar panels could supply an average of 134 W.

The battery system was designed to supplement the array under heavy power loads. This will happen for 350 cycles during transit with a depth of discharge close to 50%. In order to verify that the batteries would not degrade too much, the depth of discharge was evaluated for the entire mission duration and the battery degradation found. Over the 2 year life span the batteries will degrade by nearly 20%.

We believe the final result meets the mission need and objective statements and importantly, a realistic and feasible CubeSat design was created. The final configuration, as seen in Fig. 4, is able to accurately characterise the radiation environment. Both Artemis and Diana comply with the CubeSat standards. If launched, they will provide an extremely accurate data set. This information can be used to accurately model the interplanetary radiation environment. This will help engineers and scientists design better shielding and create new technology which will make space flight safer and more ethical. ARCHER could help solve the radiation challenge and lay the foundation for actual deep space exploration. If successful, Artemis and Diana could help facilitate the human dream to become an interplanetary species.

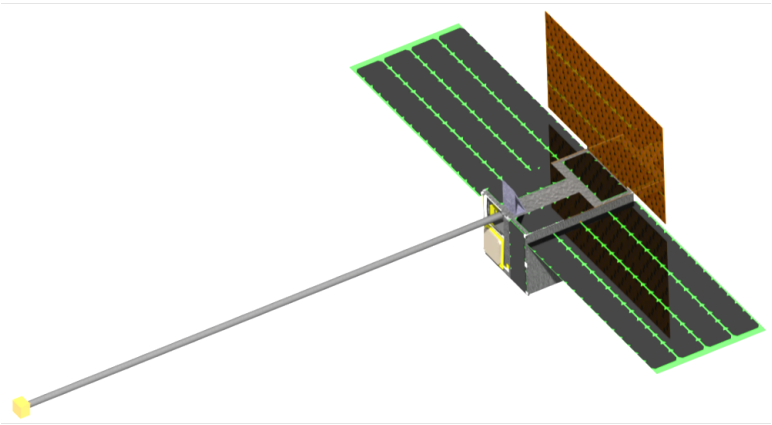

Figure 4: The final configuration of the CubeSat, which is the same for Artemis and Diana, in flight

.

1 Introduction

Welcome to Mission ARCHER. An introduction to ARCHER's story is presented in Section 1.1 followed by the project objectives in Section 1.2. Then, the project engineering and report structure will be briefly discussed in Section 1.3 and Section 1.4 respectively.

1.1. ARCHER's Story

In recent years, space exploration has experienced unprecedented growth[1]. Access to space has been made cheaper and easier by new players like SpaceX. Although the number of launches has been reasonably steady over the last 20 years[2], the number of satellites deployed has grown significantly, largely due to the increase in the use of miniaturised platforms such as the CubeSat [7].

In addition, there are new start-up companies hoping to make space travel available for the masses. The likes of Virgin Galactic [8] and Blue Origin[3] are both hoping to bring space tourists to the edge of space in the near future. However, not since the Apollo era [9], have human crewed missions gone beyond low Earth orbit. But human deep space exploration missions are very much in the public eye at present, as billionaire backed companies and national space agencies make plans to colonise the Moon and beyond. NASA's Lunar Outpost [10] and SpaceX's Mars mission [11] are examples of this.

The risks of human deep space exploration are extremely high. With little to no chance of rescue if there is an emergency, systems will need extreme reliability. Another area of concern is the radiation exposure that astronauts could receive once outside the protection of the Earth's magnetosphere [12]. This challenge is currently dismissed by some and is considered a showstopper for others. Its impact can also be difficult for the average person to quantify. Radiation is either seen as something extreme, think nuclear weapons, Chernobyl and radiation poisoning, or neglected in the public mind despite the very real dangers of lower level consistent exposure, namely, cancer [13].

The current radiation environment data-set from outside the magnetosphere is limited but there are a large number of readings within its protection. There are two components to the radiation risk. The density of the particle fluxes and their energies over time as well as the biological effects. Recently, NASA carried out a Twin Study, where one twin stayed on Earth while the other spent a year on the International Space Station. The preliminary results show the astronaut's gene expression changed by about 7%[4]. Worryingly, the effect on an astronaut's DNA and health once outside the shielding of the Earth's magnetic field is highly uncertain. The RAD radiation detector on-board the Mars Curiosity rover is one of the few measurements which can be used to estimate radiation dose absorbed during an interplanetary voyage [14]. This data was gathered both during the cruise and on the Martian surface. The results show that the dose absorbed may be higher than the currently accepted risk. However, there are uncertainties due to the lack of understanding of the biophysics involved.

---

[1] www.nasa.gov/pdf/657307main_Exploration%20Report_508_6-4-12.pdf [Retrieved 25 May 2018]
[2] www.statista.com/statistics/185460/worldwide-commercial-space-launches-since-1990/ [Retrieved 26 May 2018]
[3] www.blueorigin.com/ [Retrieved 1 June 2018]
[4] www.nasa.gov/feature/nasa-twins-study-confirms-preliminary-findings [Retrieved 1 June 2018]

All of these factors highlight a clear need and an opportunity. In order to send astronauts beyond the protection of the magnetosphere, there is a need to be able to predict the interplanetary radiation environment with high accuracy. Failure to do so puts both the spacecraft as well as the people operating these spacecraft in danger. There exists an opportunity then to satisfy this need and if a mission can be designed to accurately characterise the interplanetary radiation environment, it could potentially affect the direction of near future space exploration and allow for the safe planning of extra-terrestrial colonisation.

In order to satisfy this need and seize this exciting opportunity, the ARCHER mission was designed. ARCHER will Analyse the Radiation Challenge for Human Exploration of space. Its goal is to record charged and uncharged ionising radiation outside the magnetosphere. This will be achieved using the CubeSat platform. There has been great progress in spacecraft miniaturisation and the CubeSat platform is now capable of producing affordable space missions and has demonstrated its suitability to fulfilling scientific objectives [15]. ARCHER will use two identical CubeSats called Artemis and Diana. Artemis will take up an orbit around the Moon, relevant to planned Lunar stations. Diana will travel to the Earth-Moon Lagrange point where it can take measurements free from both the Earth's magnetosphere and interference from proximity to the Moon. This is relevant to deep space exploration.

ARCHER has the potential to hugely affect the near future of human exploration. This paper will first present mission design phase, followed by the detailed system design. The subsystem design will be presented next followed by the results and recommendations. Effectively, what follows, is ARCHER's story.

1.2. Project Objectives

The Mission Need statement is:

"To characterise the interplanetary radiation environment to aid future human space exploration."

In order to satisfy this need statement, accurate measurements are required, but the mission must deliver this scientific data in a cost effective manner. This will improve the market value of the project and thus its chances of being realised. For this purpose, a low-cost satellite platform was selected: the CubeSat.

The mission objective statement then is to:

"Develop an economically and technically feasible CubeSat mission design to be launched by 2022, capable of reliably characterising the interplanetary radiation environment, by 9 students in 10 weeks time."

This objective statement shows the desire for ARCHER to be a real-world feasible CubeSat mission, capable of providing accurate reliable data on the interplanetary radiation environment. Importantly, the team is highly motivated to present a design that is actionable and capable of being picked up by a space organisation. As such, a mission profile and a hardware system capable of carrying out the mission is to be designed.

1.3. Project Engineering

Project ARCHER required the design of both the mission profile and the mission system. This required two design cycles. In order to design the profile, the destination had to be chosen as well as the orbit. In addition, one versus multiple CubeSats had to be traded off as did a single versus multiple phased launches. While some preliminary hardware design could be done, detailed hardware engineering had to wait until the profile had been designed. In order to effectively manage the two design cycles Project Management and Systems Engineering (PMSE) was comprehensively built into the work flow and actively used to meet deadlines, guide decision processes and ensure correct engineering principles were applied.

The project evolved through several different phases. Initially, a Project Plan [16] was created which laid out the team structure, goals and deadlines. Project Management (PM) tools such as an Organogram, Gantt Chart as well as work flow and work breakdown diagrams were implemented. Importantly, these tools were continuously used to manage deliverables.

The Baseline Report [2] included a comprehensive analysis of stakeholder requirements, technical requirements and a functional analysis of the system. At this point, the sustainability policy and a large set of potential mission profiles was established.

The Midterm Report [17], reduced the potential thousands of missions to four and then carried out a detailed

trade-off, subsequently verified with a sensitivity analysis, to choose the best mission profile. At this point, the first design cycle was effectively complete. However, a preliminary architecture, or baseline, for the subsystems was also established. In addition, the PM tools where extended to cover the final part of the project in detail.

Throughout project ARCHER, Systems Engineering (SE) tools were embedded in the work flow. Design option trees, trade-off processes, risk analyses as well as verification and validation are examples of these and some will be expanded on in this report. However, Concurrent Design (CD) sessions were also used during both design cycles. This involved large collaborative team sessions trading input and output variables and iterating as necessary. This proved extremely helpful during subsystem design. In addition to this the team held a Preliminary Design Review (PDR) and a Critical Design Review (CDR).The PDR allowed the team to analyse the state of each subsystem collectively and identify potential adverse effects on, or interface problems with other subsystems. In the CDR the final design, and how each subsystem integrated into the final system, was proposed to the customer.

In addition, many subject matter experts, as can be seen in the acknowledgements, were consulted for advice and feedback. Their suggestions were integrated into the design.

1.4. Report Structure

This final report on the ARCHER project is the culmination of two design cycles and the SE process the team has been committed to following. The report effectively represents the second half of the SE V-diagram as seen in Fig. 1.1. First, a summary of the first design cycle will be presented in section Chapter 2. This includes updated work on the mission trajectories and science goals. Then, a summary of the left half of the V-diagram will be presented in Chapter 3. The report then follows the V-diagram structure presenting the subsystem design and performance and system design and performance in Chapter 4 and Chapter 5 respectively. The capability of the ARCHER to meet the mission need and goals as well as how the project can develop over the next few years to launch in 2022 is presented in Chapter 6. The report concludes with results and recommendations.

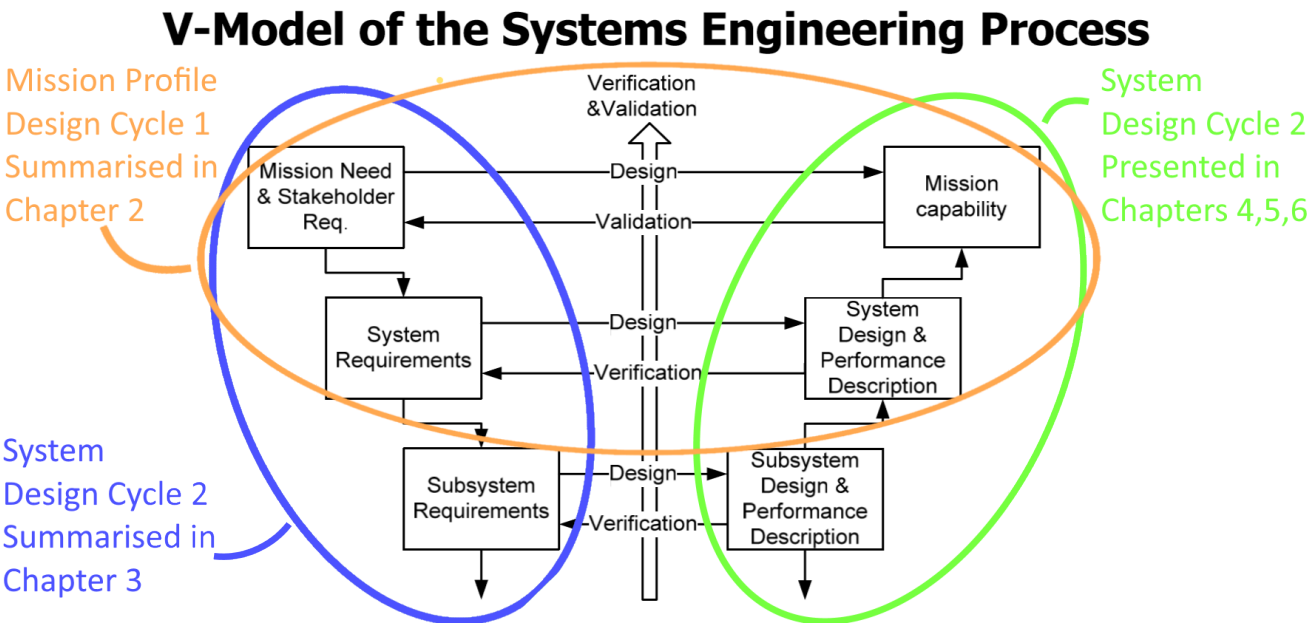

Figure 1.1: V-Diagram Report Structure [18]

2

Mission Design

This chapter summarises and expands on Design Cycle 1, the design of the mission profile. To start with, in Section 2.1 the scientific background of the mission is discussed in terms of history of radiation research, the radiation challenge we face and to conclude, the space radiation environment Mission ARCHER will be exposed to. Then, in Section 2.2 the user requirements are shown. At the start of the project, a Design Option Tree was created for the mission profile. This DOT feeds into a trade-off for the mission profile selected, shown in Section 2.3. After this, the sustainability development strategy is explained in Section 2.4. Finally, the complete and thorough analysis of the astrodynamics of the mission profile is performed and shown in Section 2.5.

2.1. Scientific Background

To begin with, in physics the term 'radiation' is intended as the transmission of energy by means of electromagnetic waves or subatomic particles. In particular, radiation can be classified into two main categories: ionising and non ionising radiation. The latter are a form of radiation which do not carry enough energy to alter the charge of the atoms or molecules it encounters. Good examples for these can be radio waves or microwaves. Generally, they are not considered to be of any major health threat. On the other hand, ionising radiation are characterised by higher energies and are able to interact with matter in a much more sever way introducing serious potential health risks. Mission ARCHER will exclusively focus on the ionising radiation present in deep space.

Despite aforementioned phenomena being omnipresent in the Universe since the Big Bang, it was only in the late 1800s when scientists started to become aware of their existance. In 1896, while conducting experiments with the purpose of better understanding X-rays, Henri Becqurel accidentally discovered the radioactive properties of uranium [19]. In those same years, inspired by the recent discoveries of Becquerel, Marie Sklodowska-Curie and her husband Pierre Curie discovered two new radioactive elements, Polonium and Radium. These discoveries would lead the three of them to share the Nobel Prize in Physics in 1903[1] and would make Marie the first woman ever to win the prize. Eventually, Marie Curie would continue her research on radioactive materials and by 1910 she would prove the existence of further elements in the periodic table by producing a metal plate purely composed or radium. These discoveries would award her a second Nobel Prize, this time in Chemistry, in 1911[1], thus becoming the first person to be awarded two Nobel Prizes. Unfortunately, these achievements came at high price, as she died at the age of 66 from aplastic anemia due to long-term exposure to radiation during her lifelong scientific research [19]. In the early 20^{th} century, the field of particle physics was in its early phases, hence still leaving room to many misconceptions about the origin and behaviour of radiation. In particular, by measuring the ionisation levels of air in the atmosphere, the scientific community at the time believed that the only source of radiation would be Earth's soil and as a consequence the levels of radiation would decrease with increasing altitude [20]. Theodor Wulf, German physicist and Jesuit priest, attempted to prove so in 1910 by taking measurements at the top (330 m) and bottom of the Eiffel Tower with a self-built electrometer (a very rough device capable of detecting charged particles) [21]. Interestingly, the experiment did show decreasing radiation levels with increasing altitude but with values far from the ones predicted and necessary to prove Earth's soil as single source of radiation

[1] `https://www.nobelprize.org` [Retrieved 15 May 2018]

[21].

In 1911, while reading the results obtained by Wulf, Victor Hess, an Austrian physicist started to broach the idea of radiation coming from the sky rather than purely from the ground [20]. Supported by his passion for ballooning, between 1911 and 1913 Hess conducted a series of ten experiments on board of balloons (five flights during the day and five in nocturnal conditions) in order to prove his thesis [20]. Indeed, Hess measurements recorded that after a small initial decrease at lower heights, radiation levels at around 1500 meters altitude would be equitable to the ones at sea level and after this point there would be a significant increase with increasing altitude [20]. Of particular interest was the first flight performed in 1912 in occasion of a quasi total solar eclipse. At around 2000 meters of altitude Hess measured radiation greater than at sea level and since the Sun was in eclipse he (mistakenly) concluded that the Sun itself was not a source of radiation. Today, it is well known that solar cosmic rays impact the Earth almost isotropically, hence proving Hess's theory wrong [20]. The findings of Hess would eventually win him the Nobel Prize in Physics in 1936 for *'his discovery on cosmic radiation'*, even though the term 'cosmic rays' would only be coined in 1928 by Robert Millikan [22], more than ten years after their actual discovery.

Radiation Challenge

As one can imagine, understanding the provenance of radiation was only a 'little' step towards the comprehension of the bigger challenge space travel is imposing today. If humankind seriously aspires to become an interplanetary species as the modern trend seems to be suggesting, a deep understanding of the radiation environment in outer space and, most importantly, its biological impact is of critical importance. Along these lines, NASA has outlined a human research roadmap[1] describing the biggest threats for human space travel [23]:

- Physiological problems caused by microgravity (or reduced gravity),
- Physiological problems caused by isolation,
- Risks caused by exposure to radiation.

In the attempt of addressing the last point of the list above, several missions have been accordingly designed and launched since the beginning of the space era. Among the most relevant and recent missions one can find the Mars Science Laboratory. More commonly known as the Curiosity Rover, it performed radiation measurements in transit to Mars in 2011 and 2012. Since then, it has been doing said measurements on the Martian surface [24]. Curiosity is packed with 11 scientific instruments of which only one, the Radiation Assessment Detector (RAD), measures radiation. On the other hand, the 2001 Mars Odyssey satellite was launched in 2001 with the objective of, among other scientific purposes, characterising the radiation environment in martian orbit [25]. Now, moving the focus from the Red planet to Earth's natural satellite, the Lunar Reconnaissance Orbiter (LRO) has been performing radiation measurements in an orbit around the Moon since 2009. Its Cosmic Ray Telescope for the Effects of Radiation (CRaTER) instrument is probably one of the most advanced radiation detectors in existence capable of detecting particles of a very broad energetic range. Moreover, CRaTER not only measures the energy deposition of charged particles, but it is also able to address to some extent the biological impact of such energy depositions [26]. Unfortunately, this advanced radiation detector is compatible with a CubeSat based mission. Finally, Chandrayaan-1 was an Indian space mission which also measured radiation in lunar orbit in 2008 and 2009, but its measurements are far from being equitable to CRaTER's both in terms of accuracy and scientific insight [27].

By analysing the aforementioned missions, it is possible to notice that all of them comprise large satellites and have had very large development and operational costs. This is where CubeSat based mission can really prove to have a significant added value. Being small relative to most satellites and having standardised characteristics, the cost of sending a CubeSat into space is much less expensive than all the missions mentioned above. Still, the main bottleneck right now for CubeSat missions is their difficulty to perform interplanetary missions. On this note, for the time being there is no CubeSat measuring radiation in deep space, this meaning ARCHER would be a pioneer of its kind. Nonetheless, CubeSat radiation measuring missions orbiting the Earth are quite common. Most try to characterise the Van Allen belts in order to understand the biological impact of radiation on astronauts on board of the ISS and model material degradation due to radiation exposure[2]. Examples of such missions are Hiscock Radiation Belt Explorer (HRBE), a one unit one kilogram CubeSat which measures the Van Allen

[1] `humanresearchroadmap.nasa.gov/` [Retrieved 5 June 2018]
[2] `www.nanosats.eu/index.html#info` [Retrieved 4 June 2018]

belts radiation with a miniature Geiger tube [28]; Robusta 1-B, again a one unit CubeSat developed by Montpelier University in France with the scope of measuring radiation induced degradation in electronic devices [29] and finally, the South Korean CubeSat mission Khusat-3, which is a pertinent mission given its strong similarities in payload and mission objective with ARCHER [30].

Space Radiation Environment

The Space radiation environment outside Earth's magnetosphere is characterised by two main sources, the Sun and the Galactic Cosmic Radiation (GCR) originating from outside the Solar System [31]. On the other hand, secondary radiation are also created from the interaction of aforementioned rays with asteroids and planetary bodies belonging to the Solar System. Eventually, the interaction of this radiation with Earth's magnetic field will create regions of trapped particles, namely Van Allen belts, which are mostly considered and relevant for missions in Low Earth Orbit (LEO). As Mission ARCHER is designed to traverse these regions of trapped particles for a small fraction of time of the entire mission duration, their impact on the CubeSat is neglected.

The Galactic Cosmic Rays (GCR) are characterised by particles that can reach energies up to 10^{20} eV. For this reason they are most probably produced by high energetic phenomena occurring in the Universe as supernova explosions or pulsars [32]. GCRs are composed by 85% of protons, 14% helium nuclei and a mere 1% of highly charged (Z), high energy (E) ions, also defined as heavy ions (HZE) [31]. Even though the HZE are in very low abundance, their biological effect is much grater than smaller ions such as protons (hydrogen nuclei) and helium nuclei (alpha particles), hence representing a bigger threat in space Travel. Nonetheless, shielding against these particles is not particularly straightforward.

An important aspect to be analysed is the influence of the solar cycle on the Galactic Cosmic Rays. It has been observed that the solar magnetic activity follows a quasi periodic cycle of around eleven years, where seven years of solar maxima usually alternate with 4 years of solar minima. Solar maxima are periods of high solar activity where solar irradiance and sunspots significantly increase in number [33]. On the contrary, solar minima are periods characterised by very poor solar activity. As the Sun increases its activity, so does its magnetic field, providing a sort of shielding for Galactic Cosmic Rays having energies below approximately 1 GeV/nucleon. As visible from Fig. 2.1 the influence of particles of lower energies decreases with periods of solar maximum and vice-versa.

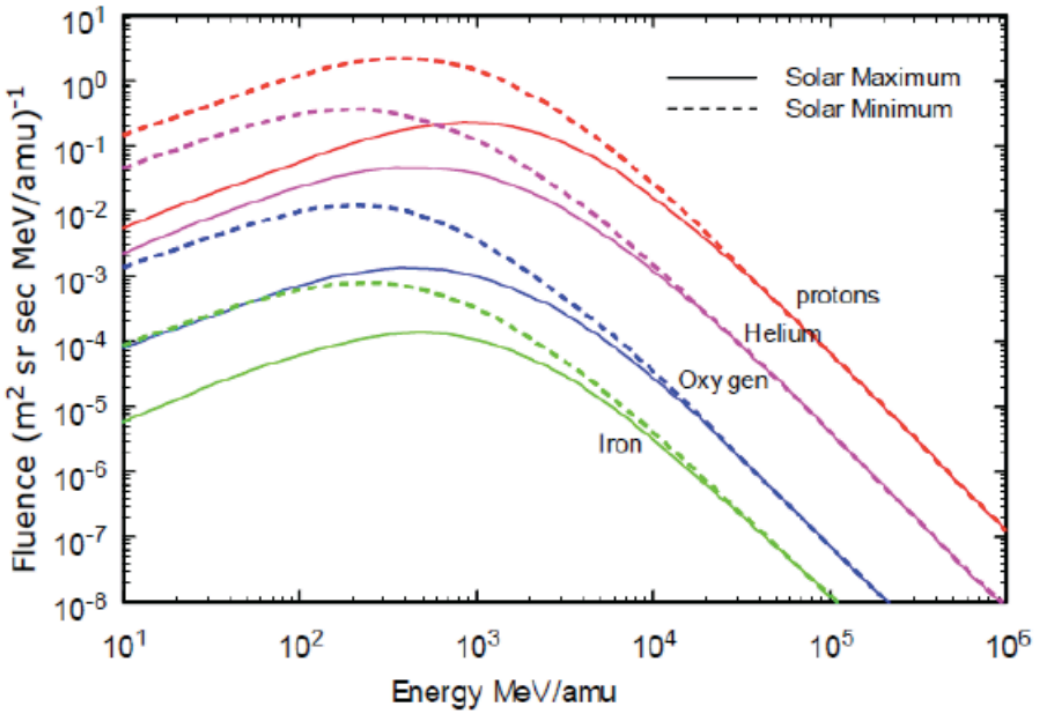

Figure 2.1: Differential Spectra of major ions caused by solar cycle [34].

As mentioned at the beginning of this subsection, the second most important source of radiation in the Solar System is the Sun. It constantly emits protons and electron of low energies ranging from around 100 eV to 3.5 keV, this radiation is called solar wind. However, given the low intensity of these particles they turn to be easily shieldable and consequently do not represent any significant biological threat. In unpredictable rate the Sun experiences local surface eruptions releasing radiation at very high energies, these local burts spiral around the interplanetary magnetic field lines originating from the Sun itself, propagating through the entire Solar System. These solar activities, more commonly known as Solar Particle Events (SPE), can vary substantially in spectrum and magnitude per event and can potentially pose a serious threat for astronauts in deep space. Generally, it is assumed that highly energetic SPEs of significant biological risk occur at a rate of one per solar cycle [31]. Along these lines, one of the most dangerous SPE of the 20th century, which would have had a serious impact on any astronaut performing an Extravehicular Activity (EVA), occurred in August of 1972, exactly in between the two very last Apollo missions, namely Apollo 16 (April, 1972) and Apollo 17 (December, 1972). [31]. Such a fortunate coincidence, outlines the incredible vulnerability of human spaceflight to such unpredictable events.

Fortunately, nowadays it is possible to have a fair estimate on the radiation environment a given mission will be exposed to if period and trajectory are known. This is achieved by making use of advanced radiation simulation models. In the particular case, for ARCHERs mission profile, the team made use of an online simulation software, namely SPace ENVironment Information System (SPENVIS) developed by the Royal Belgian Institute for Space Aeronomy (BIRA-IASB) for ESA[3].

With the use of SPENVIS, the radiation energy spectrum ARCHER is expected to be exposed to was simulated and analysed. As previously discussed, there are two main sources of radiation in outer space, the Sun and the Cosmos, each having its own composition and energy spectrum. In Fig. 2.2 and Fig. 2.3, the proton energy spectrum for both sources are displayed. Indeed, hydrogen nuclei are the most abundant particles in both GCRs and SPEs, hence simply analysing their energy spectrum can already provide valuable information on the environment.

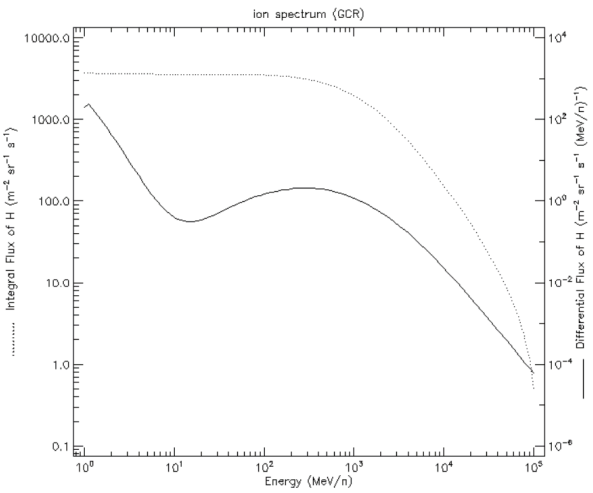

Figure 2.2: GCR spectra of protons.
Plot generated with SPENVIS.

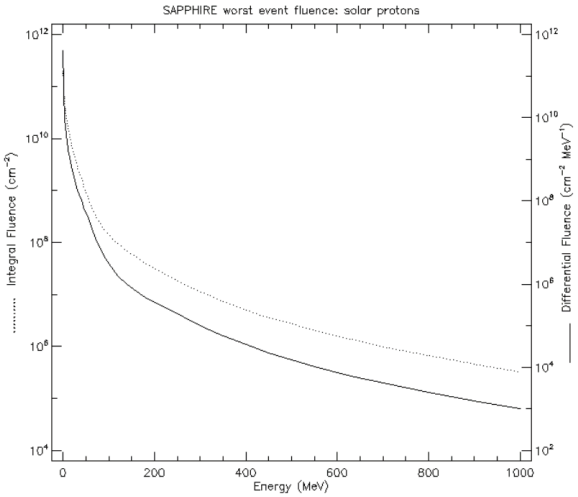

Figure 2.3: SPE spectra of protons
Plot generated with SPENVIS.

2.2. User Requirements

With the scientific background complete and the mission need established, the mission itself can be studied. This starts with a stakeholder analysis. This was carried out during the Baseline Report [2] and the following were identified:

- User/Customer/TU Delft
- Example Company - represents any potential part supplier (off the shelf)

[3] https://www.spenvis.oma.be [Retrieved 15 May 2018]

- Example Manufacturer - represents any potential manufacturer of bespoke parts
- Launch Contractor - represents any potential company providing space launch services
- Transport - represents any company which may terrestrially transport part of and/or the whole spacecraft
- Operators - represents any company involved in the daily operation of and communication with the spacecraft
- Scientists - represents scientists, academics and/or astronauts who may be interested in the measured data
- Spaceflight Community - represents parties including regulators, governments and other operators

Whilst the customer delivered a set of requirements at the beginning of the project [35], their needs were analysed and expanded on as were those of the other stakeholders. These were translated into Stakeholder requirements. These are not technical requirements and are in the language of the Stakeholder. They were used to help derive technical requirements. Only the User/Customer requirements are presented below while additional stakeholder requirements can be found in the Baseline Report [2].

User/Customer/TU Delft - Requirements

- [STA-CUS-01] The mission shall measure the radiation environment beyond Earth's magnetosphere
- [STA-CUS-02] The system shall communicate with a ground system on Earth and provide command uplink, telemetry downlink and scientific data download
- [STA-CUS-03] The scientific payload shall detect neutrons
- [STA-CUS-04] The scientific payload shall detect LET
- [STA-CUS-05] The scientific payload shall measure the ionising dose
- [STA-CUS-06] The scientific payload shall measure the ionising dose rate
- [STA-CUS-07] The scientific payload shall measure the magnetic field
- [STA-CUS-08] The spacecraft shall be able to sustain the radiation environment during the entire mission
- [STA-CUS-09] The payload shall be powered during the entire mission
- [STA-CUS-10] The overall mission's reliability shall be calculated
- [STA-CUS-11] An EOL strategy shall be identified
- [STA-CUS-12] Use of radioactive materials shall be avoided
- [STA-CUS-13] The propulsion system shall use green propellant
- [STA-CUS-14] During manufacturing and integration of the satellite, energy consumption shall be minimised
- [STA-CUS-15] The spacecraft shall be compliant with the CubeSat standard
- [STA-CUS-16] The mission shall be ready for launch by 2022
- [STA-CUS-17] The mission shall use currently available technology
- [STA-CUS-18] The spacecraft design shall be compatible with existing launch systems
- [STA-CUS-19] The cost of the mission shall not exceed 10 million euro (excluding launch and operations)
- [STA-CUS-20] An estimation of the costs for launch shall be provided
- [STA-CUS-21] An estimation of the costs for operation shall be provided
- [STA-CUS-22] The mission design shall be completed within 10 weeks
- [STA-CUS-23] The mission design shall be completed by 9 bachelor students
- [STA-CUS-24] The overall mission's availability shall be calculated

2.3. Mission Design Trade-Off

An initial mission profile Design Option Tree was created in the Baseline report and had 4950 options [2]. This was reduced to four via a trade-off process which is documented in detail in the Baseline Report. These four were then analysed and put through a trade-off to establish the best mission profile for ARCHER. The extensive trade-off process is briefly summarised below and can be seen in full in the Midterm Report [17]. The reader is encouraged to read the Baseline and Midterm reports if interested in learning more on the details of the trade-off processes used to arrive at the final mission profile.

The rest of this section will present the missions, trade-off criteria and results followed by a sensitivity analysis on the trade-off.

2.3.1. The Final Four

The four missions which made it through to the final trade off are presented in Table 2.1

Table 2.1: The four missions in the final trade-off

#	CubeSats	Destination	Detail
M1	5	Moon	Single CubeSat launched every 2 years to cover entire solar cycle
M2	2	Earth	Highly eccentric high altitude polar orbits
M3	2	Moon	Elliptical orbit and one of L4/L5 Earth-Moon Lagrangian point
M4	2	Mars	Elliptical orbits

2.3.2. Trade-off Criteria

Six main criteria were established for the final trade-off. Each of these was in turn subdivided into smaller criteria. This enabled each mission to be rated objectively on a scale of 1-5 where 1 was the worst, and 5 was the best possible score. The sub-criteria were designed so that even if exact mission parameters were not known, the missions could still be scored fairly relative to each other. Both the sub-criteria and the main criteria were also weighted. The trade-off criteria were Science, Risk, Sensitivity, Cost, Sustainability and Competitively and were divided into the following sub-criteria:

Science
Value average data point
Timescale of mission
Number of measurements at a time
Ability to communicate data

Risk
Failure to gather data
Failure to communicate
Failure to achieve orbit
Failure to support payload
Failure to meet industry standards
Unable to deliver for launch
Cost overrun

Sensitivity
EPS
COMMS
ADCS
Propulsion
Thermal
Structures

Cost
Verification and Validation
Total component cost
Total launch cost
Total operations cost

Sustainability
Space debris
Planetary protection
Earth environment

Competitively
Launch opportunity
Technology demonstration
Public interest

Examples of how these were scored can be seen in Table 2.2 and Table 2.3. Some interesting points to note are that M2 scores lower on the value of the average data point as part of the orbit passes through the magnetosphere. M1 scores highly in science timescale as it is a phased mission over ten years versus the other two year missions. Verification and Validation was expected to be the biggest cost differentiator as operations and launch, while important, were excluded from the initial budget. In addition, CubeSat hardware is relatively inexpensive. It does however, have reliability issues which are usually due to a lack of testing [36]. As a result, testing, which is costly, was considered to be extremely important. It was assumed that additional time for V&V would be required for the phased mission to the Moon, with five CubeSats, and for the Mars mission, with large amounts of time spent out of communication range, and as a result, would be more expensive than for the other missions.

Table 2.2: Scoring Scientific Value

	M1	M2	M3	M4
Value average data point	4.5	2	4.5	5
Total mission timescale	5	1	1	1
Number of measurements at a single time	2.5	5	5	5
Ability to communicate data	4	5	4	1
Total	4.1	2.75	3.53	3.4

Table 2.3: Scoring Cost

	M1	M2	M3	M4
Verification and validation	3	5	5	3
Total component cost	2	5	4	3
Total launch cost	1	5	3	2
total ground operations cost	1	5	4	3
Total	2.0	5.0	4.2	2.8

The following criteria were rejected for the trade-off.

- Electrical Power System: the electrical requirements can be fulfilled for all missions

- Mass: all missions selected fulfilled the Δv requirements therefore mass is not a limiting factor
- Command and Data Handling: mass and power required for the different missions expected to vary marginally
- Propellant: all four missions fulfilled the Δv requirements therefore, propellant was not a limiting factor
- Communications: taken into account in the main science criteria

2.3.3. Trade-Off Results

The overall results, as seen in Table 2.4, clearly show M3 is the most suitable mission. In this table, the colours range from red to green where red is the lowest score and green the highest. These colours help visually but are not necessary to interpret the table as they are represented by the numbers.

Table 2.4: Overview Trade-Off

Criteria	Weight	M1	M2	M3	M4
Scientific value	30	4.1	2.8	3.5	3.4
Risk	20	3.9	4.1	3.9	2.0
Cost	20	2.0	5.0	4.2	2.8
Sustainability	10	3.6	4.8	4.4	2.6
Sensitivity	10	4.8	4.0	4.7	3.8
Competitivity	10	3.2	2.8	4.0	3.4
		3.57	**3.80**	**3.98**	**2.97**

2.3.4. Sensitivity Analysis of Trade-Off Weighting Factor

In order to verify that the result was not a result of biased weighting, a sensitivity analysis of the trade-off weighting factor was undertaken. First, the standard deviation was checked, as seen in Table 2.5, and the clearly lower standard deviation of M3 implies that it has relatively fewer significantly outlying scores in the trade-off. Furthermore, a python script[4] was written to rapidly vary the weights in the trade-off and judge the results. Each of the six weightings was given a variation range, which was discretised seven times. For example, if a weighting was varied by +/- 10%, this 20% range was broken into 7 steps allowing for 7 different variations of the weighting. This was applied to each of the six criteria. This gave 7^6 variations or 117649 weighting combinations per trial. The highest scoring mission was evaluated at every single variation. The difference between the best mission and M3 was also recorded. Table 2.6 clearly illustrates that M3 is the best mission almost 100% of the time with moderate weighting variations and even when the weighting is varied extremely, remains the best, nine times out of ten. This gives great confidence in the trade-off output and showcases that the result is not a function of biased weighting.

Table 2.5: Trade-Off Standard Deviations

	M1	M2	M3	M4
Standard Deviation of Unweighted Scores	0.99	0.95	0.39	0.67
Mean of Unweighted Scores	3.67	3.90	4.11	3.18

Table 2.6: Sensitivity Analysis of Trade-Off

Trial	Weight varied by +/- %	% M3 was best (117649 variations per trial)
1	10	100
2	20	100
3	30	99.87
4	40	97.92
5	50	94.23
6	60	89.61

[4] https://gist.github.com/nathanvanthof/f33f0ba770cfe9e1f8396aa2f689dddd

2.4. Sustainable Development Strategy

The purpose of ARCHER is to scientifically support the advancement of human space flight. Since in a bigger context the effort is targeted towards a general growth of the space flight sector, it should also set an example as a sustainable mission. This includes dealing with Earth environmental concerns [37], space debris mitigation [38] and planetary protection [39], all of which are key in making large scale space usage and exploration possible in the long run. In this chapter the preliminary sustainability strategy is outlined. This includes a statement of the policy in Section 2.4.1 and a brief discussion of its implications on the mission design, the creation of a sustainability rubric and requirements in Section 2.4.2. A concluding evaluation of the final design sustainability is presented in Section 6.5.

2.4.1. Sustainability Policy

For the sustainability approach, a policy has been defined. This policy is the leading guideline for the project's sustainability aspect. It is defined as:

In terms of terrestrial and extra-terrestrial environmental protection and sustainability ARCHER should serve as an example to future interplanetary science missions. On the terrestrial scale, this encompasses the implementation of 'green' non-toxic propellants as well as measures for energy, (toxic) waste and environmental pollution reduction during the manufacturing and launch of the satellite. Naturally, this implies that contractors such as the suppliers of off-the-shelf components and the launch conducting agency are held to these standards, too. To minimise the risk of extra-terrestrial pollution and adverse effects on the orbital environment an end of life scenario that complies with the COSPAR [40] guidelines for planetary protection is a mandatory part of the mission.

2.4.2. Implications and Requirements

From the start, most aspects of Earth environmental protection, like the efficient use of resources during production and launch of the spacecraft, were expected to be of small impact on the mission and system design. Since the spacecraft will be secondary payload on the launch vehicle and assembled from 'mass-produced' off-the-shelf components, there is an inherent degree of resource efficiency to CubeSat missions. Since the performance of the propulsion system had the potential to narrow down the mission target options, the green propellant aspect influenced the mission design from a very early stage.

Especially during the mission profile design, extra-terrestrial protection and space debris mitigation measures had to be considered, too. According to the Committee on Space Research (COSPAR) guidelines, however, lunar orbiter missions are of no concern for planetary protection [40]. Being classified as a category II by the COSPAR catalogue, requirements merely include administrative measures, namely the documentation of pre- and post-launch reports identifying potential impact targets and strategies[4]. Furthermore, an end-of-mission report specifying impact details such as the impact location is required[4].

Regardless of the COSPAR classification, a feasible end-of-life scenario which ensures that ARCHER will - within reason - not adversely affect or endanger future missions has to be established. Since on the Moon there is "only a remote chance that contamination carried by a spacecraft could jeopardise future exploration"[4], a lunar orbiter is allowed to be disposed on the surface of the Moon without the need for an inventory of bulk constituent organics, bioload reduction or sterilisation measures. This also eliminates the need for a trajectory biasing requirement. Consequently, it was decided to dispose the lunar orbiter Artemis on the surface of the moon.

The first step of implementing the sustainability policy into the design process is to establish a system for the quantification of design 'goodness' in terms of sustainability, labelled the 'Sustainability Score'. The score is found as a weighted average of the aspects Earth environmental, planetary protection and space debris mitigation. The focus of the mission sustainability policy is on spaceflight itself. This does not imply the Earth environment is not important for the sustainable increase of future space flight activity, but it is considered less crucial than planetary protection and space debris mitigation. Table 2.7 shows how a score of the individual aspects is determined and the weight with which they impact the overall score.

---

[4] https://planetaryprotection.nasa.gov/about-categories/ [Retrieved 3 May 2018]

Table 2.7: Rubric for the derivation of the design's 'Sustainability Score'

Score / Aspect (weight)	1	2	3	4	5
Earth environment (Weight: 2)	wasteful use of resources, significant generation of toxic waste during manufacturing and launch	wasteful use of resources, significant generation of toxic waste during either manufacturing or launch	acceptable use of resources, waste from manufacturing tolerable, average pollution during launch	efficient use of resources, no toxic waste during manufacturing, pollution during launch lower than average	very efficient use of resources, no toxic waste during manufacturing, pollution during launch significantly lower than average
space debris (Weight: 3)	adverse effects on orbital environment unavoidable	adverse effects on the orbital environment likely	adverse effects on orbital environment unlikely	adverse effects on orbital environment - within reason - impossible	adverse effects on orbital environment - within reason - impossible, spacecraft sustainably disposed
planetary protection (Weight: 3)	Outer Space Treaty Article IX [39] violated	-	COSPAR [40] guidelines followed with minor exceptions	-	full compliance with COSPAR [40] guidelines

It was established, that ARCHER must achieve a score of 3 or higher in each aspect. To ensure that the internal and customer demands are kept in mind during the design process, a set of tangible sustainability requirements was derived:

- [SUS-ASD-01] The lunar orbiter shall be disposed on the surface of the Moon in a controlled, predicted manner.
- [SUS-ASD-02] The Lagrange point orbiter shall leave the region of practical stability at the end of mission.
- [SUS-ASD-03] The spacecraft shall not intersect protected LEO and GEO regions.
- [SUS-SYS-01] The mission shall not make use of any toxic materials.
- [SUS-EPS-01] The power production shall not involve any radioactive materials.
- [SUS-PROP-01] The propellant shall be no more than harmful to humans (ECHA classification III and below).
- [SUS-MNF-1] During manufacturing and integration of the satellite energy consumption shall be minimised.
- [SUS-OPS-1] The greenhouse footprint of the launch shall be neutralised.
- [SUS-OPS-2] The mission operation delivers all COSPAR class II documentation requirements.

2.5. Mission Astrodynamics

This section covers the astrodynamic mission design. In Sections 2.5.1 and 2.5.2 the common launch and transfer of the two probes, Artemis and Diana, towards the Moon is presented. Section 2.5.3 shows the insertion trajectories for each probe and how they were derived. The following Sections 2.5.4 and 2.5.5 discuss the aspects of science orbit around the Moon and the triangular region of practical stability L_5, respectively, station keeping and the end of life scenario for each of the probes. The most important characteristics and a Δv budget for both spacecraft are summarised in Section 2.5.6. Below, all requirements posed on the astrodynamic mission design are listed:

- [TEC-ASD-01] The spacecraft shall achieve an orbit which carries the payload outside the Earth's magnetosphere.
- [TEC-ASD-02] All known natural space objects with a diameter larger than 2 m shall be avoided by 1 km.
- [TEC-ASD-03] All known natural space objects with a diameter larger than 50 km shall be avoided by 50 km.

- [TEC-ASD-04] During transit and orbit, all known man-made space objects shall be avoided by 10 km.
- [TEC-ASD-05] The mission shall not depend on low availability launch opportunities.
- [SUS-ASD-01] The lunar orbiter shall be disposed on the surface of the Moon in a controlled, predicted manner.
- [SUS-ASD-02] The Lagrange point orbiter shall leave the region of practical stability at the end of mission.
- [SUS-ASD-03] The probes shall not intersect protected LEO and GEO regions.

2.5.1. Launch

For the mission, numerous launch and transfer options were considered, as shown in Figs. 2.4 and 2.5. These options were reduced until only one most viable option remained.

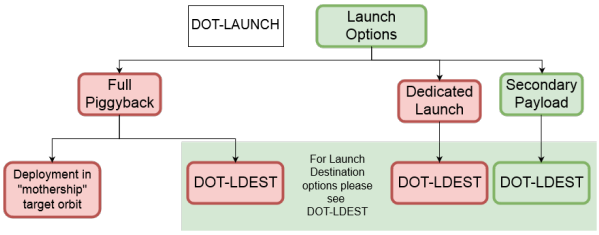

Figure 2.4: Launch design option tree

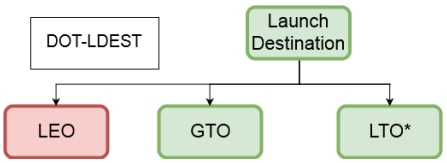

Figure 2.5: Transfer orbit design option tree

Full piggyback, where the CubeSat deployer travels with a larger satellite which provides the orbital insertion, was considered to be the most advantageous launch method, as no Δv is required from the CubeSat for transfer or capture. However, this option was dismissed from consideration due to the limited availability of opportunities for such a launch to the Moon, and complete unavailability for such a launch to the L_5 point.

Secondary payload and dedicated launch options were considered further. Dedicated launch options were evaluated based on cost and capability estimates for current and future launch vehicles. Given the size of the spacecraft and the 2022 launch requirements, the only currently operating commercial launch vehicle to fit the mission is the Electron Rocket, operated by Rocket Lab. At a standard launch cost of $4.9M (2016) [41] the Electron rocket would be feasible from a cost perspective. However, while capability information is limited, the typical mission of 150 kg to a 500 km circular Sun-synchronous orbit [41] would indicate a lack of a capacity for missions beyond LEO. More powerful launchers were too expensive for a CubeSat mission, while other options currently in development do not provide any significant advantage in capabilities over the Electron. As a result, dedicated launch was only considered as an option for launch to a LEO deployment. However, based on Δv calculations carried out during preliminary sizing, this was eliminated due to the excessive Δv requirements a transfer from LEO placed upon the spacecraft.

Secondary payload launch options are widely available from a number of commercial and non-commercial providers. Commercially, the upcoming launches of Innovative Space Logistics (ISL)[5] and Spaceflight[6] include multiple LEO and a number of Geostationary Transfer Orbit (GTO), and Lunar Transfer Orbit (LTO) opportunities. On the non-commercial front, the first launch of NASA's Space Launch System (SLS) will carry 13 CubeSats as secondary payloads on a lunar trajectory[7]. With development of the Lunar Orbital Platform-Gateway (LOP-G) scheduled to begin in 2022 with at least one launch to lunar orbit per year from then on[8], the expectation is that the availability of these secondary payload opportunities to LTO will only increase.

With secondary payload launches to GTO and LTO the only remaining options, low-thrust transfers from GTO were considered for Artemis and Diana. Following discussion with the propulsion subsystem team and a representative of Busek Co. Inc., a CubeSat propulsion system manufacturing company, the mission duration and Δv requirements placed upon the CubeSat by this profile were found to be unfeasible within the TRL requirements established in the Baseline report [2]. As a result, a launch to Lunar Transfer Orbit was chosen as the optimum for the ARCHER mission. As data from ISL on the LTO launch options they had was not available, a reference launch trajectory was assumed as that of the SLS Exploration Mission 1 (EM-1) CubeSats.

---

[5] `www.isispace.nl/launch-services/#upcoming-launches` [Retrieved 24 May 2018]
[6] `www.spaceflight.com/schedule-pricing/` [Retrieved 24 May 2018]
[7] `www.nasa.gov/press-release/nasa-space-launch-system-s-first-flight-to-send-small-sci-tech-satellites-into-space` [Retrieved 24 May 2018]
[8] `www.nasa.gov/feature/nasa-s-lunar-outpost-will-extend-human-presence-in-deep-space` [Retrieved 24 May 2018]

2.5.2. Transfer

There exist numerous investigations of low-energy transfer and insertion trajectories that connect EM-1-like LTOs to the Moon [42–45]. One of the options suggested in [45] is a low-thrust trajectory as depicted in Fig. 2.6. It requires an alteration of the EM-1 lunar B-plane target by deceleration during LTO. The lunar encounter slings the spacecraft into a high altitude out of plane arc, from which the Earth is targeted for a gravity assist. This assist puts the spacecraft on an unstable Sun-Earth manifold, from where through leveraging the gravitational attraction of the Sun the spacecraft is put on a Moon-like orbit around the Earth. On this orbit the second lunar encounter occurs and insertion from the far side of the Moon into lunar orbit is performed. In order to replicate this 231 day long trajectory up to the second encounter with the Moon [45], a spacecraft has to be able to accelerate by $5.56 \cdot 10^{-5}$ m/s^2 and deliver a total Δv of 673 m/s [45].

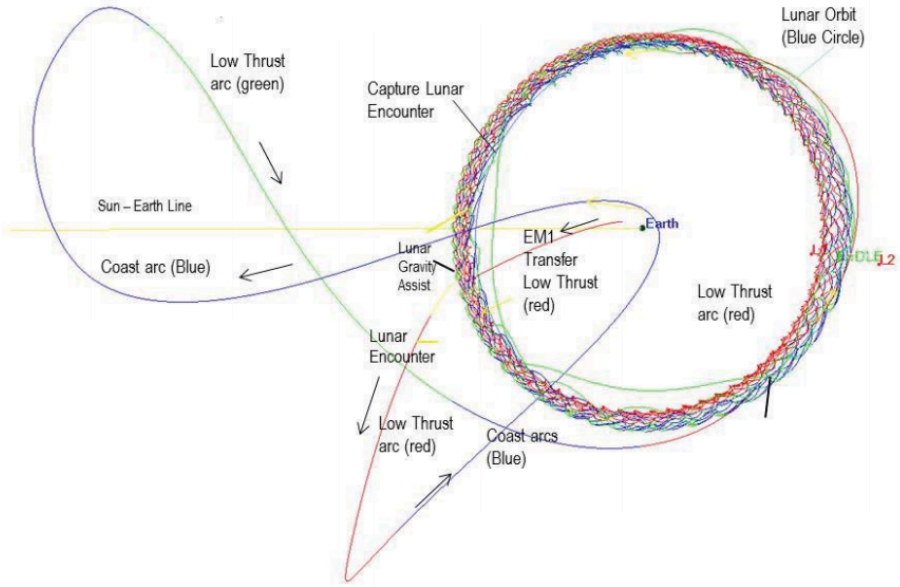

Figure 2.6: Low thrust EM-1 transfer option to the Moon [45]

Designing a low-energy lunar transfer from a constrained initial condition like the EM-1 LTO that suits the ARCHER mission profile better than the trajectory suggested above is beyond the scope of this project. Altering the transfer to suit the exact details of the ARCHER mission would be an option, however, there was not enough information accessible to make this possible. Instead, it is assumed that after small alterations a trajectory of this kind can deliver a spacecraft into the vicinity of the Earth-Moon L_2 point with a range of final conditions that will be specified in the Section 2.5.3, where insertion manoeuvres are discussed.

2.5.3. Insertion Trajectories

With the goal of providing an accurate indication on whether insertion from L_2 to the target orbit around the Moon for Artemis and to L_5 for Diana is possible, an optimisation script was developed in MATLAB®. These target orbits are derived and described in Sections 2.5.4 and 2.5.5.

This script was based on the Circular Restricted Three Body Problem (CRTBP) setup, where only three bodies (the Earth, the Moon and the spacecraft) are modelled in a frame that rotates around the Earth-Moon barycenter rotating frame with the synodic period of the two bodies. A description of the simulation functional flow followed to determine the optimal insertion trajectories is elaborated on below.

1. Setup and assumptions made: In the Circular Restricted Three Body Problem it is assumed that there are only two massive bodies, orbiting in plane around a common barycenter at constant velocity. The third body is assumed to be mass less (particle). Both massive bodies are treated as point masses, all perturbances from mass concentrations or bodies outside the system are neglected. A CRTBP analysis is performed in a rotating, non-inertial frame using canonical units, where units of distance are defined as DU = 384399 km and units of time as TU = 405648 s. This has to be kept in mind when graphics and values are consulted.

2. Optimisation model: The optimisation algorithm was based on the Genetic Algorithm (GA) solver provided by MATLAB within the Global Optimisation Toolbox. The solver uses an objective function that dictates what the goal of the optimisation is and the corresponding fitness of a certain trajectory, as quantified by the penalty value.

3. Variables: In order to discretise the properties that are being optimised, the spacecraft's trajectory was divided into 7 sections. The properties that made each section different and allowed for an optimisation of the simulation are listed below, and are illustrated in Fig. 2.7.

   (a) Elapsed time: The length in time the section was propagated for.

   (b) Thrust: The magnitude of thrust the engine delivers. It was constrained to be at the most 1.15 mN, as this is the maximum the engine can provide.

   (c) Angle: The angle at which the engine thrust towards with respect to the velocity vector of the spacecraft. This angle is in the X-Y plane. If lower than 10 deg it can be achieved by gimbaling the propulsion unit, if higher it requires Attitude Determination and Control System (ADCS) to readjust the CubeSat.

   Therefore, as there were 7 sections and three variables per section, a total of 21 variables were introduced into the simulation. Iteration through these variables resulted in different trajectories, for each of which the algorithm recorded the performance by means of the penalty value and adapted the variables until the lowest penalty was found.

4. Penalty value: In order to quantify how favourable a certain insertion trajectory was, the penalty function was introduced. The formula used to quantify the fitness of the trajectory is described in Eq. (2.1).

$$f = r_{sc-L_2} * 1000 + v_{sc-L_2} * 100 + \Delta m/100; \tag{2.1}$$

   Here, r_{sc-L_2}, v_{sc-L_2} and Δ m are the distance, velocity, and propellant mass difference between the output of the optimisation and goal conditions, as described in the following point.

5. Goal conditions: The goal conditions of the genetic algorithm for both Artemis and Diana is a state vector at a point near L_2 where both spacecraft will be delivered to after transfer. The position is 1.14 DU in the x-axis from the common barycenter of the bodies, the velocity is $-0.11\frac{DU}{TU}$ in the x-axis, and the initial mass of the spacecraft is 19.7 kg.

6. Initial conditions: The initial conditions of the genetic algorithm are the points in space where Artemis and Diana are being inserted to, namely the lunar science orbit and L_5, respectively.

7. Propagation and result filtering: The trajectory was then backwards propagated in time starting at the previously described initial conditions and the simulation was terminated when the penalty value was minimised.

8. Verification strategy: In order to verify the tool, a completely independent algorithm was developed, that used randomised starting positions along the target orbit (or region around L_5 for Diana) and backwards propagated these conditions while thrusting along or against the spacecraft's velocity vector as appropriate until the closest match to our initial position (as described by Eq. (2.2)) was met. This provided an upper bound on the requirements for insertion, as the trajectory had no variables to optimise.

$$d\left(\sqrt{(x-x_{L_2})^2+y^2+z^2}\right) = \frac{(-x_{L_2}+x)dx}{\sqrt{(x-x_{L_2})^2+y^2+z^2}} + \frac{ydy}{\sqrt{(x-x_{L_2})^2+y^2+z^2}} + \frac{zdz}{\sqrt{(x-x_{L_2})^2+y^2+z^2}} \tag{2.2}$$

where x, y, and z are the spacecraft's instantaneous position, and x_{L_2} is target position near L_2 in the synodic frame.

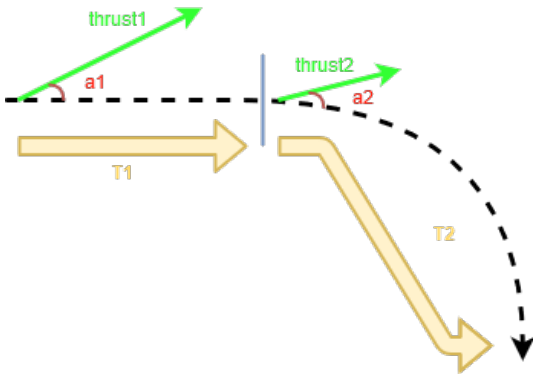

Figure 2.7: Representation of variables present in the Genetic Algorithm. The black dotted line is the path followed by the spacecraft, $T1$ and $T2$ represent the elapsed time per trajectory segment, $thrust1$ and $thrust2$ represent the thrust delivered by the engine, while $a1$ and $a2$ represent angles with respect to the velocity vector of the spacecraft.

Table 2.8: Details on Artemis insertion into Lunar science orbit. Allowable initial velocity range is with respect to the optimal initial velocity.

Axis	Position [DU]	Position [km]	Velocity [DU/TU]	Velocity [m/s]	Allowable initial position range	Allowable initial velocity range
x	1.1406	438450	-0.0822	-77.9	1.1100 to 1.1712	$\pm$0.05
y	0.0702	26985	-0.0565	-53.5	0.0329 to 0.10755	$\pm$0.02
z	0	0	0	0	N/A	N/A

Artemis Artemis' science orbit is an eccentric, inclined orbit around the moon, which is specified in greater detail and illustrated in Section 2.5.4. The insertion into this orbit was analysed in two parts: a planar trajectory, which results in an orbit equivalent to the science orbit, but at zero inclination, and a successive inclination change of 40°. For the first, planar component of the insertion, the verification algorithm provided more suitable results than the GA. Therefore, this model was used for the analysis. An illustration of the insertion provided by the verification algorithm can be found in Fig. 2.9, where the coloured contour in the background display zero-velocity lines derived by Eq. (2.7).

All the solutions of the verification model were stored in order to determine the range of initial conditions that could be handled at L_2, such that the range of workable end conditions for the transfer trajectory could be determined. These are presented in Table 2.8.

The second part of the insertion was analysed outside the CRTBP tool. The goal of the analysis is to determine an upper bound for the time and Δv required to perform the desired inclination change of 40°. To describe this manoeuvre, Gauss' form of the relevant planetary equation was chosen and adjusted [46]. Introducing a constant out-of-plane force by the low-thrust engine (T) and reversing the direction of the engine orientation when passing the line of nodes results in an expression for the inclination change per orbit:

$$\Delta i_{2\pi} = 2\int_0^{\pi} T\frac{r^3}{\mu_l p}cos(\theta+\omega)d\theta \tag{2.3}$$

where θ is the true anomaly of the spacecraft and p represents the semi-latus rectum. For simplification it was assumed that all other orbital parameters stay unaffected by the manoeuvre. Using Eq. (2.3) it was found that it takes 40.2 orbits to complete the plane change manoeuvre, which corresponds to just under 16 days and 60 m/s of Δv.

Putting the two parts of the insertion in sequence, Artemis needs at most 131.3 days and 582 m/s of Δv to get from its L_2 condition (Table 2.8) into science orbit. It is expected that these characteristics can be improved by performing the in-plane and out-of-plane parts of the insertion manoeuvre in parallel.

Diana Diana's science orbit is a stable, periodic and planar orbit around the Earth-Moon L_5, as described in Section 2.5.5. The injection to this Lagrange point showed large differences between the GA optimisation model and the verification model, with the former providing injection with more suitable initial velocities at L_2. Consequently,

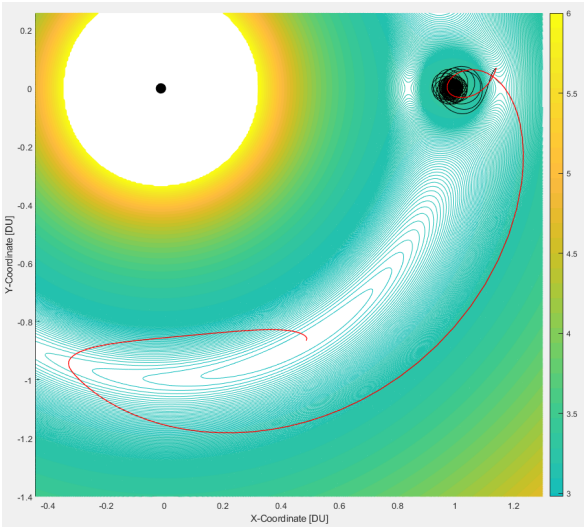

Figure 2.8: Diana insertion (in red) as optimised by the genetic algorithm. It required a Δv of 256 m/s.

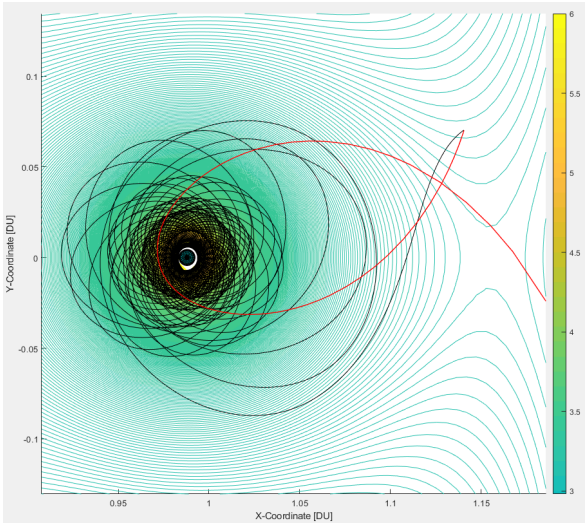

Figure 2.9: Artemis in-plane insertion (in black) as optimised by verification algorithm is the black line. This part of the insertion requires a Δv of 522 m/s.

Table 2.10: Details on Diana insertion. GA required 0.2206 kg of fuel, whereas the verification model required 0.1955 kg. However, the GA allowed for significantly lower initial velocities.

Axis	Position [DU]	Position [km]	Velocity [DU/TU]	Velocity [km/s]	Position Verification [DU]	Velocity Verification [DU/TU]
x	1.1407	434800	-0.1121	-106	1.1500	-0.446
y	0.0701	26720	-0.3440	-326	0.0002	-0.4
z	0	0	0	0	-0.0005	0.0909

the result of the GA was adopted for the mission design. An illustration of the chosen injection trajectory is shown in Fig. 2.8. The parameters describing the optimal insertion manoeuvre are catalogued in Table 2.9. The insertion takes a time of 89 days and the involved manoeuvres require 256 m/s of Δv.

Table 2.9: Optimisation parameters found by the GA for Diana's insertion. These are implemented as described in Fig. 2.7.

Segment number	Time [h]	Thrust angle [deg]	Thrust magnitude [mN]
1	81.2	170.1	0.8
2	81.2	15.3	0.2
3	81.0	-93.3	0.9
4	80.9	-7.5	0.3
5	81.0	-126.1	1.1
6	98.6	-57.6	1.1
7	2138	67.5	0.8

Implications on the transfer trajectory The launch and transfer design requires both probes to follow roughly the same trajectory to L_2. Small alterations are necessary to deliver each probe to their individual initial condition for insertion. These are listed in Tables 2.8 and 2.10, which show that the alterations have to create only a minuscule positional difference between the spacecraft, equivalent to 54.4 km. Adjusting the transfer trajectory such that L_2 conditions are so similar in position, but allow for a velocity differences of 274 m/s, is expected to be very challenging. Therefore, it is not assumed that the insertion will happen in the exact that was derived in this section. However, the preceding discussion showed that it is feasible to have both spacecraft approaching the moon from the same direction, which can be connected to an EM-1 LTO transfer trajectory and to manoeuvre them towards their specified target orbits. Furthermore, it gave well-founded estimate for the time and Δv required by these manoeuvres.

2.5.4. Artemis

Science Orbit A classical orbit around a body like the Moon can be uniquely defined using the following five Keplerian elements: Semi-major axis *a*, eccentricity *e*, inclination *i*, argument of the right ascending node Ω and argument of periselene ω. Simultaneously optimising all of these parameters to identify the most ideal science orbit is very challenging, if not impossible. Instead, it was decided to investigate the effect of each parameter in isolation or in pairs.

The semi-major axis solely determines the energy of the orbit with respect to the Moon and combined with the eccentricity defines shape of the ellipse in the plane. These two parameters were investigated under scientific and mission design aspects: For the scientific goal of characterising the radiation environment in interplanetary space, it is beneficial to avoid a measurement bias from the albedo of large astronomical bodies. This can be achieved by keeping a large distance to their surface. On another scientific note, it is very valuable to replicate the measurements of previous missions such as the Lunar Reconnaissance Orbiter (LRO), that measured the lunar neutron flux at altitudes between 20 and 165 km along its orbit [47], to allow for cross calibration. A periselene altitude of 100 km would enable a comparison with the LRO results. To generate new measurements and adhere to the mission goal a aposelene at much higher altitude is needed. From a scientific point of view there is no upper limit on the furthest distance from the Moon: The higher the aposelene altitude, the better. However, there are constraints from the astrodynamic aspect of the mission design. Pushing the aposelene to the extreme while fixing the periselene at 100 km altitude requires a large semi-major axis and eccentricity. The combination of the two can create orbits that almost escape the sphere of influence of the Moon (to use a simplified two-body model). While a science orbit at ”close-to-escape energy” greatly simplifies the insertion, it can have catastrophic consequences when perturbations, such as third body influence, introduce alterations. The study of Lunar Cube Transfer Trajectory Options [42] proposes a lunar science orbit with 6,800 km aposelene height and 100 km periselene height, which translates to a semi-major axis of 5,189.3 km and an eccentricity of 0.6456. It was decided to adopt these parameters for multiple reasons. The resulting spacecraft altitudes allow for LRO cross calibration and new measurements at a large distance from the Moon. Furthermore, because of its high energy it is easy to insert into orbit after lunar capture. This can be demonstrated by simplified two-body escape velocity calculations [48]:

$$v_r = \sqrt{2\mu_l\left(\frac{1}{r} - \frac{1}{2a}\right)} \qquad (2.4)$$

$$v_{esc_r} = \sqrt{\frac{2\mu_l}{r}} \qquad (2.5)$$

where v_r, the speed of the spacecraft in the pseudo inertial frame of the Moon at a distance r from the centre of the Moon, is given by Eq. (2.4). The standard gravitational parameter of the Moon is represented by μ_l. Equation (2.5) shows how the escape speed v_{esc_r} at any distance r from the centre of the Moon can be computed. Computing and comparing both values at periselene of the suggested science orbit shows that at a speed of 2095 m/s Artemis is only 215 m/s below the escape speed of 2,310 m/s. While this is a speed difference of only about 10%, which allows for a low Δv insertion, it also constitutes a sufficiently large margin to ensure that Artemis does not leave the lunar sphere of influence through third-body perturbations. Lastly, this orbit was chosen because it is compatible with the low-energy lunar CubeSat transfer trajectory proposed in Section 2.5.2 [45].

The inclination of the orbit is of no scientific importance, however, it dictates the eclipse times of an orbit with fixed semi-major axis and eccentricity. Accordingly, the inclination of the science orbit was determined based on an analysis of the eclipse times. This analysis was performed using AGI's STK®[9]. The specified lunar orbit was inserted at a number of inclinations between 0° and 100° and propagated over 380 days using a 48th order spherical gravity model for the Moon. Furthermore, the effects of the Earth and the Sun are accounted for by modelling the bodies as point masses at their respective distance from the orbit. Assuming a conservative reflectivity coefficient of 0.8 [49], the reference area for the solar radiation pressure was taken to be 0.6 m^2, including the solar array, reflector array area and the largest side face of the CubeSat body. The analysis is able to record eclipses caused by the Earth and the Moon to seconds precision. Furthermore, it is capable of distinguishing between umbra and penumbra and provides a maximum shade percentage for the latter.

Generally speaking, orbits with inclinations close to 90° with respect to the ecliptic plane encounter eclipses the least often and for the shortest periods of time. This trend was visible in the outcome of the STK® analysis, too. However, multiple problems have to be considered at high inclinations. While Moon eclipse times decreased

[9] `https://www.agi.com/products/engineering-tools` [Retrieved 14 May 2018]

at high inclination, the Earth eclipse duration increased compared to small inclination orbits. Furthermore, the injection into high inclination orbits either complicates the lunar transfer trajectory through significant out-of-plane components or requires a Δv expensive inclination change after lunar capture. Most significantly, due to the interaction of the high inclination with lunar mass concentrations, the semi-major axis and the eccentricity were subjected to large changes that led to unacceptable alterations of the science orbit, eventually causing the orbit to intersect with the Moon. Simple station keeping schemes, where through a series of low thrust manoeuvres around aposelene the initial periselene is raised and periodical correction burns over the lifetime of the satellite are performed, could not avert premature impact on the Moon.

The aforementioned reasons did not allow for inclinations larger than 50°. The results of the analysis performed for inclinations of 30°, 40° and 50° are presented in Fig. 2.10. It should be noted that only the outlying eclipses of long duration are caused by the Earth and consist of at least 40% penumbra. All other eclipses are caused by the Moon and almost entirely umbra.

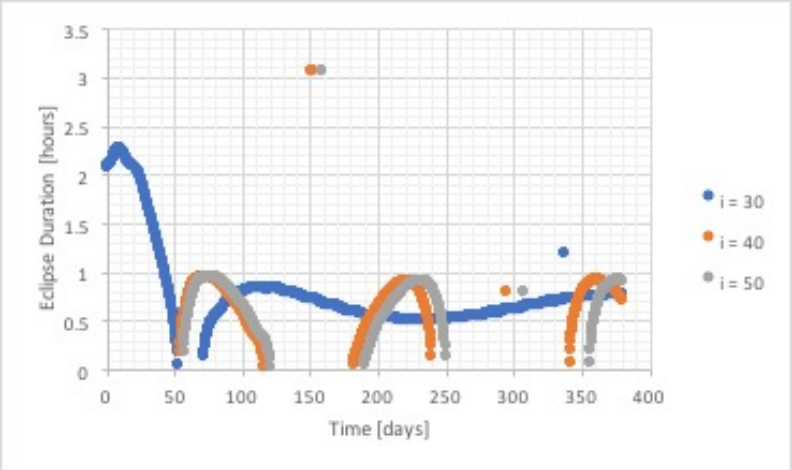

Figure 2.10: Eclipse times as function of inclination

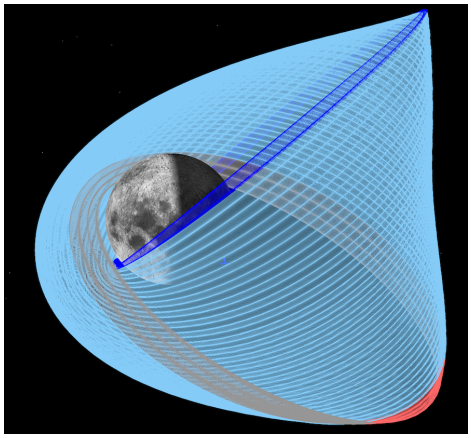

Figure 2.11: STK® render of Artemis' science orbit over the specified science orbit interval of 340 days and end of life.

Whereas increasing the inclination from 30° to 40° shows an appreciable effect on the eclipse times, an increase from 40° to 50° barely causes any improvement. It does, however, complicate the approach and insertion into the orbit. Consequently, the inclination was found to be optimal at 40°.

Ω and ω set the initial orientation of the orbit. Because there are no apparent implications on the quality of the science orbit, Ω and ω were both arbitrarily fixed at 90°. This orientation proved to be convenient during the insertion trajectory design. It should be noted that fixing an initial orientation does not lead to a constant orientation with respect to the Earth. Even if Ω and ω were to stay constant over time, the orientation of the orbit with respect to Earth would still go through a full 2π angle every synodic period. In addition to that, both parameters are subject to change over time due to obliqueness and other disturbance terms in the lunar gravity field. This means that over a time period like the Artemis mission duration the orbit will adopt a large amount of possible orientations with respect to the Moon and the Earth, which are hard if not impossible to design or even optimise for. To summarise, the final science orbit is characterised by the following Keplerian elements:

- Semi-major axis a = 5,189.3 km
- Eccentricity e = 0.6456
- Inclination i = 40°
- Argument of the right ascending node Ω = 90°
- Argument of periselene ω = 90°

Figure 2.11 shows a visualisation of this orbit over the specified science orbit interval of 340 days. The grey part of the trajectory with the red burn intervals around aposelene represents the end of life scenario, eventually leading to impact.

Station Keeping The selected science orbit was propagated in the same STK® environment as used for the eclipse time analysis. Over a time period of 340 days, active station keeping manoeuvres are not required to

avoid impact. In fact, the change in semi-major axis never exceeds 10 km. Eccentricity, however, changes in a sinusoidal fashion and reaches its minimum of 0.32 roughly halfway through Artemis' time in science orbit and recovers to almost the original value of 0.6456 at the very end of the 340 day period. A smaller eccentricity increases the periselene altitude and decreases the time during which the orbit enables cross calibration with Lunar Reconnaissance Orbiter (LRO) results to only 17%. Different correction manoeuvre schemes were applied to decrease the amplitude of the eccentricity fluctuation, none of which offered a significant improvement. Taking into account the challenging requirements that the most effective schemes posed on the ADCS and propulsion subsystems, eccentricity correction manoeuvres were discarded. Although no station keeping manoeuvres are planned for Artemis' time in science orbit, a scheme of correction burns was designed. In case of unforeseen loss of altitude due to a shrinking semi-major axis, the probe has the ability to burn at full thrust for 100 hours. If these burns are performed in two hour intervals around aposelene, this can compensate for a semi-major shrinkage of 100 km in the specified STK® environment.

End of Life Just like for station keeping, the end of life analysis was executed using the STK® environment characterised earlier in this section. According to [SUS-ASD-01], the strategy for Artemis intends to impact the Moon in a controlled fashion. An impact can be achieved through a sequence of approximately 100 orbits, during which at aposelene the engine burns with full power against the velocity vector for two hours. This sequence leads to a successful disposal within roughly 40 days, if initiated at the end of the 340 day period. Due to the periodic eccentricity fluctuations and the following raise of aposelene altitude, it is not possible to use the proposed sequence of manoeuvres to dispose the probe halfway through the mission lifetime. The scheme may only be applied in times of eccentricities larger than 0.56. This has to be taken into account when possible lifetime extensions of the mission are considered. In case of fatal damage to the spacecraft that prevents systematic manoeuvring, Artemis is predicted to deorbit naturally and to crash into the Moon after 10 years.

2.5.5. Diana

Science Orbit Diana's science orbit is a periodic, planar orbit in the triangular region of practical stability, the Earth-Moon L_5 point. In theory, one can place a particle at the very centre of the Lagrange point and it will stay in a stable, stationary position, but in reality this is not the case. Firstly, it cannot be assumed that the probe is delivered to the exact L_5 point with precisely no synodic velocity. Furthermore, the gravitational pull of the Sun is a significant source of disturbance, that destabilises the region. This means, that the properties of an orbit around the Lagrange point strongly depend on its initial conditions (i.e. the precision of insertion) and the perturbances by the Sun.

The effect of the disturbance was incorporated in the CRTBP by adding a rotating acceleration vector of constant magnitude ($3{\cdot}10^{-5}$ m/s^2) to the probe. In this simplified analysis, it was assumed that the Sun orbits in the Earth-Moon orbital plane and that the translation of the barycenter around the Sun is small during one Earth-Moon synodic period. Since the gravitational disturbance originates from the difference of acceleration that the Sun exerts on the barycenter of the Earth-Moon system and the probe on the Lagrange point, its magnitude can be straightforwardly computed by Eq. (2.6):

$$\mathbf{a} = \frac{\mu_{Sun}}{r^3_{probe/Sun}} * \mathbf{r}_{probe/Sun} - \frac{\mu_{Sun}}{r^3_{bary/Sun}} * \mathbf{r}_{bary/Sun} \tag{2.6}$$

where $\mathbf{a}$ is the disturbing acceleration, $\mathbf{r}_probe/Sun$ the position of the probe at L_5 with respect to the Sun and $\mathbf{r}_{bary/Sun}$ the position of the barycenter with respect to the Sun. It was found, that in fact not only the direction, but also the magnitude of the disturbance depends on the angular position of the Sun with respect to the system. In the simulation, the magnitude dependency was neglected and instead the perturbing acceleration was treated to be constant at its peak of $3{\cdot}10^{-5}$ m/s^2. Disturbances due to solar radiation pressure were found to be two orders of magnitude smaller, so it was decided to neglect them. Using the extended CRTBP simulation, that accounts for Sun perturbations, it was investigated for which initial conditions the probe stays in a stable orbit during its 410 days of nominal science orbit time. This investigation was performed in terms of the Jacobi integral C, which in the CRTBP reduces to:

$$C = \Omega^2 \left(x^2 + y^2\right) + 2\left(\frac{(1-\mu)}{r_e} + \frac{\mu}{r_l}\right) - v^2 \tag{2.7}$$

where Ω is the rotational velocity of the frame in inertial space, μ the mass fraction of the moon over the total mass of the system and v the velocity of the particle. Furthermore, r_e and r_l represent the distance of the particle from Earth and the Moon, respectively.

The C value is a conserved attribute of the particle in the CRTBP, that indicates which regions in the system it can access. Since in the above form it was derived from the ideal CRTBP, it does not account for the solar gravity perturbations added to the problem. A particle of low C has more 'potential' and is thus able to access more regions than a counterpart at high C. The value can also be attributed to a point in space, where it represents the amount of 'energy' a particle has to have in order to just reach this point with zero synodic velocity. To get to a point in space close to L_5, a particle has to have a C value that is at most as large as the C of the point itself. In order to achieve a stable condition in the vicinity of L_5, the value should also not be much smaller than that, otherwise the particle will easily escape the region.

It was assumed, that the insertion results in a condition of zero synodic velocity. This allowed to empirically define a region of maximum C, in which the probe would stay stable around L_5 for 410 days. This region is outlined by the outer blue contour shown in Fig. 2.12, corresponding to C = 2.98831. For verification, the evolution of a set of stationary initial conditions within this region was tested and indeed all of the tests stayed in a stable, planar orbit for at least 410 days. After the discussion of insertion trajectories in Section 2.5.3, it can be assumed that a suitable stationary initial condition can be achieved and that the proposed science orbit is compatible with the insertion strategy.

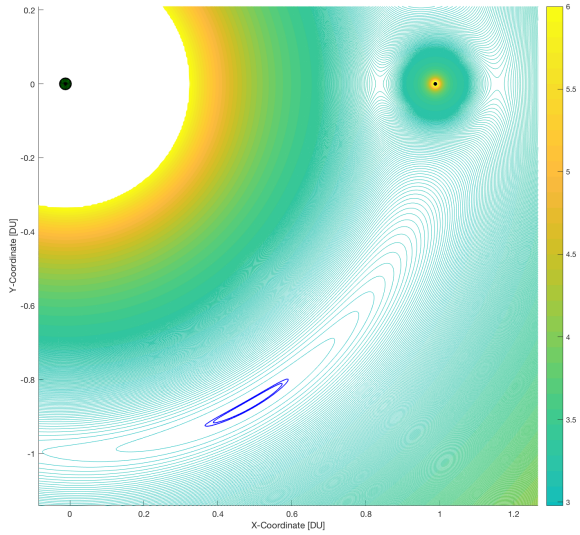

Figure 2.12: Target area for 'imperfect' but acceptable L_5 science orbits. The coloured contours mark lines of equal Jacobi constants.

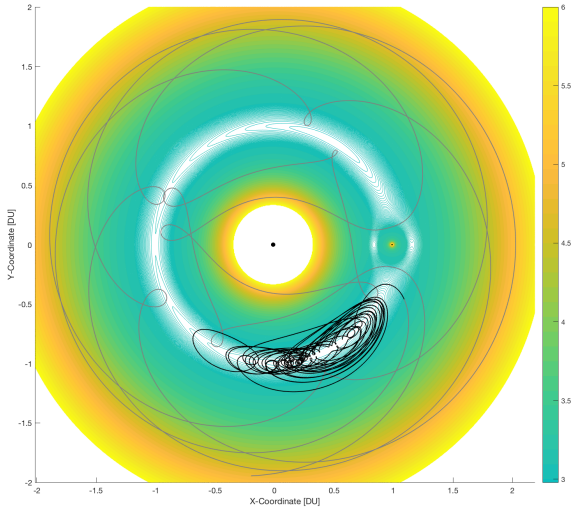

Figure 2.13: Perfect Lagrange point orbit subjected to gravitational disturbances by the Sun over 410 days. The coloured contours mark lines of equal Jacobi constants.

Station Keeping During the investigation of science orbits, it was found that, if successfully inserted in the predefined region, Diana does not require any station keeping. From a scientific and mission safety perspective, there are no orbit parameters that must be maintained. The only constraint is the stability condition over the nominal time in science orbit, which is satisfied. The development of an example science orbit around L_5 is shown in Fig. 2.13. For this specific case, the time spend in the region of stability is 1624 days and marked by the dark black line.Although no station keeping manoeuvres are planned for Diana's time in science orbit, a contingency allotment of 20 m/s Δv is given.

End of Life According to [SUS-ASD-01], the end of life objective for Diana is to clear the region of practical stability for future missions. This could be achieved through destabilisation of the orbit using low thrust manoeuvres. If due to critical subsystem failure manoeuvring is not possible anymore, it was found that depending on the initial condition the probe can stay stable for over 50 years. Since this is not compatible with the protection of the orbital environment for further use, it was decided to design an end of life strategy that does not depend on manoeuvring.

With the goal of finding insertion conditions that would make the probe clear the vicinity of L_5 within at most 10

years, the same empirical investigation that defined the allowed initial science orbit conditions was repeated. A region of minimum C, in which the test probes stayed stably around L_5 for at least 10 years, was determined. This region is outlined by the inner blue contour shown in Fig. 2.12, corresponding to C = 2.98846. The area enclosed by the two contours in Fig. 2.12 defines the optimum condition after insertion, leading to science orbits that are stable for at least 410 days and at most 10 years. For verification, the behaviour of several probes with initial conditions within that region has been tested. As expected from previous verification, the 410 day condition was met by all probes, for some, however, the 10 year condition was not. This should be subject of further investigation in future design stages.

Having left the region of stability, Diana is expected to follow a high eccentricity trajectory around the Earth. One example of such a trajectory is represented by the grey line in Fig. 2.13. A set of trajectories following other allowed initial conditions was studied. Common features were impacts and close encounters with the moon, that 'expelled' the probe from the Earth-Moon system. The closest observed approach to Earth was 58000 km, a safe distance from the GEO region. Since it complies with [SUS-ASD-02] and [SUS-ASD-03], it was decided to the adopt the passive end of life strategy.

A Δv budget of 125 m/s has been allocated for the sake of adjusting the orbit from a too stable condition to one that becomes unstable within 10 years. This value is based on the consideration, that this destabilisation will not be more than half as Δv expensive than the insertion manoeuvre.

2.5.6. Conclusion

Both probes, Artemis and Diana, will be launched on board an EM-1-like SLS launch. After small alterations of the EM-1 LTO, a lunar flyby puts the two spacecraft on a trajectory which uses an Earth gravity assists and a Sun-Earth manifold to deliver the two probes to the Earth-Moon L_2 point within 230 days. The initial conditions required for insertions into their respective target orbits have a minuscule position difference, but a considerable velocity difference, which the transfer alterations have to allow for. From there, Artemis will start its 132 day long insertion manoeuvre into science orbit around the Moon. During the first 30 out of 340 days in science orbit, Artemis will be able to replicate LRO measurements. Although Artemis does not require station keeping manoeuvres during its nominal lifetime, it is equipped with enough Δv to perform 100 hours of correction manoeuvres. Once Artemis has completed its mission lifetime, a series of low-thrust manoeuvres over 100 orbits is initiated which leads to impact with the Moon within 40 days.

Diana, the L_5 probe, requires at most 89 days to go from L_2 into its science orbit, where the probe will stay for the remaining 410 days of its lifetime. No active station keeping is required there, but a contingency allotment of 100 hours of burn time is granted. Diana naturally clears the region of practical stability at the end of life while complying with all end of life requirements. However, this might need some initial destabilisation by the low-thrust engine.

A breakdown of the probes' Δv budgets is shown in Figs. 2.14 and 2.15. The total budget is 1565 m/s, a value that will be established during the Propulsion (PROP) system design in Section 4.2.

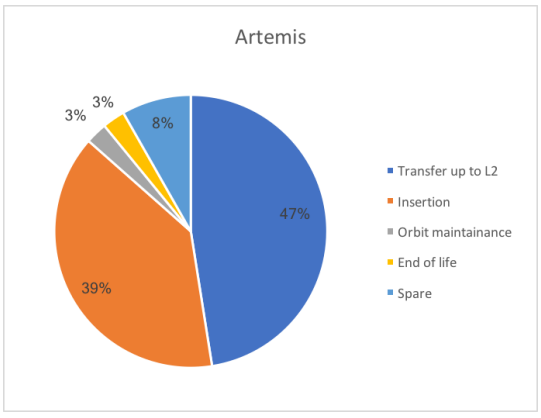

Figure 2.14: Δv breakdown of the Artemis probe. Margins are applied according to the ESA philosophy [50].

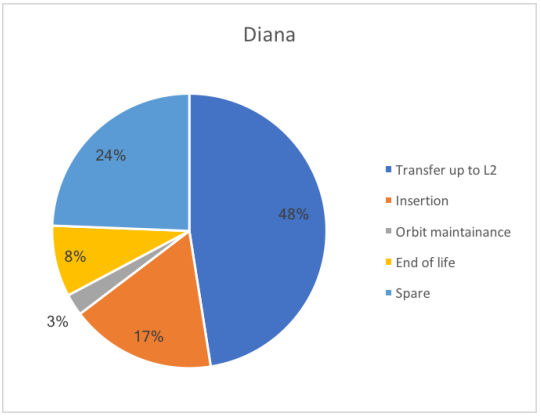

Figure 2.15: Δv breakdown of the Diana probe. Margins are applied according to the ESA philosophy [50].

3

System Planning

The system planning consists of a summary of the initial work done in design cycle one. This will be used to help design the actual hardware and integrated system. First the requirements are listed in Section 3.1. Budgets which will be used for the design can be found in Section 3.2. The functional flow and work breakdown can be found in Section 3.3. The external communication flow is presented in Section 3.4. The Reliability, Availability, Maintainability and Safety (RAMS) is analysed in Section 3.6 and the verification and validation strategy is discussed in Section 3.7.

3.1. System Requirements

System Standards

[TEC-SYS-01] The system shall use technology which complies with the EU environmental regulations
[TEC-SYS-02] The system shall use manufacturers which comply with Directive 2010/75/EU on industrial emissions
[TEC-SYS-03] The system shall use contractors which comply with EU environmental regulations
[TEC-SYS-04] The materials used for the spacecraft shall not be classed as radioactive
[TEC-SYS-05] The spacecraft shall have no pyrotechnical elements
[TEC-SYS-06] The anodized edges shall be of length 11.35 cm in contact to the P-POD [51]
[TEC-SYS-08] The spacecraft shall use units (U) of dimensions 10x10x10 cm^3

System Safety and Reliability

[TEC-SYS-09] The mission shall use technology with a readiness level of 7 or above
[TEC-SYS-10] The mission shall have at least a 50% of lasting 2 years
[TEC-SYS-11] Each individual subsystem shall have a reliability of at least 90%
[TEC-SYS-12] Spacecraft elements with a reliability below 95% shall be made redundant.
[TEC-SYS-13] The secondary redundant elements shall have a performance of at least 50% compared to the primary elements.
[TEC-SYS-14] The total reliability of a redundant system shall be no less than 90%.

System and Environment

[TEC-SYS-15] The spacecraft parts shall be able to withstand the mechanical environment.
[TEC-SYS-16] The spacecraft shall be able to withstand terrestrial transportation environment.
[TEC-SYS-18] The spacecraft shall be able to withstand the radiation environment for the mission duration.
[TEC-SYS-19] The spacecraft shall be able to withstand the standard thermal space environment during transit to and operation in the chosen orbit.

System Transport and Launch

[TEC-SYS-21] The spacecraft shall be compatible with road transportation systems.
[TEC-SYS-22] The spacecraft shall be under 24 kg as specified by the launch contractor.
[TEC-SYS-23] The spacecraft shall be compatible with the secondary payload launch system.
[TEC-SYS-24] The spacecraft shall be compatible with the secondary payload launch restraint system.
[TEC-SYS-25] The spacecraft shall be compatible with the secondary payload launcher deployment system

System Modes

[TEC-SYS-26] The spacecraft shall have an operational safe mode
[TEC-SYS-27] The spacecraft shall have a secondary nominal operational mode
[TEC-SYS-28] The spacecraft shall have a critical software error mode
[TEC-SYS-29] The spacecraft shall have an unexpected contact loss mode

Sustainability

[SUS-SYS-01] The mission shall not make use of any toxic materials.

Legal requirements

[TEC-LEG-01] The mission shall comply with the ISO-24-113 Space debris convention
[TEC-LEG-02] The mission shall comply with the 1967 Treaty on Principles Governing the Activities of States in the Exploration and Use of Outer Space, including the Moon and Other Celestial Bodies (the ”Outer Space Treaty”)
[TEC-LEG-03] The mission shall comply with the COSPAR planetary protection Guidelines
[TEC-LEG-04] The mission shall comply with the 1972 Convention on International Liability for Damage Caused by Space Objects (the ”Liability Convention”)
[TEC-LEG-05] The mission shall comply with the 1975 Convention on Registration of Objects Launched into Outer Space (the ”Registration Convention”)

3.2. Resource Allocation and Budgets

Initial mass and volume budget estimates were created in the Mid-term report [17], based on preliminary sizings and statistical estimates. These were altered slightly and used to define the preliminary resource allocations for the final design phase. The main alterations were as follows:

- At the beginning of the final design phase, more detailed astrodynamics calculations drastically reduced the propellant and engine mass from 6 kg total to 3 kg (1.5 kg dry mass and 1.5 kg propellant).
- A maximum separated mass of 20.5 kg was defined based on acceleration requirements from the transfer trajectory.
- The ESA Margin Philosophy for Science missions [50] was introduced in order to standardise the margin philosophy for the budgets. The most notable change driven by this was the introduction of the 20% system level margin.
- The harness mass was defined as 0.5 kg based on a recommendation from ISIS – Innovative Solutions In Space B.V.

The preliminary mass and volume allocations for each subsystem are shown in Table 3.1.

Table 3.1: Preliminary Mass and Volume Budgets at the Beginning of the Final Design Phase

Subsystem	**% of Nominal Dry Mass**	**Mass [kg]**	**% of Total Volume**	**Internal Volume [U]**
Payload	5.1%	0.8	13.4%	0.9
Structure and Mechanisms	15.2%	2.4	-	-
Thermal Control	3.6%	0.6	-	-
Power	42.4%	6.7	22.4%	1.5
Communications	8.9%	1.4	7.5%	0.5
CDH	2.5%	0.4	7.5%	0.5
ADCS	9.5%	1.5	10.4%	0.8
Propulsion (Dry)	9.5%	1.5	23.9%	1.6
Harness/Other	3.2%	0.5	14.9%	1
Nominal Dry Mass at Launch		**15.7**	**Nominal Volume**	**6.7**
System Margin		20%	System Margin	20%
Total Dry Mass at Launch		**18.9**	**Total Volume**	**8.0**
Propellant Mass		1.5		
Total Wet Mass at Launch		**20.4**		

Budget Flexibility

Driven by the advancing nature of CubeSat technology, the early stage of the subsystem designs, and the concurrent nature of the design approach taken it was decided not to impose these resource allocations as requirements upon the individual subsystems. Instead, the total mass of the spacecraft was managed by the systems engineers, allowing subsystems to increase and decrease mass and volume as needed so long as the total mass and volume remained below 20.5 kg and 12 U respectively.

This approach allowed for optimal use of the available total mass and volume, while the defined margins and preliminary allocations provided guidance at the subsystem level in order to prevent unnecessary bloat or ”snowballing” of any individual subsystem. In order to ensure that this was successful, a central Concurrent Design Facility (CDF) spreadsheet was maintained and iterated upon. The final spacecraft mass and volume budgets, based on the detailed subsystem designs, are presented in Section 5.1.

3.3. Functional Analysis

In this section, the functional flow and functional breakdown for ARCHER will be shown. For the functional flow, multiple levels are defined. They are elaborated on in Section 3.3.1. After this, in Section 3.3.2 the functional flow is elaborated on the second level. In Section 3.3.3 the functional breakdown is shown.

3.3.1. First Level Functional Flow

The first level description of mission ARCHER is shown in Fig. 3.1. This figure has been taken from the ARCHER baseline report [2].

3.3.2. Second and Third Level Functional Flow

The second level functional flow diagrams can be seen in Figs. 3.2 and 3.3. These second level functional flow diagrams are then further elaborated on in a third level functional flow diagram as shown in Figs. 3.4 to 3.12. All these figures have been taken from the ARCHER baseline report [2].

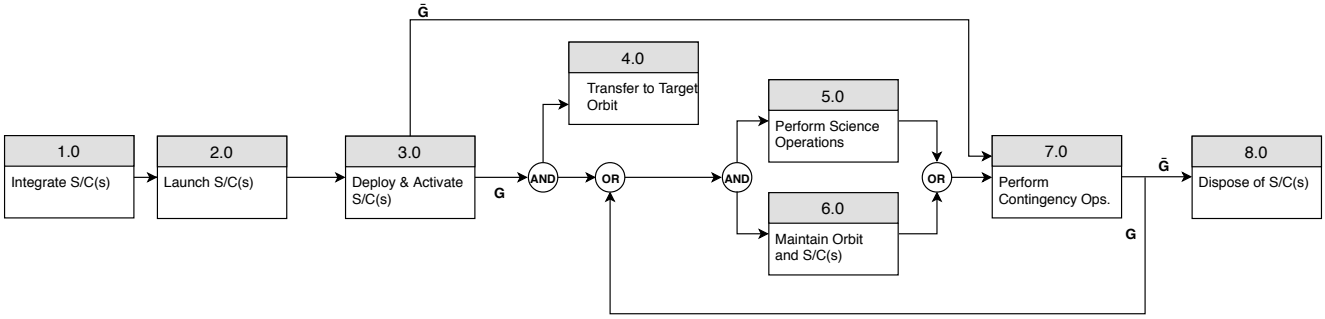

Figure 3.1: Functional Flow Level 1.

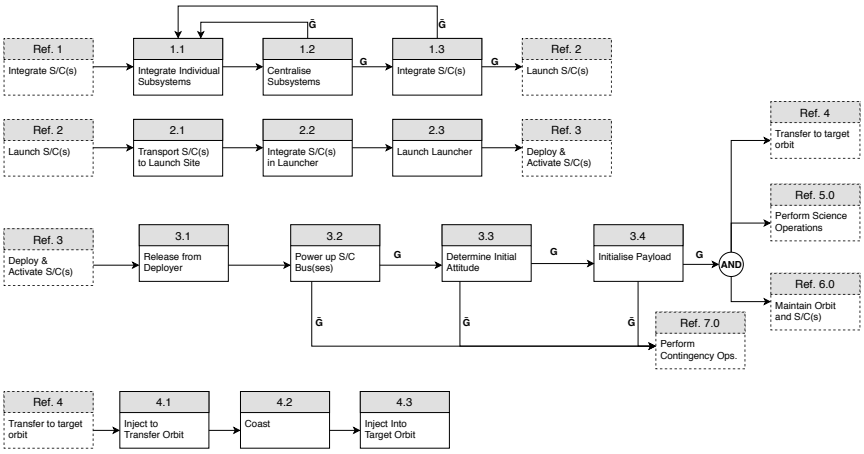

Figure 3.2: Functional Flow Level 2, part 1 out of 2.

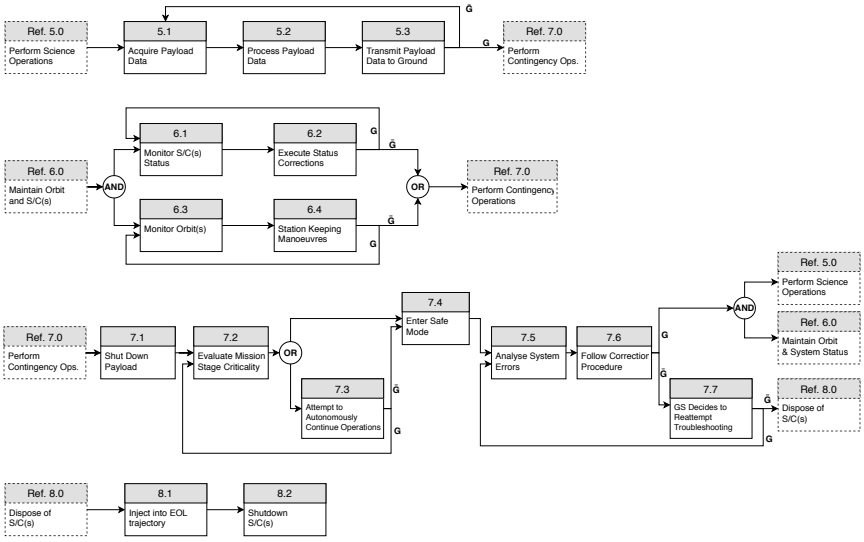

Figure 3.3: Functional Flow Level 2, part 2 out of 2.

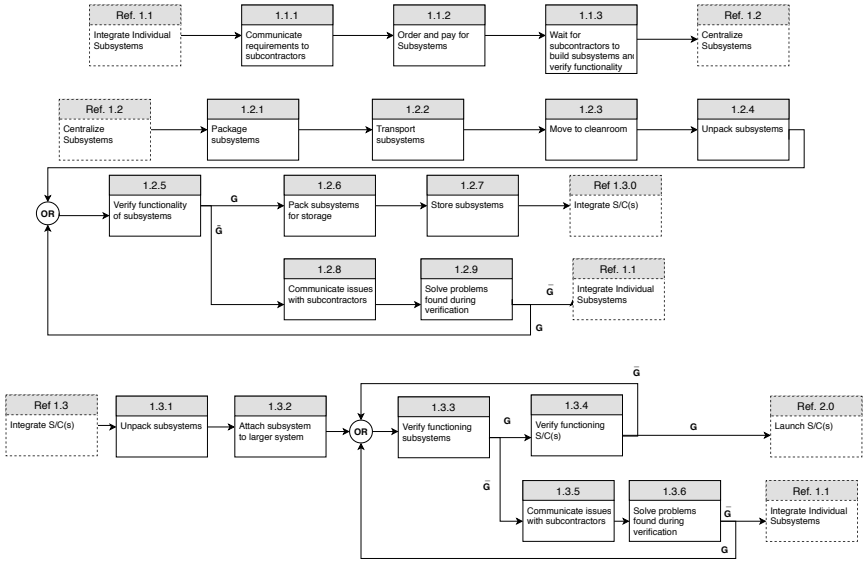

Figure 3.4: Functional Flow Level 3, Block 1.

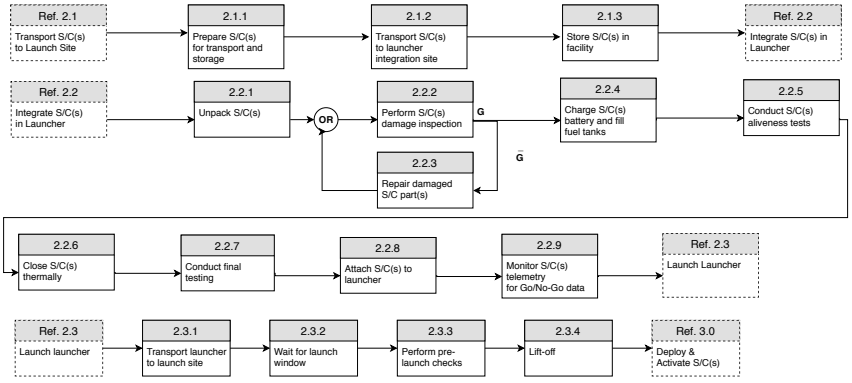

Figure 3.5: Functional Flow Level 3, Block 2.

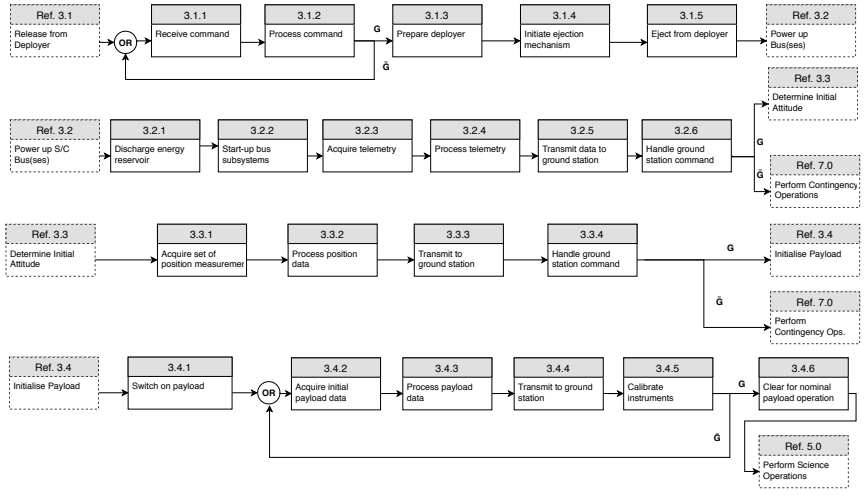

Figure 3.6: Functional Flow Level 3, Block 3.

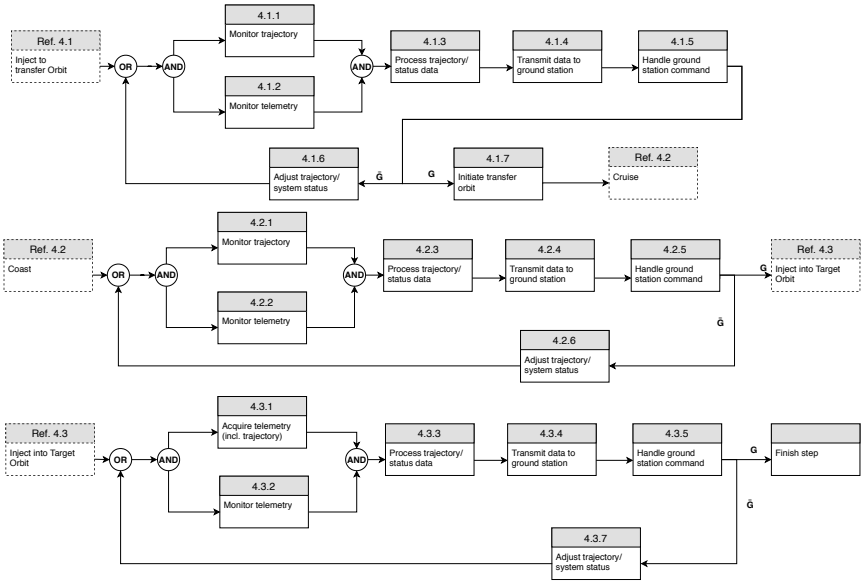

Figure 3.7: Functional Flow Level 3, Block 4.

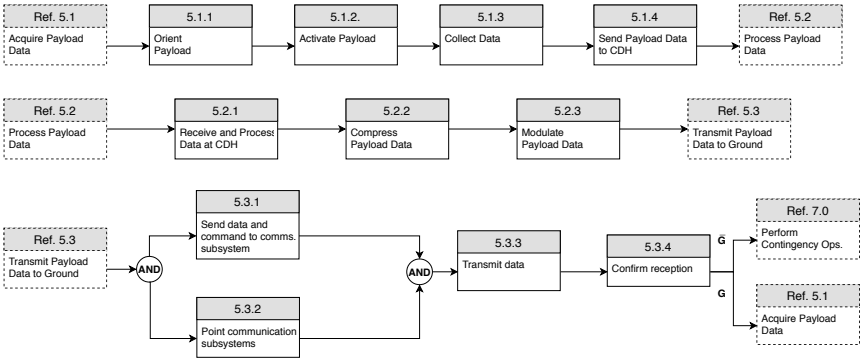

Figure 3.8: Functional Flow Level 3, Block 5.

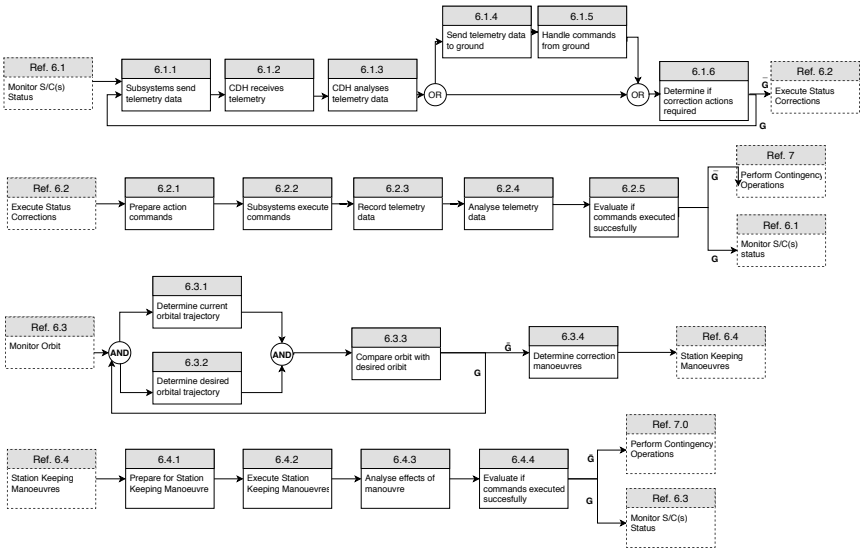

Figure 3.9: Functional Flow Level 3, Block 6.

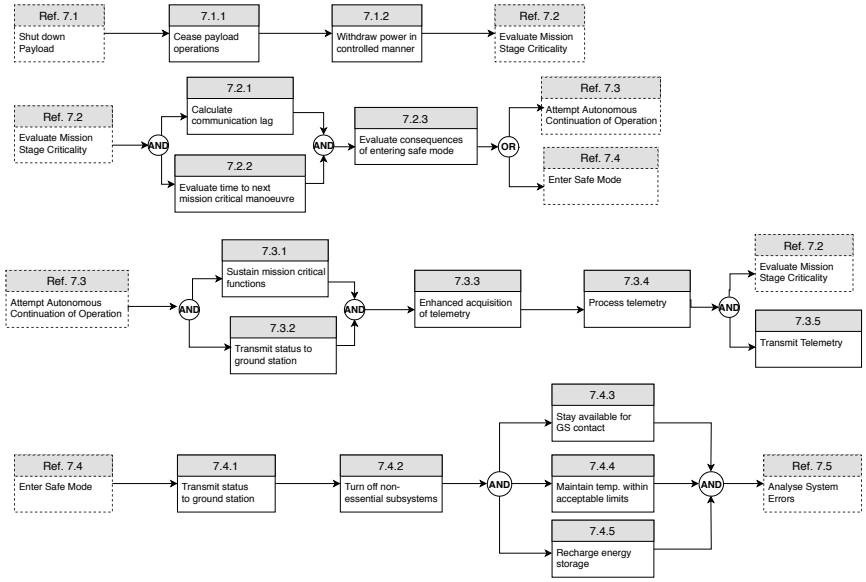

Figure 3.10: Functional Flow Level 3, Block 7. part 1 of 2.

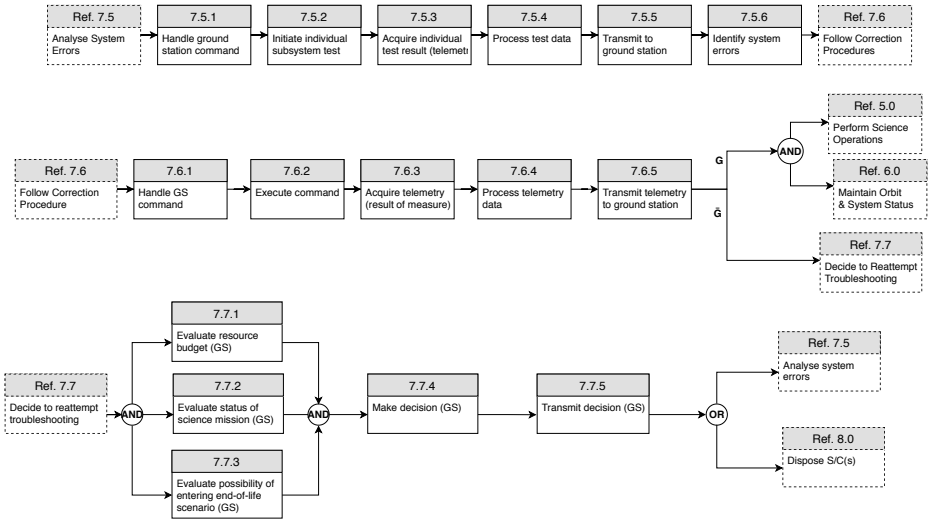

Figure 3.11: Functional Flow Level 3, Block 7. part 2 of 2.

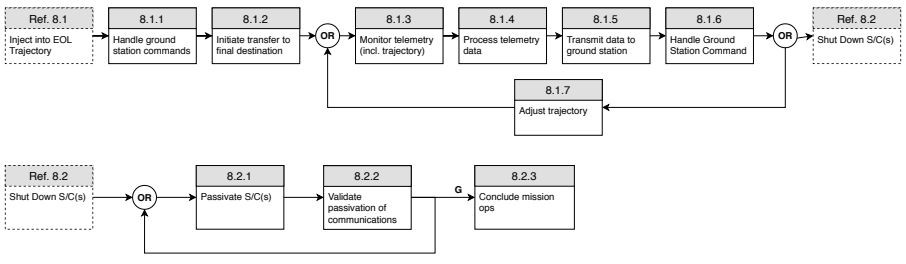

Figure 3.12: Functional Flow Level 3, Block 8

3.3.3. Functional Breakdown Diagram

The functional breakdown lists all the third level functions. For legibility, the functional breakdown is split into two halves in this report. These are found in Figs. 3.13 and 3.14. The figures are from the ARCHER baseline report.

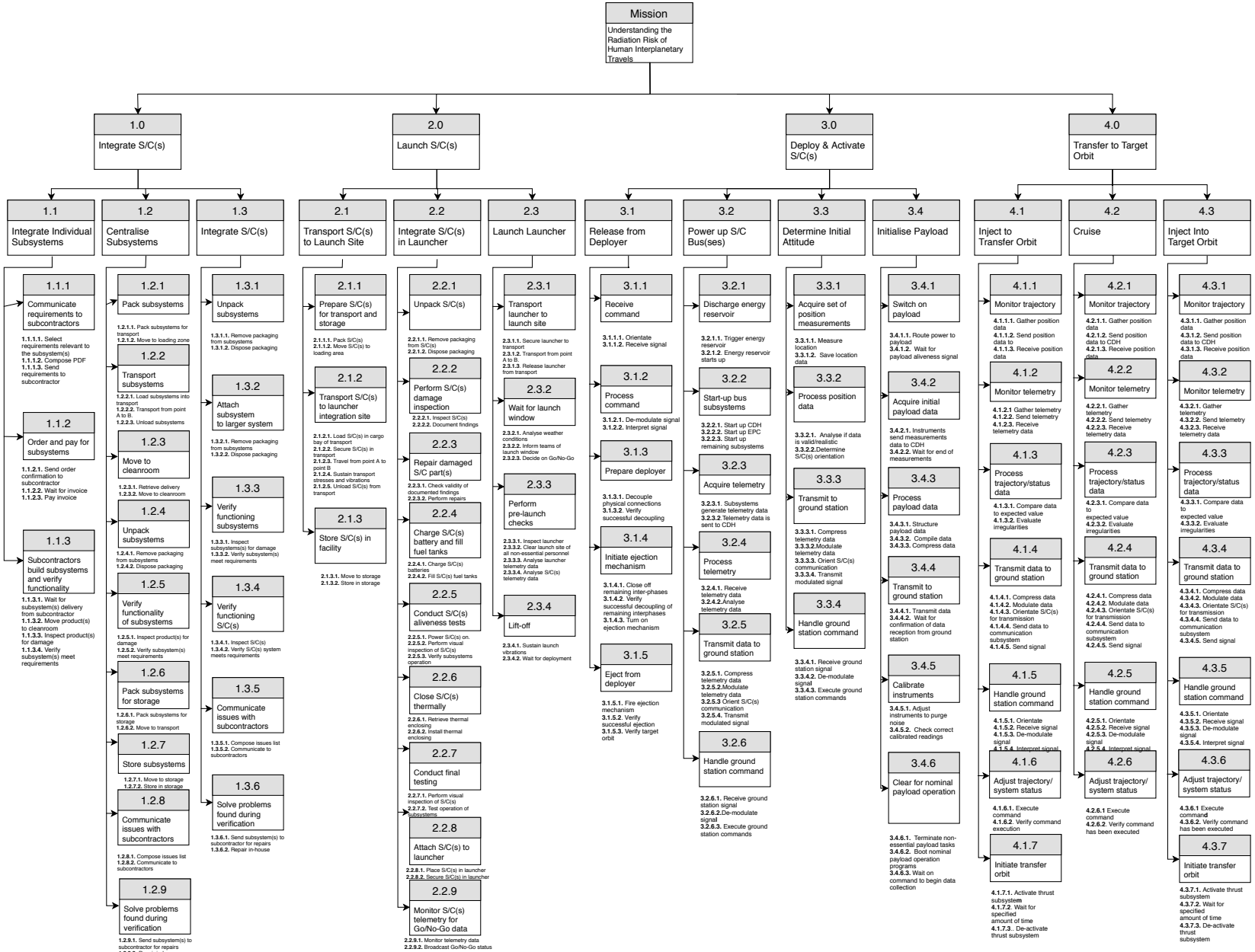

Figure 3.13: Functional Breakdown for Blocks 1 to 4.

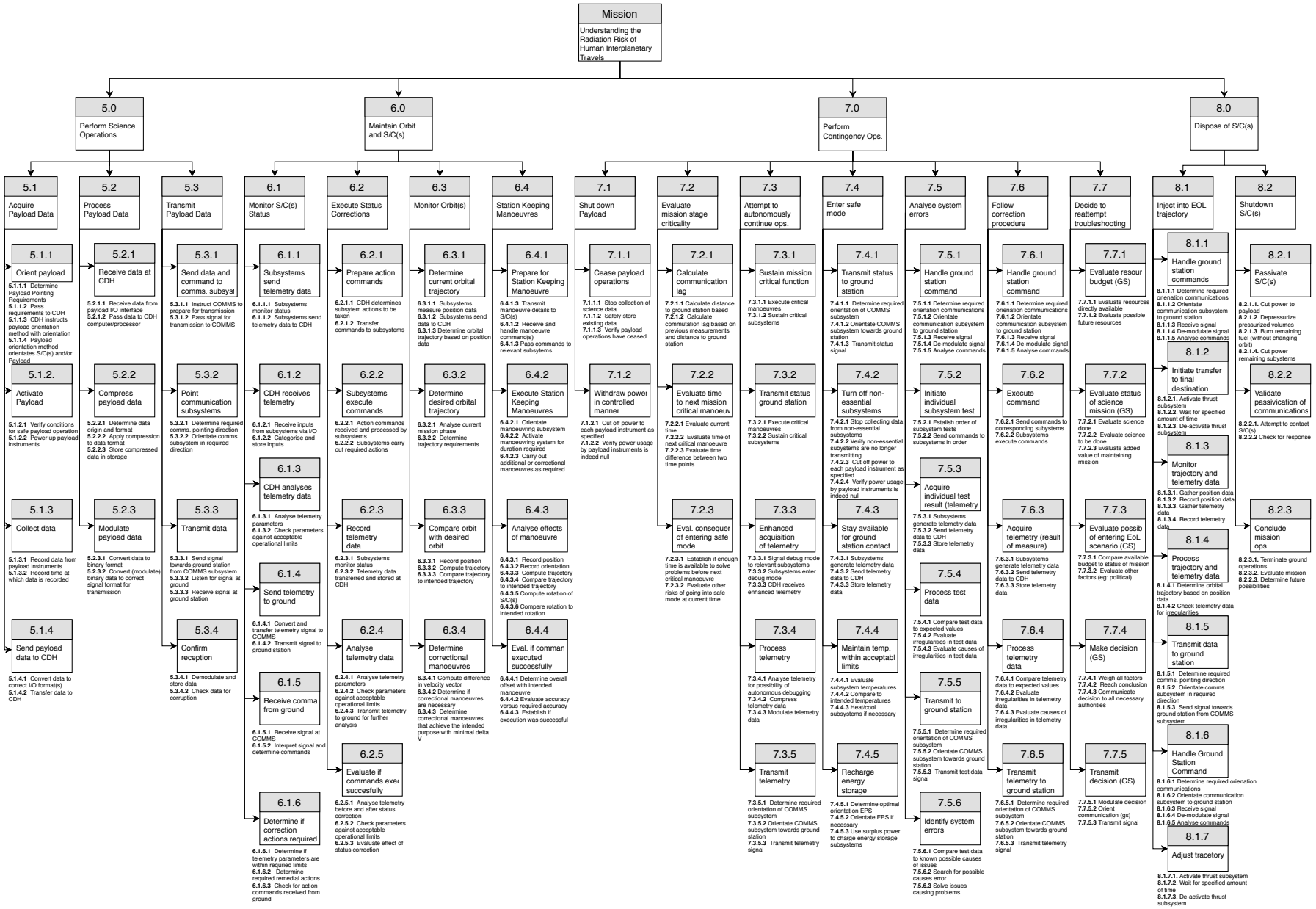

Figure 3.14: Functional Breakdown for Blocks 5 to 8.

3.4. External Communication Flow

The external communication flow diagram can be seen in Fig. 3.15. The entire system can be split up into three parts: the space environment, the satellite and the ground segment. The space environment consists of one element. This generates data to be measured by the satellite. This data is both required by the bus for maintaining orientation and by the payload to achieve the scientific goal. The satellite in turn measures data from the environment, handles this and communicates the information to the ground station. The satellite also receives commands from the ground station and executes these commands. Finally the ground segment receives data from the satellite and analyses the measurement data and telemetry. Using this information the satellite can be issued with new commands.

As can be seen, the bus and payload interact with the environment, measuring telemetry and scientific data respectively. The COMMS connects the satellite with the ground segment. These three sub-groups are connected through the CDH which controls the flow of data.

The ground segment additionally consists of the ground station, science community, and ground control. The ground station receives and transmits information to the satellite. It also communicates data to the science community which can analyse the data. Furthermore, the science community can communicate with ground control, make requests and give other feedback. Using this, and the telemetry data, ground control can decide on further commands to be sent to the ground station.

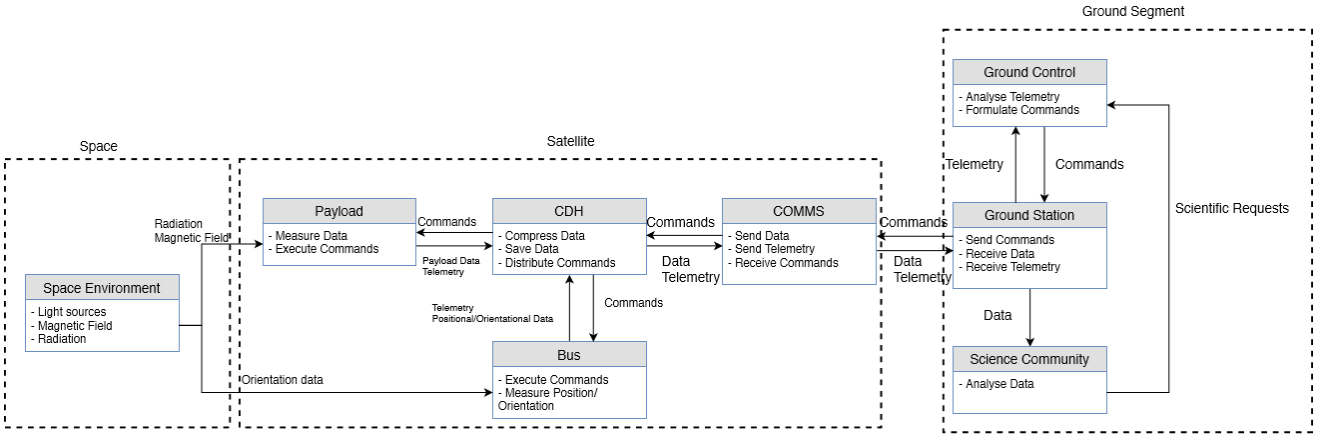

Figure 3.15: External Communication Flow Diagram for Mission Archer

3.5. Mission Risk

In this section the mission risk analysis for the ARCHER mission is performed. This is done by first mapping the elements on a risk map, then developing risk mitigation strategies for the high-risk elements and finally updating the risk map to reflect the effects the strategies have on the risk elements.

3.5.1. Risk Identification

Firstly, the risk elements are determined and this was done as follows. The second level events of the mission functional flow diagram were selected, as seen in Section 3.3.2. A risk element has been defined as said events not happening on the first try. An identification code identical to the one said element has in the mission functional flow diagram has been used. The elements in question are as follows:

[1] Integrate Spacecraft

- [1.1] Integrate Individual Subsystems
- [1.2] Centralise Subsystems
- [1.3] Integrate Spacecraft

[2] Launch Spacecraft

- [2.1] Transport Spacecraft to Launch Site
- [2.2] Integrate Spacecraft in Launcher
- [2.3] Launch Launcher

[3] Transfer to Target Orbit

- [3.1] Inject to Transfer Orbit

- [3.2] Coast
- [3.3] Inject into Target Orbit

[4] Deploy & Activate Spacecraft

- [4.1] Release from Deployer
- [4.2] Power up Spacecraft Busses
- [4.3] Determine Initial Attitude
- [4.4] Initialise Payload

[5] Perform Science Operations

- [5.1] Acquire Payload Data
- [5.2] Process Payload Data
- [5.3] Transmit Payload Data to Ground

[6] Maintain Orbit and Spacecraft

- [6.1] Monitor Spacecraft Status
- [6.2] Execute Status Corrections
- [6.3] Monitor Orbit(s)
- [6.4] Station Keeping Manoeuvres

[7] Perform Contingency Operations

- [7.1] Shut Down Payload
- [7.2] Evaluate Mission Stage Criticality
- [7.3] Attempt to Autonomously Continue Operation
- [7.4] Enter Safe Mode
- [7.5] Analyse System Errors
- [7.6] Follow Correction Procedure
- [7.7] Ground Station Decides to Reattempt Troubleshooting

[8] Dispose of Spacecraft

- [8.1] Inject into EOL trajectory
- [8.2] Shutdown Spacecraft

3.5.2. Risk Map

These risk elements were then mapped on a risk map, as seen in Table 3.2. This risk map includes both the risk positions before and after mitigation. The risks which were mitigated are underlined to show where they were before mitigation, and are emboldened to show where they are after mitigation. The severity scale is related to the ability of the spacecraft to gather science (on average), and probability shows the likelihood of events happening relative to each other.

Severity

1. [1] Minimal to no consequence
2. [2] Data gathered of tolerable quality for stakeholder use
3. [3] Data gathered of significantly reduced quality for stakeholder use
4. [4] Data gathered of insufficient quality for stakeholder use
5. [5] No data gathered

Probability

1. [1] Least likely
2. [2] Less likely
3. [3] Likely
4. [4] More likely
5. [5] Most likely

Table 3.2: Mission Profile Risk map with mitigated risks underlined before and emboldened after mitigation

5		8.1			
4			3.2, 3.3, 4.3	4.4	4.2
3		1.3	6.2, 6.4, 7.3		5.3
2	8.2	1.1	6.3 **3.2, 3.3, 4.3**	2.2, 3.1, 6.1 7.2, 7.4, 7.6, **4.4**	4.1, 4.2, 5.1 5.2, 7.5, **4.2, 5.3**
1		1.2, 2.1, 7.1		7.7	2.3
^Probability Severity >	**1**	**2**	**3**	**4**	**5**

3.5.3. Risk Mitigation Strategies

In order to increase the likelihood of the ARCHER achieving all of its mission objectives, a risk mitigation strategy has been devised for the elements which were determined to have the highest risk of failure (red area). This was done only for the high risk elements, as doing it for all of them would be cost-inefficient. It must be noted that this leaves elements in the intermediate risk cells, which is not ideal. The risk mitigation strategies are as follows:

- [3.2] Perform an extensive testing campaign to reduce the risk of engine failure during the ”Coast” mission element as much as possible.
- [3.3] Perform an extensive testing campaign to reduce the risk of engine failure during the ”Inject into Target Orbit” mission element as much as possible.
- [4.2] Perform an extensive testing campaign to reduce the risk of the spacecraft not powering up during the ”Power up Spacecraft Busses” mission element as much as possible.
- [4.3] Perform an extensive testing campaign to reduce the risk of the spacecraft not being able to determine its attitude during the ”Determine Initial Attitude” mission element as much as possible.
- [4.4] Perform an extensive testing campaign to reduce the risk of the payload not initialising during the ”Initialise Payload” mission element as much as possible.
- [5.3] Perform an extensive testing campaign to ensure proper signal strength and pointing accuracy are attained by the spacecraft.
- Component redundancy will be implemented to reduce the probability of spacecraft failure at any operational mission stage.

The result of the risk mitigation strategy dictates that more funding shall be provided to the aforementioned parts of the testing campaign. The budget manager is responsible for the implementation of said risk mitigation strategies.

3.5.4. Updated Risk Map

The implementation of the risk mitigation strategies reduces the probability and/or severity of the high-risk elements. This effect can be seen in the risk map Table 3.2. The elements which have moved have been underlined at their old locations and added in bold at their new locations. Seeing as no elements are in the high-risk cells anymore, the risk mitigation strategy is considered successful as defined by the removal of elements from high-risk cells.

3.6. Reliability, Availability, Maintainability, Safety and Redundancy

This section will describe the Reliability, Availability, Maintainability and Safety (RAMS) of the ARCHER mission. A statistical approach will be used by analysing similar past missions and evaluating their reliability. While hardware maintenance is not possible during flight operations, orbit maintenance, unscheduled fault isolation and firmware updates may be necessary.

Availability largely depends on reliability and maintainability, so for this mission, the driving factor will be reliability. However, communication time and eclipses all play a role. Safety often drives the required reliability for a product but in this case humans are not in danger during the normal operations. Therefore, safety will focus more on planetary protection and the potential for the CubeSat to cause harm or damage as space debris. This section will also discuss the redundancy philosophy.

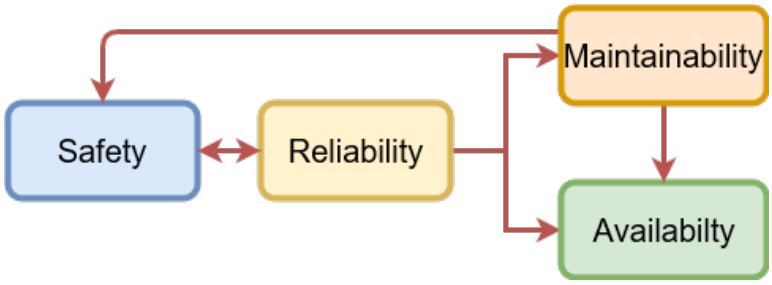

Figure 3.16: Reliability, Availability, Maintainability and Safety Relationships

3.6.1. Reliability

Reliability is defined as as the probability that a system will perform satisfactorily under specific conditions for a defined time period. There is much research at the moment on increasing reliability in space missions and improving reliability methodologies. The European Space Agency has been working on improving their methodology in this area for several years. A presentation in 2016 on New Reliability Prediction Methodology Aimed at Space Applications[1] proposed collaboration with key industry partners to design better reliability models. A few months later a white paper was published outlining how this could be achieved [52]. This has resulted in a two year project, reliability.space which hopes to create this new methodology and aims to be completed in 2019[2]. None of this however, applies to CubeSats and is focused on larger traditional spacecraft.

Little progress has been made in developing an accurate reliability model for CubeSats. However, CubeSats are more and more being considered for longer term science missions rather than quick technology demonstrators. As a result, their reliability is becoming more pressing. This is an issue ESA is aware of and the integration of CubeSats into the RAMS in orbit data exploitation (RIDE) program is being considered[3]. In this case, CubeSat in orbit telemetry would be collected in order to better understand failures and improve future models. If RIDE was extended to CubeSats, ARCHER could certainly partake in the program though it is unlikely to benefit from it. A reliability estimation tool exclusively for CubeSats is being worked on [53] and the authors were contacted to see if it had been completed but to date it has not.

In the absence of a model, statistical data will be used. However, CubeSats often have to trade testing for standardisation in order to reduce costs, it is difficult to analyse the reliability of an historic mission accurately since different missions may have widely different levels of testing and validation and this information is rarely made public.

A 2015 study by NASA analysed the reliability of CubeSat missions [7]. They analysed a CubeSat mission database of 370 missions launched between February 2000 and June 2015. There were only 96 missions with enough variables recorded to analyse mission lifetime and causes of mission failure. Using the 96 missions they found a 63% probability of a successful launch with a 60% lower confidence limit. They estimated (non-parametric) the median life of a CubeSat after successful launch to be 110 days. Upon further analysis they found that the reliability function was dependent not only on time but also satellite mass. Using a Weibull regression with mass as an explanatory variable they reassessed the median lifetime to be 85 days for a 1kg CubeSat and only 22 days for a 4 kg CubeSat. However, they note that the number of CubeSat launches in 2015 increased ten times vs 2011. It is unknown whether the analysis included mostly modern missions with a more mature CubeSat platform or mostly early platform concepts. Therefore, caution is advised when applying the results.

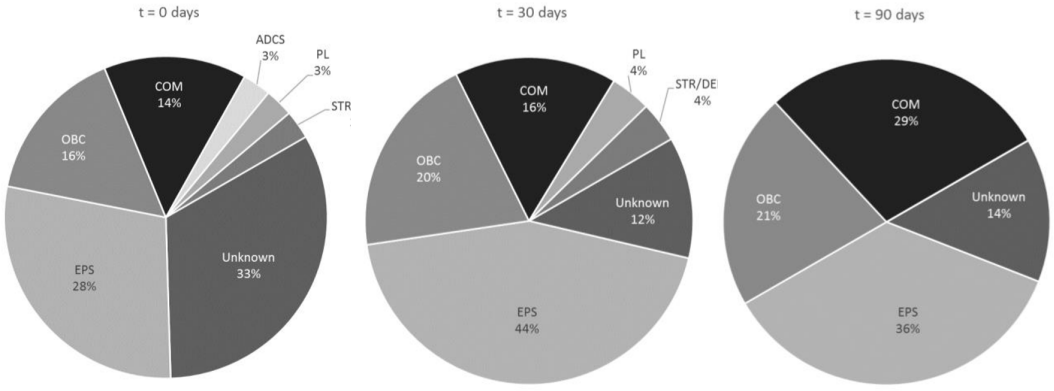

Figure 3.17: Subsystem Failures After 0, 30 and 90 days [36]

M. Langer and J. Bouwmeester created a CubeSat database in 2015 which analysed 178 missions including 70 which ended in failure [36]. Importantly, they exclude launcher failures only analysing the failure rate after successful orbit insertion. They also analyse the subsystems which were responsible for failure. The results can

[1] emits.sso.esa.int/emits-doc/ESTEC/News/NewReliabilityPredictionMethodology22042016.pdf [Retrieved 21 June 2018]
[2] www.reliability.space/project/timeline/ [Retrieved 21 June 2018]
[3] https://indico.esa.int/indico/event/189/page/1 [Retrieved 21 June 2018]

be seen in Table 3.3. Importantly, the data shows a 20% failure at day zero and that the majority of failures happen within the first 90 days. A subsystem breakdown of initial failures can be seen in Fig. 3.17. While unknown failures account for a large portion of day zero failures, this drops away quickly with the most critical systems being the EPS, On Board Computer (OBC) and COMMS. Many of the early failures are a result of inadequate system level verification testing and flight condition validation testing [54].

Table 3.3: CubeSat and Subsystem Reliability

Description	Time - days	Model	Reliability	95% Confidence
CubeSat Reliabilty	360	non-parametric	0.6	0.78-.52
CubeSat Reliabilty	730	non-parametric	0.57	0.66-0.48
CubeSat Reliabilty	720	Weibull Mixture	0.56	0.65-0.48
EPS	360	non-parametric	0.87	0.925-0.8
OBC	360	non-parametric	0.925	0.975-0.88
COM	360	non-parametric	0.925	0.975-0.875
Unknown Failure	360	non-parametric	0.86	0.92-0.81

Interestingly, the authors sent out a survey to 987 individuals associated with CubeSat programs worldwide, of which 113 were returned complete. They compiled a database[4] and found that 34% of the group didn't use any technique to quantify mission risk or reliability. It is not known however, how this correlates with mission failure.

A study for the 2017 U.S Space Command [55] largely agrees with Langer and Bouwmeester when it comes to the statistical lifetime. Again a questionnaire was sent out and a database of mission statistics analysed. There appears to be a relationship between team experience and mission success. Additionally, 27 anomalies identified were discussed during the interviews, with respondents stating that over 70% of them could have been prevented with more ground testing. A set of common themes on lessons learned was identified and a set of clear recommendations presented to improve CubeSat mission success. The recommendations can be seen in Table 3.4.

Table 3.4: Recommendations on improving CubeSat Mission Reliability [55]

#	Recommendation	Information
1	Define goals & success criteria at start	Justify these then strongly defend against growth
2	Plan ample time for integration & V&V	Consider 1/3 to 1/2 of the overall schedule
3	Conduct risk-based mission assurance	Perform risk assessment to prioritise tests & activities
4	Design for simplicity and robustness	Design for easy assembly & have respectable margins. Have robust safe modes, & few deployables Have frequent preventative satellite resets
5	Build an experienced team	Include frequent peer reviews & discussions with experts
6	Stock spare components	Supports parallel software development, can be flight spares and protects schedule during mechanical testing
7	Perform four mission assurance tests at the absolute minimum	1. Day-in-the-life (or longer) testing 2. Communication link testing with the ground station 3. Power system charge/discharge testing 4. Thermal testing (in vacuum if at all possible) - Then perform tests with the highest risk-reduction value
8	Be sceptical on vendor datasheets	Hold margin during design and verify after receipt

Results The early operational life of a CubeSat is littered with failures with the majority happening in the first 90 days. In fact, the reliability of a CubeSat changes only about 0.1 from 90 days to 2 years suggesting there is a reasonable probability that if the satellite survives the first 90 days it could go on and last the proposed mission duration of 2 years. While the correlation between those missions which did not use extensive system verification and validation has not been formally quantified, it is clear that a lack of mission condition testing results in a lower reliability. US Space Command has issued a set of recommendations which are high level, cheap and easy to

[4] `data.4tu.nl/repository/uuid:591ff8f8-b495-4d1c-9c5c-69f6f85ace78` [Retrieved 22 June 2018]

integrate into project ARCHER. The single most effective method to increase mission success is with ground testing. This should certainly reduce the risk of infant mortality. Vendor datasheets should not be trusted and margins applied until all subsystem components are verified. The EPS system has been identified as a leading failure point along with the OBC. Communications becomes more critical the longer the mission continues. As such, it is recommended to extensively test these three systems under mission flight conditions. In other words, the four assurance test should be performed and then the most risk reducing tests after that. A large percentage of the mission schedule must be set aside for V&V. Without such testing it is likely that ARCHER will only have about a 55% chance of lasting the mission duration.

3.6.2. Availability

Availability is the probability that a system will be available (functioning) for use when it is required. It can be seen as the up-time of the system and is affected by time to failure and maintenance time. H. Paul Barringer considers availability to be composed of several components as seen in equation Eq. (3.1) [56]:

$$A = A_{\text{hardware}} \cdot A_{\text{software}} \cdot A_{\text{humans}} \cdot A_{\text{interfaces}} \cdot A_{\text{process}} \tag{3.1}$$

Since Diana and Artemis can not be serviced by a human crew, the availability largely becomes a function of reliability. However, there may be scheduled firmware updates and calibration time that will need to be accounted for. Ground station availability is a factor but considering the number of stations worldwide, it should not be a limiting factor. Planning for Loss of signal (LOS) and possible anomalies is described in Section 6.3, and the maintenance strategy in Section 3.6.3. The availability of ARCHER can be computed by taking 95 % on the reliability in Section 3.6.1 [51]. Availability will be critical during the scheduled contact intervals. In addition, due to the high power demands, it is critical that the availability of the secondary power system is sufficient, during eclipses.

This being said, it is important for the success of ARCHER to optimise the hardware selection for reliability, as described in Section 3.6.1. This also means, implementing redundancy for critical systems that are shown to be less reliable. The software should also be considered, however, this can be (partially) refined by human intervention, during the mission.

As for launch availability, contingencies in the mission planning must be implemented to account for delays in logistics (manufacturing, testing, etc.). Since ARCHER is Moon/Earth-Moon-L_5 bound, launch windows will not be a significant issue, however, launch opportunities for CubeSats can be. Hence, some contingency has to be implemented.

3.6.3. Maintenance

In this section, orbit maintenance and corrections, unscheduled fault isolation and correction and software updates etc. will be considered. A Maintenance Steering Group (MSG) method can be used to help plan for scheduled maintenance such as orbit corrections, planned firmware updates, calibration time for the payload and in-flight testing of subsystems [18]. In addition, a procedure should be put in place to quickly identify faults that may happen and a solution implementation plan generated. This will allow rapid reaction to issues and ideally a quick implementation of a solution.

During the flight, it may occur that a software update is deemed necessary. Doing so involves uploading a software package to the CubeSat, which should be verified upon receipt by the CubeSat. In order to improve the reliability of the CubeSat, a separate instance of the original operating system will always be boot-able if the update renders the CubeSat not functioning properly.

In order to update the software of the distributed computer systems, it is currently assumed that the update procedure is the same as for the main computer, with the exemption that the verification of the received update file is still checked by the main OBC.

For fault detection of the OBC, a watchdog timer is implemented on the LEON-3 processor. This timer should mitigate the risk of SEE by resetting the OBC if the timer is exceeded. Furthermore, in case of a fault, the different modes of the CubeSat will be autonomously triggered in order to deal with the fault. Should there be an unforeseen hardware failure, after the CubeSat has entered safe mode and has rebooted sending down telemetry with a status report in which the fault has not been mitigated, a workaround could be found by ground ops and uploaded to the

on-board software. In the case of a Timepix failing for example, the on-board software could switch to a redundant Timepix unit. For the memory fault correcting algorithms may be implemented in order to account for errors by scrubbing the memory [57].

3.6.4. Safety

Safety is essential in reducing the risk for people and the environment in the case of a system failure. Since the system will be using an established launch vehicle the most dangerous part of the mission for humans shall be the responsibility of the launch contractor. Nonetheless, the safety record of the launcher should be taken into account when choosing a provider. During the mission itself there is hardly any threat to humans as any failed orbit insertion which directs the CubeSat back into the Earth's atmosphere will ensure it burns up before ever being a danger to people. As such, the main safety concerns are environmental via planetary protection and as space debris. The chosen mission must not carry a risk of damaging any manned missions so a safe end of life strategy must be planned for. This is discussed in detail in Section 2.4.

Results The ability to perform a safe EOL manoeuvre or enter into a safe standard orbit will be largely dependent on the propulsion system. It is essential then that the propulsion system is highly reliable as the EOL manoeuvre may take place two years into the mission. However, since the system uses electric propulsion, again the EPS system becomes critical. While it is important that the COMMS remains operational in order to issue early decommissioning commands, it is more important that the OBC is reliable. If the COMMS fail, the OBC can issue the EOL command at a predetermined time.

3.6.5. Redundancy and RAMS Summary

Redundancy is difficult to implement on a small CubeSat with limited space and mass budgets. Having spoken to several experts, such as A. Menicucci and J. Bouwmeester, there are varying opinions on whether redundancy is effective or not as it adds to the complexity of the design, which increases failure risk and testing time. If the schedule is tight, testing may then be inadequate. For example, having two identical OBCs hardly makes sense as they are both likely to fail around the same time therefore redundant components should be different to the main components. The time frame for failure should also be considered. If a component is likely to fail after a month into a three year mission, making it redundant and is hardly worth it. Again, if a component is likely to last a year and mission duration is half a year, redundancy is not beneficial. If the time scale is close to mission duration though, it can be effective. However, adding margins to critical systems, avoiding redundancy and therefore complexity while focusing on ground testing can be a better policy depending on the mission.

For this project, having margins on the solar arrays and batteries will be important but so will isolating parts of the system so a partial battery failure will not disable the entire battery system. Higher capacity batteries allow for a lower depth of discharge resulting in a longer life. Software is an area where redundancy can be greatly exploited with work-about routines, safe modes and a total reboot mode. The OBC could have more than one CPU and carry dual storage. Margins on fuel could be important if greater station keeping than expected is required and the ADCS, critical for keeping the CubeSat in plane with the Sun, must consider redundancy. One vital system is the solar array drive assembly however no redundancy is practical here. Another reason for testing and ADCS margins. Redundancy of the payload could be actively explored as it is assumed to be lightweight and not use much power. This will need to be traded off against data rate. Interfacing is an area where redundancy can be built in, for example ensuring the EPS can power each system independently so a failure in one will not prevent power reaching another. In addition, there should always be a backup ground station available at all times. For ARCHER however, the main form of redundancy is having two CubeSats instead of one. If one fails, the entire data recording ability of the mission is not lost.

Table 3.5: RAMS Analysis - Summary Features

System	Considerations	Redundancy
ARCHER	Apply extensive V&V & US Space Command recommendations	2 CubeSats
EPS	Critical risk for reliability, infant mortality availability & safety Require stringent V&V and radiation hardening Ensure primary & secondary power are independent	Apply 20% margin to power requirements Use several smaller battery packs
OBC	Critical risk for reliability, infant mortality, availability, safety and maintainability Requires stringent V&V & radiation hardening Requires fault analysis program & automated repair Requires easy subprogram & firmware updates	Include several CPUs & dual storage Dedicated ADCS and COMMS OBCs Should include Watchdog Schedule regular system resets
COMMS	High risk for reliability, infant mortality & availability Require stringent V&V and radiation hardening	Several patch antennas
PROP	Essential for EOL safety Require stringent V&V and mission flight testing Electrical propulsion heavily dependent on EPS	Fuel margin for station keeping etc.
ADCS	Important for reliability and availability Require stringent V&V	Margins on reaction wheels & thrusters Thrusters could compensate reaction wheels Additional Sensors could be used
Software	Important for reliability, availability & safety Require stringent verification, unit & system testing	Include safe mode, reboot mode & redundant process flows & workarounds
Interfaces	Important for reliability and availability Require stringent V&V and mission condition testing	Allow for independent subsystem interfacing with the EPS & OBC to ensure one failure doesn't isolate other components
Ground Ops	Important for Availability	Ensure backup station always available

3.7. Verification and Validation Plan

The verification and validation process applied throughout this project follows the systems engineering approach as seen in Fig. 3.18. Each test should be prepared, planned, executed and documented. The steps are as follows:

- Verify requirements - completed during baseline phase
- Verify and Validate model or the software tools - explained in this section, detailed as necessary in Chapter 4
- Verify component level - explained in this section, detailed as necessary in Chapter 4
- Verify system level - see Section 5.4
- Validate and flight certify the system - see Section 6.4

3.7.1. Software Verification and Validation

Verifying software tools ensures it behaves as it has been designed. Commercial industry grade software does not need to be verified or validated but its implementation should be. Both unit and system tests should be performed. Unit testing analyses the operation of sub-programs within the main program. System testing analyses the program's overall behaviour. Depending on the complexity of the software this could include:

Software Verification

Structured walk-through - This involves talking through assumptions, model parameters and methodologies with another engineer who critically analyses the logic in order to uncover any applicable errors.

Simplified Model - This involves verifying that the proposed numerical or mathematical model works on a simplified system. While this does not verify it will work with a more complex system it is a good step to ensure a minimally working model.

Anti-bugging - Applied to code units and involves programming small checks in to the code which will automatically trigger and expose a potential problem. An example could be to highlight a negative mass. This is a

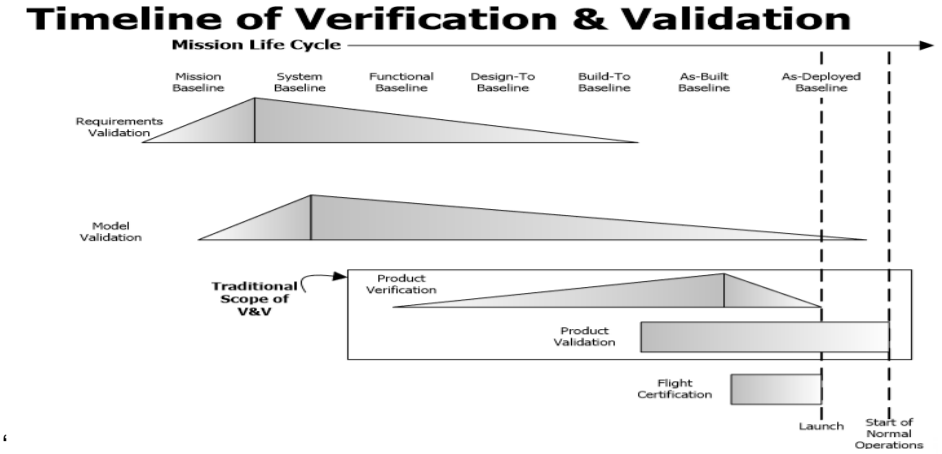

Figure 3.18: Verification and Validation Plan [58]

great time saving step which should not be skipped.

Debugging - Applied to code units. This is an essential part of any verification process and involves actively checking the code for syntax and other errors such as the incorrect use of integers or floats. Helps ensure the code behaving as designed.

Continuity Testing - Used during unit testing and involves varying input parameters slightly and observing the outputs. In general, one would expect that a slight variation in an input would result in a slight variation in the output. If this is not the case, a potential error may have been discovered.

Consistency Testing - Used during unit and system tests. Similar to continuity testing but also observes whether the outputted response is consistent to what one would expect of the model.

Error Testing - Used during unit and system tests and involves estimating the order of the error associated with a particular function.

Software Validation

Expert Intuition - Similar to a structured walk-through, a subject expert steps through the behaviour of the model and compares it to expected behaviour as learned through years of experience. Used in conjunction with additional verification tests to really challenge the model.

Real System Data - Comparison with a real system and real test data is the preferred validation method. Not always possible due to the absence of a real system or the expense associated with testing one.

Theoretical Results/Analysis - The model is compared with existing models or simulation software, or if acceptable, a more accurate theoretical model.

Software verification will be detailed as necessary in Chapter 4.

3.7.2. Component Verification

Component verification is used to ensure the components comply with requirements, can operate in the desired manner and most importantly, that the specifications actually match the vendors data sheet. This is an extremely important point, as recommended by the US Space Command [55]. Mass, centre of gravity, volume as well as specifications specific to the component such as processing power, battery capacity etc. should all be verified. This can be done using a set of general tests as follow:

- Inspection - inspect to show compliance with requirements
- Analysis - us mathematical or statistical techniques to show compliance wit requirements
- Demonstration - demonstrate compliance with requirements via operation
- Test - show compliance with requirements by test under representative conditions

Component Verification will be detailed per subsystem in Chapter 4.

4

Subsystem Design and Performance

In this chapter the subsystems design, development and component level verification are described. First, the payload is presented in Section 4.1 followed by the propulsion in Section 4.2. The COMMS can be found in Section 4.3 follwed by the ADCS in Section 4.4. The CDH and EPS can be found in Section 4.5 and Section 4.6 respectively. Lastly, the structural integrity is analysed in Section 4.7 and the thermal design is shown in Section 4.8.

4.1. Payload

For any mission a payload is necessary in order to actually be able to perform said mission. Said payload subsystem is analysed in this section. Following the requirement analysis, the final design is outlined.

4.1.1. Requirements

In addition to the system requirements as detailed in Section 3.1, the following requirements were posed onto the payload design:

- [TEC-PAY-01] The mission shall provide radiation environment measurements in an orbit beyond Earth's magnetosphere.
- [TEC-PAY-02] The scientific payload shall detect neutrons in the energetic range between 0.1 and 200 MeV.
- [TEC-PAY-03] The scientific payload shall have a sensitivity to Linear Energy Transfer (LET) between $5 \cdot 10^{-4}$ MeV cm^2/mg to 10 MeV cm^{2}2/mg.
- [TEC-PAY-06] The scientific payload shall measure the magnetic field with a sensitivity of at most $\pm$ 100 μT.
- [TEC-PAY-07] The neutron detector shall be placed internally within the spacecraft shielding structure.
- [TEC-PAY-08] The payload shall be active during the entire duration of the scientific phase of the mission.
- [TEC-PAY-09] The payload shall have a partial payload safe mode.
- [TEC-PAY-10] The payload shall have a complete payload safe mode.
- [TEC-PAY-11] The sensor surface of the charged particle detector shall not be covered by the skin of the CubeSat.

4.1.2. Scientific purpose

The ultimate goal of Mission ARCHER is to characterise the radiation environment beyond the protection of Earth's atmosphere and magnetic field. In order to achieve this goal, dedicated detectors for measuring the energy deposition of charged and uncharged particles have been accurately selected and conceptually integrated within the 12 unit CubeSats, Artemis and Diana. As will be explained in the next sections, the very same detector utilised for measuring the Linear Energy Transfer (LET) of charged particles will also be adopted for the determination of the Total Ionising Dose (TID). Finally, measurements of the magnetic field will be performed by means of a boom mounted magnetometer.

4.1.3. Evolution of final design

Before diving into the different payload components and relative characteristics, this section will first explain all the major changes and improvements done to the subsystem after the midterm preliminary design [17]. The reasoning and motives that drove these modifications will be comprehensively justified in the following sections. The goal of this initial discussion is simply to give the reader a general overview of the detectors that are going to be adopted and analysed later in the chapter.

To start, the Liulin type detector, R3D-B3, selected in first instance for the Linear Energy Transfer (LET) measurement of charged particles has been replaced by the much more advanced FITPix Lite detector [3]. The latter, currently being developed by the University of West Bohemia, Czech Republic, in collaboration with the Institute of Experimental and Applied Physics (IEAP) in Prague, is an advanced Timepix based detector that outperforms its competitors not only in terms of technological capabilities but also in weight and volume efficiency. In the next section an analysis of the FITPix Lite detector, and in particular of the Timepix characteristics and performance, will be conducted.

For the neutron detection, semiconductor pixel detectors by the Medipix collaboration were considered from the start. When coated and arranged in a telescope-like configuration they promised high-quality measurement results on a miniaturised platform. At the early design stages, the most suitable detector working off this concept seemed to be the ATLAS-TPX [59]. However, in the final design the much smaller FITPix Lite detector configuration, will be implemented.

Finally, the SpaceMag magnetometer previously selected remains unchanged. What was adjusted is its integration within the CubeSat. At first, it was planned to be mounted on the tip of one of the solar arrays to take advantage of its deployment from the CubeSat's main structure. Hence, avoiding the use of a boom that would have simply added complexity to the overall system. However, after several design iterations it was concluded that this design option was unfeasible due to a mismatching between the dimensions of the magnetometers sensor head and the space available on the solar array tip for mounting. As a result, the only obvious solution left was the adoption of a deployable boom mechanism. Fortunately, space proven booms have already been developed specifically for CubeSat applications and are available on the market. Mechanism selection, analysis and integration will be presented in the following sections.

4.1.4. Hybrid semiconductor pixel detectors

The development of hybrid semiconductor pixel detectors for radiation measurement began in the early 1990s as a joint collaboration between the European Organization for Nuclear Research (CERN), Universities of Freiburg and Glasgow, and the National Institute for Nuclear Physics (INFN) sections of Pisa and Naples, namely the Medipix1 collaboration. One of the goals of this joint effort was to outsource these highly promising technological advances developed for the Large Hadron Collider (LHC) in Geneva, to diverse applications other than high-energy physics. The first chip, also called photon counting chip (PCC), found as major application purely X-ray imaging. However, the potential foreseen in this technology after the Medipix1 chip was released, in mid-late 1990s, paved the way to further collaborations that have further developed and marketed pixel detectors. As a result, the Medipix2 collaboration was established in 1999, this time comprising a larger number of research institutes, and was intended to last only four year. However, given the wide range of applications encountered for the second version, this collaboration is still ongoing today. In particular, a major breakthrough was obtained by modifying the read out circuit integrated in the Medipix2 chip, giving it further measurement capabilities. These modifications gave birth to the Timepix.

Timepix working principle and operating modes The configuration of the Timepix can be observed in Fig. 4.1 and Fig. 4.2. The silicon sensor area of 1.4 cm^2 is subdivided in a matrix of 256x256 pixels having a pixel pitch of μm. Each and every single pixel has its own read out path which connects it, by means of bump-bonds, to the application specific integrated circuit (ASIC).

When ionising particles hit the pixel surface, electron-hole pairs are created and the charge is transferred through the bump-bond of the specific pixel. In counting mode, this will tell the electronics to add this interaction to the number of particles which have already hit that relative pixel. As visible in Fig. 4.2, the separation created, thanks to the bump-bond, between the sensor surface and the read out circuit allows to tailor the detection medium for different particles and energy ranges. In particular, it is very effective in noise-free detection of neutrons [61].

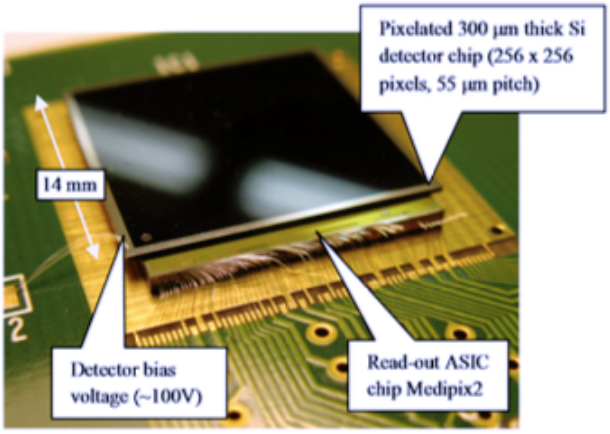

Figure 4.1: Hybrid semiconductor Timepix configuration [60]

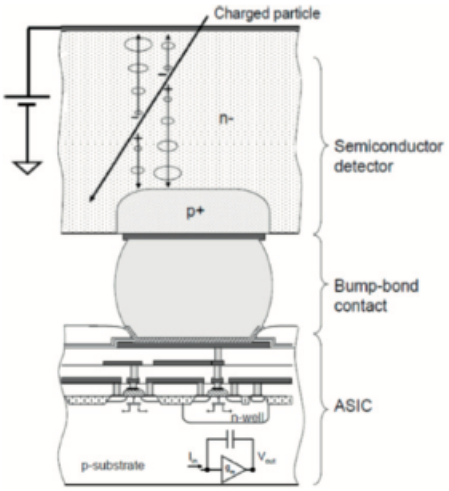

Figure 4.2: Pixel electronic overview [60]

Moreover, it is also possible to determine the energy of the hitting particle given its proportionality with the charge flowing through the bump-bonds after the particle interaction.

In addition to the counting mode already present in the Medipix, the Timepix is provided with two more operating modes. The Time-of-Arrival (ToA) mode which allows to measure the time at which the particle was detected and the Time-over-Threshold (TOT) which allows the direct measurement of energy deposited per pixel.

A very important feature of the Timepix as a pixel detector is its pattern recognition capability. It is able to differentiate between six different types of traces on its pixelated detection surface, each of which is associated with the detection of a particular group of particles. This is illustrated in Fig. 4.3.

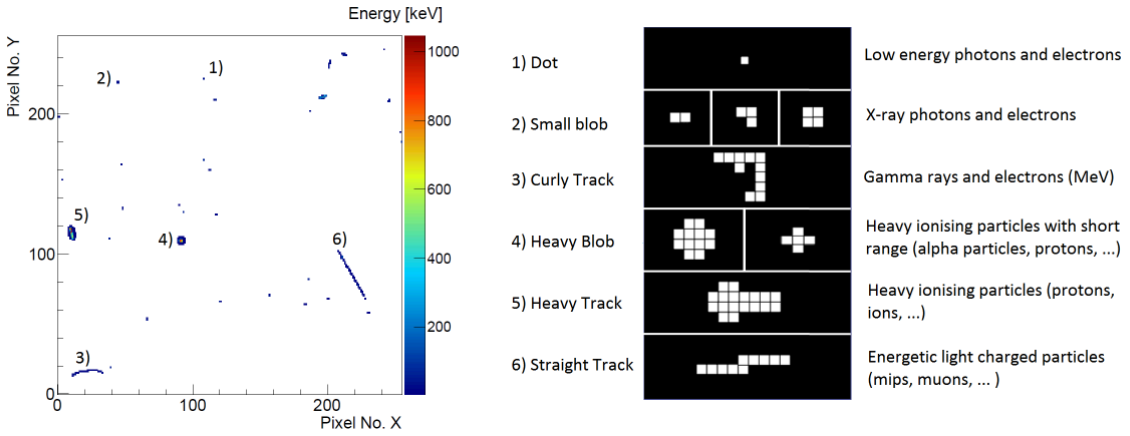

Figure 4.3: Pattern recognition capability of the Timepix detector and associated particle groups [59].

Space applications Timepix detectors for space applications are currently being operated and, given the potential of such technology, more and more applications will be found in the future. Currently, six Radiation Environment Monitor (REM) devices, Timepix based detectors, are on board of the ISS with the intention to monitor the ionisation radiation field inside the ISS and to evaluate the performance of Timepix-based detectors in the LEO radiation environment [62]. Another Space application was found through the Space Application of Timepix Radiation Monitor (SATRAM) as a technology demonstrator payload on board of ESA's Proba-V satellite [63]. The SATRAM detector is currently orbiting Earth at an altitude of approximately 820 km with the objective of characterising the radiation environment in LEO [63]. To conclude, two Timepixes were incorporated into NASA's ORION capsule, launched in 2014, in order to estimate the radiation evironement astronauts would be exposed to inside

the capsule itself [1].

4.1.5. Neutron detection application

Silicon (Si) based pixel detectors are not sensitive to neutrons. While the silicon will interact with intermediate and fast neutrons, the detection efficiency is not high enough to qualify an unmodified Timepix for neutron detection [64]. However, coating the detection surface with 'neutron activating' materials, the interaction with neutrons can be much increased. This has been shown by the ATLAS MPX/TPX modifications of the Medipix and Timepix detectors, which are currently deployed in neutron detection experiments in the Large Hadron Collider [59, 64]. Suitable coating materials should be able to efficiently react with protons and leave behind a reaction product to which the silicon based chip is more sensitive. Due to its large number of hydrogen atoms, Polyethylene (PE) is an ideal candidate for fast neutron interactions, leaving a recoil proton to be detected by the Timepix. Partially adding a thin aluminium layer between the PE and Si surfaces can shield low energy recoil protons, allowing for subtraction methods and further contrasting at the energy threshold of 4 MeV between Al covered and uncovered regions [59]. To increase the detection efficiency towards the lower side of the neutron energy spectrum, a lithium fluoride (LiF) coating can be applied. After interaction with the LiF layer, thermal and intermediate neutrons leave α particles and tritons to be detected by the Timepixn [59]. All LiF and PE reaction products are classified as heavy ionising particles and leave characteristic 'Heavy Blob' and 'Heavy Track' signatures on the detector surface (refer to Fig. 4.3). It is advised to leave a part of the silicon detector surface uncovered, to allow for subtraction of the n+Si interaction background. A full overview of the discussed coating configuration and the corresponding reactions is given in Figs. 4.4 and 4.5

Figure 4.4: Atlas-TPX neutron activation coating scheme [59]

^{6}LiF-Region Thermal neutrons through α-particles and ^{3}H from: $n + {}^{6}Li \rightarrow \alpha + {}^{3}H$, $T_n \approx 25$ meV Background from: $n + Si \rightarrow n' + Si'$, $T_n > 0.2$ MeV $n + Si \rightarrow n' + Si' + \gamma$, $T_n > 1.85$ MeV $n + Si \rightarrow Mg + \alpha$, $T_n > 2.75$ MeV $n + Si \rightarrow Al + p$, $T_n > 4$ MeV $n + Si \rightarrow nX$, $T_n > 20$ MeV non-neutron field	**PE+Al-Region** Fast neutrons detection through protons (with high enough energy to penetrate the Al-foil) from: $n + p \rightarrow n' + p'$ $T_n > 4$ MeV Background from: $n + Si \rightarrow n' + Si'$, $T_n > 0.2$ MeV $n + Si \rightarrow n' + Si' + \gamma$, $T_n > 1.85$ MeV $n + Si \rightarrow Mg + \alpha$, $T_n > 2.75$ MeV $n + Si \rightarrow Al + p$, $T_n > 4$ MeV $n + Si \rightarrow nX$, $T_n > 20$ MeV non-neutron field
Si-Region (uncovered) Used for the background subtraction. — Background from: $n + Si \rightarrow n' + Si'$, $T_n > 0.2$ MeV $n + Si \rightarrow n' + Si' + \gamma$, $T_n > 1.85$ MeV $n + Si \rightarrow Mg + \alpha$, $T_n > 2.75$ MeV $n + Si \rightarrow Al + p$, $T_n > 4$ MeV $n + Si \rightarrow nX$, $T_n > 20$ MeV non-neutron field	**PE-Region** Fast neutrons detection through protons from: $n + p \rightarrow n' + p'$ $T_n > 1$ MeV Background from: $n + Si \rightarrow n' + Si'$, $T_n > 0.2$ MeV $n + Si \rightarrow n' + Si' + \gamma$, $T_n > 1.85$ MeV $n + Si \rightarrow Mg + \alpha$, $T_n > 2.75$ MeV $n + Si \rightarrow Al + p$, $T_n > 4$ MeV $n + Si \rightarrow nX$, $T_n > 20$ MeV non-neutron field

Figure 4.5: Corresponding reactions for the creation of silicon detectable (charged) particles [59]

4.1.6. Pixel detectors in telescope configurations

Arranging two or more pixel detectors in a telescope configuration (i.e. facing each other, separated by a small distance) can significantly increase the value of the measured data. This is because charged particles can penetrate both detector surfaces [59]. The event location on both two-dimensional detection surfaces left by the same particle (coincidence event) or the fact that the particle was not able to penetrate both detector surfaces (anticoincidence event) allow to infer three-dimensional information about the path and the incidence angle of the particle. Because the event patterns on the detector surfaces are not only a function of the particle type, but also of their incidence angle [59], coincidence counts can support the pattern recognition scheme drastically and thereby contribute to the particle recognition ability of the Timepix chip. Paired with a good understanding of the angular detection efficiency, which can be obtained from extensive calibration, the insight on the incidence angle also aids the interpretation of detection count in the final set of measurements.

[1] `https://medipix.web.cern.ch` [Retrieved 20 May 2018

When it comes to neutron detection, the ability to distinguish between coincidence and anticoincidence events is crucial. In contrast to charged particles, neutrons generally do not interact with both detection surfaces [59]. Up to a neutron energy of 20 MeV their heavy blobs and tracks almost exclusively occur as anticoincidence events, which distinguishes them from the charged particle detections with similar pattern. At neutron energies above 20 MeV, neutron coincidence events can occur and the frequency of such events increases with their energy. Due to special reaction patterns like spallation reactions which are unique to neutrons [59], distinction between the detection of a charged particle or a neutron coincidence event may still be possible. However, it has to be accepted that at high energy the contrast between charged and uncharged detection gets less clear. There is another flaw in the neutron detection strategy: charged heavy ionising particles impinging on the detection surface at a shallow angle will leave heavy blob and track anticoincidences, which means those are no longer the unique signature of neutron events. This distortion can be prevented by shielding the detectors from particles approaching at shallow angles.

4.1.7. Application of the FITPixLite

A space application for the Timepix detector is currently being developed as a joint effort between the University of West Bohemia and the Institute of Experimental and Applied Physics in Prague. The FITPixLite is a compact particle detector which seems to be a perfect suit for ARCHER and CubeSat based missions in general. This device, as displayed in Fig. 4.6, is extremely weight and volume efficient. It weighs approximately 50 grams and occupies less than 3% of a CubeSat Unit. Moreover, it makes use of a telescope configuration, hence taking advantage of all the technological capabilites explained in previous sections. The FITPixLite is intended to fly in early 2019 on board of the Pilsen CUBE II, currently being developed by the same agencies mentioned above. In order to better understand how this compact detector could well integrate within Mission ARCHER, the team got in contact with the experts in the field. Unfortunately, to have access to certain information a non disclosure agreement (NDA) was required to be signed, which was beyond the scope of the project. As a result, missing information for the conceptual design was estimated from previous or similar devices. As an example, the power consumption was assumed to be equal to the miniaturised readout interface for Medipix2 detectors, USB Lite, given their similar characteristics [65]. Accordingly, the data rate was assumed to be 1 Mbit/s. Moreover, considering that the FITPixLite will be exposed to LEO radiation environment, it was assumed that its radiation hardening characteristics would be sufficient also for Mission ARCHER.

Figure 4.6: FITPixLite detector [3]

To conclude, it was decided that in order to measure the entire LET spectra required and the total ionising dose (TID), a number of two FITPixLite were necessary. As for the integration within the CubeSat, it was decided to mount the detectors in parallel providing both redundancy and cross calibration capabilities. Lastly, a calibrated, fully functional device in standby is taken on board, which can be activated in case problems with one of the nominal devices occur.

For the neutron detection aboard the ARCHER probes, one device of the same kind is used. To be applied as a neutron detector, the FITPixLite will be modified as described in Section 4.1.5. Polyethylene, lithium fluoride and aluminium coatings are applied on the silicon surface, while leaving one part uncoated.

To preserve the heavy blob and track anticoincidences as the unique signature of neutron events, a tantalum cage that shields the Timepix surfaces from shallow particles will be added. The modified detector will be placed in the interior of the probe, right behind the outer aluminium sheets of the CubeSat structure with the open face of the tantalum cage and the detection surfaces oriented parallel to the aluminium sheets. This way, the conversion from primary to secondary (neutron) radiation involves only simple, well understood geometry and materials.

Since the detector chips have a reasonable flight heritage and are designed for radiation intense environments, their feasibility in space is of no concern. The coatings, however, have to undergo a series of out-gassing treatments, evaluations and tests as specified by ESA [66]. Before system level assembly, the complete detector configuration has to undergo an extensive calibration procedure. The use of radiation testing facilities will be necessary to fine tune the pattern recognition capability, infer the exact detection efficiency at different angles and record the exact behaviour of the coincidence schemes. The time spend in expensive, power consuming test facilities can be minimised by the extensive use of Geant4 [32] Monte-Carlo simulation in advance.

4.1.8. Boom Mounted Magnetometer

As previously mentioned is this chapter, the magnetometer intended to be used for magnetic field measurements remains unchanged, the SpaceMag from Bartington Defence and Space [5]. What was re-designed was the integration of the latter within the CubeSat. Having discarded the possibility to mount the sensor head of the magnetometer on the tip of the solar array, the only viable solution left was to opt for a boom mounted configuration.

Fortunately, a retractable boom specifically designed for CubeSat applications has already been developed and flight proven on board of the 3 unit CubeSat, AlSat-1N [4]. The AstroTube Boom, developed by Oxford Space Systems, is an open-section flexible composite member with a 0.3 mm thickness. During manufacturing, Epoxy-based plain weave carbon fibre prepreg was used given its relatively high radiation tollerance. Its retractable characteristics make it the first retractable boom ever mounted on a CubeSat [4]. As for weight and volume, the boom mechanism occupies exactly 1 unit and weighs not more than 0.61 kg. The boom takes around three minutes to fully deploy (1.5 meters) consuming around 1 Watt. The boom mechanism can be better visualised in Fig. 4.7.

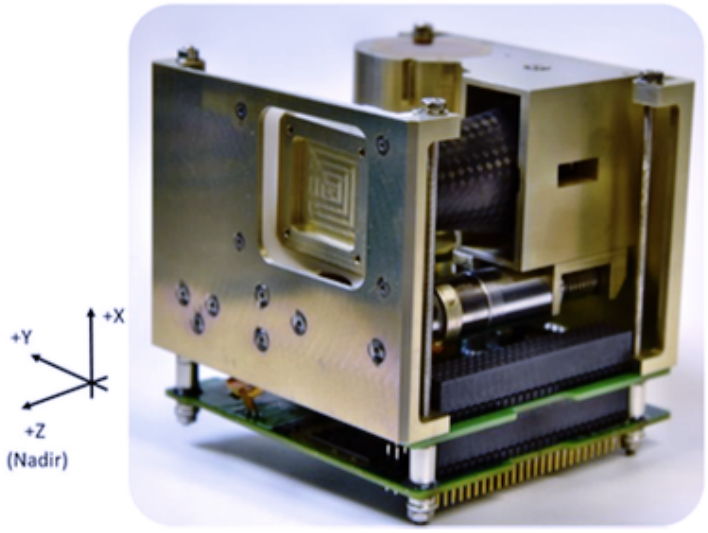

Figure 4.7: Astrotube Boom, Oxford Space Systems [4]

Before being sent into LEO, the boom underwent a series of qualification tests to prove its performance. Tests included: thermal cycling testing, deployment and retraction testing at expected in-orbit operational temperatures and vibration test campaign. All of these tests were successfully performed [4]. Furthermore, another interesting aspect of this mechanism is that, on the very same mission it was flight proven, it carried the sensor head of the smaller version of the SpaceMag magnetometer Mission Archer is intending to use. This proves a reliable integration between two components of two different companies.

4.1.9. Overall Payload Mass and Volume Budget

To conclude, in Tables 4.1 and 4.2 below an overall mass and volume budget is displayed.

Table 4.1: Mass Budget for the Payload

	Comp. Mass [kg]	Quantity	Mass [kg]	Source	Margin [%]	Inc. Marg. [kg]
FITPix Lite	0.057	2	0.114	COTS	5%	0.1197
Coated FITPix Lite	0.057	1	0.057	MCOTS	10%	0.0627
SpaceMag	0.45	1	0.45	COTS	5%	0.4725
AstroTube Boom	0.61	1	0.61	COTS	5%	0.6405
Total	-	-	2.392	-	5.23%	**1.2954**

Table 4.2: Volume Budget for the Payload

	Comp. Volume [U]	Quantity	Volume [U]	Source	Margin [%]	Inc. Marg. [U]
FITPix Lite	0.0213	2	0.0425	COTS	5%	0.0446
Coated FITPix Lite	0.025	1	0.025	MCOTS	10%	0.0275
SpaceMag	0.2798	1	0.2798	COTS	5%	0.2938
AstroTube Boom	1	1	1	COTS	5%	1.05
Total	-	-	0.5	-	5.09%	**1.4160**

4.1.10. Recommendations

The payload design involved a lot of communication with scientists at the frontier of radiation detection. While most of their recommendations were incorporated, some suggestions could not be integrated in the final design yet. This is mainly due to the difficulty of the analysis involved and the long development time of instruments compared to the short duration of this project. The purpose of this section is to draw the attention of the reader to the potential of these options.

In a private email conversation, Lawrence Pinsky, key figure in the Medipix collaboration, mentioned that a new version of the Timepix chip is in development. Final performance specifications are expected to be available late summer 2018 and it is planned to make the product available between January and July 2019. The chip will offer the same performance at smaller power consumption and will be compatible with external triggering support devices such as avalanche photodiodes and PiN diode light detectors. Usage of such devices may help to make the data output of the Timepix more efficient, which could take a lot of stress off the CDH and COMMS systems.

Secondly, it is recommended to carefully design the shielding cage around the modified FITPixLite neutron detector. The proposed shielding is very basic and in fact the effectiveness of this measure is very complex. If not designed properly, the shielding cage can trap particles from paths that would have never impinged the unshielded detector surface and alter the measurements in unknown and even disadvantageous ways. Thus, it is recommended to implement a Geant4 simulation and an optimisation, where different materials, thicknesses and geometries are considered.

Lastly, it is recommended to investigate the possibility of adding carefully selected materials between the FITPixLite neutron detector and the aluminium sheets of the CubeSat structure. One could try to replicate the material characteristics of the shielding of human space travel vehicles. Again, this requires involved Geant4 simulations, which are beyond the scope of this design study.

4.2. Propulsion

In order to attain and maintain the desired orbit it is necessary to have a reliable propulsion subsystem capable of delivering the required total impulse.

In this section the requirements at a system and subsystem level relevant to the propulsion system are addressed, followed by a trade-off on the different available types of propulsion systems. Then, the configuration of the chosen propulsion unit is detailed, followed by a discussion on possible points of failure and the redundancy applied to the subsystem. The section concludes with a description of the verification methods used to back the described subsystem characteristics.

4.2.1. Requirements

In addition to the system requirements as detailed in Section 3.1, there are other subsystem requirements also relevant to the propulsion system, these are listed below. They have to be met in order to have the highest chance of overall mission success.

- [TEC-PROP-01] The propulsion module shall provide a Δv budget of (1436.1m/s)
- [TEC-PROP-02] The spacecraft shall have a Δv budget margin of (128.8m/s)
- [TEC-PROP-03] The propulsion system shall be able to be activated and deactivated at least (400) times.

In addition to these, the subsystem implements the redundancy philosophy as detailed in Section 3.6.

4.2.2. Design and Component Selection

In this section, the selection process of the propulsion subsystem is discussed. For this, first a design option tree is constructed in order to discover all possible propulsion options, as illustrated in Fig. 4.8.

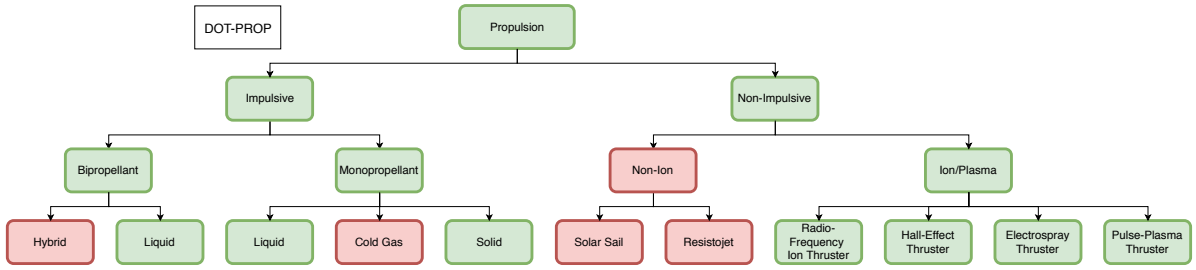

Figure 4.8: Design option tree for the propulsion subsystem

The different propulsive options can be divided into two groups: the ones that provide a high level of thrust and therefore allow for near-impulsive manoeuvres, and the ones that provide a low thrust level and will therefore need to run for extended periods of time to achieve the required Δv.

The state-of-the-art on both high-thrust and low-thrust engines that could be used on ARCHER was researched and the best option for each of these two types was brought forward. Both types had to be considered due to their significantly different characteristics. A high-thrust engine will generally require a significantly lower Δv to travel between two points, while low-thrust engines tend to have much higher fuel efficiency (I_{sp}), decreasing the subsystem mass and volume required.

High-Thrust Propulsion

For the high-thrust branch of the design option tree, only two options can be readily discarded, with the others still being possible candidates. The first one is the hybrid propulsion system of the bipropellant branch of the high-thrust branch. It can be discarded due to the fact that it has a Technology Readiness Level (TRL) of 5 [67], which violates requirement [TEC-SYS-09]. The second one is the cold gas propulsion system of the monopropellant sub-branch within high-thrust propulsion. This is due to the fact that all of the considered engines [68] have I_{sp} values inferior to other high-thrust propulsion options (maximum I_{sp} of 75 s for cold gas versus minimum I_{sp} 187 s

for Solid and liquid engines), along with a maximum thrust value below the average thrust values of the other high-thrust branches (50 mN maximum thrust for the SNAP-1 engine [68] versus 421 mN and 434 mN average thrust for the solid and liquid engines respectively [68]).

The propulsion system selected as representative for this branch is the liquid propulsion High Performance Green Propulsion (HPGP) system, due to it being (of the systems considered [68]) one of the four high-thrust systems with a TRL of 9, while having the best I_{sp} amongst them of 231.5 s, and it having an acceptable thrust level of 1000 mN. Furthermore, the thruster is light and compact at a mass of 0.38 kg and a length of 178 mm respectively[2]. While chemical propulsion subsystems are characterised by their adaptability, it has been chosen to size using a CubeSat propulsion system using the HPGP which is actually in development, as this gives a better view on the actual practical capabilities of the propulsion system. This was done using Aerojet Rocketdyne's MPS-120 propulsion system[3].

Low-Thrust Propulsion

For the low-thrust branch of the design option tree, the first option to be discarded was resistojet propulsion. This was due to the fact that it has very low I_{sp}, with its maximum value being lower than both the lowest values of the remaining high-thrust and low-thrust options respectively (maximum I_{sp} of 180 s for resistojet propulsion versus a minimum I_{sp} of 187 s and 300 s for the high-thrust and low-thrust branches respectively). Considering that the largest thrust of said engine was less than the average thrust of the engines of the high-thrust branch (30 mN maximum thrust for resistojet propulsion versus 421 mN and 434 mN average thrust for the solid and liquid engines respectively), and considering that it has no inherent power consumption advantages, it was completely inferior and thus could be readily discarded.

The next option to be discarded was the solar sail. Considering the solar reflectance of the sail, with 90% efficiency, a solar sail provides a thrust of 8.17μN/m^2 at 1 AU [69]. With this, it becomes clear that an unfeasible sail area would be required in order to obtain significant thrust such that we can perform the required Δv within the mission lifetime (100 m^2 of sail would give a thrust of 0.817 mN, so with a fully loaded 12 U CubeSat (with a total mass of 20 kg), it would take 283 days under ideal conditions per km of Δv). Overall, the low thrust of solar sails outweighs the advantage of propellant-less propulsion for our mission profile and they will thus not be further considered.

The engine selected for this branch is the RF Ion BIT-3 engine from Busek, due to it having (of the engines considered [68]) the highest I_{sp} of 2640 s and an acceptable thrust level of 1.15 mN. Furthermore, this engine has a TRL of 6, which is the highest in this thrust range, and it is expected to further increase in the very near future as it will undergo a 4000 h firing test and it is intended to be used on the Lunar IceCube NASA mission, among others. For these engines there is also the possibility of using more than one, giving a multiple of the thrust levels shown. The power requirement for this engine is a nominal 75 W. Lastly, the propellant of choice for this engine is Iodine (I_2), which is stored in solid state and provides system level benefits including low storage pressure and extremely high density.

4.2.3. Subsystem Configuration

After performing a trade-off on the different propulsion types, it was decided to use the RF BIT-3 Ion Thruster from Busek. This outcome was reached after comparing the mass, volume, and power requirements of each engine and realising the high-thrust option was driving the spacecraft design to an unacceptable extend, whereas the low-thrust option was capable of delivering the required total impulse in a manageable form factor and with higher reliability due to its COTS status and solid propellant used.

This (low-thrust) engine is currently the state-of-the-art on CubeSat electric propulsion. Its COTS characteristics are tabulated below in Table 4.5. It uses Iodine (I_2) as propellant [6], which is a very promising solid state propellant due to its high density, and efficiency comparable with the more commonly used Xenon (Xe), which cannot be stored in solid state. It would have also been possible to increase the fuel tank of the integrated subsystem in order to be able to deliver additional Δv, but that would lower the TRL and alter the dimensions and

[2] http://ecaps.space/products-1n.php [Retrieved 26 June 2018]

[3] http://www.rocket.com/files/aerojet/documents/CubeSat/MPS-120%20data%20sheet-single%20sheet.pdf [Retrieved 26 June 2018]

mass of the system and it ultimately proved to be unnecessary as [TEC-PROP-01] was met with 1.5 kg of fuel (as determined from Eq. (4.1) with M_0 = 19.0 kg, I_{sp} = 2300 s and g_0 = 9.80665 m/s^2). The Modified Commercial Off-The-Shelf (MCOTS) characteristics are tabulated in Table 4.4. A summary of the achievable Δv with different amounts of propellant and its corresponding burn times can be found in Table 4.3.

$$\Delta v = I_{sp} \cdot g_0 \cdot \ln\left(\frac{M_0 + M_f}{M_0}\right) \tag{4.1}$$

Where I_{sp} is the specific impulse of the engine in seconds, g_0 is the standard acceleration due to gravity equal to 9.80664 m/s^2, while M_0 and M_f are the initial wet mass and the fuel mass respectively in kg.

Table 4.3: Correlation between propellant mass, Δv, and burn time

Fuel Mass	Δv	Burn time
1.0kg	1029.9m/s	241.1days
1.5kg	1564.9m/s	361.7days
2.0kg	2114.1m/s	482.3days
2.5kg	2678.3m/s	602.8days
3.0kg	3258.5m/s	723.4days

Table 4.4: BIT-3 MCOTS characteristics with enlarged fuel tank

Aspect	Value
Mass	1.55kg
Max fuel mass	3.0kg
Dimensions	1.80x0.88x1.50U
Volume	2.376U

Table 4.5: BIT-3 Characteristics[6, 70, 71]

Aspect	Value
Mass	1.5 kg
Max fuel mass	1.5 kg
Dimensions	1.80x0.88x1.02 U
Volume	1.616 U
Gimbal (2-axis)	$\pm 10^\circ$
Voltage	28 VDC
Communication	RS-485
Power consumption	
↦ Nominal	75 W
↦ Warm-standby	15 W
↦ Sleep	2.8 W
Temperature range	
↦ Operational	-20 to +50 C
↦ Survivable	-30 to +80 C
Number of cycles	>400
Unit price	101 k€
Data rate	60 bit/s
Thermal dissipation load	35 W
Radiation hardening	”Rad-Hard Fence”

The engine, as listed in Table 4.5, operates at a voltage of 28 V. However, it does not require the bus voltage to be equivalent, as the BIT-3 has a built-in transformer.

Also, the integrated subsystem has a gimbal system capable or changing the direction of the thrust between $\pm 10^\circ$ in two axes. This can be used for reaction wheel desaturation if needed.

Furthermore, the engine is throttleable between 56-80 W, with the nominal thrust level being at 75 W. Under these different power levels, the engine delivers a variable thrust between 0.66-1.20 mN (see Fig. 4.11 with an also varying I_{sp} between 1400-2300 s. Three power levels are considered to be used during our mission, and these are described in Table 4.6.

Table 4.6: Thrust and I_{sp} for given power level [6, 72]

Minimum	Nominal	”Up-to”
56 W	75 W	80 W
0.66 mN	1.15 mN	1.20 mN
1400 s	2100 s	2300 s

Physically, the propulsion unit is located in the back of the spacecraft, not along its principal inertial axis. This helps minimising the empty space and allows for better thermal management. It does not have any negative

Figure 4.9: The BIT-3 propulsion unit. Image courtesy of Busek.

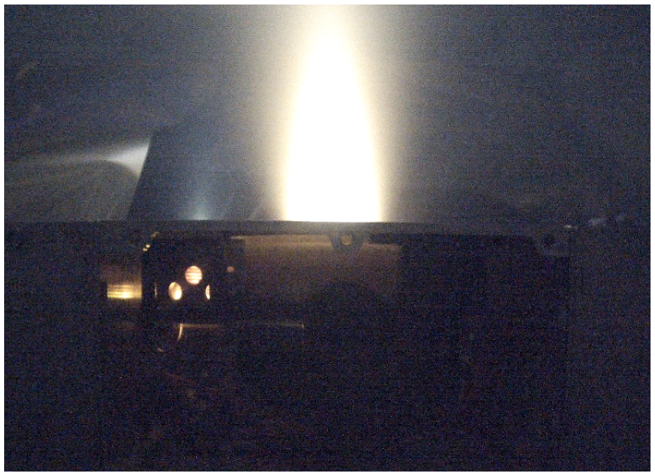

Figure 4.10: BIT-3 firing test with I_2 propellant. Image courtesy of Busek.

consequences, due to the nil atmospheric drag the spacecraft will experience. Illustrations of the BIT-3 can be found in Figs. 4.9 and 4.10.

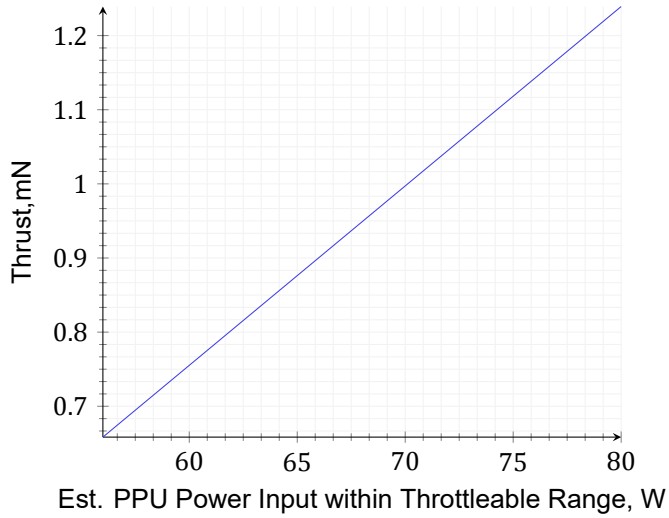

Figure 4.11: Predicted Thrust and I_{sp} Performance of Flight BIT-3 System

4.2.4. Fault Analysis

An analysis on the possible points of failure was performed with the outcomes presented below. It is formatted as a list for readability.

- Cathode ignition: The cathode is currently rated for 400 ignition cycles, while the true limit is unknown. It is desirable to use it for a larger amount of cycles, so extensive testing will be carried out to increase the confidence in higher cathode ignition cycles.
- Firing time: The engine will undergo a 4000 h firing test soon, whereas the system can theoretically fire for 20000 h. We require approximately 8000 h so extensive V&V will be required.
- Depressurisation of fuel tank: The chosen propellant for the BIT-3 is I_2, which is stored in solid state and it therefore requires very marginal pressurisation, it is therefore considered highly unlikely to fail.
- Integrated CDH Single Event Effect (SEE): Field-Programmable Gate Array (FPGA) is protected by Busek's "Rad-Hard Fence" [72], which avoids anomalies caused by SEE to cascade to other components and was

specifically designed to withstand interplanetary radiation conditions. The concrete radiation hardening of the subsystem was not publicly made available, but it can be concluded it does not pose a risk to the feasibility of the mission because the engine was selected to be used in NASA's Lunar IceCube mission[4], which follows a mission profile that is considerably similar to ARCHER's.

- Gimbal anomaly: If the gimbal were to become fixed at a certain position different from the axis-line, it would require the ADCS to counteract larger perturbations. If the gimbal were to become offline while it was correctly aligned with the axis line, it would only eliminate the possibility of using the engine for reaction wheel desaturation.
- Power anomalies: In the scenario of localised (or subsystem-wide) power outages, the subsystem would become nonoperational for the entire duration of the anomaly.
- Feed system: If the valves that regulate the flow fail, it will result in system failure.
- Debris impact: Debris may intercept with the spacecraft at high velocities, which could cause a subsystem failure. The propulsion unit is integrated in a lightweight aluminium chassis, which decreases the possibilities of failure due to impact. Furthermore, other critical subsystems are more exposed to this threat than the BIT-3 because of their lack of an additional aluminium chassis, so this event could also cascade to the propulsion system and would result in subsystem failure.

4.2.5. Redundancy

The BIT-3 engine will not have a redundant system. This is because of its size and volume, making it unfeasible to use a second BIT-3 engine for redundancy. Using a different propulsion subsystem for redundancy is also not feasible, as the BIT-3 engine is the most efficient engine volume- and mass-wise found, and thus if a second BIT-3 engine is not viable for redundancy, any other propulsion system is not viable either. Thus the propulsion subsystem is not redundant and should be made as reliable as possible, especially due to the long expected operational time.

Another aspect of propulsion redundancy is the margin on the Δv budget. This is due to uncertainties inherent in satellite operations. Said original Δv requirements along with the margins and the resulting final Δv requirements for Artemis, the spacecraft that requires the most Δv can be found in Table 4.7.

Table 4.7: Most critical Δv budget. Margins stem from ESA margin philosophy for science assessment studies [50].

Mission phase	Δv [m/s]	Margin [%]	Δv including margins [m/s]
Transfer	708	5	743.4
Insertion	581.7	5	610.7
Orbit Maintenance	20	100	40
End of Life	40	5	42
Total	1349.7	6.38	1436.1

As one can see, the mission phases for transfer, insertion and end of life all have a margin of 5%, while the orbit maintenance mission phase has a margin of 100%. Said margins are the ones used by ESA for planning their missions [50]. The reasoning for them is as follows. For any accurately pre-calculated manoeuvres a margin of only 5% is necessary. This is indeed the case for the transfer, insertion, as well as the end of life mission phases, as these have indeed been accurately pre-calculated. Orbit maintenance however, necessitates a margin of 100% according to the same design philosophy. This results in a weighted average margin of 6.38%. Comparing the resulting total Δv including margins with the available Δv of 1565 m/s gives a spare Δv of 99.1 m/s, which can be used for increased redundancy on top of the margins already used.

4.2.6. Verification

All values presented in this Section 4.2, except for the two mentioned below, were obtained from the cited references and via email correspondence with Michael Tsay, Ph.D (Director, Electrothermal Propulsion Group at

[4] https://www.nasa.gov/feature/goddard/lunar-icecube-to-take-on-big-mission-from-small-package [Retrieved 2 July 2018]

Busek).

The two values that could not be verified with the manufacturer were the exact price of the BIT-3 engine and its telemetry data rate. This information information could be made available by signing a non-disclosure agreement in the future. Thus, expected costs can only be estimated from literature. This was done by analysing the average costs per CubeSat subsystems as provided by NASA's Ames Research Center [73]. From here an average cost of $59,000 can be found. Considering that ARCHER uses a novel propulsion subsystem, it can be assumed said costs will be higher. Thus a contingency of 100% is used, resulting in a final cost of $118,000, or €98,000 as of June 25th 2018. The costs of 1.5 kg of Iodine with purity over 99.99% will cost at most €1,380[5] (this being the price of an entirely filled BIT-3 engine). This is a relatively insignificant amount compared to the final cost of €98,000, and can thus be assumed to be included in said costs.

4.3. Communications

In order to transfer the large amounts of science data, as well as commands and status information, the ARCHER spacecraft will require an advanced communications systems. This section outlines the design and analysis of that communications subsystem. First the requirements are analysed, following which components and frequencies are selected. An overview of the subsystem configuration, including mass and volume budgets, is presented. Finally, the link budget analysis of the system is shown.

4.3.1. Requirements

In addition to the system requirements as detailed in Section 3.1, the following COMMS requirements are in place:

- [TEC-COMMS-02] The communications system shall function nominally with a pointing accuracy during communications of $\pm 1^{\circ}$
- [TEC-COMMS-06] The communications system shall have a maximum payload downlink bit error rate of 10^{-5}
- [TEC-COMMS-07] The communications system shall have a link budget margin of at least 3 dB
- [TEC-COMMS-08] The communications system shall be compatible with the Estrack ground station network
- [TEC-COMMS-10] The communications system shall support an uplink minimum bit rate of 8000 bps during the science phase of the mission
- [TEC-COMMS-11] The communications system shall support a downlink minimum information rate of 1,199,416 bps during the science phase of the mission
- [TEC-COMMS-12] The communications system shall support an uplink minimum bit rate of 8000 bps during the transfer phase of the mission
- [TEC-COMMS-13] The communications system shall support a downlink minimum information rate of 1,325,670 bps during the transfer phase of the mission
- [TEC-COMMS-14] The communications system shall support an uplink minimum bit rate of 62.5 bps from any angle (”lost-in-space” case)
- [TEC-COMMS-15] The communications system shall support a downlink minimum bit rate of 62.5 bps from any angle (”lost-in-space” case)
- [TEC-COMMS-16] The communications system shall be compliant with ECSS Standards
- [TEC-COMMS-17] The communications system shall provide a ranging and tracking capability with a position accuracy of 30 km (3 sigma)
- [TEC-COMMS-18] The communications system shall provide a ranging and tracking capability with a velocity accuracy of 50 cm/s (3 sigma)

These requirements were reviewed as the project developed, with figures that had been left TBD and other specifics filled in. The figures in the downlink information rate requirements are based on the data budget determined in Section 4.5.4. The figures for the uplink and lost-in-space case are based on the maximum and minimum supportable bit rates for the selected Iris transponder (see Section 4.3.2). It is worth noting the distinction made between bit and information rates in these requirements. The information rate, also known as the net bit rate, is the amount of actual data transmitted, whereas the bit rate includes all of the transmitted bits including

[5] https://www.fishersci.nl/shop/products/iodine-crystalline-99-99-metals-basis-2/p-6827141#?keyword=iodine+crystalline [Retrieved 25 June 2018]

those used in Forward Error Correcting (FEC) schemes. As a result, the information rate can be up to 1/6 of the actual bit rate. The remaining requirements are developed based on the capabilities of other systems, legal requirements, or flowed down from system-level requirements.

In addition to these requirements, the subsystem must apply the redundancy philosophy as detailed in Section 3.6 and the sustainability strategy as outlined in Section 2.4.

4.3.2. Design and Component Selection

Based on inputs such as the functional flow of the spacecraft, the preliminary requirements, and design option trees the communications subsystem was designed. It was decided during the preliminary design, based primarily on technology readiness, that radio-based communications would be employed, eliminating concepts such as laser/optical communication. This section presents the detailed design of the radio-based communications subsystem, starting by selecting a frequency and ground network, before determining the components, namely radio and antennae, that will be carried aboard the spacecraft.

Frequency Band Selection

Frequency selection is traditionally the first step in the design of a communications subsystem [49]. A number of aspects were considered when deciding upon the frequency band for ARCHER, including:

- European Cooperation for Space Standardization (ECSS) requirements on frequency allocation.
- Required distances and data rates.
- Capabilities of available spacecraft radios and antennas.
- Capabilities of available ground stations.
- Sensitivity to atmospheric and precipitation losses.

As the ARCHER mission profile does not reach distances from the Earth of above 2 million kilometres, it is classified as a Category A mission, and is thus not allowed to use the Space Research (Deep Space) frequency bands. As a result, it must limit its frequency usage to the Space Research bands outlined by the ECSS [74] based on International Telecommunication Union (ITU) regulations.

Despite not being classified as Deep Space, the achieved distances and large payload data rates of the ARCHER mission emulate the demands of a deep space communications system. To maximise the science potential of the mission a a high data rate downlink is required. In order to achieve this, a high-gain antenna is desirable. Furthermore, ARCHER's technology and schedule requirements limit the spacecraft to the use of currently existing or under-development hardware, while the capabilities of potential ground stations add further constraints to the potential frequencies. Advantages and disadvantages of the available frequency bands are outlined in Table 4.8.

Based on Table 4.8, VHF and UHF were considered unsuitable due to the low antenna gain involved highly limiting the potential data rate. In K and Ka band, an analysis of ground station capabilities determined that there was extremely limited support for Ka band transmission in the Estrack network [75]. Furthermore, the Ka band frequencies that are supported by the Estrack network are those allocated to Deep Space transmissions, which, as stated previously, ARCHER does not qualify to use. Commercial networks, such as that operated by the Swedish Space Corporation (SSC)[6], were considered as an alternative for Ka band coverage although these are not preferred from a cost perspective. As a result, only S-band and X-band were considered for further analysis. Detailed research into hardware capabilities and link budget analysis was carried out for these frequencies.

Ground Element Selection

As the ARCHER mission is designed to be a European-operated science mission, the obvious choice for the ground station network is ESA's Estrack network. This network also supports ranging [75], as discussed further in Section 6.3.1.

With the increased ground station demand expected from future deep-space scientific missions [76], ARCHER's communications system has been designed to minimise use of the 35 m Deep Space Antenna (DSA) dishes. Dur-

[6] www.sscspace.com/ssc-worldwide/ground-station-network/ [Retreived 13 June 2018]

Table 4.8: Table of available frequencies. Frequency bands as defined by ECSS-E-ST-50-05C Rev. 2 [74].

Band	Frequencies [GHz]	Advantages	Disadvantages
VHF	Multiple*	Low pointing requirements and good omnidirectional characteristics. Rain attenuation negligible.	Very low antenna gain.
UHF	Multiple*		
S	2.025 - 2.110 (E-S) 2.200 – 2.290 (S-E)	Wide availability of compatible S/C and GS hardware. Increased gain and potential data rate compared to VHF/UHF.	Lower gain than X-band and above.
X	7.190 – 7.235 (E-S) 8.450 – 8.500 (S-E)	Widely used for downlink. Improved gain over S-band.	Limited availablity of uplink-capable ground stations. Increased precipitation sensitivity.
K	25.500 – 27.000 (S-E)	Supports high antenna gain and data rates.	Limited CubeSat hardware available. Lack of ground station support. Most sensitive to precipitation.
Ka	37.000 – 38.000 (S-E) 40.000 – 40.500 (E-S)		

* While ECSS-E-ST-50-05C does not specify any bands below S-band, multiple bands in VHF and UHF are allocated for Space Research by the ITU.

ing the science phase of the mission, Artemis and Diana will make use of the 15 m dishes in the Estrack network. It is only during the transfer, where distances from earth of up to 1.524 million kilometres are expected, and in case of emergency, that ARCHER will call upon the enhanced capabilities of the DSA dishes.

Radio Selection

The key component of the communications subsystem is the CubeSat radio. A conventional CubeSat radio consists of two elements, a transmitter and a receiver, which may be combined into a single package known as a transceiver. Many commercial options are available from European companies such as ISIS, GOMSpace, EnduroSat, and Syrlinks. Notable among these is the EWC-27 X/S band transceiver offered by Syrlinks[7] which offers a lightweight, power efficient, and high-data rate compatible option with specific deep space variant.

Operating beyond Earth's orbit places additional demands upon a spacecraft radio. Without the ability to rely upon options such as GPS or NORAD Two Line Elements to locate the spacecraft, an internal navigation capability must be included in the spacecraft. A number of options were considered for this navigation capability, such as optical navigation. However, based on the analysis carried out in Section 6.3.1 a radio-based navigation capability was considered essential to the mission.

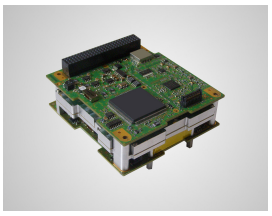

Figure 4.12: The EWC-27 transceiver from Syrlinks.

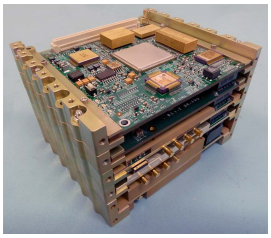

Figure 4.13: The NASA JPL Iris Transponder.

In order to carry out navigation via a radio link, the CubeSat radio must have the capabilities to carry out at a minimum ranging and two-way Doppler velocity measurements. Additional capabilities such as delta-Differential One-way Ranging (ΔDOR) enhance the accuracy of the position determination. A radio with these capabilities, known as a transceiver, is thus integral to ARCHER's operation. As a result, commercial offerings such as the EWC-27-DS are not suitable for use aboard Artemis and Diana.

[7] www.syrlinks.com/en/space/nano-satellite/x-s-transceiver-ewc27-srx [Retreived 12 June 2018]

There currently exist only two options for CubeSat transponders - the Iris radio developed by NASA's JPL and the JAXA X-band TRansPonder (XTRP). The 1 W Radio Frequency (RF) output power supported by the XTRP [77] was found to provide insufficient data rates in a link budget analysis. As a result, the JPL Iris transponder was chosen as the radio to be used on Artemis and Diana.

One challenge remains. During a discussion of the design with Dr. Stefano Speretta at the Space Systems Engineering department of the TU Delft Faculty of Aerospace Engineering it was indicated that the Iris was extremely unlikely to be made available to non-US missions. Despite this, it was chosen for the design as a result of being the only viable transceiver available. Development has begun by a consortium lead by the TU Delft on a European deep space CubeSat transponder, however this is not anticipated to be flight-ready until 2023.

A further consequence of the selection of the Iris transponder and the desire to include ranging capabilities is that the Iris V2.1 is optimised for X-band, with S-band support "under development or planned" [78]. As a result, it was decided to use X-band for both the transmission and reception bands of the spacecraft.

High-Gain Antenna Selection

In order to achieve the desired data rates, a high-gain antenna is required to improve the strength of the signal transmitted. Multiple options were explored for such an antenna in X-band. Presented in Table 4.9 are the four highest TRL options for CubeSat-compatible medium to high gain antennae. Further prospects that were considered included unfurlable reflector antennae[8] and inflateable antennae [79].

Table 4.9: Primary downlink antenna trade-off

	Peak Gain [dB]	Deployment	Internal Volume [U]	Surface Covered (Deployed) [cm]	Mass [kg]	Estimated TRL (June 2018) [-]
Deployable Parabolic Reflector [79]	green >28	red Motorised Gear System with 30 Hinged Ribs	red 1.5	sky blue 10x10, shading over a larger area	sky blue 1.4	sky blue 8
Folded Panel Reflectarray [80]	green 29	sky blue Flight-Proven Hinge	green Negligible	sky blue 10x10, shading	sky blue <1	green 9
Single Patch [81]	red 8-13	green No Deployment	green Negligible	green 10x10	green <0.1	green 9
Patch Array [82]	orange 24	green No Deployment	green Negligible	red 30x20	orange <2	orange 7

green Optimal sky blue Acceptable orange Correctable red Unacceptable

As seen in Table 4.9, only the folded panel reflectarray avoids unacceptable criteria. It has a number of advantages, as it is able to provide a high gain while not requiring internal storage. Furthermore, the fold-out deployment means that the surface upon which it was stowed can also be used for other purposes such as ADCS sensors which would be blocked by an antenna like a patch array. These factors, combined with the proven flight heritage lead to the selection of a folded panel reflectarray for use as the primary high-gain antenna aboard the ARCHER CubeSats. The antennae will be custom designed to achieve peak performance at the selected downlink frequencies in order to achieve the maximum possible data rate from the CubeSat platform.

Secondary Antennae Selection

While use of a high-gain antenna allows for high-rate payload downlink, secondary antennae are required for two purposes. Firstly, a receiving antenna along the same axis as the reflectarray will be used to provide simultaneous transmit and receive capabilities in order to reduce communication time and allow for ranging. Secondly, the high-gain provided by the reflectarray also comes with a narrow beamwidth. In order to improve the omnidirectional radio characteristics of the communications subsystem, a second pair of lower-gain antennae will also be carried aboard Artemis and Diana.

For the secondary antennae gain is not a critical requirement, and can be surrendered in favour of improved

[8] `www.oxford.space/#s-technology` [Retrieved 07 June 2018]

omnidirectional characteristics. As a result, following a brief analysis, a patch antenna was determined to be the optimal format due to its small form factor, light mass, and medium gain. A more detailed trade-off was carried out on European X-band patch antennae from EnduroSat, Syrlinks, Printech Circuit Laboratories, and Anywaves. As a result of this trade-off, not included here for reasons of brevity, the EnduroSat X-Band Patch Antenna Type I was selected based on its relatively high gain (12.4 dB) and low mass (65 g) [81]. The antennae will be modified to achieve peak performance at the selected uplink and downlink frequencies.

Modulation and Encoding Selection

The final aspect of the communications system to select is the modulation and encoding of the data to be transmitted to and from the spacecraft.

Modulation, the technique used to convert the bits to analogue signals, effects the spectral efficiency and noise tolerance of the signal. The Iris transponder employs only Binary Phase-Shift Keying (BPSK) modulation [78], meaning that no further selection of the modulation scheme was required.

In order to improve the communications link, the vast majority of spacecraft employ Forward Error Correcting (FEC) codes [83]. Iris is compatible with Consultative Committee for Space Data Systems (CCSDS) standard Reed-Solomon (255,223) and Turbo 1/2, 1/3, and 1/6 codes [78]. Table 4.10 presents the required Signal-to-Noise Ratio (SNR) for these codes for the Bit Error Rate (BER) given in [TEC-COMMS-06] of 10^{-5}.

Table 4.10: Table Iris supported Forward Error Correcting codes for a Bit Error Rate of 10^{-5}

FEC Code	Code Rate	Required SNR [dB] [83]
Uncoded	1	9.6
RS (255,223)	≈0.875	6.2
Turbo 1/2	0.5	1.1
Turbo 1/3	1/3	0.4
Turbo 1/6	1/6	-0.14

For the uplink, the large Equivalent Isotropically Radiated Power (EIRP) of the ground station antenna allowed uncoded transmission to be employed. In the downlink case, the coding scheme was varied depending on the link conditions in order to achieve the optimum combination of code rate and required SNR for each case. The selected codes for the analysed scenarios can be seen in Section 4.3.4. It is anticipated, however, that the optimum combination of coding scheme and bit rate will vary throughout the mission as the distance between the spacecraft and ground station changes.

4.3.3. Subsystem Configuration

Combining the components, we see that the communications subsystem consists of a primary antenna combination of the high-gain antenna and the parallel primary receiving patch antenna, and a secondary antenna combination of two patch antennae. This section contains further details on the antenna configuration, the communications subsystem interfaces and dependencies, and the mass and volume budgets for the subsystem.

Spacecraft Antenna Configuration

The locations of the four antennae aboard the spacecraft are shown in Figs. 4.14 and 4.15.

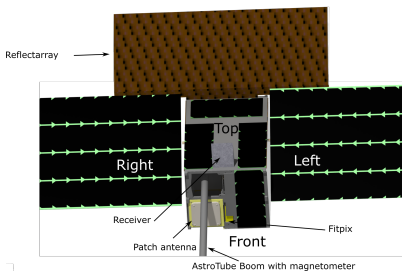

Figure 4.14: Front view of the CubeSat showing locations of high-gain reflectarray and Primary Rx Patch Antenna.

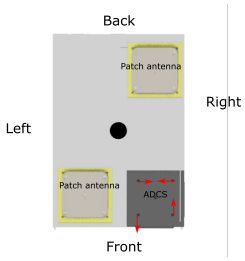

Figure 4.15: Bottom view of the CubeSat showing locations of Secondary Tx and Rx patch antennae

Interfaces and Compatibility

The Iris radio connects to the OBC via a 1 MHz point-to-point Serial Peripheral Interface (SPI) [78]. This interface allows for transfer of data to and from the LEON3-FT CPU on a Virtex 6 FPGA that acts as the transponder computer. The Iris also supports a FireCode, a specific command to reset the OBC, over this SPI link [84]. The FireCode can be transmitted from ground to the Iris even in the event that the processor is not functioning optimally, allowing for an external ”reset” of the spacecraft systems.

The uplink and downlink data format of the transponder is CCSDS compliant [84], which enables it to be compatible with the majority of Estrack ground stations. From the ground stations the data can be transmitted over high-speed terrestrial connections to the spacecraft operations centre. Figure 4.16 shows a block diagram of the full communications system, with the internal block diagram of the Iris transponder adapted from [78].

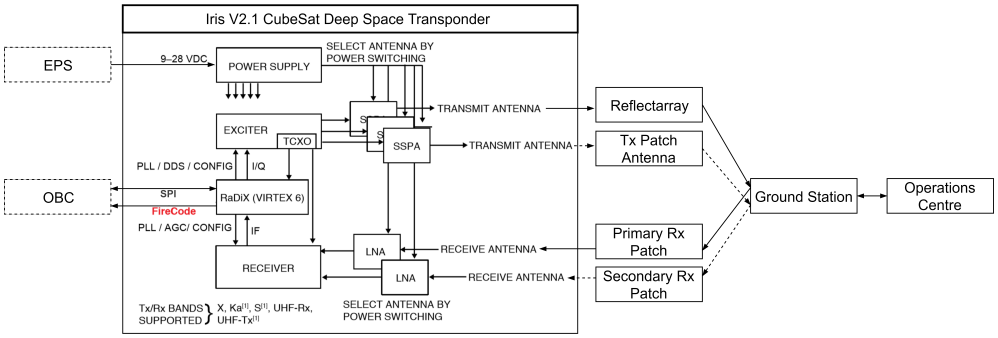

Figure 4.16: Block diagram of the communications subsystem. Internal diagram of the Iris transponder adapted from [78].

Mass and Volume Budgets

Tables 4.11 and 4.12 show the mass and volume budgets for the communications subsystem. The volume of the subsystem only includes that of the Iris as the remaining components are mounted externally.

Table 4.11: Mass Budget for the Communications Subsystem

	Comp. Mass [kg]	Quantity	Mass [kg]	Source	Margin [%]	Inc. Marg. [kg]
Reflectarray & Feed	1	1	1	MCOTS	10%	1.1
Patch Antenna	0.064	3	0.192	COTS	5%	0.2016
Iris Transponder	1.2	1	1.2	COTS	5%	1.26
Total	-	-	2.392	-	7.09%	**2.5616**

Table 4.12: Volume Budget for the Communications Subsystem

	Comp. Volume [U]	Quantity	Volume [U]	Source	Margin [%]	Inc. Marg. [U]
Reflectarray+Feed	0*	1	0	MCOTS	10%	0
Patch Antenna	0*	3	0	COTS	5%	0
Iris Transponder	0.5	1	0.5	COTS	5%	0.525
Total	-	-	0.5	-	5.00%	**0.525**

4.3.4. Link Budgets

Based on the configuration selected above, as well as a number of other potential configuration options, uplink and downlink budget analyses were carried out in order to determine the viability and the capability of the given configuration. The configuration was analysed with respect to three scenarios:

1. During the science phase, at a maximum distance of 400,000 km from the ground station, to an Estrack 15 m antenna.
2. During the lunar transfer, at a maximum distance of 1,524,000 km from the ground station, to an Estrack 35 m antenna.
3. The worst-case scenario, involving a loss of pointing control at the maximum distance of 1,524,000 km. This corresponds to the minimum possible gain of -25 dB.

A different calculation approach was taken for uplink than for downlink. In the downlink budget, Table 4.13, the equations were arranged to calculate the supportable bit rate, and thus payload data rate for a given data encoding scheme. The 3 dB required link margin was incorporated into the calculations and not used as an output. This achieveable bit rate was then rounded down to the nearest greatest Iris compatible bit rate that could be achieved, based on [78]. This allowed for optimisation of the data rate based on variations of the encoding scheme.

In the uplink case, shown in Table 4.14, the large EIRP provided by the ground stations and the low maximum uplink bit rate supported by the Iris transceiver meant that bit rate was no longer a driving factor. In this case, the link budgets were arranged in a more ”traditional” format, with the final output being the link margin which must be above the required 3 dB for the budget to close.

A number of assumptions and estimations were made in the budget analysis. These were:

1. Spacecraft pointing losses were evaluated at an accuracy of $\pm 1^{\circ}$, based on ADCS requirements. For the patch antenna no discernable change was visible on the gain diagram for this pointing variation, and thus the pointing losses for the patch antennae are assumed to be negligible.
2. The ground station EIRP and G/T values were based on an average of the values for all Estrack ground stations of the same diameter capable of transmission in that band [75].
3. Ground station pointing losses were assumed to be negligible or accounted for in the ground station figures of merit (EIRP or G/T).
4. Atmospheric attenuation was calculated based on the ITU P676 Regulation for 5 degree elevation in a standard atmosphere.
5. Precipitation losses are based on 99.5% availability for 12 GHz at the Maspolamas ground station, an ITU category E rain zone.

The ”Source” column in Tables 4.13 and 4.14 gives either the source of the value or the formula used to calculate it. Unless otherwise stated, all formulae are based on [49], where P_{Tx} is the Transmitter Power [dBW], G_{Tx} and G_{Rx} the Transmitting and Recieving Antenna Gains [dBi], f the Frequency [GHz], and R_b the Bit Rate [dB-Hz]. In addition, C/N_o is the Carrier-to-Noise Ratio [dB], G/T the Gain-to-noise-temperature [dB/K], and E_b/N_o the Signal-to-Noise Ratio [dB]. The losses, L_{out}, L_s, L_{path}, L_{atm}, L_{prec}, L_{in}, L_{point}, and L_{comb} are the Transmitter Output, Free Space, Net Path, Atmospheric, Precipitation, Receiver Input, Combined Pointing, and Combined Link Losses [dB] respectively. Finally, T_s and T_{ant} are the Effective System Noise and Antenna Noise Temperatures [K], while F_R is the receiver noise figure [K] and T_0 the reference temperature of 290 K.

Table 4.13: Downlink Link Budget

Parameter [dB unless stated]	Source	Lunar Distance	Transfer Distance	Lost in Space
Downlink Frequency [GHz]	Centre of selected ITU/ECSS band	8.475	8.475	8.475
Distance to Ground Station [km]	Astrodynamics maximum distance	400,000	1,524,000	1,524,000
Spacecraft Parameters				
S/C Transmitter Power [dBW]	[78]	5.798	5.798	5.798
S/C Tx Antenna Gain [dBi]	[80]	29	29	-25
S/C Line Loss	Assumed based on [85]	-1	-1	-1
Transmitter EIRP [dBW]	$EIRP = P_{Tx} + G_{Tx} - L_{out}$	33.798	33.798	33.798
$\pm 1°$ S/C Pointing Loss	[80]	-0.9	-0.9	N/A
Ground Station Parameters				
GS Antenna Diameter [m]	[75]	15	35	35
GS G/T [dB/K]	Assumption 2	38.467	50.450	50.450
GS Losses	Assumed based on [49]	-2	-2	-2
Losses				
Free Space Losses	$L_s = 92.45 + 20\log(d) + 20\log(f)$	-223.054	-234.672	-234.672
Atmospheric Losses	Assumption 4	-0.5269	-0.5269	-0.5269
Precipitation Losses	Assumption 5	-0.75	-0.75	-0.75
Net Path Losses	$L_{path} = L_s + L_{atm} + L_{prec}$	-224.368	-235.986	-235.986
Combined Losses	$L_{comb} = L_{path} + L_{in} + L_{point}$	-227.268	-238.886	-237.986
Link Performance				
Carrier-to-Noise Ratio	$C/N_o = EIRP + G/T - L_{comb} + 228.6$	73.597	73.962	20.862
Required SNR	Table 4.10	1.1	1.1	-0.25
Required Link Margin	[74]	3	3	3
Required SNR with Margin	Addition	4.1	4.1	2.75
Data Rates				
Supportable Bit Rate [dB-Hz]	$R_b = C/N_o - E_b/N_o$	69.497	69.862	18.112
Supportable Bit Rate [bps]	Conversion	8,906,168	9,686,664	64.74
Supportable Iris Bit Rate [bps]	[78]	8,192,000	8,192,000	62.5
Coding Efficiency [-]	Table 4.10	0.5	0.5	1/6
Downlink Information Rate [bps]		4,096,000	4,096,000	10.42

Table 4.14: Uplink Link Budget

Parameter [dB unless stated]	Source	Lunar Distance	Transfer Distance	Lost in Space
Uplink Frequency [GHz]	Centre of selected ITU/ECSS band	7.212	7.212	7.212
Uplink Bit Rate [bps]	Iris supported rates [78], uncoded	8000	8000	2000
Uplink Bit Rate [dB-Hz]	Conversion	39.031	39.031	33.010
Distance to Ground Station [km]	Astrodynamics maximum distance	400,000	1,524,000	1,524,000
Ground Station Parameters				
GS Antenna Diameter [m]	[75]	15	35	35
GS EIRP [dBW]	Assumption 2	82.8	107.5	107.5
Spacecraft Parameters				
S/C Rx Antenna Gain [dBi]	[81]	12.4	12.4	-25
S/C Line Loss	Assumed based on [85]	-1	-1	-1
S/C Receiver Noise [dB]	[78]	5	5	5
S/C Antenna Noise Temp. [K]	Assumed based on [86]	290	290	290
Losses				
Free Space Losses	$L_s = 92.45 + 20\log(d) + 20\log(f)$	-221.652	-233.271	-233.271
Atmospheric Losses	Assumption 4	-0.5269	-0.5269	-0.5269
Precipitation Losses	Assumption 5	-0.75	-0.75	-0.75
Net Path Losses	$L_p = L_s + L_{atm} + L_{prec}$	-222.929	-234.548	-234.548
Combined Losses	$L_{comb} = L_{path} + L_{in} + L_{point}$	-223.929	-235.548	-235.548
Noise				
Effective Sys. Noise Temp. [K]	$T_S = T_{ant} + (F_R - 1)T_0$ [86]	917.061	917.061	917.061
Effective Sys. Noise Temp. [dBK]	Conversion	29.624	29.624	29.624
Receiver G/T [dB/K]	$G/T = G_{Rx} - T_S$	-17.224	-17.224	-54.624
Link Performance				
Carrier-to-Noise Ratio	$C/N_o = EIRP + G/T - L_{comb} + 228.6$	70.247	83.328	45.928
Predicted SNR	$(E_b/N_o)_{\text{pred}} = C/N_o - R_b$	31.216	44.297	12.918
Link Margin	$M_L = (E_b/N_o)_{\text{pred}} - (E_b/N_o)_{\text{req}}$	21.616	34.697	3.318

As shown in Table 4.13, the spacecraft is capable of achieving the maximum bit rate of the Iris transponder, 8,192,000 bps. This is achieved through the use of Turbo 1/2 FEC, allowing a downlink information rate of 4,096,000 bps. This far exceeds the requirements during both transfer and science. In the lost-in-space case, Turbo 1/6 FEC is employed in order to overcome the extremely low gain. The link budget closes, with a low bit rate of just 10 bps. However, this should be sufficient to allow for recovery of the spacecraft signal at the ground in the event of a loss of pointing accuracy.

In the uplink case, Table 4.14, the maximum bit rate of the Iris is again achieved, with an 8000 bps uplink capacity achieved with an extremely large link margin. During the lost-in-space case the requirements are exceeded, with an uplink bit rate of 2000 bps achievable.

4.3.5. Redundancy and Sustainability

The general configuration, with two separate sets of antennae is in accordance with the redundancy strategy laid out in Section 3.6.5. The second set of antennae means that should the reflectarray fail to deploy the spacecraft will still retain the ability to communicate, albeit at a greatly reduced data rate. Furthermore, the lower gain of the second transmit antenna allows for improved re-acquisition of signal in the event of a pointing failure, improving

the capacity of the spacecraft to recover from certain failure cases.

From a sustainability perspective, aside from the items outlined in the Sustainability Policy in Section 2.4, the issue of radio spectrum pollution must also be considered during communications system design. Radio spectrum pollution occurs when ”stray” radio waves interfere with other applications such as the communications of other radio systems[9]. This is taken into account by a strict adherence to ECSS regulations on spectrum management, in order to mitigate the risk of the communications systems aboard ARCHER causing electromagnetic interference.

4.3.6. Verification

This section deals primarily with verification procedures for the functioning of the Communications subsystem itself. The link budget calculations were analytical calculations and were verified by hand calculating with the same inputs to achieve identical values and by altering the inputs to compare results with similar calculations carried out in literature.

As many of the communications system components will be custom designed, extensive verification testing will be required. Comprehensive antenna testing in an anechoic chamber will be required to characterise the antennae accurately. This characterisation will allow for an improved link analysis prior to launch of the spacecraft.

When the components are combined together, compatibility testing with the Estrack network will be required. Furthermore, upon integration of the spacecraft, electromagnetic compatibility testing will be required in order to verify the system and antenna noise figures when exposed to the interference caused by other aspects of the spacecraft.

4.4. Attitude Determination and Control System

In order to point the spacecraft in a specified direction to gather the highest quality science and due to random perturbations, it is necessary to have an Attitude Determination and Control System (ADCS). In this section, the x-axis is defined as the roll-axis, which is parallel to the primary propulsion system; the y-axis is defined as the pitch-axis, which is parallel to the solar arrays length; the z-axis is defined as the yaw-axis. Note that all torque values do not include its direction (wheel needs to spin in the opposite direction of desired body movement).

4.4.1. Requirements and Modes

In addition to the system requirements as detailed in Section 3.1, the following requirements were introduced for the ADCS:

- [TEC-ADCS-01] The spacecraft shall be able to determine attitude with an accuracy of $1°$.
- [TEC-ADCS-02] The spacecraft shall be able to control attitude with an accuracy of $1°$, 3σ.

These are more than sufficient for the payload and communication requirements, as well as being perfectly feasible. Some extra requirements have been introduced for the detailed design. These were necessary for the more detailed control modes.

- [TEC-ADCS-03] The solar panels and antenna shall be positioned in the correct direction, after deployment.
- [TEC-ADCS-04] The spacecraft shall be able to actively detumble for tip-off rates up to 10°/s. [87]
- [TEC-ADCS-05] The spacecraft shall be able to detumble within 30 minutes.
- [TEC-ADCS-06] The spacecraft shall be able to slew at least 30° in 30 seconds (1°/s).
- [TEC-ADCS-07] The spacecraft shall be able to point the antenna and solar panels in safe mode.

In addition to these, the subsystem must apply the redundancy philosophy as detailed in Section 3.6.

4.4.2. ADCS Modes

In addition to the requirements outlined in Section 4.4.1, the ADCS also depends on the propulsion, EPS and structure subsystems. Initially the ADCS needs to control the attitude during transit to its destination. When in

[9] www.ictregulationtoolkit.org/toolkit/5.2.5 [Retrieved 29 June 2018]

orbit, the mission pointing requirements are leading. Modes, with activated devices, can be found in Table 4.15. With the devices described in Section 4.4.5.

Table 4.15: Activated ADCS devices during the modes

Mode	Description	Devices
Acquisition (detumbling)	For detumbling, the IMU is used for attitude determination, reaction wheels for completely stopping the spacecraft and the thrusters for decreasing tumbling rates and desaturation of the reaction wheels. For initial acquisition, the IMU and sun sensors are used to point the solar arrays and antenna in the correct direction. Reaction wheels used when necessary.	Sun sensors IMU Reaction wheels Thrusters
Normal mission	The star tracker is the main attitude determination device, reaction wheels will be used to control the attitude and thrusters to desaturate the reaction wheels, when necessary.	Star tracker Reaction wheels Thrusters
Slew	Same as the normal mission mode. Used for orientating the spacecraft.	Star tracker Reaction wheels
Contingency (safe)	The sun sensors and IMU will be used to determine the attitude and keep the solar array pointed towards the sun. Thruster are used to control the attitude, if necessary. Used in emergencies or in the case of disabled systems.	Sun sensors IMU Thrusters

As obtained in Section 4.6 and Section 4.3, the mission requires small, continuous, rotations to be performed; the ADCS will be designed for stand-alone performance. However, to increase efficiency, the stored momentum can be used for some of these rotations, which decreases the total impulse required to desaturate.

4.4.3. Characteristics, Stability and Control

For designing the ADCS, the stability and control characteristics will need to be computed. Variables can be found in [17], when applicable, changes will be stated. Assuming the worst case mass of 24kg (maximum mass of 12U CubeSat, according to the standard), equally distributed with the centre of mass at the geometrical centre; the mass moment of inertia of the undeployed and deployed spacecraft can be found in Eq. (4.2) and Eq. (4.3) respectively. For the computation of these values, the rigid-body assumption is made.

$$J_{\text{initial}} = \begin{bmatrix} 0.374 & 0 & 0 \\ 0 & 0.365 & 0 \\ 0 & 0 & 0.221 \end{bmatrix} [kg \cdot m^2] \quad (4.2) \qquad J_{\text{deployed}} = \begin{bmatrix} 0.549 & 0 & 0 \\ 0 & 0.354 & 0 \\ 0 & 0 & 0.365 \end{bmatrix} [kg \cdot m^2] \quad (4.3)$$

A new parameter (from [17]) to be computed is the total impulse required for detumbling, see Eq. (4.4). In Eq. (4.4); J_{ii} is the mass moment of inertia from Eq. (4.2); ω_t is the tip-off rate (in rad/s) that needs to be countered, and L_i is the thruster arm (assumed to be 0.05 m along all axes). Initially the thrusters are used to decrease the angular rates, followed by the use of reaction wheels, at rates of 0.5 °/s, to bring the spacecraft to a complete stop. The momentum that needs to be stored in the reaction wheels for this, is: $(J_{ii}\omega_{t_{wh}}) = [3.27, 3.19, 1.93]^T$ $[\text{m}Nms]$. With this method, the total impulse that is required will stay the same, due to desaturation. Since no power is produced before deployment, consumption needs to be limited; this way, detumbling can be done accurately while still limiting power consumption.

$$I_{tot_{de}} = \sum_{i=1}^{3} \frac{J_{ii}\omega_t}{L_i} = 3.35\ [Ns] \quad (4.4) \qquad T_{\text{slew}} = \frac{4\theta J_{jj}}{t_{\text{slew}}^2} = \begin{bmatrix} 1.28 \\ 0.82 \\ 0.85 \end{bmatrix} [\text{m}Nm] \quad (4.5)$$

The required torque, to achieve [TEC-ADCS-06], is computed in Eq. (4.5) [49]. With the angular displacement (θ) and the slew time (t_{slew}). Note that J_{jj} is obtained from Eq. (4.3).

$$F_{req} = \frac{J_{ii}\omega_t - J_{ii}\omega_{t_{wh}}}{L_i t} = \begin{bmatrix} 0.676 \\ 0.673 \\ 0.409 \end{bmatrix} [\text{m}N] \quad (4.6)$$

The thrust required for [TEC-ADCS-05] is provided in Eq. (4.6). Note that this is the minimal thrust required, where $(j_{ii}\omega_{t_{wh}})$ is subtracted due to the last 0.5 °/s being detumbled by the reaction wheels.

Disturbance torques

As discussed in [17], the solar radiation pressure (T_{SRP}) will be the dominating disturbance torque throughout the normal mission, and can be computed with Eq. (4.7). Note that it does not account for counteracting cyclic moments, which would decrease the net torque. In addition, it is assumed that only the solar arrays and reflectarray produce a torque. Although the gravity gradient torque (T_{GGT}) is much lower, as computed in Eq. (4.8), it is accounted for. Furthermore, external disturbance torques are assumed equal during transit.

$$T_{SRP} = \begin{bmatrix} r_x \\ r_y \\ r_z \end{bmatrix} \times \frac{E_e}{c}(1+q)\cos(\theta)\hat{N} = \begin{bmatrix} 0 \\ 0.557 \\ 0 \end{bmatrix} [\mu Nm] \quad (4.7) \qquad T_{GGT} = \frac{3\mu}{2R}|J_x - J_z|\sin(2\theta_P) = \begin{bmatrix} 0 \\ 37.7 \\ 0 \end{bmatrix} [\mathrm{n}Nm] \quad (4.8)$$

The average irradiance (E_e), the speed of light (c), the reflective factor (q) of 0.6, the angle of the principal axis (θ_P) of 5° and the gravity constant (μ) of the moon, are taken from [17]. The distance between the centre of solar pressure and centre of mass (r_x) is conservatively assumed to be 10 cm. This is due to the positioning of the solar array, at the top. Note that it assumes the worst case, which is the solar incidence angle (θ) of 0°, in combination with the solar array parallel to the roll-axis. In this case the unit force vector ($\hat{N}$) is in one direction, and thus, the torque is maximised. The sunlit area (A_s) is 0.36 m^2 as computed in Section 4.6. In addition, it is assumed that the centre of mass is located at the geometrical centre of the spacecraft, in the deployed state. Because the solar array is symmetrically deployed, the torque around the roll-axis is counteracted; the centre of pressure is located perpendicular to the yaw-axis. As a result, all momentum is stored in the pitch-axis. The acceptability of this assumption is shown in Section 4.4.7. Note that T_{SRP} consists of two different values; the solar arrays use the variables as mentioned earlier, and for the reflectarray, the sunlit area is 0.18 m^2 as determined in Section 4.3, r_x is 20 cm and q is assumed to be a factor of 0.8. The reflectarray location also gives a non-zero r_z, however, due to the assumed unit force vector this does not create a torque. The momentum stored, in one orbit, is computed with Eq. (4.9) [49].

$$h_y = \frac{T_D P \frac{1}{2}\sqrt{2}}{4} = 3.58\ [\mathrm{m}Nms] \qquad (4.9) \qquad I_{tot_{ex}} = \sum_{i=1}^{3} \frac{h_i}{L_i} = 143.03\ [Ns] \qquad (4.10)$$

The disturbance torque (T_D) is the sum of Eq. (4.7) and Eq. (4.8). This method assumes momentum is accumulated in a quarter of the period (P) and is the same for transit. In Eq. (4.10), the total impulse required to dump the momentum of the external disturbance torques, accumulated in 2000 orbits, is computed. Note that the stored momentum (h_i) is in the pitch-axis.

In addition to the external disturbance torques, internal disturbance torques such as thruster misalignment need to be accounted for. As discussed in Section 2.5, no orbit maintenance is required, however, some Δv is allocated for backup. In the event that this would be necessary, it is minimised due to the gimbal of the BIT-3, which means thruster misalignment poses a minor issue.

Other, smaller, internal disturbance torques to consider are: Pointing rotation of the solar arrays, deployment of the antenna, solar arrays and boom for the magnetometer. Propellant slosh, which is only created by the RCS thrusters since the BIT-3 uses solid propellant, and is negligible [88]. Finally, for reaction wheel imbalance, misalignment is assumed to be negligible.

An improvement for the design can be made by using, more, in-depth modelling of the disturbances, rather than using conservative computations. However, this should only be done for the driving disturbances as modelling increases cost, which, at a certain point, is not worth the better tailored design.

4.4.4. Component Selection

In this subsection, the trade-offs for the ADCS hardware will be executed. These trade-offs will have different parameters, depending on the critical aspects, and will have the value of the COTS item in the table. Mass, volume, power and TRL will always be considered; cost will not be considered because the budget will not be violated for the COTS items. Some costs are not specified by companies, however it can be assumed that the costs will not be considerably higher and hence does not pose a problematic constraint.

European options are preferred, but only if the performance is not significantly affected. All parameters in the trade-off will be considered with equal weight. However, since mass and power will be more limiting than the volume, these will be the deciding factors, given that all requirements are satisfied.

Actuators

As discussed in [17], reaction wheels will be used for attitude control. Since four wheels will be required, three for axis control and one for redundancy, mass will be a large constraint. The accuracy of 1° will not be an issue and hence, this is not considered for the trade-off. The reaction wheel trade-off can be seen in Table 4.16.

Table 4.16: Reaction wheel trade-off

Parameter / COTS	Momentum [mNms]	Torque [mNm]	Mass [g]	Volume [cm^3]	Peak power [W]	TRL [-]
Hyperion RW400 [89]	green 60	sky blue 2	red 340	sky blue 68.75	sky blue <2.5	orange 7
GSW-600 [90]	sky blue 19	sky blue 2	sky blue 180	sky blue 52.27	sky blue 2.55	sky blue 8
BCT RWP050 [91]	green 50	green 7	orange 240	sky blue 84.1	sky blue <1	green 9
BCT RWP015 [91]	sky blue 15	green 4	green 115	green 33.52	sky blue <1	green 9
CubeWheel Medium [92]	sky blue 10	orange 1	sky blue 140	sky blue 66.65	sky blue <1.5	orange 7

blue European | yellow Non-European | green Optimal | sky blue Acceptable | orange Correctable | red Unacceptable

Hyperion RW400 can be discarded due to the mass. BCT RWP050 can be considered with a reduction to three wheels. This would increase the momentum storage in each axis and thus decrease the amount of desaturation manoeuvres required (minimises jitter). However, it would also eliminate the redundancy, and still increase mass by 56.5% compared to four BCT RWP015. Furthermore, the more frequent desaturation manoeuvres, is of lesser significance for environmental measurement missions. The BCT RWP015 satisfies the requirements, as calculated in Section 4.4.3, and it allows for redundancy. The only disadvantage is the country of origin (US). Hence, four GSW-600, in combination with the pyramid mount, provided by GOMspace, will be used.

Using reaction wheels requires momentum management, which can only be done by thrusters due to the lack of a magnetic field. In the case of ARCHER, a separate thruster system is required because the propulsion system uses the BIT-3 engine; an alternative option is to use gimbals. However, complexity increases significantly due to this; mass is not an issue because the standard BIT-3 has a gimbal mounted. Furthermore, this option was discussed with Dr. A. Cervone (TU Delft), who discouraged the use of gimbals due to perturbations caused by the BIT-3.

Many propulsion options are available for said microthruster system. However, only two are not readily unfeasible which are cold gas and electrospray thrusters. The reasons are as follows: Both bipropellant and monopropellant liquid propulsion systems are too heavy, the first one due to the feed system, and both due to the sum of the thruster masses; hybrid, resistojet and pulsed-plasma propulsion systems, at the scale required, have a TRL level below 7; solid propulsion contains pyrotechnics, which violates the CubeSat standard; the power consumption of, both, ion and hall thrusters violates the requirements.

For desaturation, at least four thrusters are required, with more being better for redundancy and a more flexible configuration. The trade-off for the thruster options can be seen in Table 4.17. Furthermore, VACCO has been contacted, and they have indicated that their MiPS units can be delivered in any size above the minimum; with a linear relationship between mass and volume, and a polynomial[10,11] relating mass and total impulse. Using the values from the system data sheets one can size for the exact total impulse required, and thus their thrusters will be sized accordingly. In addition, only thrusters with the ability to be placed in any orientation within the CubeSat are considered. For example, the VACCO CuSP Propulsion System, was excluded, as it can only be stacked on top of other subsystems. For the TILE 50, four single thrusters are considered.

[10] Standard $I_{tot} = 1.087 \cdot 10^{-20}x^2 + 0.292926x - 114.729$ (based on four COTS options, x in [g])
[11] End-Mounted $I_{tot} = -2.14665 \cdot 10^{-6}x^2 + 0.299138x - 108.325$ (based on four COTS options, x in [g])

Table 4.17: Thruster trade-off

Parameter / COTS	Total impulse [Ns]	Thrust [mN]	Mass [kg]	Volume [cm^3]	Peak power [W]	TRL [-]
yellow MiPS Standard [93]	sky blue 143	green 10	sky blue 0.88	sky blue 640	sky blue 10	green 9
yellow MiPS End-Mounted [94]	sky blue 143	green 10	sky blue 0.85	sky blue 790	sky blue 10	green 9
yellow MarCO propulsion [95]	green 755	green 25	orange 3.49	orange 254.7	sky blue 10-15	green 9
yellow TILE 50 [96]	green 240	red 0.05	green 0.20	green 100	green 1.5	orange 6-7

blue European | yellow Non-European | green Optimal | sky blue Acceptable | orange Correctable | red Unacceptable

Although the TILE 50 has very advantageous budget properties and could even function as a fully redundant stand-alone ADCS [97, 98], insufficient thrust makes it unfeasible. Considering that the thrust of the TILE 50 is 0.05 mN, 14 thrusters on the pitch- and roll-axes, and nine thrusters on the yaw-axis would be required to satisfy [TEC-ADCS-05]. This would result in reliability and spatial distribution issues, which is a significant risk factor; it would also require a power of 27 W for 30 minutes, which is unfeasible before the solar array is deployed. Hence, only the cold gas thrusters remain.

Of the cold gas thrusters, the MiPS Standard is the superior option: With only a slightly higher mass than the MiPS End-Mounted, the volume is significantly lower. This is due to the fact that the MiPS End-Mounted makes use of the ”tuna can” volume, which cannot be utilised in ARCHER´s design. This makes the option space-inefficient and would limit the thruster placement as well.

Sensors

The sensors are quite small and light and will thus not pose a constraint. Several considered sensors can be seen in Table 4.18. Note that more COTS sensors have been considered but one optimal per company has been chosen, not including different types. As discussed in [17], only sun sensors, star trackers and gyroscopes will be considered. Initially, a combination of sun sensors and gyroscopes was chosen, however after consulting with ISIS Delft, it was decided to include a star tracker.

Table 4.18: Stand-alone sensor trade-off

Parameter / COTS	Accuracy [°](3σ)	Slew rate [°/s]	Mass [g]	Volume [cm^3]	Peak power [W]	TRL [-]
blue Hyperion ST400 [99]	green 0.0028 (pitch,yaw) 0.033 (roll)	orange >0.5 (tip,tilt) >1 (roll)	sky blue 280	sky blue 261.95	sky blue 1	green 9
yellow BCT Standard NST [99]	green 0.0017 (pitch,yaw) 0.011 (roll)	green >10	sky blue 350[12]	sky blue 275	sky blue <1	green 9
yellow MAI-SS Space Sextant [100]	green 0.0011 (pitch,yaw) 0.0075 (roll)	sky blue >2	sky blue 170	sky blue 250.25	red 2.31	sky blue 8
blue Hyperion SS200 [101]	red <1	red -	green 2	green 1.8	green 0.04	sky blue 8
yellow NFSS-411 [102]	sky blue <0.1	red -	green 35	green 21.76	green 0.13	green 9
blue nanoSSOC-D60 [103]	sky blue <0.5	red -	green 6.5	green 3.55	green <0.115	green 9

blue European | yellow Non-European | green Optimal | sky blue Acceptable | orange Correctable | red Unacceptable

[12] Including baffle

In Table 4.18, it can be seen that the accuracy is not a problem, even for the sun sensors, but the slew rate can be. Note that Table 4.18 is for a stand-alone sensor, the sun sensors can thus be used in combination with the star tracker. The Hyperion ST400 could satisfy the slew rate requirement by combining it with an IMU. However, no baffle is included yet and the mass, volume and power advantages are negligible; it leaves no room for redundancy and ITAR is of a lesser concern for CubeSats. The result is the selection of the Blue Canyon Technologies Standard NST. It more than satisfies the requirements and fits within the allocated mass and power budget. An extra advantage is that it has been tested in deep space by MarCO[13] and the Lunar IceCube[14].

Coarse sun sensors will be used for ADCS functioning in safe mode and acquisition. For this, six Hyperion SS200 are selected to cover all axes. The accuracy for initial acquisition is adequate for both the nanoSSOC-D60 and SS200; the TRL is lower for the SS200, but the mass and power consumption is also much lower. Hence, the SS200 is selected. After initial acquisition, the star tracker will be driving.

Gyroscopes and accelerometers will be combined to form an IMU (Inertial Measurement Unit) for 3-axis control. The IMU is used to determine both the attitude between star tracker updates (when necessary) and the initial detumbling of the spacecraft (post launch). The trade-off can be seen in Table 4.19.

Table 4.19: IMU trade-off

Parameter / COTS	Angular rate [°/s]	Acceleration [g]	Mass [g]	Volume [cm^3]	Peak power [W]	TRL [-]
blue STIM300 [104]	green ±400	green ±10	sky blue <50	sky blue 37.18	red 2	sky blue 8
yellow GyroCube3F [105]	green ±150	green ±2	green 8.2	green 18.20	green 0.205	sky blue 8
blue DMU11 [106]	green ±300	green ±10	green 4	green 5.13	sky blue 0.5	orange 7

blue European | yellow Non-European | green Optimal | sky blue Acceptable | orange Correctable | red Unacceptable

Considering that the European STIM300 requires significantly more power and mass, it is discarded. The O-Navi GyroCube3F is optimal, because little power is required and its capabilities are well within the requirements. However, it is American, and thus the DMU11 from Silicon Sensing is selected.

Conclusion

For European CubeSat launches, ITAR is less restrictive[15]as compared to most countries. However, there is always a probability that problems will arise; it is opted to take European options, or at least non US, wherever possible. For the micro propulsion system, no equivalent alternative is available; the star tracker could be designed with European options. However, this would require the constant use of the IMU during slew, and thus should only be used in the event of ITAR issues.

4.4.5. Subsystem Configuration

After the selection of the components, the configuration can be finalised. Instead of using the on-board computer, it was decided to implement a dedicated ADCS computer. This way, some decentralisation is build-in, in case of partial CDH failure, and the on-board computer can accommodate the processing needs of the payload better. Given the composition of the design, the integrated electronics based on the Blue Canyon Technologies XACT is a good option. It uses an European processor, as such, it is ITAR free. The processor board consists of: An FPGA with LEON soft-core processor (LEON3FT IP); Synchronous Cynamic Random-Access Memory (SDRAM), Dual-Ported Random-Access Memory (DPRAM) and Flash memory; interfaces for the reaction wheel and thruster drivers, A2D converters, SPI and Inter-Integrated Circuit (I2C), GPSR data interface and microsecond 1PPS timing; latching relay for image boot selection and volt regulators.[107] It is capable of enduring the 'deep space'

[13] https://directory.eoportal.org/web/eoportal/satellite-missions/m/marco [Retrieved 8 June 2018]
[14] https://directory.eoportal.org/web/eoportal/satellite-missions/l/lunar-icecube [Retrieved 8 June 2018]
[15] https://www.lexology.com/library/detail.aspx?g=f1958030-537d-40dd-aeef-1f363dcd1797 [Retrieved 2 July 2018]

radiation environment, as it is used on MarCO[13] and Lunar IceCube[14] as well as Earth orbit MinXSS[16].

Extra considerations are: Uncertainties in the variation of the moments of inertia, caused by consumption of propellant and the rotating solar panels; friction of the reaction wheels due to discontinuity (can be mitigated by implementing triangle wave dither in the voltage input of the wheel motor [108]), and the small perturbations of constant solar radiation pressure can reduce control accuracy. However, this can be mitigated by using an extended state observer to estimate the effect of the disturbances and compensate for them in the control [109]. To reduce jitter even more, a passive vibration source isolator can be included for each axis.

As for software; multi-rate system with real-time OS, commands (SLOC 1,000), telemetry (SLOC 3,500), fault protection & autonomy (SLOC 11,500), attitude orientation command (SLOC 1,000), attitude determination & control (SLOC 10,800), time keeping (SLOC 700), orbit propagation (SLOC 8,500), high-precision reference vectors (SLOC 4,000), momentum control (SLOC 3,000), wheel control (SLOC 1,200), thruster control (SLOC 600-1,200) and table management (SLOC 5,800) will be implemented. This can be done using Matlab/Simulink [107]. In addition, a Kalman filter (SLOC 6,000-10,000) will be implemented for the attitude determination [110]. With Source Lines of Code (SLOC) estimated, based on [49]. A fast quaternion Triaxial Attitude Determination (TRIAD) algorithm would require two star trackers and hence, will not be used [111].

Furthermore, planned control manoeuvres, such as pointing for communication, can be initiated earlier (preventing large rotations) to reduce the required demands on the system. For attitude control a Proportional, Integral and Derivative (PID)-controller is usually used, and can be modelled as function of time, in reaction to attitude deviations (delta-signal ϵ); with the respective PID-controller parameters (K), the control variable ($u(t)$) is being updated in an effort to minimise the error [51]:

$$u(t) = K_P\epsilon(t) + K_I\int \epsilon(t)dt - K_D\frac{d\epsilon(t)}{dt} \qquad \omega_n \approx \left(\frac{K_P}{J_{jj}}\right)^{\frac{1}{2}}$$

The bandwidth of the control system (ω_n) is mostly determined by the proportional gain (K_P), which can be set to any value that satisfies: ($K_P > T_D/\theta_{\max}$), with $\theta_{\max}$ being [TEC-ADCS-02] [49]. The optimal value of K_P is determined by trading-off more accuracy (for higher values), with higher stability margin (for lower values). To compensate for the decreased stability margin, the derivative gain (K_D) can be increased but this will slow the response. There are many methods for determining the optimal values of these gains, such as the linear-quadratic regulation (LQR) and other state space methods [49]. In contrast to a PD-controller, the PID is capable of removing the steady-state error (caused by continued presence of disturbances) at the cost of a reduction in stability margin. Unfortunately, a more detailed software design cannot be provided, as this is not within the scope of the current report. The configuration of the ADCS is depicted in Fig. 4.17.

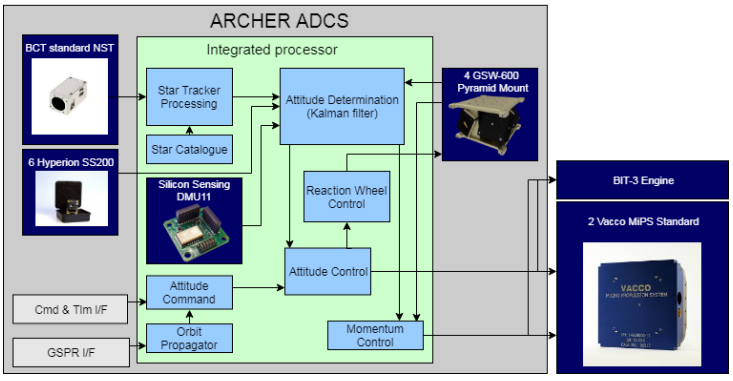

Figure 4.17: Configuration of Attitude Determination and Control System

For the reaction wheels; the pyramid mount of 30°, provided by GOMspace, is used. There are several optimising algorithms for the tetrahedral configuration angle [112, 113], however, this would require designing a mount and thus not using COTS. Furthermore, although the roll-axis requires the most torque (highest inertia and most rotations), almost all momentum is stored in the pitch-axis; torque is no issue, as computed, hence the placement

[16] https://directory.eoportal.org/web/eoportal/satellite-missions/m/minxss [Retrieved 13 June 2018]

around the pitch-axis. This changes the torque and momentum storage, as derived from the capacity of the four wheels, in each axis to:

$$\begin{bmatrix} 0 & \frac{1}{2}\sqrt{3} & 0 & -\frac{1}{2}\sqrt{3} \\ \frac{1}{2} & \frac{1}{2} & \frac{1}{2} & \frac{1}{2} \\ \frac{1}{2}\sqrt{3} & 0 & -\frac{1}{2}\sqrt{3} & 0 \end{bmatrix} \begin{bmatrix} T_1 \\ T_2 \\ T_3 \\ T_4 \end{bmatrix} = \begin{bmatrix} 3.46 \\ 4 \\ 3.46 \end{bmatrix} [\mathrm{m}Nm] \quad \begin{bmatrix} 0 & \frac{1}{2}\sqrt{3} & 0 & -\frac{1}{2}\sqrt{3} \\ \frac{1}{2} & \frac{1}{2} & \frac{1}{2} & \frac{1}{2} \\ \frac{1}{2}\sqrt{3} & 0 & --\frac{1}{2}\sqrt{3} & 0 \end{bmatrix} \begin{bmatrix} h_1 \\ h_2 \\ h_3 \\ h_4 \end{bmatrix} = \begin{bmatrix} 32.91 \\ 38 \\ 32.91 \end{bmatrix} [\mathrm{m}Nms]$$

The momentum that will be stored due to the disturbance torques can then be obtained with the (Moore-Penrose) pseudo-inverse of the transformation matrix. In one orbit, using the pure pitch-axis momentum from Section 4.4.3, this results in the storage division:

$$\begin{bmatrix} 0 & \frac{1}{\sqrt{3}} & 0 & -\frac{1}{\sqrt{3}} \\ \frac{1}{2} & \frac{1}{2} & \frac{1}{2} & \frac{1}{2} \\ \frac{1}{\sqrt{3}} & 0 & -\frac{1}{\sqrt{3}} & 0 \end{bmatrix}^T \begin{bmatrix} h_x \\ h_y \\ h_z \end{bmatrix} = \begin{bmatrix} 1.79 \\ 1.79 \\ 1.79 \\ 1.79 \end{bmatrix} [\mathrm{m}Nms]$$

With this worst case situation, desaturation will have to be executed every 10.63 orbits, which is often. However, as mentioned in Section 4.4.4, the jitter caused by more frequent desaturation is of lesser concern for environmental measurement missions.

Furthermore, two sun sensors will be placed on every axis, for full field of view. Since the SS200 has low mass and power consumption this is preferred, because no sun searching algorithm to account for insufficient field of view has to be implemented. The BCT standard NST determines the attitude by obtaining data of the stars in space, which is compared to an on-board catalogue of more than 23,000 stars to identify known constellations and calculate the precise three-axis orientation. Note that the output consists of quaternions, which significantly reduces the I/O handling and accompanied processing but potentially makes fault tolerance more difficult, after failure.

Thruster design

For the thruster system, two VACCO Standard MiPS are used, placed on the upper left and lower right of opposing sides, as shown in Section 5.1.1. This increases the effective arm with respect to the assumed arm in Section 4.4.3, and thus decreases the total impulse (I_{tot}) required. In addition, no standard exhaust hole placement and orientation needs to be used according to VACCO, which means that these can be optimised. This was realised by using a script discussed in this section. Note that the placement takes into account that most of the momentum will be stored in the pitch-axis.

The exact placement was limited to a square formation due to the scope of the project, with exhaust holes thrusting at an angle of 90° relative to each other. In order to keep development and manufacturing costs to a minimum both blocks were assumed to be identical, with one being turned 90° relative to the other. The current thruster configuration can be seen in Fig. 5.2, with the arrows pointing in the direction of cold gas expulsion. However, this configuration is subject to change.

It was determined that the best moment arm around the pitch-axis for both thruster blocks was achieved at an angle of 30° relative to the face of the block. The results are depicted in Table 4.20 and Table 4.21. These have been calculated by the means of a Python program. This Python program has been verified by comparing some of its results with results calculated by hand. These were found to match exactly.

Table 4.20: Effective thruster arms of the ”engine” block

Thruster	Roll-axis [m]	Pitch-axis [m]	Yaw-axis [m]
Top right	0.02	0.17	-0.01
Top left	-0.06	0.00	-0.04
Bottom left	-0.11	0.06	-0.12
Bottom right	0.11	0.06	0.07
Middle	0.00	0.15	-0.05

Table 4.21: Effective thruster arms of the ”antenna” block

Thruster	Roll-axis [m]	Pitch-axis [m]	Yaw-axis [m]
Top right	-0.01	-0.17	0.02
Top left	-0.17	-0.04	-0.06
Bottom left	0.09	-0.01	0.02
Bottom right	-0.01	0.12	-0.02
Middle	-0.05	-0.05	0.00

Using Eq. (4.10) with the optimal arm, a total impulse of 42 Ns is required to desaturate the stored momentum due to external disturbances. In addition, momentum around the roll- and yaw-axes will be dumped at a less optimal arm, and due to the risk of (partial) failure, a margin of 100% is added. An additional reason for the margin is the increased complexity of the firing sequence to account for net-forces. Hence, the blocks are designed for a total impulse of 84 Ns. This includes detumbling, since the total impulse required is negligible. This means that two 0.3 U (the smallest possible dimension) MiPS Standard thrusters can be used for a total of 88 Ns. Furthermore, an improvement could be made when more exact angle options are provided by VACCO. With this configuration, and neglecting the complex thrust sequence, dumping 38 mNms in the pitch-axis would take ~ 22 s given a thrust of 10 mN.

The thrusters are radiation tolerant depending on customer request, hence this is no issue, and a minimum resistance of 20 kRad is expected to be achievable. The block uses a RS422 digital interface, includes an integral sensor suite and closed-loop, vector pointing and thrust vector control. It is recommended that further development takes place in collaboration with VACCO in order to ensure most efficient exhaust hole placement and orientation, as well as sufficient radiation tolerance.

Components

In Table 4.22, the final component composition can be seen. Note that this includes the relevant margin for COTS and MCOTS. It exceeds the preliminary budget mentioned in Section 3.2, as a result of the inclusion of the thruster system.

Table 4.22: Budget allocation of the components

Component	Quantity [-]	Mass [g]	Dimensions [mm]	Cost [€]
GOMspace - Pyramid mounted GSW-600	1	987	96.6×96.6×62.7	67,200
Blue Canyon Technologies - Standard NST	1	367.5	101.7×68.5×50.8	64,135.89
Hyperion Technologies - SS200	6	2.1	20.3×15.3×6.1	4,000
Silicon Sensing - DMU11	1	4.2	22.4×22.4×10.8	213.2
VACCO - Standard MiPS (price estimate)	2	569.1	101.7×101.7×30.5	100,000
Dedicated OBC (estimate based on NanoMind Z7000 [114])	1	77	69.2×42.6×7	25,000
Total	-	2586.5	1.6 [U]	380,549.1

4.4.6. Redundancy

As discussed in Section 3.6.5; designing for redundancy is a complex matter, which has no uniform consensus. For a complex system such as the ADCS, it is of utmost importance to implement some redundancy.

The design includes four reaction wheels, one for redundancy, placed in a pyramid configuration. Furthermore, to reduce jitter, desaturation will be done before reaching 19 mNms (10 orbits), where the wheel rate, and thus the internal disturbance, is largest. The design includes a contingency for stopping desaturation, to account for the net-force of the thrusters. Momentum management is an integral part of control using reaction wheels, as such, some redundancy for this has to be implemented. It was considered to use one block on a centre axis. However, due to configuration constraints, it was opted to implement two separate blocks for nominal functioning, and the BIT-3 gimbal for redundancy. If one fails, momentum management can still be performed.

Furthermore, computations to test the possibility of 'complete' redundancy, using the thrusters were executed. To determine this, the equation relating the minimum impulse bit (I_{min}) and the arm (L_i) with the angular momentum, the equation relating the angular momentum with angular velocity, and the equation relating angular velocity with angular displacement (θ) are combined as seen in Eq. (4.11).

$$t = \frac{\theta J_{jj}}{L_i \times I_{min}} \tag{4.11}$$

In this equation, it is assumed that attitude control manoeuvres always result in an overcompensation of a full impulse bit. Higher values of time (t) are desired, since this allows for sufficient accuracy for longer. The worst case scenario occurs when the ratio of effective arm to the moment of inertia is maximised. By dividing the

respective largest value of the smallest non-zero arms from Table 4.20 and Table 4.21 by the respective moment of inertia from Eq. (4.3), one finds that the z-axis is the critical axis, with a moment of inertia of 0.365 kg· m^2 and an effective arm of -0.06 m. With a minimum impulse bit of 0.05 mNs Eq. (4.3) and the requirement of [TEC-ADCS-02], a time of 2123 s (or 35 minutes and 24 seconds) is obtained. This is deemed to be an acceptable value. In conclusion, the thruster blocks can temporarily replace the reaction wheels.

The full field of view sun sensors (six in total) in combination with the IMU can be used as redundancy for the star tracker.

4.4.7. Verification

For every design, a verification has to be performed before production can begin. In the case of a complex system like the ADCS, this is of the utmost importance, and will therefore also include a Fault Detection, Isolation and Recovery (FDIR) module [51]. As mentioned in Section 4.4.3, the computations will be verified; the assumption that the disturbance torques in roll and yaw are cancelled out, which can be verified by implementing a random off-set in the centre of mass with respect to the centre of pressure. An offset of 1 cm in the pitch-axis (r_y), resulted in a disturbance torque of ~ 0.026 μNm around the roll-axis. This is a large off-set and still produces a negligible torque. The yaw-axis is perpendicular to the solar array configuration used, and hence is irrespective of centre position. In reality, some momentum will be stored in the other axes, but much less than in the pitch-axis. This is due to the orientation of the solar array with respect to the sun and spacecraft. For example, a shade on one panel moves the centre of pressure in the the pitch-axis, and thus creates a torque around the roll-axis. This is also possible for the yaw-axis, depending on the array inclination.

An extra consideration is the off-set due to propellant being consumed; the propellant is located at the bottom of the spacecraft. Hence, the centre of mass moves in the positive direction of the roll-axis, which decreases the torque produced. It can thus be concluded that the worst case situation is designed for.

Regarding the assumed tip-off rates; due to a malfunction of the deployment canister, the tip-off rates can increase drastically. Although very rare, tip-off rates up to 200 °/s have been observed with CubeSat missions [115]. Since a contingency has been included for the total impulse, and the IMU operates for rates up to 300 °/s, this will not be an issue. The thrust remains the same, hence the total time to detumble increases, which drains the battery.

On a component level all components are COTS, as such, they have been tested extensively. From Section 4.4.4 it can be seen that the TRL of all components is quite favourable. For the reaction wheels, an imbalance test using Jitter Environment Measurement System (JEMS) and a Servo-Loop Performance test have to be performed. For the star tracker, test results of the baffle performance and Root Mean Square Error (RMSE) vs slew rate have have yielded favourable results [107]. In addition, it was successfully used on the aforementioned missions. For the thrusters, material tests and thrust performance tests have been performed. For the sun sensors, contact with Hyperion Technologies revealed that units have been subjected to thermal cycles (no vacuum), T-VAC tests and vibration tests. The only component that would require additional testing is the IMU, as it has no description of tests in space environment.

4.5. Command and Data Handling Architecture

Controlling the spacecraft and handling all data at the heart of the system is the Command and Data Handling (CDH). The On Board Computer (OBC) is the most important part of the CDH and arguably one of the most important parts of a spacecraft. It is the brain of the spacecraft drives and most of the subsystems. In this section, the entire data infrastructure for the ARCHER CubeSat is considered.

4.5.1. Requirements

In addition to the system requirements as detailed in Section 3.1, the following CDH requirements are driving:

- [TEC-CDH-01] Data shall be compressed according to maximum data rate constraint
- [TEC-CDH-02] Data processing operations shall be compliant with power requirements
- [TEC-CDH-04] The OBC shall be able to handle all relevant interfaces
- [TEC-CDH-05] The OBC shall at least be radiation tolerant

In addition to these, the subsystem must apply the redundancy philosophy as detailed in Section 3.6.

4.5.2. Radiation Hardness Assurance

One of the driving factors of the design of the OBC architecture is the effect radiation has on the subsystem. The following effects are defined [116]:

1. Total Ionising Dose (TID). Due to cumulative energy deposited in the material the TID causes a degradation of the subsystem.
2. Single Event Effect (SEE). A SEE is an effect that is caused by a charged particle hitting the device and causing an anomaly in the system.

The SEE's can be divided into two types, soft errors and hard errors. The soft errors cause a change in device output and are entirely device specific. Usually a device reset solves the issue. The hard errors are potentially killer events, due to the damage caused on the subsystem. Most of hard errors are again device specific and can be critical to the system [116].

Soft errors can be split up into:

1. Single Event Upset (SEU)
2. Single Event Transient (SET)
3. Single Event Latchup (SEL)

SEU's are a change in state of a storage element due to a strike of a particle. SET is a change of state due to a strike, which travels to and is saved in a storage element. SEL causes the circuit to behave differently and causes high-current draw by the circuit. This can potentially result in a hard error. A system reset has to be performed [117].

In order to have a reliable OBC the subsystem should be able to handle all types of radiation induced effects for the lifetime of the CubeSat. In order to be able to handle these effects, various measures can be taken which will reduce the radiation effects on the OBC such as including a watchdog. Selecting an OBC that is able to deal with the TID accumulated and has immunity to SEE is vital.

4.5.3. Payload Data Compression

The Timepix is operated in event-by-event mode with 1 second exposures. Due to this, the detector generates a large amount of digital data which cannot be sent directly to the ground station on Earth without processing as it greatly exceeds the data-rate the CubeSat communication system can achieve. Therefore, it needs to be compressed. The compression strategy followed to reduce the data-rate is based on sparse matrix data reduction algorithms, which take advantage of matrices that have a large amount of zero-valued cells which corresponds to the usual data output of the Timepix, as most pixels in a single frame do not capture any event. Since the zero valued cells do not provide any value, they are stripped from the matrix. Furthermore, the location (pixel position) of the non-zero valued cells is also not critical, so that the cell index of these events does not need to be recorded either. All in all, this allows for histograms to be build, so that only the magnitude of the events and the number that occurred is recorded. This allows for compression factors of 10-100 [118], depending on the number of fragments (events of different magnitude) that occur in a single frame. In our calculations an average compression factor of 20 for the scientific data was assumed, which is equivalent to a compression rate of 95%. This is a highly conservative data compression factor, as depicted in Fig. 4.18.

However, as the compressed data is more prone to transmission errors, an overhead needs to be added to the data packets to ensure their correctness. Furthermore, a small computing overhead will also be added to the data-rate to account for the ancillary information that needs to be encapsulated in the frames. The data on board will be compressed as described in Table 4.23.

Table 4.23: Payload Data Compression

Frame Size [kbit]	1000
Frame Rate [Hz]	1
Compression Rate [%]	95
Computing Overhead [%]	10
Transmission Overhead [%]	20
Effective Compression Rate [%]	93.40
Compressed Data Rate [kbit/s]	66

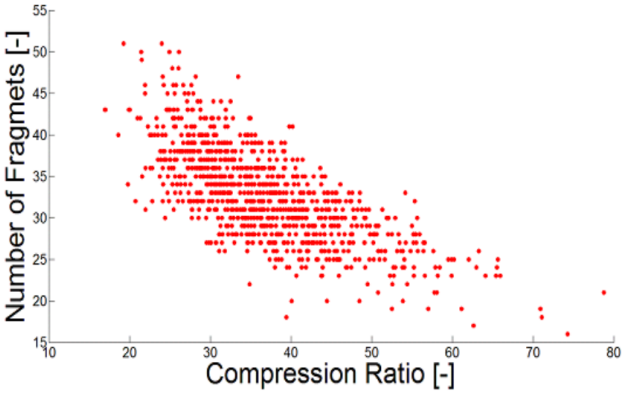

Figure 4.18: Data compression factor versus number of fragments. The mean compression factor is 31. [118]

Summarising, on board processing of the data is required in order to reduce the data-rate to a magnitude that can be transmitted by the on-board communications system. By applying sparse matrix data reduction algorithms together with the construction of histograms (Run-Length Encoding), the data rate can be reduced on average by at least a factor of 14.35, depending on the quantity of fragments and events.

4.5.4. Data Budget

In order to quantify the amount of telemetry that has to be sent down, a data budget is defined, as shown in Table 4.24. The data budget displayed is an adaption of the data budget displayed in [57], with a 100% safety margin applied to account for uncertainties. As such, this housekeeping budget should be considered a quantitative estimate.

Furthermore, the payload is of course a part of the data budget. The payload data rates, after compression, are also shown in Table 4.24.

Table 4.24: Data Budget

Element	Estimated Data Rate [bit/s]
EPS	25
CDH	35
Thermal	5
COMMS	72
Propulsion	110
ADCS	320
Nominal Housekeeping	567
Housekeeping Budget Margin	100%
Total Housekeeping	**1134**
TimePix 1	66000
TimePix 2	66000
TimePix 3	66000
Magnetometer	66000
Total Payload	**264000**
Total Data Rate	**265134**

As can be seen, the data rate of the housekeeping is estimated to be only a fraction of the data rate of the payload. This also means that in case of a safe-mode emergency the nominal data rate can be brought down to only a fraction off the normal data rate.

4.5.5. OBC Trade-off

After defining the data budget and interfaces, the OBC was selected based on a trade-off (see Table 4.25). It was determined that for the configuration a single, safe-life COTS OBC was preferable. At the top level, a decision on the redundancy approach is made. Following a meeting with Jasper Bouwmeester (TU Delft) the conclusion was drawn that on the top level, redundancy could be achieved by having different OBC's in a redundant configuration, also supported by [119]. The reasoning behind this is that failure of the OBC is a high risk factor and it might therefore have to be redundant. However, having two or more identical OBC's means that the radiation degradation of the computers is nearly identical and therefore the redundancy is not effectively implemented [116]. Considering that having two different OBC's greatly increases system complexity and might therefore reduce reliability, the decision was made to choose a single, safe-life, computer instead of two. The reason a COTS option was chosen over a custom computer is the assumption that a COTS OBC would greatly reduce costs in comparison to a custom build.

After that, taking into account the harsh radiation environment and recognising the need for the OBC to be able to withstand this environment, the decision was made to choose a radiation-tolerant OBC. This decision greatly reduces the possible choice for the OBC. Processing power was considered as well as mass and power characteristics. Since processing power can be hard to compare between processors, it is only quantified as "sufficient" or "insufficient", based on the expert opinion of A. Menicucci. Some aspects that were not considered for the trade-off were interfaces and memory size. This is because the assumption was made that this could influence the trade-off towards a less than optimal solution, and because the memory size could easily be adapted. Also, since a USB space-grade interface does not exist the interfaces would have to be adapted in any case. For the trade-off some parameters were unknown. Where possible, these parameters were requested to the provider of the OBC. If for some reason the TID was left unknown, it was considered to be non-existent or "worst-case". For example, all OBC's without a TID rating were considered not to be radiation hardened, even though this may not be true in all cases. The first selection was based on the radiation hardness in terms of TID. Considering this parameter, the minimum radiation was based on the requirement [TEC-CDH-05], which states that the OBC shall at least be radiation tolerant (in order to make the OBC as safe-life as possible, due to the vital nature of the OBC). Radiation tolerant (in terms of TID) is typically defined as a TID tolerance of 20-50 krad [120]. Then, the SEE immunity was considered. For this, according to the ECSS standard on radiation hardness assurance (ECSS-Q-ST-60-15C), any parts rated at an LET value above 60 MeVcm^2/mg are "considered immune to SEE in the space environment" and therefore preferable [121].

Table 4.25: Trade-Off OBC

Parameter / COTS	TID [krad]	SEE [MeV-cm2/mg]	Mass [g]	Power Required [mW]	Processing [-]
blue Endurosat OBC [17]	sky blue 41	orange UNKNOWN	green 58	orange UNKNOWN	green Sufficient
blue ISIS OBC [122]	red UNKNOWN	orange UNKNOWN	sky blue 94	green 550	green Sufficient
yellow CubeSpace CubeComputer [123]	orange 20	orange UNKNOWN	sky blue 70	green 200	red Not Sufficient
blue IMT Cubesat OBC [124]	red 15	orange UNKNOWN	green 38	green 300	green Sufficient
blue Hyperion CP400.85 [125]	orange 25	orange UNKNOWN	green 7	green 550	green Sufficient
yellow Cubic SBC [126]	green 50	green 87	sky blue 125	orange 5000	green Sufficient
yellow Vorago Rad-hard OBC [127]	green 300	green 110	orange UNKNOWN	orange UNKOWN	red Not Sufficient
yellow Proton200k™ Lite [128]	sky blue 30	sky blue 36	sky blue 200	sky blue 1500	green Sufficient

blue European yellow Non-European green Optimal sky blue Acceptable orange Correctable red Unacceptable

All OBCs with red parameters are discarded. Out of the remaining OBC's, the Cubic SBC is the highest scoring computer in terms of TID hardness and SEE immunity. Since these are identified as the leading requirements, the Cubic SBC was selected.

4.5.6. Data Flow and Interfaces

A top-level data flow diagram and interface diagram were made to explore the data flow and interfaces of the CubeSat. First, the data flow throughout the system is explored on a high level in Fig. 4.19. Here the links between the subsystems in terms of data transfer are displayed. The square blocks are the different dedicated computers present in the CubeSat. As can be seen, a distributed system is chosen. This is due to most of the COTS items having the computers integrated into the subsystem.

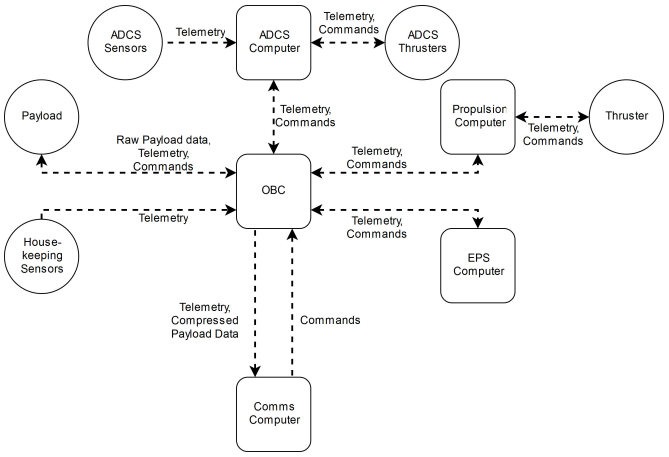

Figure 4.19: Internal Communication and Data Flow Diagram

In Fig. 4.20 the data sources consist of the payload and the different subsystems. As can be seen, due to the TimePixes having a USB interface, a USB controller is needed in order to connect them to the OBC. One such controller is the CM18407HR by RTD Embedded Technologies. It has the PC/104 form factor and PCI expansion bus. It can therefore be stacked upon a CubeSat standard OBC. Its power consumption is 0.5 W [18]. It has, however, not been radiation tested. Therefore, an assumption is made that a device similar to this device will be developed in order to have enough radiation hardening, as rad-hard USB controllers could not be found.

Most of the housekeeping data from the sensors is supplied as an analogue signal and will require processing. For this, analogue to digital converters are a necessity. One of the converters that could be used is the RHD5950 by Aeroflex. This analogue to digital converter takes in 16-channels of analogue signals and converts the signal to a digital signal which can be supplied to the digital bus. Its radiation hardness is 100 krad [129]. It is assumed that this chip is used, and that it will be connected using an SPI interface to the OBC. The power consumption is estimated to be 0.3 W.

Furthermore, the data provided by the payloads is estimated to be 1 Mb/s per TimePix. Since 3 of these devices are present and are generating data during experiments, the total data rate of these payloads is 3 Mb/s. Also, the magnetometer produces an analogue signal which should be converted to a digital signal, using a 24bit digitizer according to corresponding with the manufacturer of the magnetometer, Bartington. For this, the ADS1282-SP Radiation Tolerant High-Resolution Delta Sigma ADC from Texas Instruments is chosen. It uses an SPI interface to connect to the OBC and is assumed to use 0.2 Watt. Its radiation tolerance is 50 krad.[130] The output of this payload is estimated to be about 1 Mb per second as well. This makes the total payload data rate 4 Mbit/s.

Lastly, in order to interface the OBC with the two RS serial interfaces, a serial communication interface will have to be added. As again a radiation hardened variant could not be found, a reference is used. This reference is the MPL OSCI. It uses 0.7W of power and has a mass of 90 g. It uses a PC/104-Plus interface with PCI[19]. All CDH components characteristics have been tabulated in Table 4.27.

[17] //www.endurosat.com/products/cubesat-onboard-computer-obc/ [Retreived 20 July 2018
[18] www.rtd.com/PC104/UM/network/cm18407.htm [Retrieved 21 June 2018]
[19] https://www.mpl.ch/t2863.html [Retrieved 19 June 2018]

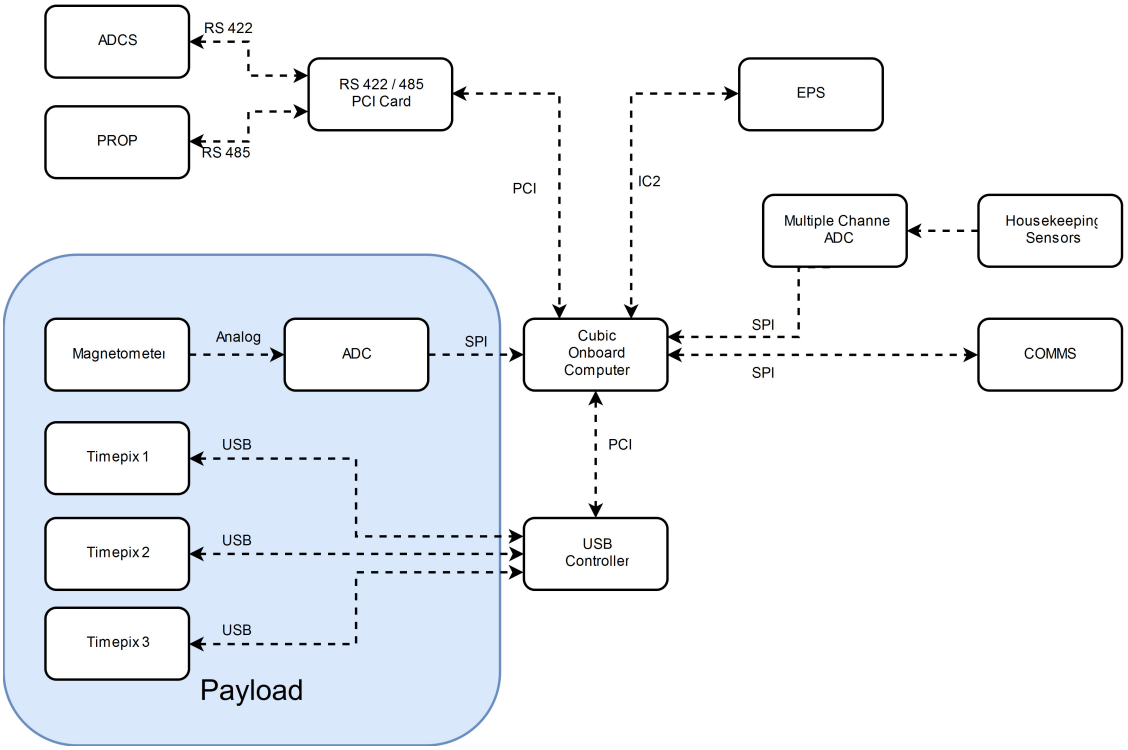

Figure 4.20: Interface Diagram

In Table 4.26 the throughput of the different bus types can be seen. The required throughput for the subsystems is an estimate based on payload data rate and on housekeeping data rate. For SPI the throughput is not defined in the standard but is dependant on the master and slave. The actual throughput will be well above the required since in general the SPI throughput is an order of magnitude above 1 Mbit/s[20].

Table 4.26: Throughput Verification Bus Architecture[21]

Interface	Throughput	Required Throughput
PCI	2.133 Gbit/s	4 Mbit/s
USB	480 Mbit/s	4 Mbit/s
SPI	Undefined	1 Mbit/s
I2C	100 kbit/s	1 kbit/s
RS 422	10 Mbit/s	1 kbit/s
RS 485	10 Mbit/s	1 kbit/s

4.5.7. OBC Characteristics

The system diagram for the OBC is provided in Fig. 4.21. This shows the internal Single Event protection by means of a Watchdog Timer (WDT), which is connected to a reset control on a separate FPGA. This WDT will reset the computer if the timer is exceeded due to a single event. Furthermore, the memory bus is displayed as a separate block, consisting of NAND Flash and SDRAM with Error Detection and Correction (EDAC). The flash unit will have to be expanded to 17 GB as required by COMMS. After applying a safety marging the final size is set at 32 GB and is also one of the weak points in terms of radiation tolerance, as its radiation tolerance is about 30 krad [57]. In order to mitigate the risk of corrupting the operating system, a storage unit could be implemented with a more radiation resistant architecture, such as MRAM.

[20] www.byteparadigm.com/applications/introduction-to-i2c-and-spi-protocols/ [Retrieved 15 June 2018]
[21] en.wikipedia.org/wiki/List_of_interface_bit_rates [Retrieved 15 June 2018]

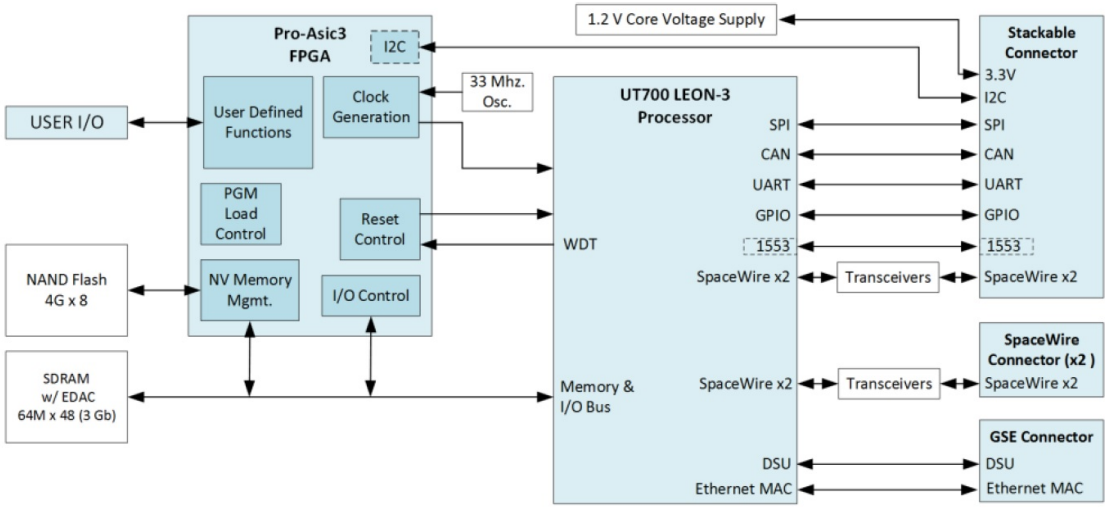

Figure 4.21: OBC System Diagram [126]

Furthermore, it has to be noted that the OBC can be made PC/104 compliant according to correspondence with Cubic Aerospace, making it stack-able, which is convenient for the implementation of peripherals.

Table 4.27: CDH Components and Characteristics

Component	Mass [g]	Power Consumption [W]	TID [krad]	Cost [Euro]	Volume [U]
Cubic SBC	125	<5	50	83250	0.2
ADC multiple channel	30	0.3	100	200	0.05
ADC Payload	30	0.2	50	200	0.05
USB Controller[22]	60	0.5	0	2000	0.2
RS Controller[23]	90	0.7	0	2000	0.2

In Table 4.27 all preliminary characteristics of the different OBC components are presented. It is expected that the TID levels of the USB and RS controller can be as high as the other components, but currently they have not been rated yet. All presented values are without margins. For the cost estimations, the Cubic SBC cost is an estimate provided by Cubic in e-mail correspondence. The other costs are based on given prices, except in the case of the USB and RS controller for which very general estimates are made by adding a factor of 10 to the non-radiation hardened price.

4.5.8. Software

For the software, an operating system should be selected as well as dedicated software for the different distributed computers. The requirements for the software are that it should be reliable, maintainable and verified to be as error-free as possible. Furthermore, it should require as little processing power and memory as possible. Examples of possible operating systems are Linux, free-RTOS, Pumpkin Salvo RTOS etc. A trade-off of the operating system will not be performed at this stage, but is planned to be a part of the further development of the OBC.

One of the other requirements for the selection of the operating system is that is should be compatible with the chosen processor and peripheral drivers. Furthermore, having separate processors for ADCS, COMMS, etc. purposes requires separate software for these goals.

The development of a large amount of software is costly and therefore it is preferable to choose a COTS option. The software should be able to handle the different spacecraft modes as outlined in Section 4.6.

4.5.9. Verification

In order to verify the CDH subsystem, on a component level all components should be tested to be up to the expected radiation levels. After this, the bus throughput and processor performance should be verified by testing with reference data on ground. The software design should be verified by performing day-in-the-life testing and iterated until of sufficient quality.

The storage size will have to be tested by the day-in-the-life testing as well. During this testing, power usage should be verified. Mass and volume can be verified by inspection.

4.5.10. Recommendations

Continuing the development of the ARCHER OBC, it is recommended to search for an European alternative to the Cubic SBC. One of these alternatives with similar characteristics may be the SkyLabs OBC, according to T. Szewczyk and G. Furano from ESA in an e-mail correspondence. Currently, Skylabs could not be reached for specifications.

Furthermore, it is recommended to add an extra, redundant, memory unit with read-only capabilities (fixed PROM for example) for the operating software in order to increase the reliability by reducing the chances of a Single Event occurring in the operating system memory addresses. Next to that, the amount of interface controllers might not be necessary if an OBC is found that could handle the interfaces used out-of-the-box. This means that the complexity could be reduced.

Lastly, it is recommended to investigate a less distributed layout of the OBC as the current layout increases the complexity by having multiple computers in a non-redundant layout. This means that there are multiple single points of failure, which is not beneficial for reliability. If possible, a more powerful OBC could provide the required processing capabilities for reducing the amount of computers.

4.6. Electrical Power System

The Electrical Power System (EPS) is a complicated subsystem which is made up of several components. The primary power system will consist of solar cells, the solar array and/or body mounted panels, the Solar Array Drive Assembly (SADA) as well as the Power Control Unit (PCU). The secondary power system will include the batteries but it must also interface with the PCU. In addition, the system must distribute power to all other subsystems. Different power modes, which indicate which subsystems are active at which times, need to be identified and then the power requirements for each mode calculated. The solar array must be designed such that it can generate enough power to cover nominal operations while allowing a margin for charging. Battery dependent modes need to be identified and eclipses considered in order to adequately size the batteries. Degradation of both the primary and secondary power system must also be accounted for.

In order to meet these demands the EPS was designed as follows. The EPS requirements are presented in Section 4.6.1. In Section 4.6.2, possible components were researched and traded-off to find the most suitable components. With the component power requirements and inefficiencies quantified, an accurate set of power modes was drawn up, as seen in Section 4.6.3. The primary array and secondary battery system was then sized and designed using the components chosen in Section 4.6.4. The final configuration, characteristics and the electrical block diagram are presented in Section 4.6.5 and Section 4.6.6 respectively. Finally, a verification plan was put in place as detailed in Section 4.6.7.

4.6.1. Requirements

In addition to the system requirements as detailed in Section 3.1, the following EPS requirements are driving:

- [TEC-EPS-02] The spacecraft array shall be able to provide at least 100W average power in Earth Orbit under direct sunlight.
- [TEC-EPS-03] The spacecraft shall be able to provide 40 W peak power.
- [TEC-EPS-04] The spacecraft shall have minimum battery capacity of at least 50% of original capacity at end of mission.
- [TEC-EPS-05] The spacecraft secondary power system shall be able to maintain basic operations for all schedule eclipses with a 20% margin.

Table 4.28: Total Power and Voltage Component Requirements

Subsystem	Component	Number of	Operating Power [W]	Standby Power [W]	Voltage [V]
ADCS	Reaction Wheels	1	3.05	1.26	5
”	Star Tracker	1	0.79	0.53	5
”	Sun Sensor	6	0.25	0.01	5
”	IMU	1	0.5	0.525	5
”	ADCS Thruster	2	21	0.53	8-12.6
”	ADCS Processor	1	0.53	0.11	1.5
CDH	Cubic OBC	1	5.25	3.15	3.3
”	USB Controller	1	0.53	0.525	5
”	ADC	2	1.1	1.050	3.3
”	RS Controller	1	1.1	1.050	3.3 & 5
COMMS	IRIS Transceiver	1	36.75	0.525	18
Payload	Fitpic lite	2	5.25	1.16	5
”	Fitpix lite coated	1	2.63	0.53	5
”	Magnometer	1	0.63	0.36	16
”	Boom	1	1.05	0	5
Propulsion	Bit3	1	75	2.94	28
Structures	12 U	0	0	0	0
Thermal	Battery Heaters	2	6	0	5

- [TEC-EPS-06] The spacecraft shall have a power budget margin of at least 20%.
- [TEC-EPS-07] The payload shall be powered during nominal operations.
- [TEC-EPS-08] The power allocated to the scientific payload shall be sufficient for nominal payload performance
- [SUS-EPS-01] The power production shall not involve any radioactive materials.

The EPS must distribute power to all other subsystems, manage the different voltage interfaces and apply the redundancy philosophy as detailed in Section 3.6.5. The component basic power requirements and voltages are listed in Table 4.28. All COTS components have a 5% margin applied to their power requirements except for the engine which can be throttled and therefore will not be sent more than 75 W in nominal flight.

4.6.2. EPS Component Selection

Before designing the final configuration, components were researched, analysed and traded-off. This section details the considerations for choosing a solar cell, SADA, the batteries and power management system.

Several solar cells were considered as can be seen in Table 4.29. Some interesting points to note; the power per cell was calculated solely as a function of the cells efficiency and an irradiance of 1361 W/m^2[24]. The Solaero IMM-alpha [131] has exceptional efficiency however it is still undergoing space qualification. The Spectrolab cells [132] & [133] have good heritage but the cell size is noticeably smaller than the others. The Solaero ZTJ+ [134] has been optimised for high radiation environments and so should suffer less from degradation than the other cells. As a result, this would be the optimal choice. However, considering this is a European mission seeking European funding, European components are desired. The Azur cell [135] is comparable with the ZTJ+ in every category and is made in the EU and as a result this cell was chosen. One other thing to note is that only the Azur cell comes fully integrated with cover glass and bypass diode. This explains why the mass per cm^2 is higher than the other cells. For all other cells, the mass per cell includes a one gram estimate for cover glass and diode.

[24] nssdc.gsfc.nasa.gov/planetary/factsheet/moonfact.html[Retrieved 06 June 2018]

Table 4.29: Solar Cell Trade-off

COTS \ Parameter	Efficiency [%]	Area per cell [cm^2]	Power per cell [W]	Mass [mg/cm^2]	Mass per cell [mg/cm^2]	TRL [-]
yellow Spectrolab XTJ	skyblue 29.5	red 26.6	red 1.07	skyblue 84	skyblue 3249	green 9
yellow Spectrolab XTJ Prime	skyblue 30.7	orange 27.4	orange 1.14	skyblue 80	skyblue 3207	green 9
yellow Solaero IMM-alpha	green 32	green 30	green 1.31	green 49	green 2485	orange <9
yellow Solaero ZTJ+	skyblue 29.5	green 30	skyblue 1.20	skyblue 84	skyblue 3535	green 9
blue Azur 3G30A	skyblue 29.5	green 30.18	skyblue 1.21	skyblue 120	skyblue 3621	green 9

blue European | yellow Non-European | green Optimal | sky blue Acceptable | orange Correctable | red Unacceptable

As the BIT-3 is a low thrust engine, it needs to fire for long periods of time. As such, it is not feasible to use the ADCS to constantly align the solar panels with the sun as this would change the thrust vector. Therefore, a SADA is required in order to maximise power generation. There are many options for larger satellites such as those from Thales[25], Surrey[26] and Ruag[27]. However, only one fully developed design for a CubeSat was found. The specifications for the SADA from HoneyBee Robotics can be found in Table 4.30. There is however, much interest in the area and research papers were found from projects in China [136], Italy [136] and France [137] as well as a design for a picosat [138]. The French group responded to say their SADA is currently undergoing development and they expect it will be TRL 7 within two years. They would not however, disclose specification. In addition to this, a tender from the European Space agency was put out in 2017[28] though no further details have been found. Finally, GOMSpace make reference to sun tracking arrays on their website [29]. They have been contacted and have yet to confirm details. Given the TRL requirement the only option is to move forward with the HoneyBee SADA while reserving the option to replace this with a European option if one becomes available at a later date.

Table 4.30: HoneyBee SADA Characteristics [139]

Origin	Mass [g]	Output Step Angle [°]	Power through put [W]	Temperature range [C]	Range of motion [°]	Radiation tolerance [krad]	TRL [-]
USA	180	0.009	120 (up to 550)	-30 to 85	180	10	8

When considering which battery to choose, it is worth considering both the batteries and the power management system together. It is not certain that one particular battery will interface well with a particular power system and often they come bundled together. Several batteries were analysed as can be seen in Table 4.31. Both Clydespace options[30][31] come integrated with the power management system which explains their large mass and why they are not immediately disqualified due to mass. Interestingly, the BA0X from the Ecuadorian Civilian Space Agency has an impressive power to mass ratio, outstripping all others. However, other than the company's data sheet [140], very little information was found on the component. In addition, simple errors were spotted on the companies data sheet such as a 16 cell battery weighing less than a 12 cell. Being sceptical of vendor data sheets, as per advice of the US Space command [55], it was decided to stick with more well known alternatives until the BA0X has a greater flight heritage. The GOMSpace BPX [141] has the next highest power to mass ratio,

[25] www.thalesgroup.com/en/solar-array-and-drive-mechanisms[Retrieved 22 June 2018]
[26] www.sst-us.com/getfile/b6f8a873-e0d5-4aaa-ac08-8e46fb29f897[Retrieved 22 June 2018]
[27] www.ruag.com/en/products-services/space/spacecraft/satellite-mechanisms/solar-array-drive-mechanisms[Retrieved 22 June 2018]
[28] www2.rosa.ro/index.php/en/esa/oferte-furnizori/2144-miniaturised-solar-array-drive-assembly-for-6u-12u-cubesats-expro-plus [Retrieved 22 June 2018]
[29] gomspace.com/large-platforms.aspx [Retrieved 22 June 2018]
[30] www.clyde.space/products/61-high-capacity-microsat-power-bundle [Retrieved 22 June 2018]
[31] www.clyde.space/products/47-cs-high-power-bundle-c-eps-80whr-battery [Retrieved 22 June 2018]

Table 4.31: Battery Trade-off

Parameter / COTS	Watt hours [Whr]	Nominal voltage [V]	Amp hours [Ah]	Mass [g]	[Wh/g]	Built in heater / PCU [-]	TRL [-]
blue Clydespace 80 Whr	skyblue 80	skyblue 6-8.4	sky blue 10.4	orange 1042	orange 0.077	green yes / yes	green 9
blue Clydespace 150 Whr	skyblue 80	skyblue 9-12.6	sky blue 13	orange 1910	orange 0.079	green yes / yes	green 9
yellow EXA BA0X	skyblue 53.2	skyblue 7.2,14.4	sky blue 7.4,3.7	green 180	green 0.296	orange no / no	green 9
blue German Orbital Systems	skyblue 40	skyblue 3.7	skyblue 7.8	skyblue 325	skyblue 0.123	orange no / no	green 9
blue Gomspace BPX	skyblue 77	green 7.4,14.8,29.6	green 10.4,5.2,2.6	skyblue 500	skyblue 0.154	skyblue yes / no	green 9

blue European | yellow Non-European | green Optimal | sky blue Acceptable | orange Correctable | red Unacceptable

Table 4.32: Power Conditioning and Distribution Trade-off

Parameter / COTS	Regulated Bus [V]	Maximum Power Point Tracking	Mass [g]	Includes Batteries [-]	Modular [-]	TRL [-]
blue Clydespace 80 Whr	skyblue 3.3, 5, 12	skyblue Yes - analogue	orange 1042	green yes	skyblue no	green 9
blue Clydespace 150 Whr	orange 3.3	skyblue Yes - analogue	orange 1910	green yes	skyblue no	green 9
blue Clydespace FlexU	skyblue 3.3, 5, 12	skyblue Yes - analogue	green 148	skyblue no	skyblue no	green 9
blue Gomspace P60	green 3.3, 5, 8 12, 18, 24	skyblue yes - per channel	green 191	skyblue no	green yes	green 9

blue European | yellow Non-European | green Optimal | sky blue Acceptable | orange Correctable | red Unacceptable

offers many voltage combinations and has integrated thermal protection. As such, it is favoured as a stand alone battery. However, the power management system must also be considered before confirming a choice.

For the power management system, both Clydespace bundles were considered as well as a standalone Clydespace PCU, the FlexU[32]. The GOMSpace P60 [142] was the other option in trade-off Table 4.32. As there were sufficient quality European options, nothing from outside Europe was considered. At this stage, the 150 Whr bundle becomes difficult to justify due to mass as two GOMSpace BPXs and the P60 collectively gave as much power with around 700 g of mass saving. Relatively similar savings can be found when pitched against the 80 Whr bundle. More analysis is required though before a choice can be made. With the P60's flight heritage, proven reliability and modular design, allowing for easy addition of extra array conditioning units and power distribution modules as well as the greater range of regulated voltage buses, it becomes a very strong contender. In addition, it is designed to operate with the BPX, the first choice standalone battery. It would make little sense to match the BPX with the FlexU, and the combination of GOMSpace battery and power management system outperforms the Clydespace bundles.

4.6.3. Power Modes

The power modes detail which subsystems are active at a given time or during a given set of operations and are used to calculate the power used during that mode. Fig. 4.22 presents the final power modes including final design power generation. Throughout the design cycle the modes underwent constant iteration. They were designed to

[32] `www.clyde.space/products/5-3rd-generation-3u-eps` [Retrieved 22 June 2018]

be modular modes which could be combined in series to cover any eventuality during the mission. It would be beneficial to present the different mission phases and then detail all sets of modes within that mission phase. However, due to practical limitations on space, this modular approach was taken. It is however, a very useful way to approach the modes as it allows for quick and easy calculations while also building in extreme flexibility.

The modes are defined across the top of Fig. 4.22. Here, Acquisition refers to either acquiring the sun for power generation or acquiring the Earth for communications. The table details which subsystems are active during each mode. Each mode block lasts either an hour or 0.1 of an hour if generally very short. A non-integer string of blocks in series can make up any length of time required. The system is not limited to an hour or 0.1 hour blocks, rather this simplifies the calculations. The power required for each mode and the total Whrs needed for that modular block and displayed at the top. A power margin of 20% is applied to every block, as per requirements and the efficiency of the EPS system is accounted for. The power balance per block is also displayed and is positive or negative depending on power requirements and power generation.

Modular Power Modes mean any combination can in theory be put together. A limited set of examples follows:

- 1 - Deployment: Startup block x1, detumbling block x1, acquisition block x1
- 2 - Thrusting: Powered flight block x4, powered+ flight block x4, powered flight block x4
- 3 - Momentum Dumping: Acquisition block x1, momentum dumping block x1, acquisition block x1
- 4 - Eclipse: Eclipse block x(eclipse time), acquisition block x1, unpowered block flight x3

Example 1 demonstrates the string of blocks that will likely happen immediately after deployment through to acquiring and aligning with the sun. It is of course possible that detumbling may require more time. Example 2 demonstrates a cycling between thrusting at 75 W in nominal powered flight mode and then at 80 Wm using the powered+ modes where the engine is boosted by the batteries. Example 4 illustrates how the craft enters eclipse mode, stays there for the length of the eclipse then reacquires the sun before entering unpowered flight mode to charge the batteries.

Power critical modes need to be identified in order to quantify the maximum likely series of power negative blocks. The batteries must then be able to safely power the craft for this length of time with a margin. Power critical modes are listed in Section 4.6.4 during battery design.

			Detumbling	Acquisition	Powered Flight	Powered + Flight	Comms Flight	Unpowered Flight	Comms Transmit	Eclipse mode	Startup mode	Safe/Test mode	Emerg Battery	Momentum Dumping	Decommissioning
		Hours	0.1	0.1	1	1	1	1	1	1	0.1	1	1	0.1	1
		Power Req	26.20	22.50	94.10	99.10	105.50	33.70	56.10	28.30	28.10	26.30	16.70	32.20	88.40
		Margin 20%	31.44	27.00	112.92	118.92	126.60	40.44	67.32	33.96	33.72	31.56	20.04	38.64	106.08
		efficiency	0.92	0.92	0.92	0.92	0.92	0.92	0.92	0.92	0.92	0.92	0.92	0.92	0.92
		Total Wh	3.42	2.93	122.74	129.26	137.61	43.96	73.17	36.91	3.67	34.30	21.78	4.20	115.30
		Power Gen	0.00	0.00	133.89	133.89	133.89	133.89	133.89	0.00	0.00	133.89	0.00	0.00	133.89
		Balance/block	-3.42	-2.93	11.15	4.63	-3.72	89.93	60.72	-36.91	-3.67	99.59	-21.78	-4.20	18.59
		Balance/hr	-34.17	-29.35	11.15	4.63	-3.72	89.93	60.72	-36.91	-36.65	99.59	-21.78	-42.00	18.59
		W	on/off	on/off	on/off	on/off	on/off	on/off	on/off	on/off	on/off	on/off	on/off	on/off	on/off
Power	Generation	133.8913372	0	0	1	1	1	1	1	0	0	1	0	0	1
EPS	Dist Solar	see efficiency	0	0	1	1	1	1	1	0	0	1	0	0	1
	Dist Batt	see efficiency	1	1	0	1	1	0	0	1	1	0	1	1	0
	Standby	0.6	0	0	0	0	0	0	0	0	0	0	0	0	0
Payload	Science	8.1	0	1	1	1	1	1	1	1	0	0	0	1	0
	Standby	2.4	1	0	0	0	0	0	0	0	1	1	1	0	1
ADCS	Detumbling	12.4	1	0	0	0	0	0	0	0	0	0	0	0	0
	Acquisition	3	0	1	0	0	0	0	0	0	0	0	0	0	0
	Dumping	12.7	0	0	0	0	0	0	0	0	0	0	0	1	0
	Normal	2.8	0	0	1	1	1	1	1	1	0	0	0	0	1
	Contingency	12.5	0	0	0	0	0	0	0	0	0	1	0	0	0
	Standby	2.9	0	0	0	0	0	0	0	0	1	0	1	0	0
OBC	On	7	1	1	1	1	1	1	1	1	1	1	1	1	1
	Standby	3.6	0	0	0	0	0	0	0	0	0	0	0	0	0
COMMS	In	12.6	0	0	0	0	1	1	0	0	1	0	0	0	0
	In and Out	35	0	0	0	0	0	0	1	0	0	0	0	0	0
	Standby	1.2	1	1	1	1	0	0	0	1	0	1	1	1	1
Propulsion	Thrust	75	0	0	1	0	1	0	0	0	0	0	0	0	1
	Thrust	80	0	0	0	1	0	0	0	0	0	0	0	0	0
	Standby	3.2	1	1	0	0	0	1	1	1	1	1	1	1	0
Thermal	On	6	0	0	0	0	0	0	0	1	0	0	0	0	0
	Standby	0	1	1	1	1	1	1	1	0	1	1	1	1	1

Figure 4.22: ARCHER Power Modes

4.6.4. Designing the EPS

In this subsection the design process along with the actual design of the EPS are shown.

Primary Power

As seen in Fig. 4.22, nominal powered flight consumes 123 W. This includes a generous 20% margin and the efficiency of the EPS. Comms flight however, is the ideal nominal mission mode as the IRIS receiver is also powered on, unlike in powered flight. This is ideal as switching the COMMS subsystem on and off is risky. If a system problem arises while the receiver is switched off, the reset command from Earth will not be received. As such, maintaining the receiver on at all times is important. Comms flight requires 138 W. The large power requirements for both modes is largely due to the engine and the skewed effect the 20% power margin regulation has as a result. The solar array must at a minimum be capable of powering the craft during powered flight and there must be a power surplus in order to charge the batteries. The array must deliver around 125 W for powered flight or 140 W for Comms flight.

To investigate whether this is possible, the power each Azur 3G30A cell could deliver was calculated as per Eq. (4.12). In this equation, E_e is the irradiance of 1361 W/m^2 and A is the cell area. An offset of 1 degrees was assumed for the solar incidence angle, θ. The inherent degradation, D_i, accounts for losses due to shadow, temperature variations and assembly errors. It can be estimated to range from 0.49 to 0.88 or above [49]. Artemis and Diana need the arrays to be in plane with the sun and will be using a SADA to keep the panels facing the sun. Few appendages are in a position to cast shadow on the array and excellent thermal control has been applied to maintain the panels temperature close to optimal, see Section 4.8. As a result, a factor of 0.88 was used for the inherent degradation.

SPENVIS was used to analyse the expected radiation the cells should receive over the 2 year mission. The results can be seen in Fig. 4.23. As can be seen, SPENVIS expects the cells will be exposed to about 5E+13 MeV [e/cm^2] over the mission duration. The 3G30A datasheet [135] claims that the expected EOL efficiency will drop by less than 1% after experiencing 2.5E+14 MeV [e/cm^2] suggesting an even smaller drop for the lower exposure level. However, the potential for error between SPENVIS and the actual radiation the cells receive is large. Considering, ARCHER is designed to record datawhich can be used to improve models like SPENVIS, this result should be treated with caution. As a result, and being quite conservative, The yearly degradation D_y was assumed to be conservatively 1% a year applied over L, the mission lifetime of 2 years.

Cell: Azur 3G30 (SR-NIEL 21eV)

Electron/proton damage ratios:
P_{max} = 1135.0
V_{oc} = 1325.0
I_{sc} = 613.0

Coverglass

material: SiO2
density: 2.32 (g/cm^3)

Coverglass thickness			Total			Solar protons		
g cm^{-2}	mils	micron	P_{max}	V_{oc}	I_{sc}	P_{max}	V_{oc}	I_{sc}
0.0232	3.9	100.00	4.486E+13	5.237E+13	2.423E+13	4.486E+13	5.237E+13	2.423E+13

Figure 4.23: SPENVIS Analysis of Azur 3G30A Cell for 2 Years.

$$P_{cell} = E_e \cdot \eta_{cell} \cdot A \cdot cos(\theta) \cdot D_i \cdot (1 - D_y)^L \qquad (4.12)$$

This resulted in 1.045 W per cell. In order to just cover the powered flight requirements, 117 cells are needed. In order to cover comms flight, 132 are needed. The standard Azur 3G30a is 80x40mm. 20 cells can be arranged tightly on a 3x2U face. Fig. 4.24 is an example from EnduroSat on how to arrange this. While the dimensions of the 3x2U fact suggests there is potential for a denser packing, in practice this would prove very difficult and would likely increase the inherent degradation. As such, 20 cells per face was considered and a two wing trifold array was designed. In total this means 120 cells will be placed on the solar tracking arrays.

GomSpace offer large trifold power arrays for 12U missions as custom designs. A concept can be seen in Fig. 4.25. ISIS are currently not offering a trifold deployable arrays. Pumpkin Space and MMA both do but are both American. In the interests in buying European, and considering the easy interfacing with other parts of the

[33] www.endurosat.com/cubesat-store/all-cubesat-modules/custom-6u-solar-panel/ [Retrieved 22 June 2018]
[34] gomspace.com/large-platforms.aspx [Retrieved 22 June 2018]

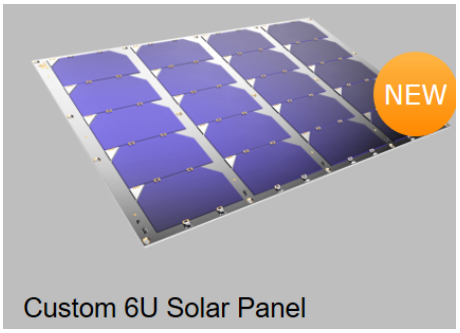

Figure 4.24: EnduroSat 20 Cell Panel[33]

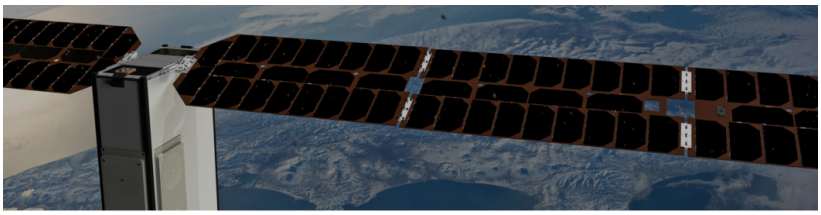

Figure 4.25: GomSpace large trifold array[34]

EPS, it is recommended to commission the array from GomSpace. They have been contacted regarding our specification but at time of writing have not confirmed the details.

To boost power, body mounted panels were considered. Due to the potential shadow from the reflector array, cells were only placed on two faces, a 2x2U side panel and 3x2U top panel. Due to the necessity for other components to use surface area, 5 cells were placed on the side and 15 on top. These can not receive direct sunlight at all times. A python program was written to calculate the power these cells would generate as the sun changed position from - 90°, directly behind the CubeSat, to 0°, where the side panel is in direct sunlight, to +90°, directly in front of the CubeSat and the top panel is in direct sunlight. Once the sun moves past the 180°mark, the reflect array will cast shadow on the top panel. This will trigger the ADCS to rotate the CubeSat around the thrust vector axis by 180°. This will bring the front face back into sunlight and move the side panel to the sun side. As the sun then moves to the 270°mark the side panel again comes into direct sunlight. This mode will not affect the SADA, as they will track the sun regardless and readjust after the CubeSat flips. It also ensures the body mounted panels receive as much sunlight as possible maximising the value from only two panels.

Fig. 4.26 shows the power generated solely by the body panels and Fig. 4.27 shows how this works with the array. The body panels add a minimum of 0 W only when the sun is directly behind the CubeSat, a maximum of 16.5 W and an average of 8.3 W. This brings the total generated power to just under 134 W when considering the average power from the body panels. This is more than enough to run in powered flight with surplus to charge but not enough to run in the ideal Comms flight. While extending the array may be feasible, it would require folding the array over the engine during deployment, a high risk manoeuvre. Instead, an interesting battery design will be considered in order to ensure Comms flight can be maintained.

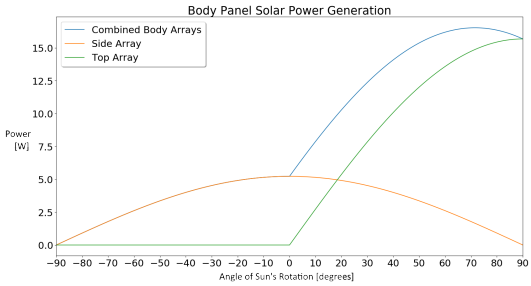

Figure 4.26: Body Panel Power Power Generation

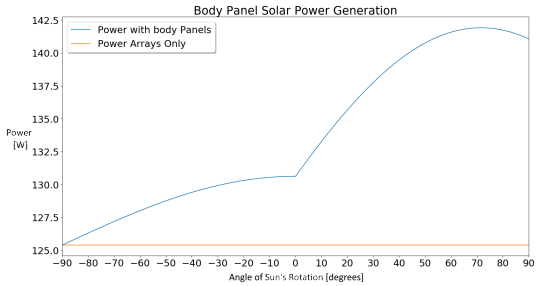

Figure 4.27: Body Panel and Array Power Power Generation

Secondary Power

The secondary power system will be designed to ensure the COMMS subsystem can remain on during transit while the engine is firing. As COMMS is scheduled to transmit on a 20% duty cycle, or for 4.8 hours every 24 hours during transit, this requires using the batteries to make up the shortfall for keeping the COMMS on for 19 hours a day and there must be enough time to recharge during the 5 hr transmission window when the engine is powered off. During the science orbit, the engine is not firing other than when station keeping is needed and as such, there will not be a problem powering COMMS from the solar array at this point. Only the most critical case

will be considered, that for Artemis as Diana will rarely encounter eclipse.

The following mission phases will require battery use:

- Transfer time of 230 days
- 1 day cycles during transfer
- Transfer Power Modes - Comms Flight block x 19, acquisition block x1, Comms transmit block by 4.8, and acquisition block x0.1
- 160 day insertion into lunar orbit
- 120 days no eclipses and 40 days with eclipses during insertion equivalent to 100 eclipses
- Insertion eclipse = 0.65 hours (average science eclipse as insertion eclipses not calculated in Section 2.5)
- 380 days in science orbit
- Eclipse times vary in science orbit as calculated in Section 2.5
- End of life for 40 days
- Eclipse times as per extended science orbit as calculated in Section 2.5

In order to model the most critical case it was assumed that the 120 days of non eclipse insertion happens consecutively with the transfer. This gives 230 + 120 = 350 days where the Transfer Power Mode will be operating. The batteries will have to provide the power balance required to ensure the COMMS can remain in receiving mode during these 19 hours. 3.92 W for 19 hours is a total of 74.5 Whrs. The batteries will have 5 hours to recharge during the Comms transmit blocks. Since the engine is switched off to allow transmission, this is possible as there is a potential surplus of 300 W over the 5 hours.

The Gomspace BPX is a 77 Whr battery. A single battery pack would require almost a 100% Depth of Discharge (DOD) to cover the 350 cycles for the transfer power modes. This would do considerable damage to the batteries. With two battery packs, the DOD drops to below 50%.

It is essential to analyse whether this is actually feasible in order to better understand the battery degradation and to confirm that the batteries are capable of running the power mode, Comms Flight x 19, acquisition x0.1, Comms transmit by 4.8, acquisition x0.1, for 350 cycles. As can be seen in Fig. 4.28, taken from the data sheet including efficiency losses, the batteries will take 10.25 hours to fully charge with a 0.1C charge rate. While it is possible to charge it more quickly, it would be ideal to work with 0.1C in order to use the data from the graph. 15.4 W of power at the appropriate voltage, discussed below, equates to 0.1C. During Comms transmit, there is far more than this available. nonetheless, 15.4 x 5 hours is 77 Whr of power. The batteries will have discharged 74.5 Whrs. Therefore, a 0.1C charging rate can feasibly charge the batteries during the 5 hour transmission window.

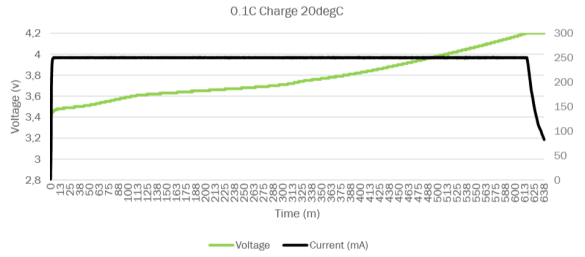

Figure 4.28: BPX Charge Time [143]

Depth-Of-Discharge [% used]	80% remaining capacity 25°C, +1C/-1C, 4.2 V EOCV [cycles]	65% remaining capacity 25°C, +1C/-1C, 4.2 V EOCV [cycles]
100%	350	430
50%	1000	1200
25%	1700	2100

Figure 4.29: BPX Depth of discharge losses[143]

In order to accurately model how the power modes affect the batteries a python program was written. It first runs a 350 day cycle, draining the batteries by 74.5 Whrs over 19 hours and then recharging them over 5 hours at 0.1C. This program was then extended to cover the insertion eclipse orbits with each eclipse being the average science eclipse as provided by astrodynamics in Section 2.5. Then the actual science orbit, including all eclipses were modelled for a further 380 days. Finally, the EOL phase was modelled as a 40 day extension to the science mission and including the calculated corresponding science mission eclipses.

The DOD cycle figures in the data sheet use 1C which is far less efficient than 0.1C. These figures will be used nonetheless both as they are the only figures provided and also to act as a margin. This small dataset was plotted and a quadratic interpolant fitted. Using the interpolant the number of cycles to reduce battery capacity from 100 to 80% can be found. Dividing (100-80)% by the number of cycles then gives the average percentage of capacity lost for that cycle. The number of cycles per DOD when dropping from 80 to 65% of capacity can similarly be

interpolated. The interpolants can be seen in Fig. 4.30. Finally, any DOD under 25% was modelled as 25%. This will cause higher degradation of the batteries but it was felt, with only 3 data points, extrapolation was not ideal.

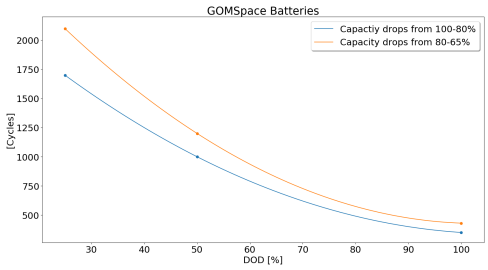

Figure 4.30: BPX DOD losses vs cycle # interpolants

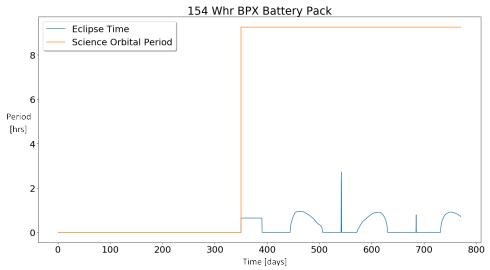

Figure 4.31: Eclipse vs Orbital Period

The program first calculated the power used in a cycle. During transit this was 74.5 Whr and during eclipse it varied depending on eclipse length. During insertion the eclipse length was considered to be 0.65 hours, the average science orbit eclipse. During eclipse, power used was calculated as Eclipse mode x eclipse time + acquisition x 0.1. On the rare occasion the eclipse lasted more than two hours, the system switched to emergency battery mode to save power. In addition, all eclipse times were increased by 20% as per [TEC-EPS-05]. One other point to note, that once out of eclipse, 2 hours was set aside to fire the engine for station keeping. This was purely a reserve but did eat into potential charge time. In addition, Comms transmit was active for 6.3 out of 28.5 hours, or three orbits. This would not affect the batteries as the engine would be switched off.

With the power used known, the DOD could be found simply dividing by the battery capacity. Using the interpolant, the percentage capacity lost for that single cycle could be calculated and the new reduced battery capacity found. If the new battery capacity dropped below 80%, the second interpolant would be used. This was applied over 770 days, with 350 high drain cycles during the Comms flight modes followed by more than 500 eclipses. The capacity loss for each individual cycle was found and applied before the next cycle. The eclipse times versus the average period of 9.25 hours in science orbit can be seen in Fig. 4.31. The DOD during the mission and how the capacity dropped as a percentage of the original battery capacity can be seen in Fig. 4.32. The power used, power levels and battery capacity over mission life can be seen in Fig. 4.33. One final thing to note, it was assumed that a cycle with a DOD of 25% was applied during the eclipse gaps. This was to cover any battery degradation due to lack of use. The EOL capacity was just over 80% which meets [TEC-EPS-04].

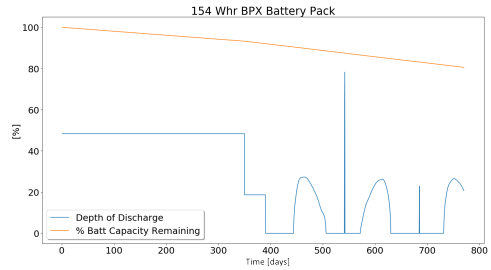

Figure 4.32: BPX depth of discharge and remaining capacity over mission life

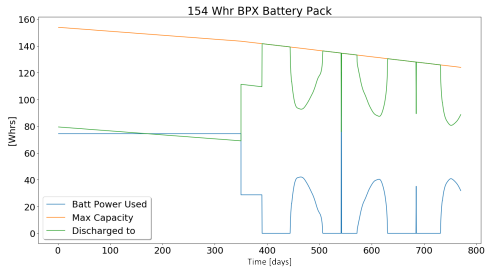

Figure 4.33: BPX power used, power levels and battery capacity over mission life

4.6.5. Subsystem Configuration

The final system consists of an array with 2 wings, each with 60 Azur 3G30A cells. This is capable of generating over 125 W. 20 body cells will add an average of 8 W and a maximum of 16W. The cells are arranged in strings of 5. These will be connected in series giving 12 V before any inefficiencies are taken into account. 4 strings will be connected in parallel giving 2 amps. Each 5 x 4 module is a set of 20 cells or one fold of a wing. There are 6 wing folds in total, each a 3x2U area. There is one set of body mounted panels again in a 20 cell configuration. The array can be seen in Fig. 4.34 and Fig. 4.36 while the positioning of the body panels can be seen in Fig. 4.35. The Azur cell can be seen in Fig. 4.37. As mentioned before, GomSpace will be contracted to deliver this array.

A concept of their own can be seen in Fig. 4.25.

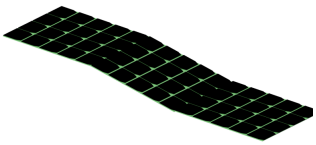

Figure 4.34: Single wing of solar array

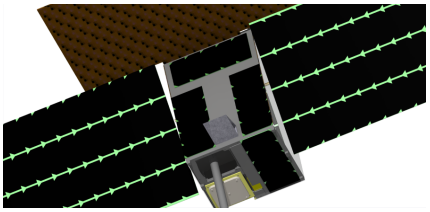

Figure 4.35: Solar array body panel configuration

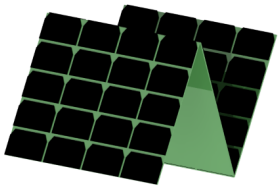

Figure 4.36: Solar array wing in trifold configuration

Two GomSpace BPX 77 Whr battery packs, as seen in Fig. 4.38 will be used with a total of 154 Whr and an expected EOL capacity of around 124 Whr. The P60, as seen in Fig. 4.39, with its modular ACU [144] and PDU [145] design will control and distribute power to and from the batteries and solar array. The P60 modular power management has an ACU with 6 channels rated for 2 amps and up to 25 volts. As there are 7 PV channels a second ACU will be added to the modular design. The PDU has 9 channels and so 2 are required. 7 of the nine channels per PDU can run either 3.3, 5 or 8V. Two channels and one regulator per PDU can also run either 12, 18 or 24. In order to best cover the voltage requirements of the components, one PDU will send 18 V to the magnetometer and IRIS transceiver. The other PDU will send 24 V to the engine. While the engine requires 28 V it comes with an inbuilt converter. All other channels will run in the standard configuration of 3.3, 5 or 8 V. For specifics, please see the Section 4.6.6. The The final EPS configuration specifications can be seen in Table 4.33.

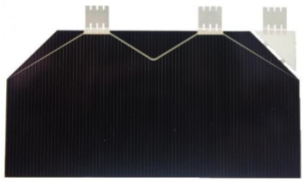

Figure 4.37: Azur 3G30A Cell [135]

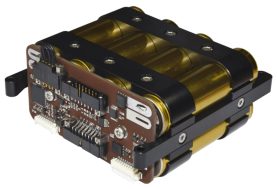

Figure 4.38: GomSpace BPX 77 Whr Battery Pack [141]

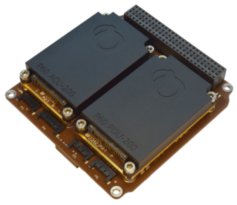

Figure 4.39: GomSpace P60 Dock, ACU and PDU [142]

Table 4.33: EPS Final Characteristics

Component	Quantity	Total Mass + 5% [kg]	Total Internal Volume [U]	Temp Range [C]	Radiation Hardening	Total Cost [k euro]
3G30A	140	0.57	External	-150 to +250	26.6% efficient @ 5E+15 MeV [e/cm²]	33.6
Solar Array	2	1.2	External	-150 to 250	To be confirmed	To be confirmed
BPX Batteries	2	1.05	0.735	-40 to +85	Min 2 years LEO	10
P60	1	0.09	0.09	-35 to +85	Min 2 years LEO	5
PDU	2	0.120	0.025	-35 to +85	Min 2 years LEO	12
ACU	2	0.115	0.025	-35 to +85	Min 2 years LEO	12
SADA	1	0.2625	0.06825	-30 to +85	10 [Krad]	To be confirmed
Total	-	3.4075	0.94325	-	-	-

P60 to CDH interface – I2C

WData on radiation hardening to be confirmed for the BPX,P60, ACU and PDU it is likely to be in the same order as the SADA and therefore will need to be protected. 3G30A numbers include body mounted cells.

4.6.6. Electrical Block Diagram

The Electrical block diagram as seen in Fig. 4.40 presents the power and subsystem component interfaces.

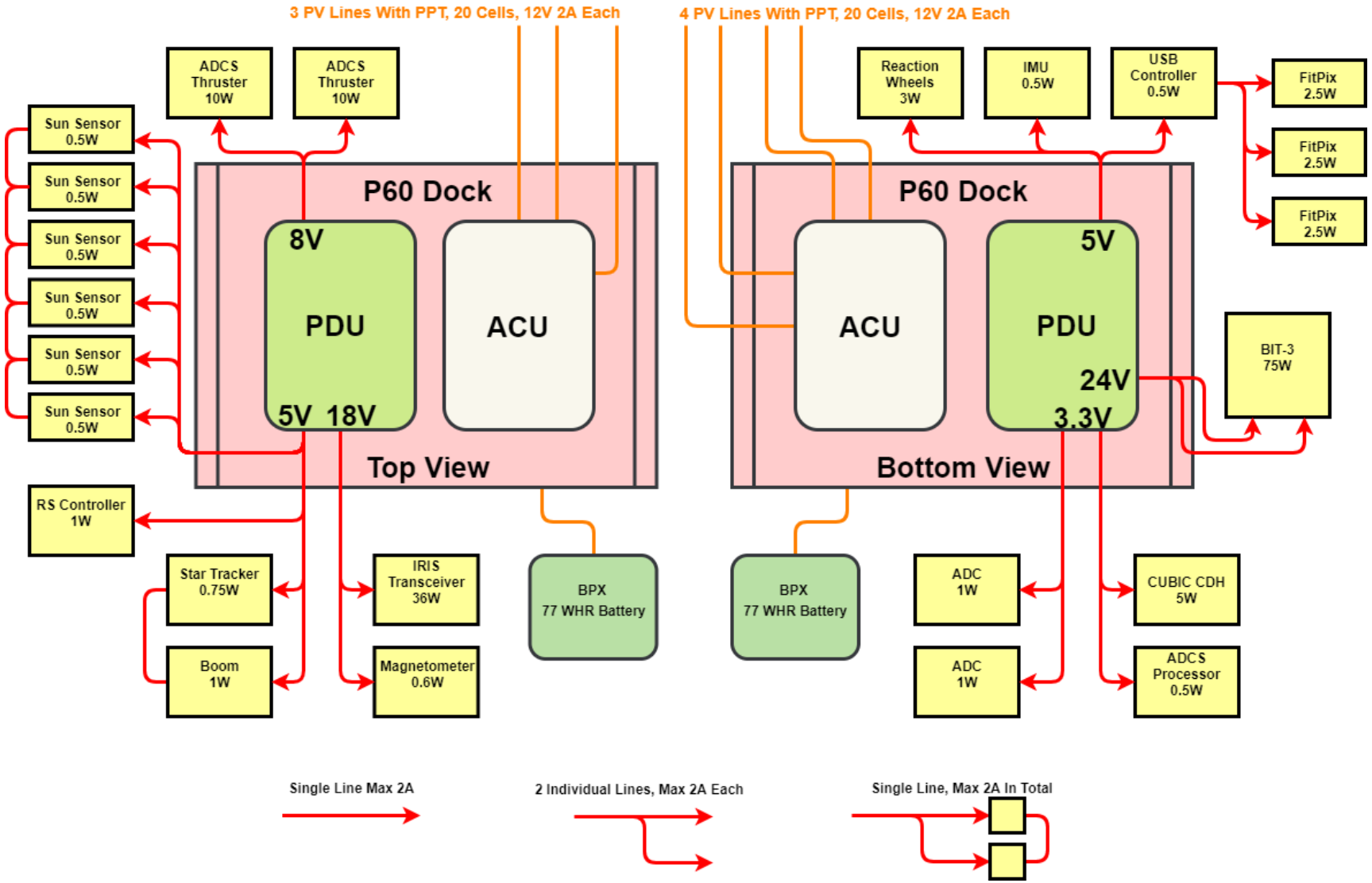

Figure 4.40: Electrical Block Diagram

4.6.7. Verification

The EPS components must be verified. It is important to test against vendor datasheets and ensure that the correct product was delivered and it can meet the requirements set. These tests will be carried out on a component by component level. These will not be the only tests carried out on the EPS. System level EPS testing will take place during system verification. This is detailed in Section 5.4 and largely involves the solar array and the interfacing of the components together and the interfacing of different subsystems together. System validation will also take place as detailed in Section 6.4 and will include day in the life testing etc.

Azur 3G30A

- Basic tests: verify mass, dimensions, volume, coverglass thickness etc.
- Solar Irradiance test: verify power, voltage and current levels under ideal conditions.
- Series & Parallel test: verify total voltage and current when cells are arranged in series and in parallel.
- Heat test: verify can operate within stated temperature ranges.
- Radiation test: Expose cells to predicted radiation levels then repeat the solar irradiance test to verify cell degradation.
- Vendor test: verify 3G30A meet all other vendor datasheet specifications.

GomSpace BPX Battery

- Basic tests: Verify mass, dimensions, volume, coverglass thickness etc.
- Heat test: verify can operate within stated temperature ranges.
- Charge/discharge test: verify charge/discharge time and capacity.
- Heat test: verify can operate within stated temperature ranges.
- Vendor test: verify BPX meets all other vendor datasheet specifications.

GomSpace P60 Dock, ACU and PDU

- Basic tests: Verify mass, dimensions, volume, coverglass thickness etc.
- Connection tests: verify voltage, current flowing through each ACU, PDU line.
- Heat test: verify can operate within stated temperature ranges.
- Vendor test: verify P60 meets all other vendor datasheet specifications.

HoneyBee SADA

- Basic tests: Verify mass, dimensions, volume, coverglass thickness etc.
- Torque test: verify the rotating and holding torque.
- Step test: verify number of steps per 360°.
- Range of motion test: verify full range of motion.
- Voltage/Power test: verify the SADA can pass the correct power and voltage through its connections.
- Heat test: verify can operate within stated temperature ranges.
- Vendor test: verify SADA meets all other vendor datasheet specifications.

GomSpace Solar Array

- Basic tests: Verify mass, dimensions, volume, coverglass thickness etc.
- Heat test: verify can operate within stated temperature ranges.
- Vendor test: verify array meets all other vendor datasheet specifications.

4.7. Structures

One of the most critical subsystems within a spacecraft is the structure, as its failure in general results in the irreversible failure of the spacecraft as a whole. In this section the design of and analysis of the spacecraft structure is described.

4.7.1. Requirements

In addition to the system requirements as detailed in Section 3.1, the following requirements for the structure have been formulated:

- [STA-LAN-03] Spacecraft shall be inert under normal launch operations
- [STA-LAN-04] Spacecraft shall not resonate at dangerous vibration frequencies during launch
- [STA-LAN-08] Spacecraft shall include attachment points in order to secure spacecraft during launch as per launcher guide
- [STA-LAN-09] The spacecraft shall be compatible with the launcher deployment system
- [TEC-PAY-07] The neutron detector shall be placed internally within the spacecraft shielding structure
- [TEC-STR-03] The outer structure of the spacecraft shall provide (TBD) protection against space debris impacts with an energy of (TBD) J/m^2 - (beyond the scope of this design phase)
- [TEC-STR-04] The structure shall maintain the needed sensor alignment and positioning despite structural and thermal loads and vibrations
- [TEC-STR-08] The spacecraft shall withstand accelerations in the range (TBD) m/s^2

The requirements for a secondary payload for all Arianespace launches are taken [146], a 20% contingency is added to mitigate the risk of incorrect assumptions in the analysis causing a failure.

- [STA-LAN-04] The spacecraft lowest eigenfrequency, while in stowed position, should be:
  - 54 Hz in lateral direction
  - 108 Hz in longitudinal direction
- [TEC-STR-08] Spacecraft shall be inert under:
  - lateral accelerations from -4.8 g to 4.8 g
  - longitudinal accelerations from -17 g to 12.4 g

Furthermore, requirement [TEC-STR-03] was found to be unfeasible to determine in this stage of the mission design. As such it is ignored in this report.

4.7.2. Trade-off

Several different options exist for the structure[35]. Most notable are:

- Modular structure
- 3D printed structure
- Standardised structure

The modular structure allows for more freedom than the standardised structure. However, as a standardised 12U configuration is used, this does not add much value. However, the structural properties of these logically are less than the standardised structures designed to be a 12U. Furthermore, it appears no modular CubeSat structures are on the market for CubeSats larger than 3U.

The 3D printed structure allows for a far larger freedom for designing the layout. However, similar to the modular structure, this does not add any real value as the layout has been designed to fit almost completely within the standardised structure. Furthermore, CubeSats using this technology larger than 1U do not appear to be launched yet [147, 148].

The standardised structures are a high TRL, and as such low risk, solution. There are several producers of such structures on the market. However, the amount of manufactures working on 12U CubeSat structures are relatively limited. Given that some, probably minor, adjustments have to be made to the structure to fit the engine, it was decided to opt for a local manufacturer. The only manufacturer fulfilling these requirements is ISIS, with a 12U structure with primary mass of 1500 g[36].

---

[35] https://sst-soa.arc.nasa.gov/06-structures-materials-and-mechanisms [Retrieved 22 May 2018]
[36] https://www.isispace.nl/product/12-unit-cubesat-structure/ [Retrieved 20 June 2018]

4.7.3. Radiation Shielding

For the determination of the necessary radiation shielding required for ARCHER, all the sensitive components present within the CubeSat structure as on-board computers (OBC), printed circuit boards (PCB) and FPGAs were analysed in order to establish which of these would be the least resistant to radiation. After conducting the analysis it resulted that the microcontroller electronics within the Solar Array Drive Assembly (SADA) were the least resistant component, being able to withstand only up to a maximum of 10 krad of total ionising dose (TID). Bearing this in mind, the skin of the CubeSat must be designed in such a way that, over the entire span of the mission life, the total ionising dose would never exceed 10 krad, except in case of unpredictable strong solar particle events.

The determination of both the material and the appropriate skin thickness was possible by means of an on-line radiation simulation software, SPENVIS. The simulation model used was MULASSIS (Multi-layered shielding simulations), a Geant4 toolkit. Geant4 is simply a toolkit for the Monte Carlo simulation of the passage of particles through matter.

As the SPENVIS software only allows to simulate GCRs and SPEs separately, by scrutinising the results it was noted that, in an orbit resembling the lunar orbit, the vast majority of the contribution in total ionising dose was due solar particle events (SPE). Results showed that the ionising dose produced by SPEs was at least two to three orders of magnitude greater than the contribution any ion of the GCRs would provide. For this reason and for the sake of simplicity, it was decided to determine the total ionising dose inside the CubeSat purely based on radiation coming from the Sun.

To start, the skin of the CubeSat will be assumed to be composed purely of pure aluminium. In early stages of the project, combinations of aluminium and lead were tested proving to be very good shielding effective. Unfortunately, the use of lead is not compatible with [SUS-SYS-01] requirement, hence its use was discarded. This said, simulations were run multiple times having at every run a different skin thickness as input. Eventually, the plot in Fig. 4.41 was produced, better known as the dose-depth curve. As one can observe, a skin thickness approximately ranging between 0.7 and 0.8 millimetres would just be enough to obtain 10 krad of ionising dose during the entire mission. A 50% margin was added for safety and to improve reliability, increasing the thickness to 1.2 mm. With dimensions of 0.34x0.22x0.22 cm and a total cutout area of 300 cm^2 to account for openings for thrusters, sensors, and the boom, and a density of 2770 kg/m^3 [49] this means the radiation shielding weighs 1.22 kg. Applying the 20% component-level mass margin for custom designed components [50], the total mass of the shielding becomes 1.46 kg.

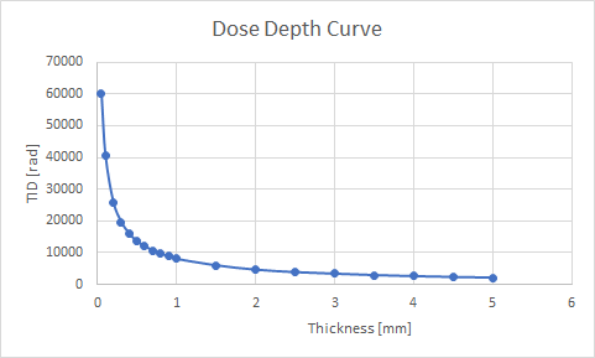

Figure 4.41: Dose-Depth curve for solar protons interacting with a finite aluminium planar slab.

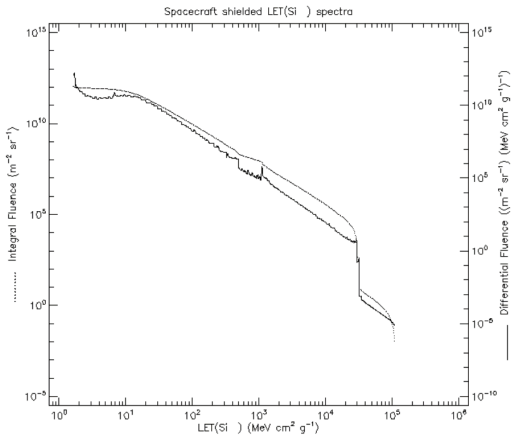

Figure 4.42: Spacecraft shielded LET spectra for the total mission duration

Finally, with SPENVIS it was also possible to 'predict' what would be the Linear Energy Transfer (LET) spectrum of the entire mission duration. As visible in Fig. 4.42, after a quasi linear proportionality between the influence and the LET of charged particles until deposited energies of around $2*10^4 cm^{-2} g^{-1}$, a sudden drop occurs, significantly reducing the influence of highly energetic particles.

4.7.4. Frequency Analysis

The eigenfrequencies of the CubeSats were analysed using ANSYS. A simplified version of the CAD model that modelled all the internal components as boxes of the corresponding shapes. The densities of these boxes were chosen to accurately reflect the masses of the corresponding components. For lack of a better approach, the Young's Modulus was estimated for these boxes using Eq. (4.13) such that the stiffness per unit mass is 80% of that of aluminium.

$$E = E_{aluminium} \cdot \frac{\rho_{component}}{\rho_{aluminium}} \cdot 0.8 \tag{4.13}$$

The solar panels were modelled as three layers of 2 mm thick PCB, with mechanical properties as shown in Table 4.34. The solar cells are assumed not to have any influence on the structural properties of the solar panels. These panels were modelled as having a completely connected edge on one long edge, on the opposing edge they were connected to the pin of the SADA.

Table 4.34: Mechanical properties PCB [149]

Axis	Young's Modulus [GPa]
x	28.9
y	28.9
z	13.7

Table 4.35: Results of the frequency analysis on the CubeSat in stowed position

Number	Component	Frequency [Hz]
1	Reflectarray	85.576
2	Reflectarray	122.06
3	Solar panel	222.28
4	Reflectarray	234.72
5	Solar panel	259.99
6	Solar panel	267.3

The reflectarray was modelled as a cuboid with dimensions 2 x 200 x 300 mm, with mechanical properties the same as the copper alloy in ANSYS, with a Young's Modulus of 110 GPa. This, because the reflect array is mostly made of copper, weighs slightly under 1 kg, and has dimensions of 200 x 300 mm when stowed, see Section 4.3. Furthermore, the panel housing the magnetometer was constrained as fully constrained, while the opposite panel was constrained as compression only. The corners of each long side were constrained by compression only as well. Using this, the six lowest eigenfrequencies of the model were calculated using ANSYS. The results are summarised in Table 4.35. Of these, only the first, shown in Fig. 4.43, does not fulfil the given requirements. In order to increase the stiffness of the reflect array it is pinned at the side as well using fishing cable of 1 mm diameter, with properties from the ANSYS library for Nylon.

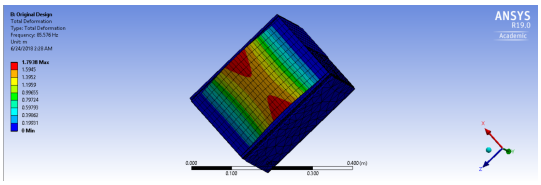

Figure 4.43: The response of the CubeSat at the lowest eigenfrequency, before adjustments were made.

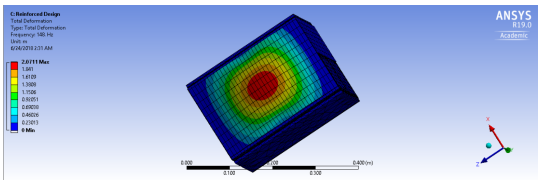

Figure 4.44: The response of the CubeSat at the lowest eigenfrequency, after adjustments were made.

After doing so, the eigenfrequencies were computed again, resulting in Fig. 4.44. Which is compliant with the requirements regarding the eigenfrequencies as stipulated in [STA-LAN-04], as can be seen in Table 4.36.

Acceleration Analysis

The geometry used in the frequency analysis was also used for the acceleration analysis. This meant only the boundary conditions had to be adjusted. The boundary conditions applied can be seen in Fig. 4.45. The layout consists out of 4 important factors:

Table 4.36: Results of the frequency analysis on the CubeSat in stowed position, after reinforcing the reflect array

Number	Component	Frequency [Hz]
1	Reflectarray	148.
2	Solar panel	222.28
3	Reflectarray	234.94
4	Solar panel	259.99
5	Solar panel	267.3
6	Solar panel	275.24

Table 4.37: Resulting stresses from accelerations
With faces as described in Chapter 5

Direction	Face	Acceleration [g]	Maximum stress [MPa]
Longitudinal	Top	17	13.3
Longitudinal	Bottom	12.4	10.0
Lateral	Front	4.8	25.4
Lateral	Back	4.8	26.8
Lateral	Left	4.8	6.5
Lateral	Right	4.8	7.2

- Acceleration, is applied in the opposite direction as the objects actually accelerate in, as specified in the ANSYS manual [37]
- A force opposing the acceleration is applied to the four corners on the bottom plate
- The side edges were placed under a compression-only restraint, as they would be kept in place by the P-Pod
- The side opposite to the face where the force is applied is fully constrained, this to allow ANSYS to converge to a result

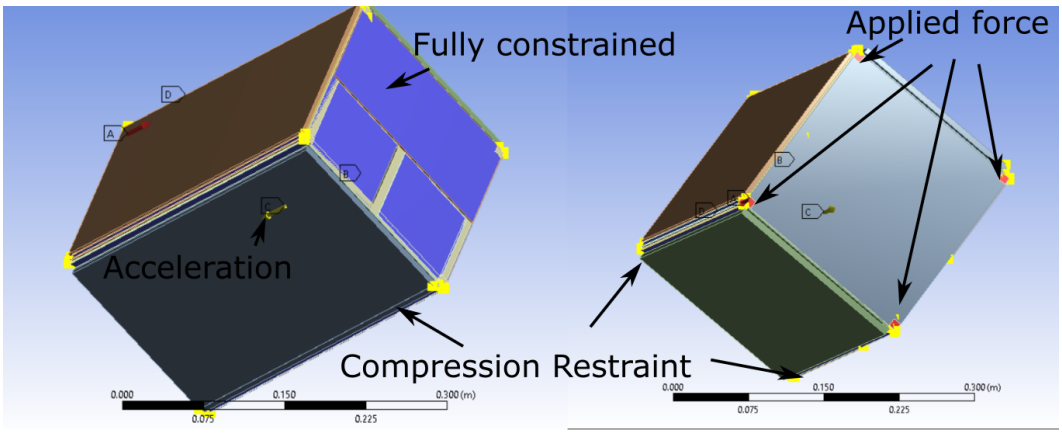

Figure 4.45: Model used to simulate launch conditions

The results show that all stresses are far lower than the maximum yield stress of 280 MPa, as taken from the ANSYS library. However, each of the columns still has to be checked for column buckling. This is done using Euler's formula, as represented in Eq. (4.14). Here k is a factor accounting for the end condition. The structure fixes both ends, and as such k is taken as 0.5. The moment of inertia is taken about the side with the lowest thickness, as that is the critical side.

$$F = \frac{\pi^2 \cdot E \cdot I}{(k \cdot L)^2} \tag{4.14}$$

[37] https://www.sharcnet.ca/Software/Ansys/17.0/en-us/help/wb_sim/ds_Acceleration.html [Retrieved 24 June 2018]

As mentioned earlier, the model was simplified in order to meet computational requirements. This meant all the columns were assumed to have the same thickness. Using weight estimations from ISIS, at 1.5 kg[38] and Gomspace [39] 730 g for a 6 U structure, the total weight was assumed to be 1.5 kg, the columns were computed to have dimensions of 8.5 x 8.5 mm. This meant the maximum applied force before buckling would occur, without taking into account the added reinforcement of other components, was set at 177 N, or a stress of 2.5 MPa.

As the stress was applied non-uniform, the stress was taken at the middle of the column. Comparing these between load cases, the maximum stress was found to be below the buckling stress in all cases except for the longitudinal loading with acceleration of 17 g. Here the maximum stress was found to be 3.6 MPa in the corner columns, see Fig. 4.46. However, as the side plates prohibit buckling in both directions in these columns, this was assumed not to be an issue. Furthermore, the simplified model, with the same mass as the actual design, is expected to handle the applied accelerations worse than the structure optimised for this specific load case.

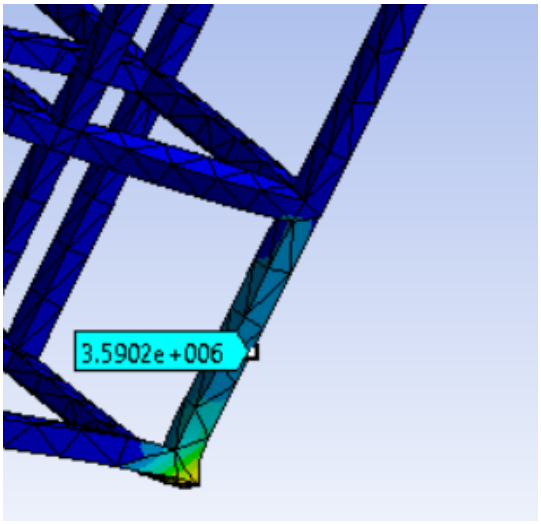

Figure 4.46: The maximum stress during launch

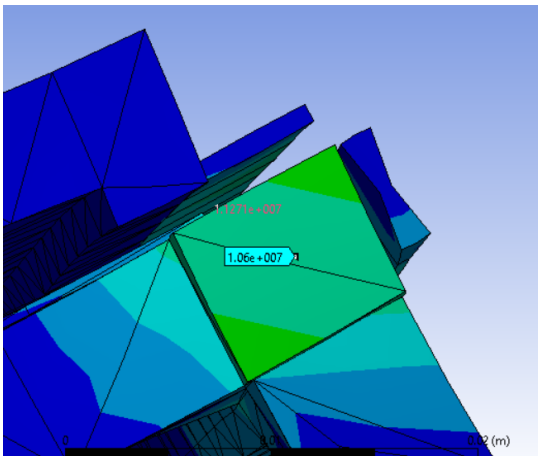

Figure 4.47: Stress in corners in Pa

4.7.5. Verification

Lastly, the structural analysis is verified. This is done using analytical formula which have been proven to be correct.

Frequencies

In order to verify the result, the lowest eigenfrequency was analysed analytically. This was done by assuming the reflect array is a uniform beam with fixed ends, such that Eq. (4.15) can be used [150].

$$f = \frac{K}{2 \cdot \pi} \sqrt{\frac{E \cdot I}{m_l \cdot l^4}} \tag{4.15}$$

Here K is a constant, depending on which mode is analysed, set at 22.4 for the first mode. E is 133 mm^4, I is 110 GPa, m_l was 0.0033 g/mm. The length l is set at 297 mm, this as the connection at each side was drawn as 1.5 mm wide such that the length between the two ends was 3 mm less than the total length of 300 mm. Using this approximation, the lowest eigenvalue was expected to be found at 83.9 Hz, relatively close to the actual found number of 85.5 Hz. Based on this, it is concluded the simulation was run correctly.

[38] https://www.isispace.nl/product/12-unit-cubesat-structure/ [Retrieved 24 May 2018]
[39] https://gomspace.com/Shop/subsystems/structures/6u-structure.aspx [Retrieved 24 May 2018]

Stresses

To find if the maximum stress is computed correctly, the total applied force is divided by the total area. Here, the maximum force in longitudinal direction is 3.4 kN, as the maximum allowable mass was set at 20.5 kg, see Chapter 5, with an acceleration of 17 g. The area where the force is added consists of the four edge columns: 289 mm^2. This means the stress here would be expected to be 11.7 MPa. However, as can be seen in Fig. 4.47, it was slightly lower. This is probably due to the relatively large mesh, required to limit the computational effort.

4.8. Thermal Control

In this section the thermal properties of Artemis and Diana are analysed. Using the obtained results, adjustments are made to fulfil the requirements. It is verified that the requirements are met. Lastly the entire section is summarised and some recommendations for future thermal design are made.

4.8.1. Requirements

In addition to the system requirements as detailed in Section 3.1, each of the subsystems had to stay within specific bounds, the exact values of these are described in Table 4.38.

Table 4.38: Temperature ranges for each of the subsystems
As specified by designer of each corresponding subsystem

Component	Survivable temperature range [°C]	Operational temperature range [°C]
Reaction wheel	-40/80	-40/80
ADCS thruster	-24/60	0/60
Magnetometer	- 55/125	- 55/125
FITPix	-50/80	-40/60
Bit-3 engine	-30/80	-20/50
Solar panels	-150/250	-50/30 optimally/50
Batteries	-20/60	5/45
Patch antenna	-20/60	-20/60
Iris transponder	-20/50	-20/50
Reflectarray	-	-20/50
OBC	-40/105	-40/105

4.8.2. Trade-off

In order to allow the requirements to be met, a thermal control system will have to be in place. This control system can be designed either to be passive or active. Furthermore, both passive and active control can be done through multiple means.

Firstly, the thermal control will be done entirely passively if possible. This to minimise the requirements on the EPS. However, if it turns out that this cannot be achieved, an active thermal control will be considered. A wide variety of passive control elements are available. However, in consultation with ISIS it was decided to only use heat sinks and insulation materials, as these are the simplest forms of thermal control to design with.

The thermal analysis can be done using a multitude of simulation programs available to the students of TU Delft. Dr. R. Hedayati recommended the use of ANSYS as it is an industry standard, yet it is simple enough that it would be feasible to analyse the thermal properties using it within the given timeframe.

4.8.3. Subsystem Configuration

First, a simplified model of the entire system was modelled using ANSYS. The results, a video illustrating the temperature, will be used to see which simplifications may be made. Figs. 4.48 and 4.49 were added as an illustration of this result, but the entire result is used to understand the interactions. Lastly, the entire system was modelled again including the implemented changes to verify the thermal requirements are met.

The thermal analysis is further split up into two parts: the hot case and the cold case. Here the hot case will be

Table 4.39: Model of the Solar Panels [151]

Layer	Thickness [mm] [mm]	Material	Density [kg/m^3]	Thermal Conductivity [W/(m K)]	Specific Heat [J/(kg K)]	α [-]	ϵ [-]
1	1	Solar Cell	5316	46.05	350	0.88	0.85
2	2	PCB	1900	0.1	1200	-	0.85

modelled as a static thermal solution where the spacecraft is in the sun, and each of the subsystems is functioning at maximum power. This as there is no possible way for the system to heat up beyond that level. The cold case will be modelled by running the spacecraft through normal operations for 10^5 seconds, normal operations being the average power each subsystem would use over time, to allow all the subsystems to reach a nominal temperature, followed by either 2142 seconds of total eclipse or 9862 seconds of eclipse with only 60% of the nominal flux, as described in Section 2.5.4. Both will have all subsystems turned off except for the CDH, batteries and the reaction wheels.

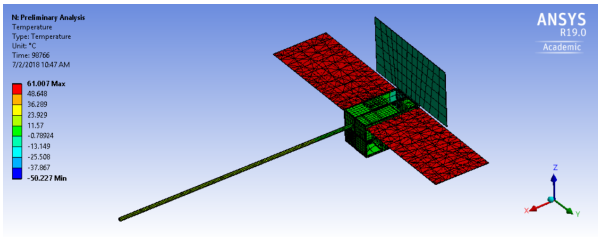

Figure 4.48: Preliminary analysis of the CubeSat in the hot case

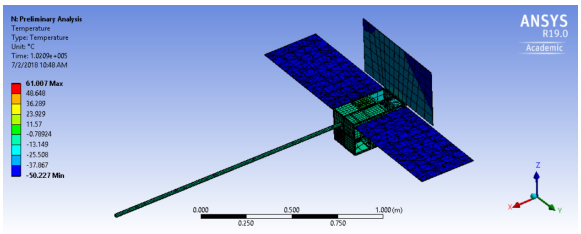

Figure 4.49: Preliminary analysis of the CubeSat in the cold case

Solar Panels

The maximum temperature of the solar panels were found to be almost completely independent from the rest of the system. This was due to their large size and small connection to the main body. As such, the thermal design for these was done independently from the rest. Using this, the solar panel was modelled as a flat plate of two layers, the exact properties are outlined in Table 4.39. This is not a perfect approximation as the coldest temperature is significantly lower than the one found in the preliminary analysis. The irradiance was taken at 1361 W/m^2 while in the sun[40], assuming the irradiance from the Moon negligible as the solar panels will not be aligned with this flux. In the cold case, the irradiance of the Moon was taken into account, as the solar panels would be pointed here to retain heat as much as possible. The Moon has a black body temperature of 271 K, and with a radius of 1737 km the surface area is 37.9 10^{12} m^2 [41]. As the solar panels are designed for the absolute worst case, the maximum distance to the moon, 6800 km, was used, this way the irradiance was established to be 13 W/m^2.

$$E_e = \frac{\sigma \cdot 1 \cdot (T_1 - T_2)^4 \cdot A}{4 \cdot \pi \cdot (r + d)^2} = 13 W/m^2 \tag{4.16}$$

All this was modelled using ANSYS. It was found that in order to ensure the solar panel stays within the given limits, it had to be cooled. Initially it heated up to almost 61°C as seen in Fig. 4.50, a figure confirmed by literature [49]. However, after adding a heat sink with emissivity of 0.85 and total added surface area of 0.22 m^2 per solar panel, it stays well within the requirements as can be seen in Fig. 4.51. Assuming the thickness of the heat sink to be 0.4 mm, and it to be made of aluminium[42], the total mass of the heat sinks would be 0.24 kg. However, a preliminary design iteration showed that the thermal control on the bus would add only a very minimal amount of mass. The thermal control subsystem has a mass budget of 410 grams total, 2% of the total mass [49]. As no detailed design on the heat sink was done, the mass is allowed to increase up to 400 grams, ensuring the mass will not go over budget in a later design phase.

[40] https://nssdc.gsfc.nasa.gov/planetary/factsheet/Earthfact.html [Retrieved 21 May 2018]
[41] https://nssdc.gsfc.nasa.gov/planetary/factsheet/moonfact.html [Retrieved 20 June 2018]
[42] http://www.alphanovatech.com/ [Retrieved 25 June 2018]

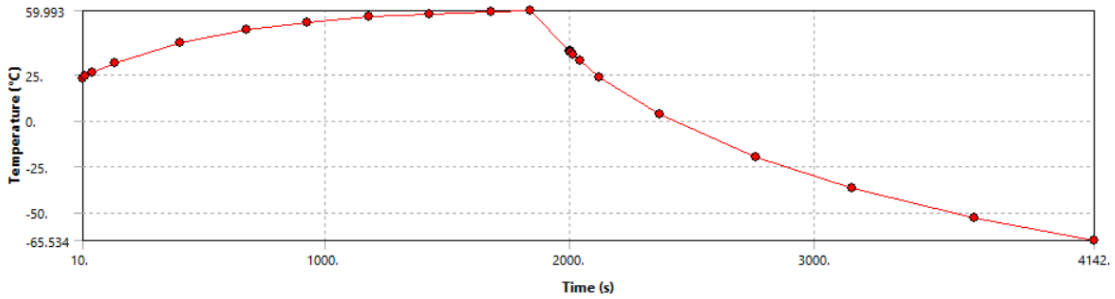

Figure 4.50: The average temperature of the solar panels throughout one orbit without adding a heat sink

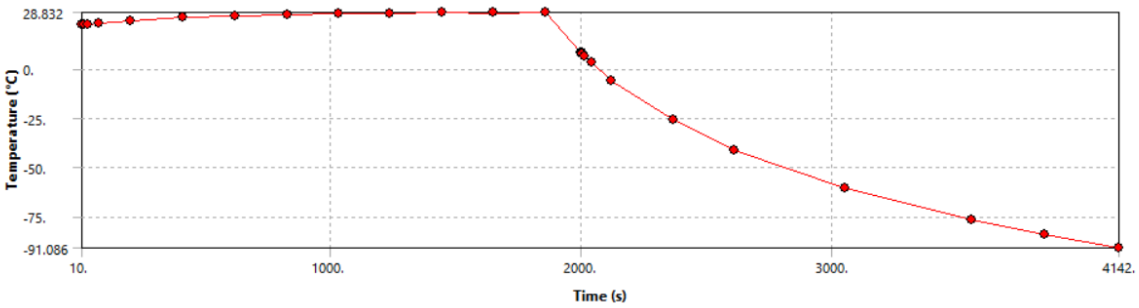

Figure 4.51: The average temperature of the solar panels throughout one orbit with a heat sink.

Reflectarray

As the thermal requirements are not known for the reflectarray, no thermal design can be conducted for this component. It is therefore assumed the temperature of the reflectarray can be maintained using the same approach as ISARA[43]. However, from the preliminary analysis it did appear the reflectarray functioned as a type of heat sink. As such it is taken into account in the further design process. It was modelled as a copper plate, with the properties used from the ANSYS database. The maximum incident power was taken at 200 W/m^2, which is a conservative estimate as the reflectarray is extremely reflective, and so in reality it would heat up less.

Magnetometer

The magnetometer sticks out from the rest of the CubeSat on a 1500 mm long rod. This means the interaction between the rest of the system and the magnetometer will be extremely minimal. Furthermore, as the magnetometer is designed to function in this environment, it is assumed no further thermal design is required. However, as the rod may function as a sort of heatsink it cannot be neglected when analysing the interaction between the subsystems.

OBC

Using ANSYS, it quickly became apparent that the OBC becomes far hotter than the surrounding environment. Furthermore, the board the components are placed on insulates well [151]. A simplified model of the entire CubeSat thermal properties shows that the effect of the environment on the OBC is negligible. However, the OBC is a standard component meant for CubeSat applications. As the environment has no large effect on the thermal properties, it is assumed the OBC will not overheat while in standard use. This means that no detailed analysis of the OBC has to be done.

As mentioned earlier, the OBC does have an effect on its surroundings. In order to simulate the entire spacecraft, a simplified version of the OBC has to be added. This simplified version consists of a single block in a steady state temperature, as the OBC is always turned on, generating 9 W of heat.

[43] https://directory.eoportal.org/web/eoportal/satellite-missions/i/isara [Retrieved 22 June 2018]

Transponder

Similarly to the CDH, the transponder becomes far hotter than its surroundings as can be seen. As for the thermal control, the transponder has been designed to ensure it does not overheat [84]. This means no further analysis on this component has to be done with regards to the hot case. However, as it is not in use during the cold case, the minimum temperatures still have to be investigated.

Remaining Subsystems

The remaining subsystems generate relatively little heat of their own, meaning their temperature is a function of the surroundings. As such they are all modelled together. All, except for the engine, are modelled as a single block with the same overall properties as the corresponding subsystem. The engine consists of two components: a thin aluminium hull covers the core. The core is the only component in the engine that generates heat.

The emissivity of components was modelled using data from [151]. For outward facing components such as the ADCS thrusters where the emissivity was not known, the emissivity was assumed the same as the structure at 0.88, this because both are made largely from aluminium. Similarly, components for which no information was available were assumed to have the same thermal conductivity, 171 W/(m K), and specific heat, 920 J/(K kg), as the structure for the same reason. For the body, the irradiance was taken at 38.5% of that of the solar panels as that is the average as calculated previously in Section 4.6. The first analysis before adding any insulation are summarised in Table 4.40 which shows the maximum and minimum temperatures for all the subsystems for different temperature cases.

Table 4.40: Temperature ranges for each of the subsystems before thermal design has been implemented, as found during simulation using ANSYS
N/A: Not Analysed

Component	Hot Case [°C]	Cold Case no Penumbra [°C]	Cold Case Penumbra [°C]
Reaction wheel	-4	-16	-38
ADCS thruster	0	-28	-36
FITPix	-1	-13	-36
Bit-3 engine	25	-20	-41
Batteries	9	-11	-30
Patch antenna	4	-24	-44
Iris transponder	N/A	-12	-35

Overall, it is clear that every subsystem can still heat up significantly before the upper bound of the operational range is reached. However, when the lower bound of the survivable range is considered, the system cools down far too much. It should be noted that the batteries heat themselves when they cool down to below 5°C with 6 W per battery pack. However, it would be better to limit the cooling to save power. Based on this it was decided to to use Multi-Layer Insulation (MLI) in a similar fashion to [151]: 12 layers of 0.00635 mm of aluminized Myler, sandwiched in between two layers of 0.0254 mm thick aluminized Kapton. This has has an absorptivity of 0.8 and an emissivity of 0.45. This was applied to the entire outside of the spacecraft. At a density of 350 kg/m^3, this adds a total of 7 g.

After applying these layers, the entire simulation was run again. The results are summarised in Table 4.41. It should be noted that while the minimum temperature of the battery is at -3°C, this is only one corner. Almost the entire battery stays above 10°C at all times. As mentioned before, if necessary, the battery can be kept at a warm temperature relatively easily using the built heaters.

4.8.4. Verification

In order to verify that the thermal requirements are met, the entire system is simulated in all three worst case scenarios. By doing so, the assumptions made previously that specific subsystems can be designed for separately are checked. The results are compared to the requirements in Table 4.42. Doing so clearly indicates all the requirements have been met. Only the reflectarray may cool down too much, but the survivable temperature is not known and as such this cannot be verified.

Table 4.41: Temperature ranges for each of the subsystems after thermal design has been implemented, as found during simulation using ANSYS with the simplified model
N/A: Not Analysed

Component	Hot Case [°C]	Cold Case no Penumbra [°C]	Cold Case Penumbra [°C]
Reaction wheel	31	21	0
ADCS thruster	34	9	-9
FITPix	33	22	2
Bit-3 engine	34	18	-3
Batteries	26	20	-3
Patch antenna	33	14	-6
Iris transponder	N/A	24	4

Table 4.42: Verification that the thermal requirements have been met, as found during simulation using ANSYS with the non-simplified model
NA: Not Analysed

Component	Survivable temperature range [°C]	Operational temperature range [°C]	Hottest temperature [°C]	Coldest temperature [°C]
Reaction wheel	-40/80	-40/80	31	0
ADCS thruster	-24/60	0/60	31	-9
Magnetometer	- 55/125	- 55/125	NA	NA
FITPix	-50/80	-40/60	33	2
Bit-3 engine	-30/80	-20/50	35	-2
Solar panels	-150/250	-50/30	30	-77
Batteries	-20/60	5/45	30	-3
Patch antenna	-20/60	-20/60	34	-5
Iris transponder	-20/50	-20/50	N/A	3
Reflectarray	N/A	-20/50	21	-36
CDH	-40/105	-40/105	N/A	N/A

With regards to the validation of the software: ANSYS has been validated extensively [152–154] and is an industry standard.

While ANSYS is an industry grade commercial program, in order to verify that the software was implemented correctly its results were compared to an expected result calculated using python. Here thermal influx was used as an input parameter, the radiation power was modelled using the Stefan-Boltzmann law Eq. (4.17). Emissivity was the same as was used in the ANSYS simulation. Lastly, the temperature change was modelled using Eq. (4.18). Temperature transfer between the layers of the solar panel was assumed to be immediate. This equation simply states that the difference in energy divided by the total specific heat and mass results in a temperature change over time. This resulted in Fig. 4.52, illustrating that the difference between the ANSYS result and the expected result is negligible.

$$P_{out} = \sigma \cdot \epsilon \cdot (T_1 - T_2)^4 \cdot A \tag{4.17}$$

$$dT = \frac{P_{in} - P_{out}}{\Sigma m_i \cdot c_i} \cdot dt \tag{4.18}$$

4.8.5. Conclusion and Recommendations

The thermal properties of the CubeSats have been analysed using ANSYS. Using this, adjustments were made to ensure the components stay within acceptable temperature ranges.

Both Artemis and Diana control their temperatures by passive control. Each of the solar panels needs a heat sink with emissivity of 0.85 and total added surface area of 0.22 m^2, with an estimated mass of 0.4 kg. Also, the entire outside of the CubeSat will be covered with 12 layers of 0.00635 mm of aluminised Myler, sandwiched

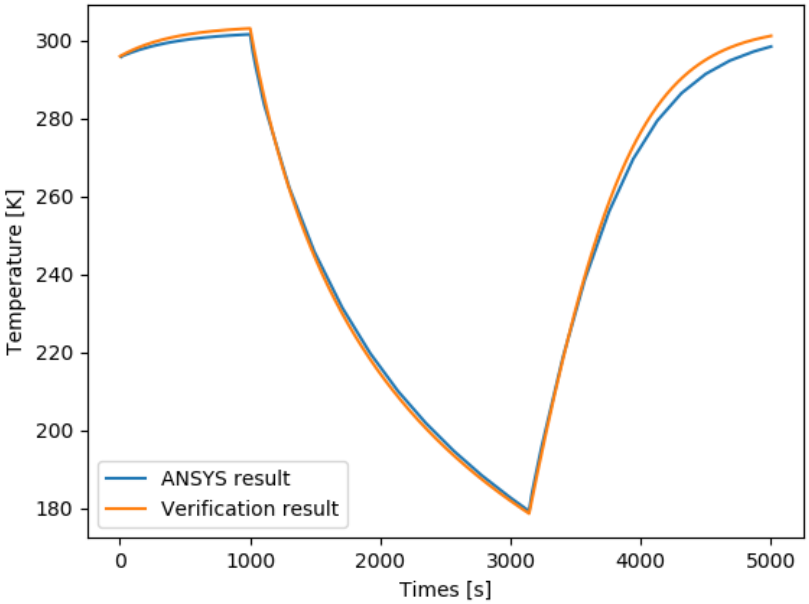

Figure 4.52: Comparison with ANSYS and the verification.

between two layers of 0.0254 mm thick aluminised Kapton, adding a negligible 7 g to the entire structure.

With regards to the thermal analysis, future recommendations are:

- Acquire more accurate information on the thermal properties of the components
- Acquire an ANSYS license without a limitation on mesh size
- Simulate several orbits to take into account the effect of not being in steady state before going into eclipse

5

System Design and Performance

This chapter outlines the system configuration and general system performance. First the system configuration is described in Section 5.1. The sensitivity of the system is analysed in Section 5.2, together with the risk in Section 5.3. The system verification and manufacturing is described in Section 5.4 and Section 5.5 respectively.

5.1. System Configuration and Characteristics

The entire CubeSat is designed to have a total wet mass at launch of 20.5 kg, 1.5 kg of which is propellant mass. These figures do include margins dependent on TRL, and a final margin of 20% is placed on the overall system. The exact distribution of mass is shown in Table 5.1.

Table 5.1: Mass Distribution CubeSat including margins
*Stored outside the CubeSat and is thus neglected

Subsystem	Component	Amount	Total Mass [kg]	Total Volume [U]
ADCS	Reaction wheels	4	0.98	0.58
	Star tracker	1	0.36	0.35
	Sun sensor	6	0.01	0.011
	IMU	1	0.004	0.005
	Thruster system	2	1.25	0.83
	Processor	1	0.077	0.019
CDH	Cubic OBC	1	0.22	0.2
	USB Controller	1	0.066	0.2
	ADC	1	0.063	0.1
	RS PCI card	1	0.22	0.15
COMMS	Reflectarray	1	1.1	0*
	Patch Antenna	4	0.064	0*
	Iris Transponder	1	1.26	0.53
EPS	Solar Array	2	1.7	0*
	Body Mounted Solar modules	1	0.07	0*
	Batteries	2	1.05	0.7
	PCU	1	0.084	0.09
	ACU/PDU	4	0.0.235	0.05
	SADA	1	0.2625	0.06825
PAY	FITPix Lite unmodified	2	0.119	0.044
	Spacemag Magnetometer	1	0.472	0.29
	FITPix Lite coated	1	0.062	0.022
	AstroTube Boom	1	0.64	1.05
PROP	Engine	1	1.575	1.7
	Fuel	-	1.5	0.3
STR	Primary Structure	-	1.57	0*
	Shielding	-	1.88	0*
THERM	Insulation	-	0.01	0*
	Heat sinks	-	0.29	0*
Total Dry			16.58	7.1
Total Dry With 20% Margin			18.90	8.52
Total Wet			20.40	8.82

Using the layout as described in the next two sections, this puts the centre of mass at a distance of 0.7 and 3 mm sideways as seen from the engine and 8 mm up from the geometrical centre when the CubeSat is in stored position, well within the requirements of the CubeSat standard of 3.2.10 which specify it should be less than 45, 20 and 70 mm from its geometric centre in [93]. With all the deployables extended, the centre of mass is located 2.1 and 0.1 mm to the side, and 17.6 mm up from the geometrical centre, easily allowing the Bit-3 to align the

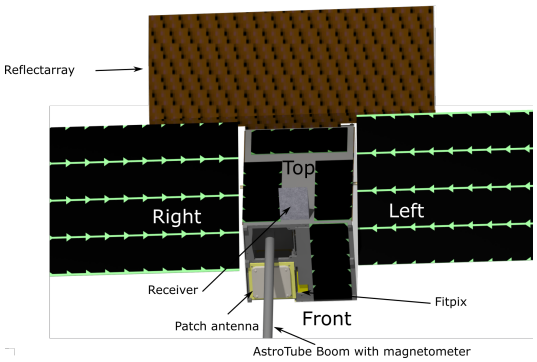

Figure 5.1: Front view of the CubeSat

thrust vector with it.

The entire volume is smaller than the maximum allowed volume of 12U. This allows for easier assembly. This, combined with other factors such as the components not interacting with each other, increases reliability [55].

5.1.1. Configuration

For the best possible performance of the spacecraft not only the characteristics of the subsystems are important, but their configuration within the spacecraft itself as well. Said configuration is described in this subsection.

External Configuration

The external configuration is illustrated in Fig. 5.1. Most notable is the fact that four deployables are present. The solar panels fold up onto the left and right side panel, with the solar cells facing outward. The reflectarray folds up on the top. While it may seem from the pictures that the reflectarray and the solar panels would touch when the solar panels turn, this is not the case. A 10 mm gap has been left open at the bottom of the reflectarray, allowing the solar panels to turn a complete 360°. The last deployable, the boom, is rolled up, and only unrolls after launch.

With regards to communication, three patch antennas and one reflectarray are used. Opposite of the reflectarray, a feed is placed toward which the reflectarray is aimed. Furthermore, one patch antenna is aligned with the reflectarray, as can be seen in Fig. 5.1, allowing the system to downlink and uplink simultaneously. The other two are placed on the bottom face, as shown in Fig. 5.2, these are used as secondary antennae. Non of these patch antennae are covered by any deployables, ensuring uplink is possible even if a mechanical failure were to occur.

Furthermore, two ADCS thruster blocks are pointed outwards at opposite sides of the CubeSat. Each of these thruster blocks have 5 thrusters pointing outward under an angle. The position of the thruster blocks and the direction of the corresponding thrusters is indicated in Figs. 5.2 and 5.3.

There are three patches of body mounted solar panels on the top face. Furthermore, the front face also has a solar panel. On the same panel, two FITPix Lite are positioned on the front panel and are open to receive radiation. One FITPix Lite with coating is placed on the back panel behind the aluminium panels. In Fig. 5.3 the last FITPix is shown with the aluminium panel hidden to illustrate the exact position.

Lastly, on each face a sun sensor is placed. However, as these are relatively small and can fit practically anywhere, their exact location can still be changed relatively easily and as such have not been drawn in.

With regards to the interaction with thrusters and the payload, no issues are expected. The ADCS thrusters use cold gas and should have no influence on the radiation measurements. The BIT-3 ion engine could interact with the payload, but it will not do so as it is pointed away from the spacecraft.

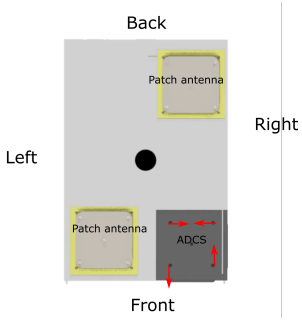

Figure 5.2: Bottom view of the CubeSat

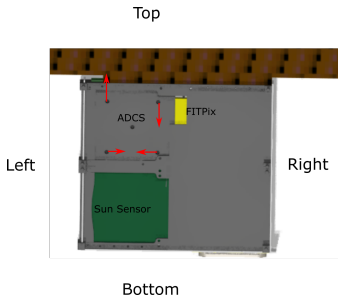

Figure 5.3: Back view of the CubeSat

Internal Configuration

The CubeSat consists of two layers. The top layer can be seen in Fig. 5.4. In the centre a SADA covers the top. Underneath the SADA two battery packs with a PCU and four reaction wheels are housed. Furthermore, the AstroTube and magnetometer are also placed in the top layer. The Iris transponder is placed as close as possible to the feed and patch on the front panel to reduce system noise. Lastly, one ADCS thruster block is placed facing the back.

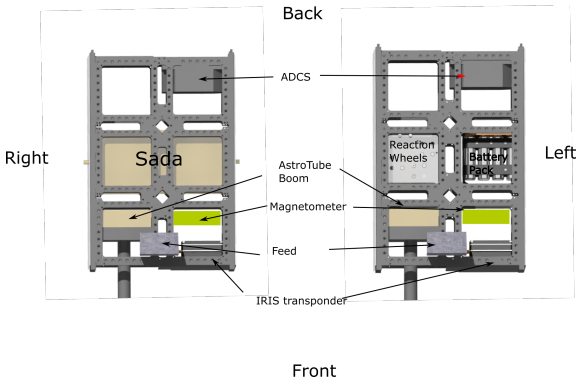

Figure 5.4: Top layer of the CubeSat

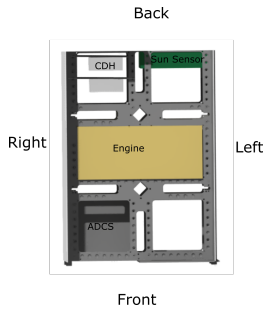

Figure 5.5: Bottom layer of the CubeSat

The second layer can be seen in Fig. 5.5. Most notable is that the thruster of the engine is placed along a lateral axis. This was done to allow the thrust vector to align with the centre of gravity, minimising the torque this would cause, while the structure would (barely) have to be changed. This also solved issues regarding the ADCS as it increased the moment arm the thrusters would have. The reason most satellites thrust along the longitudinal axis is to minimise drag. This is not a design issue for Artemis or Diana as both will be going to deep space. After consulting experts from the Technical University of Delft, it was found that this layout would be feasible.

The CDH is placed opposite of the Iris transponder. This was necessary to keep the centre of gravity centralised. One drawback of this is that the wiring from and to major components such as the FITPix, magnetometer and transponder will be relatively extensive. While the CDH is drawn as two blocks, this effectively consists out of numerous components placed on several boards.

Lastly, one sun sensor is placed facing outwards and will not be covered by any deployables during launch.

5.2. Technical Sensitivity

Some parameters involved in the design of the probes are subject to uncertainty. This can be due to a number of reasons: the analysis required to determine the parameter with absolute certainty can be too complicated and an approximation had to be used instead. Environmental parameters can sometimes behave in an unpredictable manner and it may not only be complicated, but entirely impossible to predict them reliably. One example for this

is the solar activity, which directly influences the solar flux experienced by the probes. In this section the technical sensitivity of the design to such aspects will be analysed.

5.2.1. Solar Flux

The solar flux played a fundamental role in the sizing of the solar arrays and the thermal analysis of the system, so it seems natural to investigated how these aspects of the design develop with changing solar flux. However, fluctuations of the solar flux are generally in the order of +/- 0.2%[1], such that the investigation showed no relevant effects.

5.2.2. Compression Rate

The maximum allowed compression rate is expected to be related to the saturation and quality of the radiation environment measurement data, which in itself is not reliably predictable. Sparse measurements enable better compression of the data [118], which can take stress of the on-board processing units and the link budget. But if the saturation of the measurement increases, compression may become an issue of concern, because the loss-free compression scheme may not be able to generate frames that fit within the available downlink budget. This can be handled by either using more rigorous compression schemes, which lead to information losses within each measurement frame, or by operating the payload for only a fraction of the available time. Whereas generally the former is recommended, either option is not ideal and should be avoided.

Because FITPix-specific research in this area has been very limited and only one source is available at this point [118], it is not possible to establish a quantitative relation between the measurement saturation and the downlink budget. It should however become clear from the qualitative discussion, that such an analysis has to be performed in future design stages.

5.2.3. Astrodynamics

The suggested transfer involves some unknown alterations along the trajectory, which may very well have an impact on the spacecraft's maximum distance to the ground station. In the sizing of the COMMS subsystem, this parameter sets the minimum data rate during transfer. The sensitivity of this minimum data rate was investigated as a function of variations in the maximum ground station distance. From the result shown in Table 5.2 it can be seen that decreasing the maximum ground station distance by 10% can improve the data rate by a significant 23.5%. On the downside, however, a variation of 10% in the opposite direction can decrease the downlink rate by more than 17%. Considering that the transfer trajectory will be subjected to changes in order to fit it perfectly for the ARCHER mission, a maximum ground distance variation of 10% can occur. As a consequence of this insight, it is recommended to strictly monitor the effect on the link budgets throughout the detailed design of the transfer trajectory.

Another uncertain design parameter associated with the astrodynamics of the mission is the power available to the engine during the insertion of the Artemis probe. This is due to the complexity of the eclipse time analysis of the insertion trajectory and the uncertainty of contact time requirements during this phase of the mission. While the trajectory has been designed based on the availability of 75% total thrust, the sensitivity of the required insertion time and Δv to a change in the available thrust was investigated, too. As shown in Table 5.2, it was found that for a 20% reduction of the thrust level, the insertion time and Δv only increased by 4.2% and 5.6%, respectively.

5.2.4. Pointing Accuracy

It is now known that the downlink data rate is a strong function of the distance to the ground station, however, it was found that it is also very sensitive to the pointing accuracy of the antenna. Its nominal accuracy is limited by the +/-1° error of the ADCS. If for some reason this system fails to perform at this accuracy and the pointing error increases by +/-2°, the data rate is cut drastically by 50%.

The pointing error of the ADCS also translates into the incidence angle on the solar arrays and consequently the power generation. The consequences are much less pronounced: a increased pointing offset by +/-2° (from +/-1° to +/-3°) causes less than one percent loss of generated power.

---

[1] `en.wikipedia.org/wiki/Solar_cycle#/media/File:Solar-cycle-data.png` [Retrieved 20 June 2018]

System	Aspect	Design value	Variable parameter	Amount of variation	Value after variation	deviation [%]
EPS	average power generation	133.89 W	average incidence angle	+/-2°	133.73	-0.122
COMMS	downlink rate	1.319 MBit/s	pointing error	+/-2°	0.661 MBit/s	-50
COMMS	downlink rate	1.319 MBit/s	maximum distance to Earth	-10%	1.629 MBit/s	+23.5
COMMS	downlink rate	1.319 MBit/s	maximum distance to Earth	+10%	1.09 MBit/s	-17.36
ASD	transfer time	115 days	thrust level	-20%	119.8 days	+4.2
ASD	transfer Δv	547.75 m/s	thrust level	-20%	578.31 m/s	+5.6

Table 5.2: Sensitivity study of sizeable subsystem key aspects

The study shows that the EPS system can handle incidence angle variations very well. Furthermore, the insertion trajectory parameters proved to be robust to changes in the available thrust level. The downlink data rate was found to be the most sensitive element. It shows great dependency on the distance from the ground station and the antenna pointing error. It is recommended to perform a detailed link budget analysis for possible alterations of the transfer trajectory, pointing offsets and measurement saturation to avoid a disadvantageous interaction between these parameters that could significantly decrease the scientific value or even lifetime of the mission.

5.3. Technical Risk

In this section, the technical risk analysis for the ARCHER mission is performed. This is done by first identifying all of the risk elements. These are then put into a risk map visualising their risk. A mitigation strategy for the highest-risk elements is then presented after which an updated risk map follows.

5.3.1. Risk mapping

The risk elements are defined as all of the spacecraft components in all of the subsystems. These have been identified by their respective subsystem managers and listed as follows.

Risk elements

- [1] BIT-3 engine (PROP)
- [2] VACCO MiPS Standard (ADCS)
- [3] FITPixLite (Payload)
- [4] USB Network Module (CDH)
- [5] Nanopower BPX (EPS)
- [6] Azur 3G30A (EPS)
- [7] SADA (EPS)
- [8] Array (EPS)
- [9] P60 PCU (EPS)
- [10] Structure (STR)
- [11] Solar Panels (THERM)
- [12] Body (THERM)
- [13] CDH and IRIS (THERM)
- [14] Neutron FITPix (Payload)
- [15] Magnetometer (Payload)
- [16] AstroTube Boom (Payload)
- [17] Small launch inaccuracy (ASTRO)
- [18] Large launch inaccuracy/failure (ASTRO)
- [19] RS Serial Adapter (CDH)
- [20] Reaction Wheels (ADCS)
- [21] Star Tracker (ADCS)
- [22] Sun Sensor (ADCS)
- [23] IMU (ADCS)
- [24] Dedicatied OBC (ADCS)
- [25] Reflectarray (COMMS)
- [26] IRIS (COMMS)
- [27] Patch Array (COMMS)

As one can see, first the number identifying the risk element is provided and then the component itself along with its subsystem are stated. This generates a list with the relevant risk elements to be assessed.

5.3.2. Risk map

The risk elements from the risk element list are then mapped on the risk map, as seen in Table 5.3. This risk map shows both the probability and the severity of the element failure. The probability and severity are defined as follows.

Severity

- [1] Reduced redundancy
- [2] Action from ground required for nominal operation
- [3] Somewhat worse science gathering capabilities
- [4] Much worse science gathering capabilities
- [5] Mission death

Probability

- [1] Flown many times
- [2] Flown once or twice
- [3] To be flown
- [4] Ready to be flown
- [5] Not ready to be flown

The probability criteria are used as an initial placement tool into the risk map. For the updated risk-map the probability is taken as relative probability concerning all components. The scale of severity for the updated risk-map remains unchanged. Multiplying the severity and probability scores gives the risk score. Said quantities of risk have been colour-coded, with low, medium and high risk being visualised using green, yellow and red respectively. The elements in the high risk area are underlined.

Table 5.3: Technical Risk map with mitigated risks underlined before and emboldened after mitigation

5	23				
4	22	7			
3	17	12		3, 14	4, 19
2		20	1, 11,16, 25	2, **3, 14**	8, 24, 26, **4, 19**
1	6, 27	5, 21	15		9, 10, 13, 18
^Probability Severity >	1	2	3	4	5

5.3.3. Risk mitigation strategies

In order to increase the value of the spacecraft the individual risks should be minimised. Seeing as due to schedule-constraints this is unfeasible to be done for all risk elements, it was only done for the high-risk ones using respective risk mitigation strategies. It was found that the main reason for elements being put into the high-risk part is due to the fact that those are the elements most susceptible to failure due to radiation. A general risk mitigation strategy was thus adopted to decrease said probability of failure. This is done by spending more time and financial resources to ensure a more rigorous and accurate test campaign, with a focus on testing radiation hardening and solving any issues found. Furthermore, it should be noted that the team has built up a network of specialists for the respective components and subsystems, which reduces the general technical risk by increasing overall design expertise.

5.3.4. Updated risk map

Implementing said risk mitigation strategy moves all of the high-risk elements to medium-risk, as seen in Table 5.3. The elements moved are underlined at their old position and emboldened at their new position. This change greatly reduces the overall risks of mission failure caused by technical components, which results in an increase in the value of the mission. This also increases the likeliness of this mission actually being chosen and becoming a reality.

5.4. System Verification

System level verification is used to determine if the system meets the design solution specifications and requirements. Testing must be performed on the built system to ensure this is so and if it is discovered that the system does not meet the requirements or specifications, it must be modified. Component level testing was done on each component and is explained in the relevant subsection in Chapter 4. System testing analyses does not focus on just a component but verifies the entire system and how it functions as an integrated whole. Once verified, it can be validated and flight qualified as explained in Section 6.4. How the system verification integrates with the proposed project schedule can be seen in Section 6.7.

It is important to test basic parameters such as volume, mass, centre of gravity. Each test should be prepared, planned, executed and documented. In addition to the basic parameter measurements, the following system level tests should be carried out, as seen in Table 5.4.

Table 5.4: System Level Verification Tests

Test	Area	Explanation
Power charge/discharge	EPS	Verify capacity & charge time (one of the four essential tests [55]).
Thermal vacuum cycling	System	Verify thermal modelling results (one of the four essential tests [55]).
Power modes	EPS	Verify the actual power used in each mode.
Vibration	System	Verify eigen frequencies. Verify cabling, connectors etc. do not break.
Strength	Structure	Verify buckling stress.
Compatibility	Interfaces	Verify components work together and can communicate.
Torque	ADCS, SADA	Verify rotational torque adequate to rotate CubeSat & array.
Shock	System	Verify the system can survive sudden mechanical shocks.
Deployment	Deployables	Verify array and magnetometer will deploy as designed.
Field of View	Sensors	Verify they can operate correctly and are not obscured.
Communication	COMMS	Verify transceiver operates correctly & interfaces with the antennas.
Radiation	System	Verify radiation protection of the structure & shielding.
EM Compatibility	Electronics	Verify electronic components do not interfere with each other.

5.5. Manufacturing, Assembly and Integration

In this section, the Maintenance, Assembly and Integration plan (MAI) is presented. The current MAI is largely based on the preliminary MAI presented in [17].

5.5.1. Production Plan Flowchart

Due to the nature of the project, which is using off the shelf parts, manufacturing of the subsystems and individual parts is not considered here as they are assumed to all be off the shelf. In Section 5.5.1 the basic flow chart for the integration of ARCHER can be found.

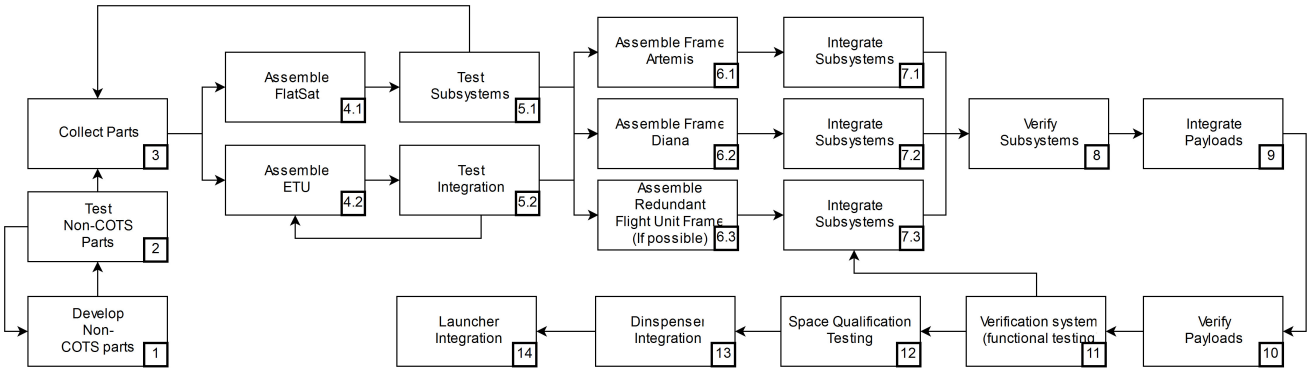

Figure 5.6: Flow Diagram MAI plan

During all steps, it is important that all work performed should be well documented. For example, photo's should be taken at set intervals or at important steps during integration. This is important for troubleshooting and continuity in the integration team, and prevents "reinventing the wheel" [155].

Firstly, in block 1, the development of non-COTS part is displayed. This rather general description of a manufacturing element describes the steps involved in either developing the elements that are not available off the shelve or modifying the COTS parts that are not applicable as-is. After this, the parts that are not yet qualified for use in space, will have to be tested and qualified. Tests include random vibration testing, shock tests, thermal and vacuum tests as well as radiation tests. In Section 6.4 these tests will be elaborated on for the system, but in some cases also apply to the components in development.

As stated in [17], according to the NASA CubeSat Launch Initiative [155], in parallel with constructing the flight unit, it is wise (if the budget allows it) to also produce an Engineering Testing Unit (ETU) for testing subsystems and integration. Furthermore it is recommended to create a FlatSat (a complete satellite excluding the structure [155]) for testing and troubleshooting the systems. Lastly it is recommended to build two flight units for redundancy and for having a choice in selecting the best unit. Therefore, steps 4 and 5 include the assembly and testing of a FlatSat and an ETU. From the testing of the subsystem and the integration test a feedback loop is present back to block 3 and 4.2 to display the possibility of having to adapt the design and even the possibility of having to re-select parts. The units will remain involved in the rest of the manufacturing process in order to troubleshoot the flight units without compromising them.

Then the manufacturing of the flight units will begin, in all blocks 6. As can be seen, the possibility of having a redundant 3rd flight unit is considered if the budget allows it. This would allow for redundancy and to select the best flight unit out of the three for the actual mission. Next block, the subsystems can be integrated according to the process tested in block 5.2. After this, all units will have to be tested and verified to be working correctly. Continuing, all payloads should be integrated (block 9) and tested to be functioning correctly (block 10). After the integration and internal development testing of the flight unit(s), the CubeSat should be verification tested [155]. After this testing, no more changes to the CubeSat can be made or it would have to be qualification tested again [156]. Due to the payload performing radiation measurements, part of these tests may have to be done in a radiation testing facility. Then the functional testing of the entire system should be performed. This testing is an important part of the manufacturing process, as the lack of proper testing is a cause of CubeSat failures [53]. Results from these test feedback into the integration of the subsystems, as possible errors will have to be addressed.

After block 11, the whole system will have to undergo rigorous qualification testing, which will be further elaborated Section 6.4. Once qualified, the CubeSat will be integrated in its dispenser and launcher, respectively.

During all steps of manufacturing, energy consumption should be kept at a minimum according to requirement [SUS-MNF-1]. This should be considered mainly during the testing campaign, where the reproduction of the environment will cost a considerable amount of energy. The only way to minimise this is to conduct these tests not more often than is strictly necessary. Therefore, in the production plan, no feedback loop is present from qualification testing: it is considered to only be performed once.

6

Mission Capability and Future Development

This chapter will highlight the finished product's capabilities and showcase how the design satisfies the mission need. First, how it will operate within the market will be presented in Section 6.1. Then, the general mission plan will be presented including the launch and deployment in section Section 6.2 and the operations and logistics in section Section 6.3. Then, the final product validation is explained in Section 6.4. The sustainability assessment and requirement compliance will be shown in Section 6.5 and Section 6.6 respectively. This chapter will round of by looking at how the project can be developed into the future in Section 6.7, the associated costs, in Section 6.8, and the project Gantt chart in Section 6.9.

6.1. Market Analysis

This section will analyse where ARCHER fits into and affects the market. It will explore target and future markets and detail the expected return on investment.

6.1.1. Stakeholders

An initial analysis identified several generic stakeholders. This has been extended and added to with actual suppliers and partners as seen in Table 6.1.

Table 6.1: Stakeholders

Type	Name
Customer	TU Delft, European Space Agency
Company/Manufacturer	Innovative Solutions In Space, GOMSpace, Hyperion Technologies HoneyBee Robotics, Jet Propulsion Lab, Cubic Aerospace, many others
Launch Contractor	SpaceX, Arianespace, United Launch Alliance, Indian Space Research Organisation, International Launch Services, Orbital ATK
Transport	DHL, FedEx, UPS, many others
Operators	ESTRACK, TU Delft
Scientific World	Universities, Astronauts, Scientists, Academics, Students
Spaceflight Community	NASA, European Governments, United Nations, SpaceX Blue Origin, Virgin Galactic , Genral Public

6.1.2. Strengths, Weaknesses, Opportunities and Threats

A Strengths, Weaknesses, Opportunities and Threats (SWOT) analysis was carried out to better understand how ARCHER can position itself in the market. As a result risks can be better addressed and the economic viability of the mission ensured. The results can be seen in Table 6.2.

Table 6.2: Market SWOT analysis

	Strengths	Weaknesses
Internal	• Relatively low cost satellite bus • High budget • Valuable research subject • High spec miniaturised science payload • 2 CubeSats for reliability and resolution	• Short time frame for mission design • Platform reliability issues • ITAR restricted technology • Ground station expense
	Opportunities	Threats
External	• Greatly extend knowledge on interplanetary radiation • Potential to open up new technology markets • Potential to make space flight safer and more ethical • A need to better understand radiation risks • In expensive technology demonstration	• Important technology delayed • Production/launch delay • Superseded by large mission • Loss of funds

This project has many strengths and opportunities and these are expanded on in Section 6.1.4 and Section 6.1.5. One weakness is the short time frame to design, develop and launch the mission. In addition, the CubeSat platform has had reliability issues in the past. This requires extensive mission testing to verify and validate the design. However, the short time frame complicates this. Currently, the design uses an American engine. Due to International Traffic in Arms Regulations (ITAR), this may become unavailable before launch. A big threat would be a highly funded larger mission with the same scientific goal reducing the need for ARCHER.

6.1.3. Market and Cost Requirements

It is essential that the ARCHER mission reliably characterises the interplanetary radiation environment with a high degree of precision. Other missions have had radiation detectors on board, see Section 2.1. Their data however, has been limited in either range or precision. If ARCHER is to add value to the available scientific body of knowledge, it is required that the data the mission delivers is consistently of high quality, covers a broad range with good resolution and is made freely available to the scientific community.

In addition, ARCHER must deliver this value at a reasonable cost. While most CubeSat missions are relatively cheap, with the cost per satellite being less than $0.1 million[1], project ARCHER is expected to cost 5.5 million euro's as detailed in Section 6.8. ARCHER though has some telling differences versus most other CubeSat missions. For example, it is required to exit the Earth's magnetosphere not just float in LEO. It is planned to last 2 years where the median lifetime of a CubeSat is about 90 days [7]. Often, CubeSats are built by students but the extreme reliability required by ARCHER will require the use of paid professionals. Finally, there are only 2 satellites in the ARCHER mission while many CubeSat missions design swarms of satellites which reduces the cost per unit significantly[2]. As a result, it falls into a category with the likes of some of NASA's CubeSat missions.

NASA has indicated that deep space CubeSat missions in the range of $ 10-100 million are possible [157] and has already invested $ 13 million in the MarCO CubeSats[3]. ARCHER's budget of 10 million euro for the mission should then be feasible considering the potential benefits it could bring to human space exploration.

6.1.4. ARCHER's Market Edge

With so many deep space exploration missions planned there is a clear need to better understand the radiation risks to human interplanetary travel [12]. Therefore, in order to satisfy the market requirements, the payload was thoroughly investigated and extensively analysed. A high spec miniaturised payload suite consisting of three FITPix devices designed will cover 0.1 and 200 MeV neutron range with a sensitivity of $5 \cdot 10^{-4}$ MeV cm^2/mg to 10 MeV cm^2/mg. The FITPix devices have yet to be used in deep space and have never flown in such a configuration. Add to this the resolution that comes from having two CubeSats at different locations, one at the Moon an one at the Earth-Moon L_5 point and the result is that ARCHER will deliver premium, high value data with unprecedented resolution.

[1] nanosats.eu [Retrieved 1 May 2018]
[2] www.nanosats.eu/index.html [Retrieved 4 May 2018]
[3] www.planetary.org/blogs/guest-blogs/van-kane/0708-marco-planetary-cubesats.html [Retrieved 1 May 2018]

In addition, hardware and software verification and validation, as required by the RAMS analysis in Section 3.6 and detailed in Chapter 4, Section 5.4 and Section 6.4, was extensively employed in order to ensure both Artemis and Diana will reliably last the mission duration. This is extremely important as CubeSats have not always been reliable in the past (Section 3.6). The fact that two CubeSats will record and transmit data adds not only resolution but also redundancy adding further value to ARCHER.

Finally, while there is a risk that a larger mission may supersede ARCHER, it is unlikely that a larger mission could be designed, developed and launched before ARCHER. Add to this, the fact that no large mission could compete with ARCHER on a cost level. ARCHER could therefore easily be a cheap precursor to test vital hardware.

6.1.5. Target/Future Markets

ARCHER, as a concept will be competing against other micro satellite missions and will be courting funding from large space agencies such as the ESA. However, since it is relatively cheap for a deep space science mission it could easily be funded by national governments or private industry. To date, only large missions have taken radiation measurements in deep space, as detailed in Section 2.1. Due to the size and cost of these missions ARCHER will not be in direct competition with them. ARCHER will be in direct competition for funding with other micro satellite missions and examples of these are presented in Section 6.1.6. ARCHER will have to prove why it deserves funding. However, its distinct market edge and the ability to return a scientific value comparable with much larger and more expensive missions places it in a very strong position.

The data recovered from ARCHER will greatly extend a small body of knowledge and will do so with unprecedented resolution. As such, it is not in direct competition with other data-sets. It will be made freely available to the academic world but has the potential to affect and open up many markets. It will be extremely valuable in helping to accurately model the interplanetary radiation environment in order to better understand the radiation challenge to deep space human exploration. In addition, it will have uses in developing spacecraft shielding technology, in aerospace materials research and bio-medical fields. For example, a more accurate knowledge of the radiation environment would allow for more accurate radiation hardening designs potentially lowering weight and saving money. Accurate data could be of great value in future scientific research in ways currently not known.

As a technology demonstration, the mission will showcase the use, versatility and potential of the CubeSat platform. If successful, it is envisioned that ARCHER will blaze the way for CubeSats to be routinely used as stand alone deep space science platforms or to be packaged along with bigger missions opening up a whole new market of technically advanced reliable CubeSats. The potential of the platform once reliability and self-sufficiency have been demonstrated is immense and ARCHER could be a leading example of what is possible.

6.1.6. CubeSat Competition Analysis

The following list is not exhaustive but highlights similar type CubeSat missions which ARCHER could be in competition with for funding.

Mars Cube One (MarCO) is the first interplanetary CubeSat mission and was launched in early May 2018 as part of the NASA Mars Interior Exploration using Seismic Investigations, Geodesy and Heat Transport (InSight) mission [158]. While it will correct its course en-route, the majority of the required ΔV is provided by its larger companion. It will not measure radiation, instead acting as a communication relay for the InSight Mars Lander.

BioSentinel is a NASA mission planned to launch in late 2019 as secondary payload of the SLS[4]. Its primary objective is to study the impact of radiation on living organisms exposed for a long period of time beyond LEO [159]. To achieve this, BioSentinel will carry bio-sensors containing yeast as organism models. Radiation sensors and dosimeters are carried as secondary payload for data comparison. Identical payloads will also be delivered into LEO for comparison in order to better understand the Earth's magnetic field's shielding effect.

IceCube is a NASA mission sending a 6U CubeSat to the Moon to prospect for water [42]. It will be injected from the same SLS launch as BioSentinel, and use an ion engine and a lunar gravity assisted multi-body transfer trajectory. Though it has a different science mission, it is likely to have a similar configuration to ARCHER.

LunaH is another 6U CubeSat going to the Moon and will search for hydrogen deposits [160]. It will also be carried on Exploration Mission-1 and be inserted into a highly elliptical orbit centered around the South Pole of the Moon.

[4] `www.nasa.gov/feature/around-the-moon-with-nasa-s-first-launch-of-sls-with-orion` [Retrieved 5 June 2018]

6.1.7. Expected Return on Investment

ARCHER is not a commercial venture. As such, the return on investment can not be measured in returned dollars. Rather instead, it should be judged on returned value. If successful, the data generated will be freely distributed to the scientific community and could have many benefits economically and socially. Better radiation models for interplanetary space could be developed which in turn could lead to a host of spin off opportunities.

One area where this could pay dividends is in the space weather sector. Improving prediction models could be of great interest to utilities such as power generation and electrical grid maintenance etc. Better protection and regulation of the grid could lead to cost savings and a reduction in damage.

Huge business opportunities also exist in developing lighter and more effective component shielding. This in turn could allow for longer space missions using components which previously may not have survived the radiation levels. This could lead to a new set of scientific missions to further enhance our knowledge of the universe.

When considered in the scope of human interplanetary travel, a range of new technology and businesses could benefit from ARCHER's data. New ways to harden spacecraft could be developed as well a brand new opportunities explored such as active shielding which can adapt to the surrounding radiation levels. This in turn could be one of the main catalysts in realising the much talked about Moon and Mars colonisation missions. ARCHER's data could lay the foundation for new space businesses, missions and expansion from asteroid mining to hotels in space providing not only a host of economic benefits to the world, but ever changing the course of Humankind. To make the dream of becoming an interplanetary species a reality the radiation challenge must be met. But perhaps when judging missions ARCHER's returned value we need only consider one thing. If the data Artemis and Diana send back to Earth helps make space travel safer and therefore ethical and ultimately saves the lives of astronauts, then the return on investment is priceless.

6.2. Launch and Deployment

The launch consists out of three main steps: pre-launch documentation, on site launch campaign and the actual launch and deployment.

6.2.1. Pre-Launch Documentation

The pre-launch documentation generally has to be done several months in advance [49] for larger satellites. As Diana and Artemis are CubeSats, this documentation may be done with less margin, seeing how CubeSat can be developed over the course of a few months. It was decided that for this step the normal schedule would be adhered to as the ARCHER will be built over the course of four years, allowing enough time for the paperwork.

So far ahead of time, an accurate schedule would not make sense, but the following paperwork will have to be delivered [49], some of the paperwork suggested by this source has been removed as it is not applicable to a CubeSat mission:

- Systems Safety Program Plan
- Safety Data Package
- Launch Site Operations Plan
- List of GSE Plastics, Films and Adhesives Used
- Submit Radio Requency Authorization
- Payload Procedures
- Personnel Deployment Plan
- Material Safety Data Sheets
- Final Arrival Plan
- Launch Checklist

Most of this will be standardised for CubeSat launches, allowing it to be done relatively easily compared to most missions.

Table 6.3: Schedule for the launch campaign, as seen in [49]

Day	Activity
-8	Arrival Unpack
-7	Aliveness tests Thermal closeouts
-6	Fueling Leak testing
-5	Testing of electrical and mechanical components
-4	Testing of electrical and mechanical components
-3	Communications check Functionality check
-2	Fairing installation Transport to pad
-1	Final vehicle closeouts Launch Rehersal
0	Management Review Launch

6.2.2. Launch Campaign

SMAD [49] explains in detail how the launch campaign is done, and reserves about three weeks for this. However, the exact same procedures can be done in about three days when the satellite concerns a CubeSat [5]. As a risk mitigation procedure, all three CubeSats will be prepared for launch. If one of the two models intended to launch fails unexpectedly, the launch spot can still be filled with the remaining option. As such, it was decided to schedule a total of nine days for the launch campaign.

Using these sources as well a schedule was made for the complete launch campaign, as seen in Table 6.3. It may be noticed that two days have been scheduled for the testing of electrical and mechanical components. This is because each CubeSat features four deployables: two solar arrays, a reflectarray and a boom. Three of these, the solar arrays and the reflectarray, are of such importance that if they were to fail it would mean the goals of the mission would become unattainable. The communications and functionality checks have been moved to before the fairing installation as the P-POD eliminates the possibility of most testing.

6.2.3. Launch and Deployment

After launch, the ARCHER will be deployed. It is necessary to do this as quickly as possible and start thrusting as soon as possible in order to achieve the intended trajectory.

The first step to be taken, waiting after deployment, has been outlined carefully [1] for 6U, there does not appear to be a 12U standard so it was decided to follow these guidelines:

- 3.3.1: The CubeSat shall be in a power safe mode during deployment.
- 3.4.4: Components that can be deployed will only do so after de-tumbling is completed.
- 3.4.5: No RF signals shall be sent or received in the first 15 minutes after de-tumbling.

Directly after the initial separation, the CubeSat will power on and start its initial acquisition (de-tumble) mode. It can start measuring telemetry but cannot yet communicate this back to the ground station. After the activation of this mode, the CubeSat has to de-tumble. Using the strategy described in Section 4.4, with the component configuration from Section 5.1.1, this will be executed in 59.34 s with the worst-case arm around the roll-axis of 11 cm. A margin of 100% is added to account for the firing sequence, and an additional margin of 2 min is used for start-up. This brings the total de-tumble time to ~ 4 minutes.

The solar panels and omnidirectional antenna can be deployed 30 minutes after deployment from the launch vehicle. This can be done under 10 seconds [161].

[5] http://www.esa.int/Education/CubeSats_-_Fly_Your_Satellite/Launch_campaign_started_CubeSats_arrived_at_Kourou_spaceport [Retrieved 26 June 2018]

After another 15 minutes, 45 minutes after separation from the launcher, the CubeSat can start sending and receiving RF signals. The next steps to be taken are, in order [49]:

- first station acquisition
- communicate telemetry and execute V&V
- orbit determination
- engine turn on
- normal operations

It is expected the entire time between detachment from the launcher to normal operations will take in the order of 8 hours [162]. However, it is highly dependent on whether or not all subsystems work as expected after deployment. This adds a risk factor: if any of the steps fail, or if the entire sequence takes longer than expected, the CubeSat will not be able to reduce its velocity fast enough and will miss the intended trajectory.

6.3. Navigation, Operations and Logistics

In order to successfully carry out their mission in space, Artemis and Diana will have to have the capability to operate autonomously with minimal input from the ground.

6.3.1. Navigation

A critical capability in order to support the CubeSats will be the ability to have a knowledge of the current and future locations of the CubeSats in space, to a degree sufficient to allow for ground station tracking for communications and precise in-space manoeuvring of the CubeSats. CubeSats beyond Earth's orbit cannot rely on the conventional methods such as GPS or regular ground-based tracking by the U.S. Air Force. As a result, navigation must be carried out by systems aboard the satellite itself, either with or without cooperation from the ground.

The conventional method employed for navigation is tracking and ranging during communications. This is done via a compatible transponder radio and requires semi-regular communication with the ground in order to ensure regular and accurate knowledge of the spacecraft position and velocity. In order to reduce the dependence on ground stations, a number of alternatives for autonomous navigation of CubeSats have been investigated. These range from simple optical celestial navigation to complex pulsar astronomy based navigation.

Of the multiple navigation techniques under investigation around the globe, ground-based radio navigation remains the only flight-proven technique compatible with operations at a distance from any planet or body, a requirement for the operations Diana will carry out in the L_5 region. Ground-based radio navigation with modern high-precision ground stations and radios also provides an extremely high accuracy when compared to optical-based navigation techniques. As a result, radio navigation will be employed as the primary navigation technique aboard Artemis and Diana.

However, ARCHER should still retain the capability to estimate position should the radio transponder experience issues or contact with the ground not be an option for an extended period of time. To ensure that this is the case, Artemis' and Diana's ADCS computer shall be capable of celestial triangulation with the star tracking camera carried aboard. This action reduces dependance on expensive ground station time for navigation, while improving the redundancy of the ARCHER CubeSats' navigation capabilities.

6.3.2. Operations and Logistics

The operation phase, after the launch of the spacecraft, reveals whether the planning of the mission is proven to be correct, resulting in a successful mission. This section will show the process, with the sustainability requirements regarding operations, stated below.

- [SUS-OPS-01] The greenhouse footprint of the launch shall be neutralised.
- [SUS-OPS-02] The mission operation delivers all COSPAR class II documentation requirements.

The requirements under the classification, COSPAR category II, merely include administrative obligations, namely the documentation of pre- and post-launch reports identifying potential impact targets and strategies. In addition, an end-of-mission report, specifying impact details such as the impact location, is required. ARCHER makes use

of references and draw.io to design the flow. Alternatively, modelling software like Enterprise Architect, from sparx, could be used to design the operations concept. For the first step, the typical mission evolution of ESA can be seen in Fig. 6.1.

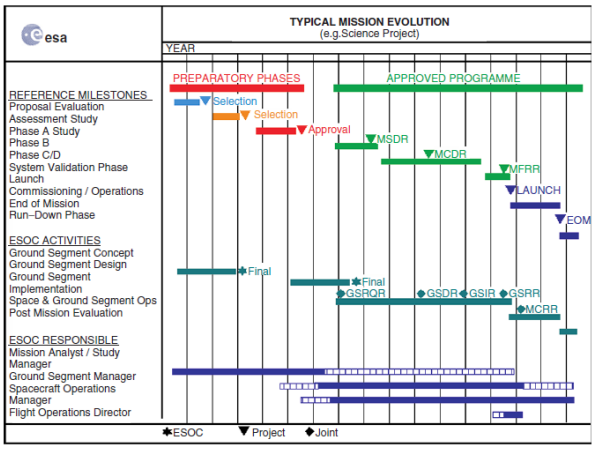

Figure 6.1: Typical mission evolution from the mission operations perspective. [51]

Where phase B is the definition; phase C is design, development and implementation; phase D is test, training and simulation; phase E is launch and operations, and phase F is the run-down phase.[51] The top level operations and logistics flow diagram of ARCHER can be seen in Fig. 6.2. This includes the pre- and post-launch report.

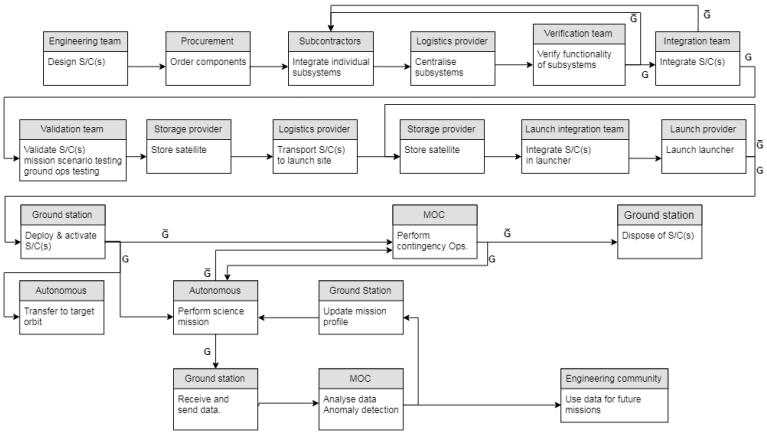

Figure 6.2: Operation and Logistics flow of ARCHER

Note that MOC is the Mission Operation Centre. The operational validation scheme and the mission control team, as used by ESA, is depicted in Fig. 6.4 and Fig. 6.3 respectively.

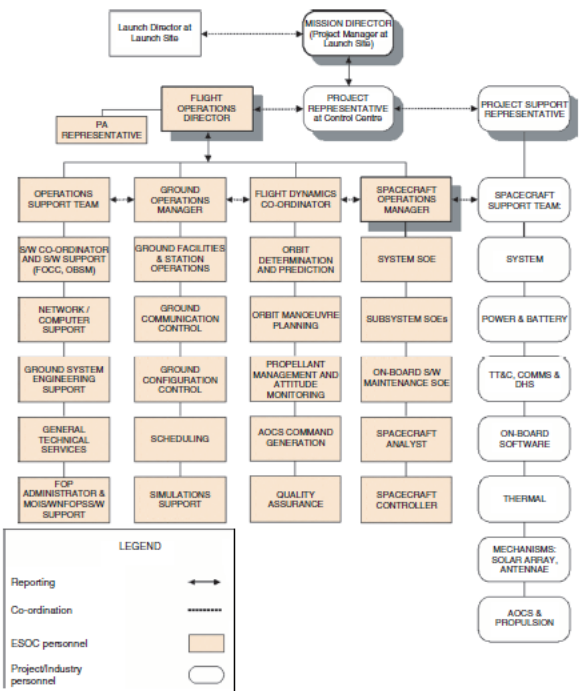

Figure 6.3: Mission control team. [51]

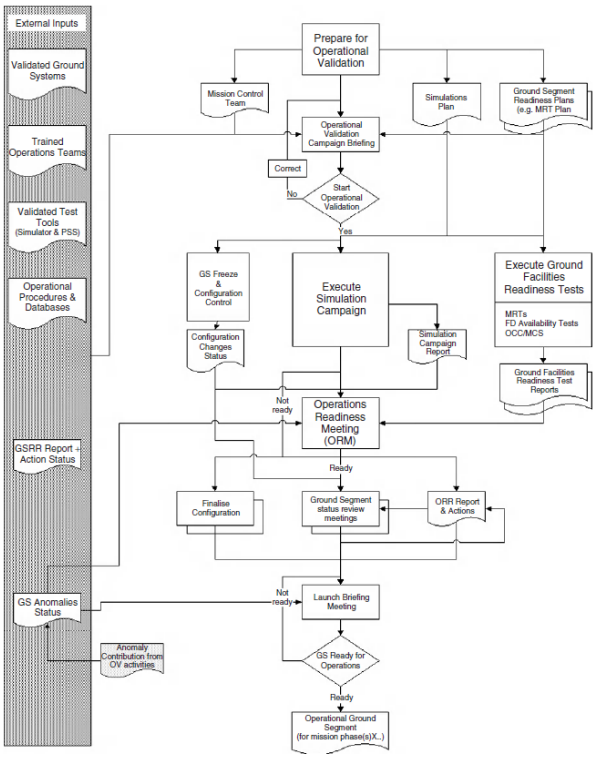

Figure 6.4: Operational validation scheme. [51]

A detailed flow of the anomaly detection process can be seen in Fig. 6.5, with stored state-of-health (SSOH) and loss of signal (LOS). The flow is based on [49]. Note that the documentation is an integral part, as the anomaly may resurface in the mission life. Impacts fall under the anomaly detection and hence, [SUS-OPS-02] will be satisfied, with regards to the impact documentation.

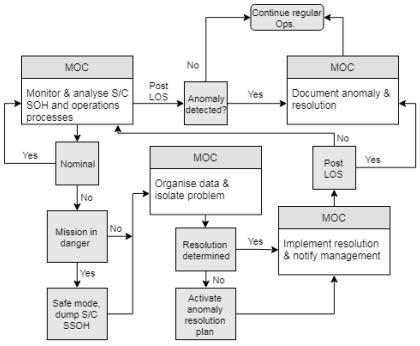

Figure 6.5: Operations anomaly detection protocol of ARCHER

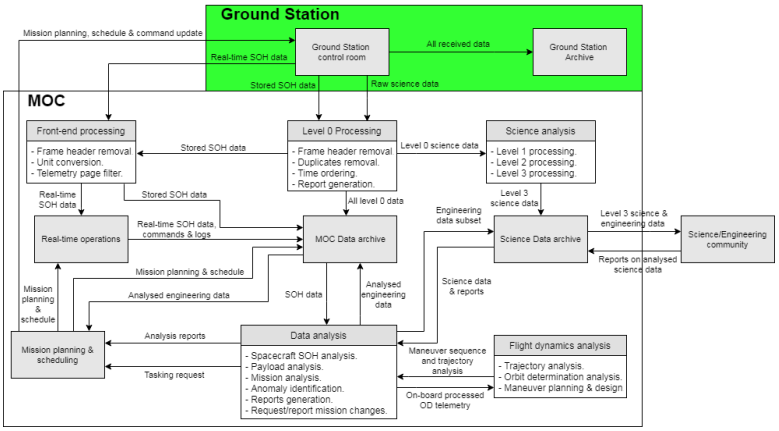

Figure 6.6: Data processing and management flow of ARCHER

In Fig. 6.6, a more detailed flow of the data processing and management is shown, with OD being Orbital Dynamics. This is the most sizeable part of the operations in phase E. In the data processing, planning & scheduling includes all the reports as specified by [SUS-OPS-02].

6.4. System Validation and Flight Certification

After the components have been verified, as detailed in Chapter 4, and the system as been verified, as explained in Section 5.4, the system must then be validated.

System validation checks whether the product accomplished the intended purpose. In other words, can the system carry out the mission? This is partly met by meeting system requirements, i.e. verification, assuming the requirements are appropriately set. However, additional validation testing is required as a system which meets vibration, shock and strength tests may not necessarily carry out the intended science mission. Each test should be prepared, planned, executed and documented. Important validation tests can be seen in Table 6.4.

Table 6.4: System Validation Testing

Test	Explanation
Mission Scenario	Validates the flight hardware can execute the mission under flight-like conditions. Validates the flight software is nominally functional (one of the four essential tests [55]).
Communication link	Validates the satellite radio frequency pattern is accurate & there are minimal losses. Use comparable or actual ground equipment (one of the four essential tests [55]).
End-to-End	Validates compatibility of the information systems and end-to-end data flow.
Command	Validates the operating system correctly executes command.
Fault Isolation	Validates the fault isolation sub-routines are effective & correct software problems.
Operation Readiness	Validates the ground operations can accomplish the mission plan in real time. Must account or software, hardware and people.
Stress and Simulation	Validates that the system can react and cope with variations in performance.

Flight certification generally consists of a mixture of some system verification tests, as seen in Section 5.4, and some of the above validation tests. A complete CubeSat mode should be flight qualified to maximum design limits. This verifies the design can handle the maximum design case. Additional flight units should undergo flight assurance testing. In this case, the flight units are tested up to nominal flight conditions. How the system validation and flight certification integrates with the proposed project schedule can be seen in Section 6.7.

6.5. Design Sustainability Assessment

Planetary protection As hinted in Section 2.4.2, planetary protection measures do not pose any requirements on the design. Full compliance with COSPAR guidelines, ranking at a score of 5 in the sustainability rubric (Table 2.7), can simply be achieved through appropriate documentation prior, during and after the mission. The pre-launch identification of possible impact targets and strategies is covered in in Sections 2.5.4 and 2.5.5. Handling of the remaining mandatory administrative work has been accounted for in Section 6.3.

Space debris All requirements regarding EOL and space debris mitigation concerns have been successfully implemented in the designs. Artemis will be disposed on the surface of the moon and Diana will clear the region of stability around the Lagrange point to not interfere with future missions. In order to completely diminish the chance of adverse effects on the orbital environment, the Earth flyby during transfer of both probes and the after-life trajectory of Diana have to be analysed in great detail to ensure that they pose no threat to LEO and GEO regions. It is recommended to implement trajectory biasing measures during the detailed redesign of the transfer trajectory that minimise the chance of intersecting protected orbital regions even if control over the probes is lost.

Earth environment Both probes use electrical propulsion systems running on iodine, which is ECHA classification III[6] and thus complies with [SUS-SYS-01], [SUS-PROP-01] and [STA-CUS-13] the 'green' propellant customer requirement. Since iodine is much safer to handle and poses less environmental threats than Hydrazine based chemical propellants [163, 164], ARCHER has a significant edge on conventionally propelled missions. The R-134a propellant used by the momentum dumping thrusters also satisfies all three applicable requirements[6]. In fact, it requires even less caution when handled and does not have adverse effects on the environment.[6]

[6] https://echa.europa.eu/substance-information/-/substanceinfo/100.028.585 [Retrieved 20 June 2018]
[6] https://echa.europa.eu/substance-information/-/substanceinfo/100.006.027 [Retrieved 20 June 2018]

Not only the PROP and ADCS subsystems avoid the use of toxic and environmentally harmful materials, but the entire system complies with [SUS-SYS-01]. One great example on how this requirement has impacted the final design of the spacecrafts can be seen during the radiation shielding sizing in Section 4.7.3. Altough lead performed better than any of the other shielding materials in consideration, it was discarded because of its high environmental toxicity and significant adverse effects to human fertility, health of organs and unborn children.[7]

The ARCHER environmental sustainability policy is not limited to the design of the spacecraft. As stated in Section 2.4.1, special attention is payed to the sustainability standards of the launch agency and the hired vehicle. The current design is based on the SLS Block 1B launch vehicle, which uses Liquid Hydrogen (LH_2) and Liquid Oxygen (LOX) for the main engines of all its stages. The reaction of these two propellants is carbon neutral and leaves no toxic products behind. While this sounds like a great environmental record, one must not forget that the emitted water vapour is a powerful greenhouse gas with a significant impact on global warming. It is not possible to accurately compute the Global Warming Potential (GWP) of water vapour, which makes a direct comparison to carbon emissions impossible. However, scientists agree on the fact that the H_2O GWP is lower than that of CO_2. This gives launch vehicles like the SLS and Ariane 6, which use Liquid Hydrogen (LH_2) and Liquid Oxygen (LOX), an edge over the other LTO capable launch systems such as the Altlas V, Soyuz-5 or Falcon 9 rockets. Both 'water-fuelled' systems make also use of solid rocket boosters.

The SLS boosters employ APCP and PBAN, which exhaust mostly water, carbon dioxide, hydrogen chloride, and aluminium oxide. According to NASA investigations [37], the use of these kind of boosters do neither cause short-term nor long-term adverse effects on local air quality. However, the same study found records of booster exhaust product deposits on the soil, mainly consisting of hydrogen chloride and aluminium oxide.

This is to demonstrate that even by choosing the most advanced and environmental friendly launch systems, ARCHER will impact the environmental in an undesirable way. This issue cannot be solved, but the impact may be minimised by aiming for a miniaturised design of the spacecraft and making them suitable to be placed as secondary payload aboard a CubeSat 'mass launch'. Both of these measures apply to the ARCHER probes, reducing the mission specific environmental pollution of the launch. The following derivation is to show just how small the pollution footprints of such a CubeSat mission can be.

The SLS main stage runs off 2 million liters of liquid hydrogen[8]. The payload launch capability of the same rocket is 70 tons [165], which makes the ARCHER CubeSats about 0.06% of the payload mass. Comparing the fuel consumption to the payload mass fractions, it was found that ARCHER is responsible for only 1.2 litres of hydrogen. LH_2 is power consuming during production (51 kWh) [9] and tracing back the carbon emissions of the energy generation (500 g/kWh)[10], one can derive a carbon footprint about 2.2 kg for the 1.2 litres. This is almost negligible, but does not account for the contribution of the solid boosters. Running on the same APCP-PBAN propellant combination, SLS boosters are basically a 25% upsized version of the spaceshuttle boosters[11]. This motivates the assumption, that the CO_2 emissions are also 25% larger. Scaling the 28 tonnes CO_2 emission of the space shuttle launch[12], it can be estimated that an SLS launch emits 35 tonnes of CO_2. Again, using the payload mass fractions, it was found that ARCHER can be held responsible for 21 kg of these emissions. With only 23.2 kg the carbon footprint of the mission launch is estimated to be so small, that it can be offset by planting a single large tree.

To conclude, the sustainability evaluation of the final ARCHER mission design, the rubric introduced in Section 2.4.2 will be applied. The design scores very well (**4**) in the Earth environment aspect: the use of toxic materials is avoided, production and testing procedures will be optimised for energy efficiency and by the nature of standardisation and miniaturisation resources and the environment is spared. To be awarded the highest score, a more detailed breakdown of the component production properties is required.

Since ARCHER will be able to comply with all COSPAR guidelines required from a class II mission, its planetary protection score will be at maximum (**5**).

Due to the design of suitable end of life strategies for both probes, adverse effects on the orbital environment are - within reason - impossible (**4**). Since there is no impact or burn up intended for the Diana probe, it cannot

---

[7] `https://echa.europa.eu/substance-information/-/substanceinfo/100.028.273` [Retrieved 22 June 2018]
[8] `https://www.nasa.gov/xploration/systems/sls/multimedia/fuel-tank-for-sls.html`[Retrieved on 22 June 2018]
[9] `http://www.fsec.ucf.edu/en/consumer/hydrogen/basics/production-solar.htm` [Retrieved 22 June 2018]
[10] `https://www.electricitymap.org/?page=map&solar=false&remote=true&wind=false` [Retrieved 22 June 2018]
[11] `en.wikipedia.org/wiki/Space_Launch_System` [Retreived 22 June 2018]
[12] `http://discovermagazine.com/2007/dec/a-spaceport-for-tree-huggers` [Retrieved 22 June 2018]

be classified as sustainably disposed, which denies the mission design the optimum score.

Table 6.5: Sustainability score of the final mission design based on the ARCHER sustainability rubric.

Aspect	Earth Environmental	Planetary Protection	Space Debris	**Total Weighted Score**
Score	**4** efficient use of resources, no toxic waste during manufacturing, pollution during launch lower than average	**5** full compliance with COSPAR guidelines	**4** adverse effects on orbital environment - within reason - impossible, probes sustainably disposed	**4.375**

6.6. Compliance Matrix

For designing, it is important to verify if all the requirements are satisfied. This verification is performed in this section and can be seen in Table 6.6, with the rationale for an unsatisfied requirement.

Table 6.6: Compliance matrix

Code	Description	Satisfied	Rationale
[SUS-ASD-01]	The lunar orbiter shall be disposed on the surface of the Moon in a controlled, predicted manner	☑	Added requirement, planned for
[SUS-ASD-02]	The Lagrangian point orbiter shall leave the region of practical stability at the end of mission	☑	Added requirement, planned for
[SUS-ASD-03]	The probes shall not intersect protected LEO and GEO regions	☑	Added requirement
[SUS-EPS-01]	The power production shall not involve any radioactive materials	☑	Added requirement
[SUS-MNF-1]	During manufacturing and integration of the satellite energy consumption shall be minimised	☑	Added requirement, planned for
[SUS-OPS-1]	The greenhouse footprint of the launch shall be neutralised	☑	Added requirement, planned for
[SUS-OPS-2]	The mission operation delivers all COSPAR class II documentation requirements	☑	Added requirement, planned for
[TEC-ADCS-01]	The spacecraft shall be able to determine attitude with an accuracy of 1°	☑	
[TEC-ADCS-02]	The spacecraft shall be able to control attitude with an accuracy of 1°, 3σ	☑	
[TEC-ADCS-03]	The solar panels and antenna shall be positioned in the correct direction, after deployment	☑	Added requirement
[TEC-ADCS-04]	The spacecraft shall be able to actively de-tumble for tip-off rates up to 10 $^{\circ}/s$	☑	Added requirement
[TEC-ADCS-05]	The spacecraft shall be able to de-tumble within 30 minutes	☑	Added requirement
[TEC-ADCS-06]	The spacecraft shall be able to slew at least 30° in 30 seconds (1 $^{\circ}/s$)	☑	Added requirement
[TEC-ADCS-07]	The spacecraft shall be able to point the antenna and solar panels in safe mode.	☑	Added requirement
[TEC-ASD-01]	The spacecraft shall have no more than 1 km deviation from its target trajectory at any point of its actual trajectory	☒	Currently not quantifiable
[TEC-ASD-02]	The spacecraft shall have no more than a 1 m/s deviation from its target velocity at any point of its actual trajectory	☒	Currently not quantifiable
[TEC-ASD-03]	All known natural space objects with a diameter larger than 2 m shall be avoided by 1 km	☑	Specified requirement
[TEC-ASD-04]	All known natural space objects with a diameter larger than 50 km shall be avoided by 50 km	☑	Specified requirement
[TEC-ASD-05]	During transit and orbit, all known man-made space objects shall be avoided by 10 km	☑	Specified requirement
[TEC-CDH-01]	Data shall be compressed according to maximum data rate constraint	☒	Currently not quantifiable
[TEC-CDH-02]	Data processing operations shall be compliant with power requirements	☑	See power budget
[TEC-CDH-03]	The spacecraft shall be within an uplink error rate of at most $10^{-}6$	☒	Currently not quantifiable
[TEC-CDH-04]	The OBC shall be able to handle all relevant interfaces	☑	Added requirement
[TEC-CDH-05]	The OBC shall at least be radiation tolerant	☑	Added requirement
[TEC-COMMS-01]	The required data rate shall not exceed 500kbps	☒	Removed after discussion with customer
[TEC-COMMS-02]	The communications system shall function nominally with a pointing accuracy during communications of ±1°	☑	Specified requirement
[TEC-COMMS-03]	The spacecraft shall be able to send its telemetry to a receiving station	☒	Redundant, removed and replaced with TEC-COMMS-10 to TEC-COMMS-15
[TEC-COMMS-04]	The spacecraft shall be able to send its measured data to a receiving station	☒	Same as TEC-COMMS-03
[TEC-COMMS-05]	The sent data shall be coherent	☒	Redundant, removed and replaced with TEC-COMMS-06
[TEC-COMMS-06]	The communication system shall have a maximum payload downlink bit error rate of 10^{-5}	☑	Specified requirement
[TEC-COMMS-07]	The communication system shall have a link budget margin of at least 3 dB	☑	Specified requirement
[TEC-COMMS-08]	The communication system shall be compatible with the Estrack ground station network	☑	Specified ground station
[TEC-COMMS-09]	The maximum period without contact shall be at most 21000 seconds	☒	Removed as redundant due to increased autonomy

[TEC-COMMS-10]	The communication system shall support an uplink minimum data rate of 8000 bps during the science phase of the mission	☑	Achieved, Section 4.3.4
[TEC-COMMS-11]	The communications system shall support a downlink minimum information rate of 1,199,416 bps during the science phase of the mission	☑	Achieved, Section 4.3.4
[TEC-COMMS-12]	The communication system shall support an uplink minimum data rate of 8000 bps during the transfer phase of the mission	☑	Achieved, Section 4.3.4
[TEC-COMMS-13]	The communications system shall support a downlink minimum information rate of 1,325,670 bps during the transfer phase of the mission	☑	Achieved, Section 4.3.4
[TEC-COMMS-14]	The communication system shall support an uplink minimum data rate of 62.5 bps from any angle (”lost-in-space” case)	☑	Achieved, Section 4.3.4
[TEC-COMMS-15]	The communication system shall support a downlink minimum data rate of 62.5 bps from any angle (”lost-in-space” case)	☑	Achieved, Section 4.3.4
[TEC-COMMS-16]	The communication system shall be compliant with ECSS Standards	☑	Achieved
[TEC-COMMS-17]	The communication system shall provide a ranging and tracking capability with a position accuracy of 30 km (3 sigma)	☑	Hardware capability
[TEC-COMMS-18]	The communication system shall provide a ranging and tracking capability with a velocity accuracy of 50 cm/s (3 sigma)	☑	Hardware capability
[TEC-CST-01]	The total mission cost shall not exceed 10 million euro (2018) excluding launch and operations	☑	
[TEC-CST-02]	The mission launch costs shall not exceed 1 million euro (2018)	-	Not possible at this stage
[TEC-CST-03]	Mission operations costs shall not exceed (TBD) euro (2018) per month	-	Not possible to define at this stage
[TEC-CST-04]	The mission design phase costs shall not exceed (TBD) euro (2018)	-	Not possible to define at this stage
[TEC-CST-05]	The preliminary mission design phase shall not exceed 3600 man hours	☑	
[TEC-EPS-01]	The total required power for the spacecraft shall not exceed 40 W	☒	Unachievable with electric propulsion Discussed with customer
[TEC-EPS-02]	The spacecraft array shall be able to provide atleast 100W average power in Earth Orbit under direct sunlight	☑	Achieved
[TEC-EPS-03]	The spacecraft shall be able to provide 40 W peak power	☑	Achieved - peak at 135 W
[TEC-EPS-04]	The spacecraft shall have minimum battery capacity of at least 50 % of original capacity at end of mission	☑	Achieved - EOL at 80%
[TEC-EPS-05]	The spacecraft secondary power system shall be able to maintain basic operations for all schedule eclipses with a 20% margin	☑	Achieved - All eclipses with margin powered
[TEC-EPS-06]	The spacecraft shall have a power budget margin of at least 20%	☑	Achieved
[TEC-EPS-07]	The payload shall be powered during nominal operations	☑	Achieved
[TEC-EPS-08]	The power allocated to the scientific payload shall be sufficient for nominal payload performance	☑	Achieved
[TEC-LEG-01]	The mission shall comply with the ISO-24-113 Space debris convention	☑	
[TEC-LEG-02]	The mission shall comply with the 1967 Treaty on Principles Governing the Activities of States in the Exploration and Use of Outer Space, including the Moon and Other Celestial Bodies (the ”Outer Space Treaty”)	☑	
[TEC-LEG-03]	The mission shall comply with the COSPAR planetary protection Guidelines	☑	
[TEC-LEG-04]	The mission shall comply with the 1972 Convention on International Liability for Damage Caused by Space Objects (the ”Liability Convention”)	☑	
[TEC-LEG-05]	The mission shall comply with the 1975 Convention on Registration of Objects Launched into Outer Space (the ”Registration Convention”)	☑	
[TEC-OPS-01]	The launch window shall be factored into mission profile selection	☑	
[TEC-OPS-02]	The mission shall be ready for launch by no later than end of 2022	☑	Excluding unforseen delays
[TEC-OPS-03]	The mission shall have a duration of 2 years	☑	
[TEC-PAY-01]	The mission shall provide radiation environment measurements in an orbit beyond Earth’s magnetosphere	☑	
[TEC-PAY-02]	The scientific payload shall detect neutrons in the energetic range between 01 and 200 MeV	☑	
[TEC-PAY-03]	The scientific payload shall have a sensitivity to Linear Energy Transfer (LET) between $5 \cdot 10^{-4}$ MeV cm^2/mg to 10 MeV cm^{2}2/mg	☑	
[TEC-PAY-04]	The scientific payload shall measure the magnetic field with a sensitivity of at most $\pm$ 100 μT	☑	
[TEC-PAY-05]	The neutron detector shall be placed internally within the spacecraft shielding structure	☑	
[TEC-PAY-06]	The payload shall be active during the entire duration of the scientific phase of the mission	☑	During nominal mission
[TEC-PAY-07]	The payload shall have a partial payload safe mode	☑	
[TEC-PAY-08]	The payload shall have a complete payload safe mode	☑	
[TEC-PAY-09]	The sensor surface of the FITPixLITE shall not be covered by the skin of the CubeSat.	☑	
[TEC-PROP-01]	The spacecraft shall have a Δv budget of 1564.9m/s	☑	
[TEC-PROP-02]	The spacecraft shall have a Δv budget margin of 99.1m/s	☑	
[TEC-PROP-03]	The propulsion system shall be able to be activated and deactivated at least 400 times	☑	
[TEC-STR-01]	The spacecraft shall be able to withstand the expected loads with a margin of at least (TBD)	-	Not possible to define at this stage
[TEC-STR-02]	The spacecraft shall be inert compared to the launcher during launch operations	☑	
[TEC-STR-03]	The outer structure of the spacecraft shall provide (TBD) protection against space debris impacts with an energy of (TBD) J/m^2	-	Not within the scope of the project

[TEC-STR-04]	The structure shall maintain the needed sensor alignment and positioning despite structural and thermal loads and vibrations	☑	
[TEC-STR-05]	The maximum spacecraft diameter shall be under the maximum allowed launcher diameter of (TBD)	-	Not possible to define at this stage
[TEC-STR-06]	The spacecraft structure shall be able to support the payload and all subsystems at all times, including ground operations	☑	
[TEC-STR-07]	The natural frequency of the spacecraft shall be within (TBD) launcher specifications	-	Not possible to define at this stage
[TEC-STR-08]	The spacecraft shall withstand accelerations in the range 17 g longitudinally and 4.5 g laterally	☑	
[TEC-SYS-01]	The system shall use technology which complies with the EU environmental regulations	☑	
[TEC-SYS-02]	The system shall use manufacturers which comply with Directive 2010/75/EU on industrial emissions	☑	
[TEC-SYS-03]	The system shall use contractors which comply with EU environmental regulations	☑	
[TEC-SYS-04]	The materials used for the spacecraft shall not be classed as radioactive	☑	
[TEC-SYS-05]	The spacecraft shall have no pyrotechnical elements	☑	
[TEC-SYS-06]	The anodized edges shall be of length 11.35 cm in contact to the P-POD	☑	
[TEC-SYS-09]	The mission shall use technology which may be developed to minimum TRL 7 before Q1 2020	☑	Specified requirement
[TEC-SYS-10]	The mission shall have at least a 50 % of lasting two years	☒	Currently not quantifiable
[TEC-SYS-11]	Each individual subsystem shall have a reliability of at least 90 %	☒	Currently not quantifiable
[TEC-SYS-12]	Spacecraft elements with a reliability below 95 % shall be made redundant	☒	Currently not quantifiable
[TEC-SYS-13]	The secondary redundant elements shall have a performance of at least 50 % compared to the primary elements	☒	Currently not quantifiable
[TEC-SYS-14]	The total reliability of a redundant system shall be no less than 90 %	☒	Currently not quantifiable
[TEC-SYS-15]	The spacecraft parts shall be able to withstand the mechanical environment	☑	
[TEC-SYS-16]	The spacecraft shall be able to withstand terrestrial transportation environment	-	Currently not quantifiable
[TEC-SYS-17]	The spacecraft shall be able to withstand the radiation environment encountered during the mission	☑	
[TEC-SYS-18]	The spacecraft shall be able to withstand the radiation environment for the mission duration	☑	Excluding unforeseen malfunctions
[TEC-SYS-19]	The spacecraft shall be able to withstand the standard thermal space environment during transit to and operation in the chosen orbit	☑	
[TEC-SYS-20]	The spacecraft shall be able to withstand an magnetic field of 25 μ Tesla	☒	Currently not quantifiable
[TEC-SYS-21]	The spacecraft shall be compatible with (TBD) road transportation systems	-	Cannot be defined at this stage
[TEC-SYS-22]	The spacecraft shall be under 24 kg as specified by the launch contractor	☑	
[TEC-SYS-23]	The spacecraft shall be compatible with the (TBD) launch system	-	Not defined at this stage
[TEC-SYS-24]	The spacecraft shall be compatible with the (TBD) launch restraint system	-	Not defined at this stage
[TEC-SYS-25]	The spacecraft shall be compatible with the (TBD) launcher deployment system	-	Not defined at this stage
[TEC-SYS-26]	The spacecraft shall have an operational safe mode	☑	
[TEC-SYS-27]	The spacecraft shall have a secondary nominal operational mode	☑	
[TEC-SYS-28]	The spacecraft shall have a critical software error mode	☑	
[TEC-SYS-29]	The spacecraft shall have an unexpected contact loss mode	☑	
[TEC-TH-01]	The batteries shall be operational between 10 to 30 °C	☑	Exceeded requirement 5 to 45
[TEC-TH-02]	The batteries shall survive between 0 to 40 °C	☑	Exceeded requirement -20 to 60
[TEC-TH-03]	The solar array shall be operational between -150 to 110 °C	☒	The actual values range from -50 to 50 °C, the thermal subsystem has been designed with this in mind
[TEC-TH-04]	The solar array shall survive between -200 to 130 °C	☒	The actual values range from -150 to 250 °C, the thermal subsystem has bee designed with this in mind
[TEC-TH-05]	The antennas shall be operational between -100 to 110 °C	☒	The actual values range from -20 to 60 °C, the thermal subsystem has been designed with this in mind
[TEC-TH-06]	The antennas shall survive between -120 to 120 °C	☒	Same as TEC-TH-05
[TEC-TH-07]	The system shall be able to transfer excess thermal energy to internal sources in accordance with applicable interface specifications	☑	

6.7. Project Design and Development Logic

Even though technical and mission design during the project is concluded, the ARCHER mission is far from finished. Apart from getting approval and receiving funding, some components still need to be designed and

tested to be made flight-ready, a launcher has to be found and contracted and the entirety of the system needs to be verified. All of this takes time and planning to perform successfully, and thus a preliminary continuation plan has been developed. An overview of this can be found in this section, starting with the Project Design and Development Logic Fig. 6.7.

It is divided into 6 stages which are further subdivided into individual elements. The approximate timeline is shown as well, with the expected years during which a certain stage is executed being shown. The more detailed explanation about the individual is as follows.

Final Design Stage

During the Final Design Stage the spacecraft design will be finalised in every aspect as a large part of spacecraft design is not only dependent on technical capabilities, but also on various unknown constraints. For example, the final performance of the communication subsystem will in large be determined by the bandwidth and the connection time. During this final stage the technical and mission design will be finalised including individual spacecraft components. However, before that will happen, the project needs to get actual approval and funding in order to be feasible at all. Thus that precedes any other elements within the figure.

Test Campaign

After having designed the spacecraft and operations to feasibly fulfil all of the requirements, it must be tested in order to see if the system indeed functions as intended. This is done during the Test Campaign, which is also the longest stage of all. This is due to many uncertainties inherent in testing which require a lot of contingency time. During this stage firstly the system and subsystem test are performed. This is done in order to ensure that all the components as well as the spacecraft as a whole work as intended. When this is not the case, a subsystem of system redesign is performed to address this issue, afterwards another test is performed. This continues until all tests are passed successfully. Then the design is frozen. The spacecraft are then manufactured and assembled, after which the performance of the spacecraft is tested for manufacturing deficiencies. Any such possible deficiencies are addressed until no deficiencies are present.

Launch Campaign

After the final spacecraft are built, they are launched into space. This happens during the launch campaign, where first the spacecraft are integrated into the launcher, after which the spacecraft are launched into their initial orbit.

Operations

During this stage all of the ground operations are performed in order to ensure the spacecraft perform their mission successfully. This is done by ensuring that scientific data is collected and that the spacecraft operate correctly. Issues with any of these two are dealt with by performing spacecraft contingencies, which are supposed to ensure the relevant spacecraft returns to nominal scientific data collection and general operations. If this is not the case, the spacecraft enters the End of Life stage. This stage is also entered when the mission is concluded successfully.

End of Life

For the sake of sustainable space exploration End of Life operations are performed. During this stage the spacecraft gets boosted into their respective final orbits. For Artemis this means colliding into the moon, and for Diana this means simply leaving the L_5 point. Artemis is expected to stop operating after impact, while Diana will be shut down from the ground after ensuring it has entered the desired graveyard orbit.

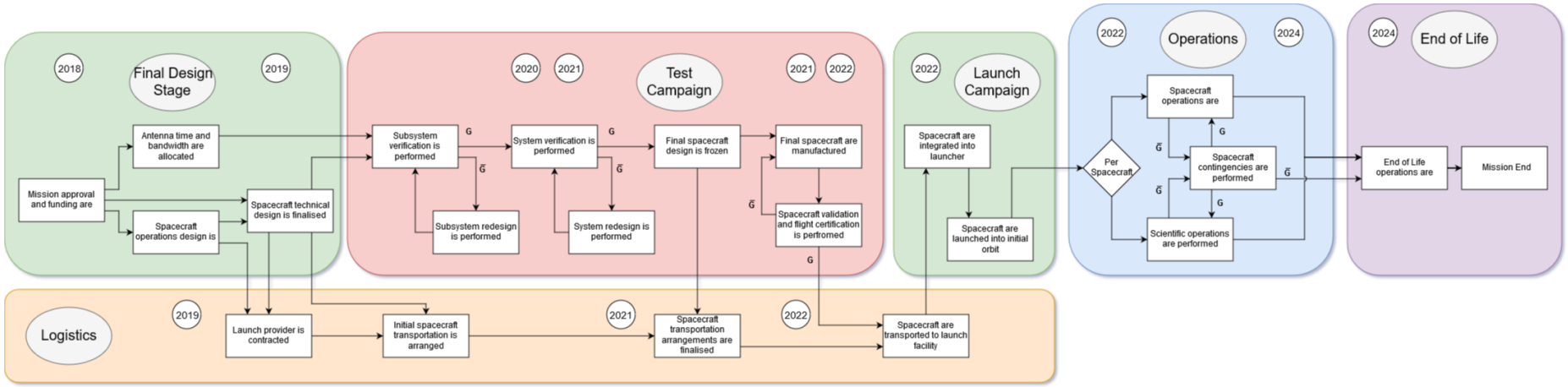

Figure 6.7: Project Design and Development Logic

Color-coding	TRL Now	What	2018 Q3	2018 Q4	2019 Q1	2019 Q2	2019 Q3	2019 Q4	2020 Q1	2020 Q2	2020 Q3	2020 Q4	2021 Q1	2021 Q2	2021 Q3	2021 Q4	2022 Q1
Design	5	FitPixLite															
Manufacturing	5	Neutron FITPIX															
Verification Testing	6	BIT-3															
Delivery	7	IMU															
	6	RS Serial Adapter															
	6	USB Network Module															
	7	OBC															
	6	Reflectarray															
	6	Patch Antenna															
	2	European Transponder															
	7	Solar Array															

Figure 6.8: Technology Development Plan

Logistics

During the first three stages logistical operations are performed in order to ensure launch will actually take place. Firstly, the launch provider is contracted when the exact spacecraft design and mission profile are known. After this, contractors for spacecraft transportation to the launch site can be contracted as well. However, due to possible changes to the spacecraft during the testing phase, this is not yet final. The final contracting is done after the final design is known and frozen. Afterwards, the actual transportation to the launch site takes place.

6.7.1. Technology Development Plan

As has been stated, in order to ensure the success of the ARCHER mission development and testing need to be performed, and thus planned. For this, the Technology Development Plan has been made, which can be seen in Fig. 6.8. In said figure one can see the expected time for components with a Technology Readiness Level of below 8 to be flight-ready, assuming a starting time of Q3 2018. One can see the expected time for the design, manufacturing, verification testing and delivery. The later the delivery, the less time there is for said component to be integrated and tested within the system. This means that resources should be allocated for the elements which are expected to take the longest to be delivered.

The exact Technology Development plan can be found in Fig. 6.8. Here one can see the plan to make components with a technology development level of below 8 flight-ready on time. As can be seen, the timeline is divided into quarters. The green colour shows the design phase, yellow means manufacturing, purple means verification testing and blue means delivery for integration into the spacecraft. This timeline is simply an estimation and is subject to change.

As can be seen, most of the components to be developed have a technology readiness level of below 7, which is exactly the reason they are included in the technology development plan, as to not violate requirement [TEC-SYS-09]. The exact reasons are as follows. Both the FitPix components, while already functional, still need to be radiation tolerant and rated. The BIT-3 engine, while already scheduled to fly in 2020 [43], will need to be verification tested to be rated for 8000 hours of firing, which it theoretically is capable of doing. Currently, it will undergo verification testing for 4000 hours of firing, as seen in Section 4.2. Thus an extensive verification campaign will be held. The IMU needs to be tested, as while it has desirable characteristics, no documentation can be found of it having been verification tested, and thus the assumption needs to be made that this is yet to be done. The RS Serial Adapter, the USB Network Module and the OBS are yet to undergo a full development cycle, but their performance is based on existing hardware, the characteristics of which are assumed to reflect the expected performance of the radiation tolerant and redundant components to be developed. The Reflectarray, Patch Antenna and the European Transceiver are still yet to undergo a full development cycle as well. However, taking US counterparts as examples (like the MarCO antenna [82] for the European Transceiver) gives a general idea on the technology development timeline which can be expected. Moreover, seeing as the technology has already been proven in the US, it can be expected that the development in Europe will take less time than the development for the US counterparts did. Finally, the Solar Array needs to be redesigned to meet the requirements of our mission, which will take long due to the criticallity of this component.

As can be seen, two elements can be seen as most critical, as these are the ones which have less than one year between delivery. They are the Reflectarray and the European Transponder. As delays in technical development are commonplace, this poses a big risk of a component not being delivered on time, resulting in a delay and possible cancellation of the mission. It is thus necessary to direct resources towards the development of said two components, as this offers great value for the invested money due to a significant decrease in risk. Apart from that, the RS Serial Adapter and the USB Network Module, and to a lesser extent the BIT-3, the OBC and the Solar Array should also be closely monitored for signs of possible delays, as with respectively 1 year and 1.5 years of contingency time on a scale of 3.5 years it is a possibility that the development of any of these four components could also extend into 2022, delaying the mission. Thus it is recommended that these components should be closely monitored for signs of possible delays, with appropriate steps (depending on the situation) taken when unacceptable delays are expected to threaten the mission timeline.

6.8. Cost Analysis

In order to ensure the project can realistically be funded and will thus be viable for approval from a financial standpoint, it is necessary to perform a cost analysis. This is performed in this section.

6.8.1. Requirements

In order to be able to properly quantify whether the funding for the project can realistically proceed, requirements have been put in place that the spacecraft needs to fulfil. The driving requirements are as follows:

- [STA-CUS-19] The cost of the mission shall not exceed 10 million euro (excluding the launch cost and operation)
- [TEC-CST-01] The total mission cost shall not exceed 10 million euro (2018) excluding launch and operations
- [STA-LAN-05] Spacecraft shall fit within the launcher as specified in launcher guide
- [STA-LAN-07] Spacecraft diameter shall be no more than specified by the Launch Contractor as per diameter of launcher cargo hold
- [STA-LAN-09] The spacecraft shall be compatible with the launcher deployment system

6.8.2. Cost Breakdown Structure

For a proper cost analysis a cost breakdown structure is of great benefit, as it indicates what costs can be expected at what stage of the mission. The cost breakdown structure is shown in Fig. 6.9. All of the elements shown in colour represent the elements from the Project Design and Development Logic, as seen in Fig. 6.7. The text underneath said elements shows the actual expected sources of cost during each phase of the mission. As one can see, during the Final Design Stage the funding is received and spent on research and development. During the Test Campaign funds are directed towards manufacturing and testing, and possibly redesign. During operations funds go towards antenna time, ground operations and data storage and distribution, which is also the case for the End of Life operations. Finally funds for logistics go towards fees and transportation costs.

Of these, the Final Design Stage, Test Campaign are to be financed by the €10 million expected to be allocated for this project, while the funds for the other stages falls outside of our requirements. However, it is still useful to be able to approximate some of the costs for which it is possible, and to see if all of the €10 million is required to be able to fund the Final Design Stage as well as the Test Campaign.

6.8.3. Costs

By taking all the subsystem costs and adding them together, one finds the total costs, which can be seen in Table 6.7. Due to requests from some experts to avoid publishing the component prices, only the total subsystem prices are provided without any breakdown. Furthermore, it should be noted that the high number of components for the EPS is due to the large number of individual solar cells (140).

Table 6.7: Subsystem costs

Subsystem	Cost [€]	Number of components
ADCS	380,549	12
CDH	114,900	5
COMMS	159,000	5
EPS	80,100	146
PAY	260,000	4
PROP	98,000	1
STR	13,500	1
Total	1,106,049	174

Seeing as there will be three fully functional built (one engineering model for rigorous testing and two flight models), the total price will be €3.3 million. Seeing as most of the price is derived from the reliability and radiation hardening of the components, the flat-sat (which will test whether the components actually work together, and thus does not need to be very reliable nor radiation hardened) is expected to not cost a significant amount. Assuming it to cost the equivalent of the Total Component Cost would be a gross overestimation.

Unfortunately, these prices sometimes do, and sometimes do not include development costs, while at the same time not accounting for buying components in bulk for testing. Seeing as any development costs included would be overestimated three-fold, it can be assumed that the development costs are included in the above figure. And even if this was not the case, around 67% of the budget is left to be spent after investing in the spacecraft

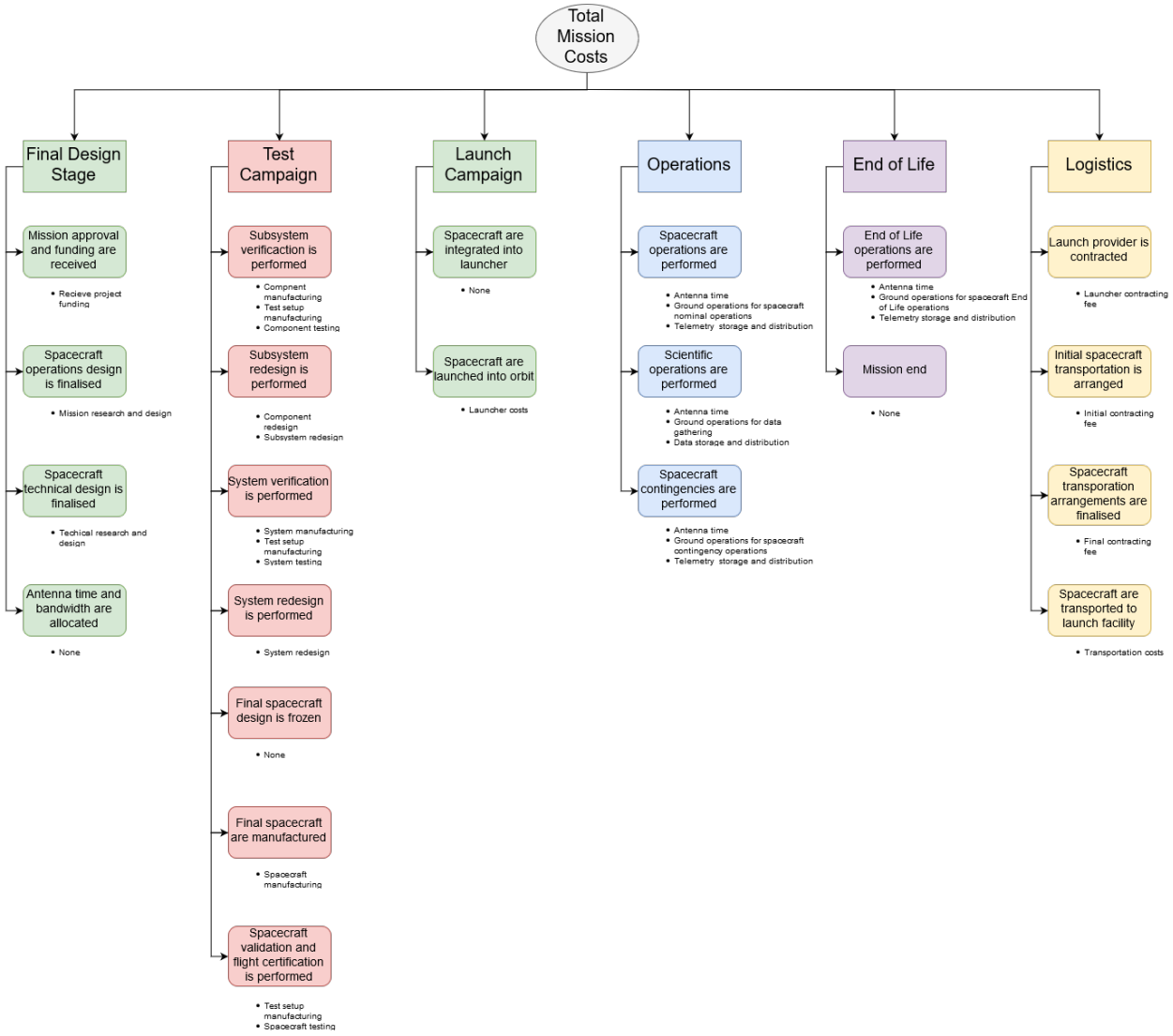

Figure 6.9: Cost Breakdown Structure

hardware, which can be assumed to be enough for development. Furthermore, this can be spent in case of a contingency when a component is in danger of not being flight-ready on time, as is very much a possibility in the case of the European Transponder and Reflectarray, as stated in Section 6.7. Thus it can be assumed that €10 million is enough for the development of the ARCHER mission.

The only other costs that can be somewhat confidently approximated are the launch costs, which are excluded from the aforementioned €10 million as according to requirements [STA-CUS-19] and [TEC-CST-01]. These have been obtained as follows. Firstly, it has been assumed that Diana and Artemis will launch as secondary payloads, possibly along with other CubeSats as is the case in NASA's Exploration Mission 1[13]. It is also assumed that rockets currently in use with the capability to do so will launch to the moon at random intervals, thus any such launcher is a potential candidate for the ARCHER mission. Finally, seeing as a launch profile provided by an SLS rocket is assumed, the SLS has been chosen for preliminary calculations. In order to estimate the actual launch costs the following was done. NASA states that the TLI payload capabilities of SLS block 1 are over 26 tons[14], thus 26 tons is assumed. Now, it is known that the a single SLS launch costs roughly $500 million[15], which gives €430 million euro. Taking the weight of the Diana and Artemis spacecraft and adding a margin of 100% to account

[13] www.nasa.gov/feature/around-the-moon-with-nasa-s-first-launch-of-sls-with-orion [Retrieved 26 June 2018]
[14] https://www.nasa.gov/sites/default/files/atoms/files/sls_lift_capabilities_and_configurations_508_03152018_0.pdf [Retrieved 2 June 2018]
[15] https://www.space.com/17556-giant-nasa-rocket-space-launch-cost.html [Retreieved 2 June 2018]

for both the deployer mass as well as other inefficiencies, dividing this by the total lifting mass into a TLI orbit and multiplying this by the launch price of €430 million, one gets a price of €0.66 million. This is well within the price range of €10 million, accounting for the total component price of €3.3 million. However, seeing as this is a very rough estimation, a large margin should be used for any further calculations using this value.

6.9. Project Gantt Chart

All high-level project phases that still need to be performed are planned out, based on the project design and development logic. They are put into a Gantt chart (Fig. 6.10 which shows interdependence and some milestones. In Table 6.8 the Excel sheet used to make the Gantt chart is presented. The current launch date is set in 2022, in accordance to requirements.

Table 6.8: Detailed Design Phase Gantt Excel Sheet

Grouping	Package	Job	Code	Start	End	Duration Years	Assigned
1 Final Design Stage	1.1	Secure Mission Funding	1.1.1	7/1/2018	12/30/2018	0.5	Sales Rep.
1 Final Design Stage	1.1	Secure Mission Approval	1.1.2	7/1/2018	12/30/2018	0.5	Sales Rep.
1 Final Design Stage	1.2	Finalise Spacecraft Operations Design	1.2.1	7/1/2018	7/1/2019	1	Operations
1 Final Design Stage	1.2	Aquire Antenna Time and Bandwith Allocation	1.2.2	7/1/2018	7/1/2019	1	COMMS
1 Final Design Stage	1.3	Develop and Finalise non-COTS parts	1.4.1	12/30/2018	12/30/2019	1	Engineering Dept. Test Engineers Suppliers
1 Final Design Stage	1.4	Finalise Spacecraft Technical Design	1.4.1	12/30/2018	12/30/2019	1	Engineering Dept.
2 Test Campaign and Manufacturing	2.1	Verify Subsytems	2.1.1	12/30/2019	3/30/2020	0.25	Engineering Dept. Test Engineers
2 Test Campaign and Manufacturing	2.1	Verify System	2.1.2	3/30/2020	6/30/2020	0.25	Engineering Dept. Test Engineers
2 Test Campaign and Manufacturing	2.1	Freeze design	2.1.3	6/30/2020	9/29/2020	0.25	Engineering Dept.
2 Test Campaign and Manufacturing	2.2	Manufacture Spacecrafts	2.2.1	9/29/2020	12/29/2020	0.25	Manufacturing Dept.
2 Test Campaign and Manufacturing	2.3	Validate Spacecraft	2.3.1	12/29/2020	10/17/2021	0.8	Engineering Dept. Test Engineers
2 Test Campaign and Manufacturing	2.3	Certify Spacecraft	2.3.2	10/17/2021	12/29/2021	0.2	Engineering Dept. Test Engineers
3 Launch Campaign	3.1	Integrate Spacecraft into launcher	3.1.1	12/29/2021	3/12/2022	0.2	Launch Provider
3 Launch Campaign	3.2	Launch Spacecraft	3.2.1	3/12/2022	4/18/2022	0.1	Launch Provider
4 Operations	4.1	Perform Transfer Orbit	4.1.1	4/18/2022	4/18/2023	1	Ground OPS
4 Operations	4.2	Perform Science Mission	4.1.2	4/18/2023	5/23/2024	1.1	COMMS Ground OPS
5 End of Life	5.1	Perform end of life operations	5.1.1	5/23/2024	8/4/2024	0.2	COMMS Ground OPS
6 Logistics	6.1	Contract Launch Provider	6.1.1	12/30/2018	7/1/2019	0.5	Logistics
6 Logistics	6.2	Arrange Spacecraft Transportation	6.2.1	12/30/2019	6/30/2020	0.5	Logistics
6 Logistics	6.3	Finalise Spacecraft Transportation Arrangement	6.3.1	6/30/2020	12/29/2020	0.5	Logistics
6 Logistics	6.4	Transport Spacecraft to Launch	6.4.1	10/17/2021	11/23/2021	0.1	Logistics

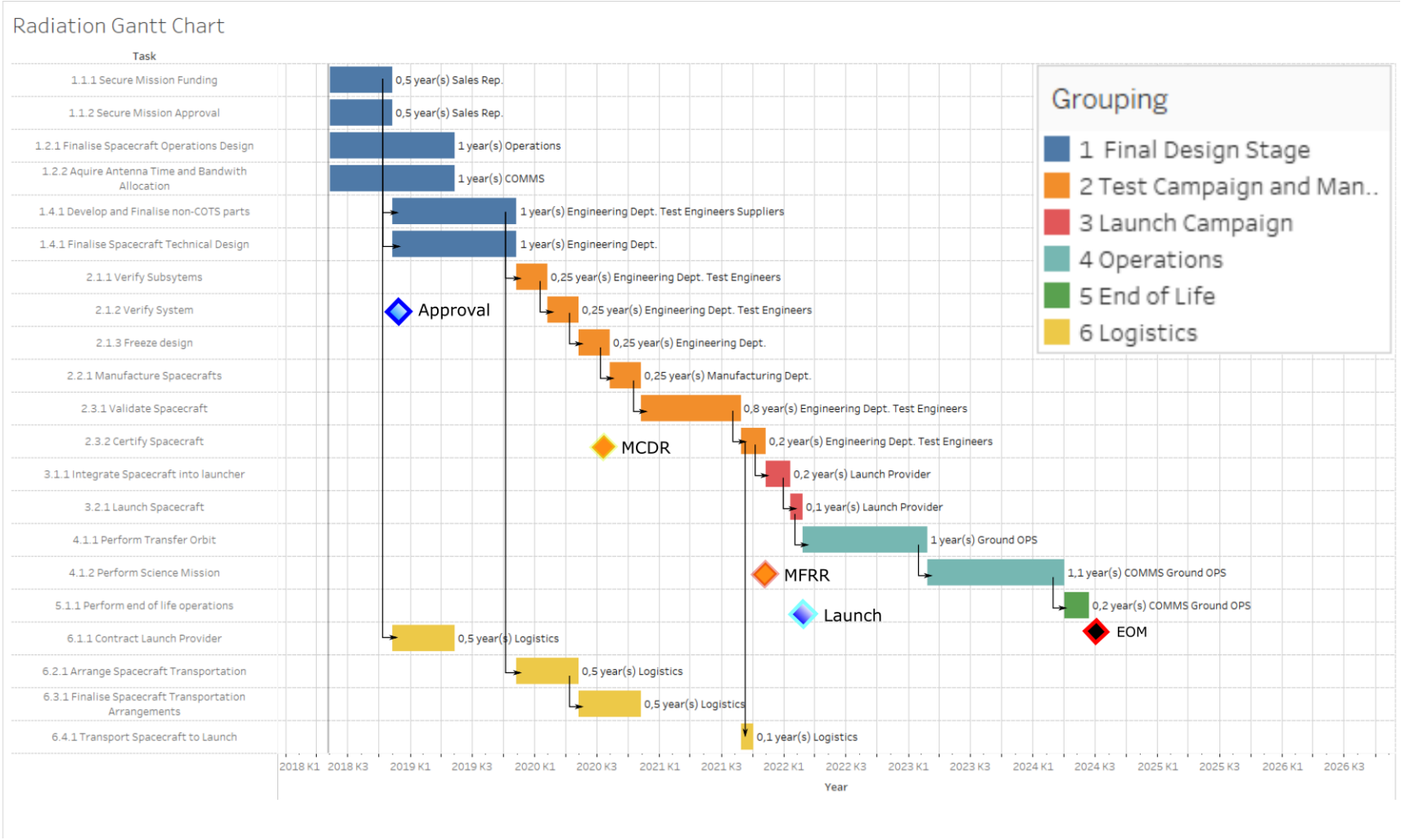

Figure 6.10: ARCHER Project Gantt Chart

7

Results and Recommendations

This chapter will give the results of project ARCHER and present a short list of future recommendations.

7.1. Results

Two design cycles were completed during this project. The first design cycle, the Mission Design resulted in a trade-off where 4950 potential mission options were reduced to one. An intense sensitivity analysis left no doubt that this was the best option for ARCHER and with the project complete, the team is as certain as ever that this is the case. The mission consists of two 12 U CubeSats, Artemis which will go to the Moon and Diana will go to the Earth-Moon L_5 point. They will be injected into a lunar transfer orbit and must then power themselves to their final destination. In order to calculate their trajectories, the team developed a Matlab program to and then optimised the trajectories with a genetic algorithm. This proved to be very successful. In addition, STK was used to predict eclipse times at destination. This resulted in a detailed and complete picture of ARCHER's astrodynamics.

The second design cycle involved designing the system hardware that could successfully carry out the mission. This was an intensive process which analysed every subsystem and designed them in detail. Even the component interfacing was devised to ensure the data flow and power flow were mapped and were feasible. An impressive miniaturised payload suite consisting of three FitPix lites, one specially coated to detect neutrons, will be operated in conjunction with a highly sensitive magnetometer. This helps quantify how strong the magnetic fields are in the CubeSat vicinity and also allows Artemis and Diana to validate that they have left the magnetosphere. Four million bits of scientific data per second will be recorded by ARCHER's payload suite. In addition, the distance between the two spacecraft, or the spatial resolution will allow for an unprecedented and unparalleled characterisation of the interplanetary radiation environment.

To ensure this data could be transmitted to Earth, a link budget tool was created to calculate the achievable data rates. A high-gain reflectarray antenna was coupled with a JPL Iris transceiver to maximise data downlink on the X-band. In order to ensure the recorded science was delivered to Earth, a downlink of close to 5 hours is required every day during transit. In lunar orbit, Artemis has to downlink for nearly 6.5 hours every three orbits.

A power hungry ion engine, the Busek BIT-3, was chosen to propel the CubeSats. This is cutting edge technology but the large power requirements put great strain on the EPS system. A trifold dual wing solar array with 120 Azur 3G30A cells coupled with an innovative and breakthrough solar array drive assembly which rotates the panels to track the sun went some way to satisfying the power needs. An extra 20 body mounted cells gave an average generated power of 134 W. However, this was not enough to ensure powered flight and the JPL IRIS receiver could operate in unison. Two GomSpace BPX batteries with a combined 154 Whr and a flexible modular set of power modes was implemented to make up the shortfall. During transit, the batteries will be drained for 19 each day and are able to recharge during the 5 hour down link window. This ensures all power requirements can be met and that the CubeSats can power both the engines and the transceiver simultaneously. A small program was designed to plot the battery degradation over the 770 day mission to ensure the EPS system would last the full mission. EOL capacity of the batteries was found to be 80%.

ARCHER faces many technological challenges before it can undertake its mission and harvest such high quality

data. Artemis and Diana will join the first generation of deep space CubeSats, the first being NASA's Marco mission launched on 5th May 2018. Many of the technologies it will use are cutting edge and never before has such a configuration been integrated together. This will cause problems and challenge reliability, an area CubeSats are notoriously weak on. A strong verification and validation plan has been put in place including component, subsystem and system level testing. In addition, day in the life testing and mission scenario testing will round out an extensive set of investigations which will help ensure that both CubeSats survive the mission duration of two years. By doing so, they will prove the utility of the CubeSat platform as serious scientific instruments while demonstrating the extreme limits of current technology.

If successful, the result will be a large dataset with an extremely fine resolution. This will be used to better analyse the radiation challenge to human interplanetary space travel. The first step would be to improve the current radiation models. These in turn can be used to study the ill effects on humans exposed to radiation for a prolonged time thereby helping to avoid significant harm. Better shielding both for humans and components could be developed as well as new technologies such as active shielding. The information could form the backbone of the push to make deep space exploration safe and importantly, ethical. This in turn could lay the foundation for the true expansion of humankind as we transition to a multi-planet species.

ARCHER, a small mission with big goals will send out two CubeSats, Artemis and Diana, both at the forefront of technology, which, if successful will result in a wealth of scientific knowledge and help push open the door for real, safe and ethical Human deep space missions.

7.2. Recommendations

ARCHER has great potential to deliver a large return on investment, when judged on returned value rather than euro. However, there are many challenges that must be overcome in order to successfully complete the mission. The following recommendations, if implemented, would help reduce mission ARCHER's sensitivity to the technical challenges it faces and improve the chance of a high value return. In addition to the following, component level recommendations can be found in appropriate sections in Chapter 4.

- The project design and development plan should be followed.
- The full end-to-end trajectory, from launch to EOL should be designed and integrated.
- Radiation hardening of components should be further researched in order to better design the radiation shielding.
- The computer system is currently distributed over several subsystems, ADCS, OBC, EPS. It is recommended that a more centralised solution be found, reducing subsystem complexity.
- If power, mass and volume budgets allow, an additional payload should be considered.
- The FitPix manufacturers are currently upgrading the FPGA. It is recommended to make contact with and work with the manufacturers to help steer the direction of future updates in a direction most useful to ARCHER. Upgrading to a more space proven interface for example would be beneficial. Interesting configurations could be used such as aligning two FitPix beside each other to contrast their measurements or covering one in lead to isolate particular neutron ranges.
- VACCO industries has indicated that the exhaust holes on the ADCS thrusters are variable in terms of position and orientation. It is recommended to optimise the the position of the holes to maximise the ability of the thrusters to momentum dump and control the CubeSat while minimising mass and volume.
- Currently, critical and essential technology such as the BIT-3 engine, the HoneyBee SADA and the JPL IRIS transceiver as well as the reflect array are American technologies. While it is envisioned that there would be no export restrictions on these technologies, it is recommended to collaborate with European initiatives in order to help drive and direct replacement European technologies in order to ensure that no geopolitical event could restrict access to critical technology.
- If funding allows, a third CubeSat would allow for a greater data set, better resolution and would open up new mission opportunities. It could be sent on a deep space trajectory, sent to another lagrange point or kept in LEO for comparison with the data from outside the magnetosphere.

8

Conclusion

The main objective of project ARCHER was to deliver an economically and technically feasible CubeSat design which could realistically carry out the mission and characterise the interplanetary radiation environment. The feasibility of the design is an area that the team passionately pursued. This required a deep analysis of the many problems facing ARCHER. To answer this challenge, the team wrote programs to plot lunar trajectories, calculate battery degradation, calculate average solar cell power generation, to optimise the heat sinks, to find the angular impulse and to calculate the link budgets. Industry standard software was then used to really push the limits of the projects engineering. STK, ANSYS, CATIA and SPENVIS were used to ensure accurate results, understand the conditions the CubSats would face ad really test the robustness of the design. The project went as far as to establish the interfacing between different subsystems, both for power and data flow.

In addition to this, two design cycles were carried out, one for the mission profile and one for the system. Throughout both, systems engineering and project management was deeply embedded in every activity. This helped set deadlines, keep deadlines, guide decision making processes and ensure the project engineering adhered to strict and high standards. Systems engineering tools were not treated just as deliverables, but were actively used to engineer the subsystems, choose components and track changes. Concurrent design was also implemented to help iterate quickly through the early phases of the system design.

To increase the team's knowledge base experts from many fields across the world, were sought out and consulted. Specialists from the European Space Agency, from CubeSat technology companies, experts in redundancy and reliability as well as component experts, were consulted and their feedback integrated into the design. Their advice was very beneficial to the team and effectively, boosted the teams experience level. Every avenue was pursued to better the design and pursue the teams goal of designing something with the potential to be real.

Importantly, throughout the entire project, the team worked hard and pulled together. From the start, we actively pursued a good team atmosphere and built in extracurricular team building activities. This certainly helped the team remain cohesive when under stress. Every member of the team advanced their learning and a real passion for the project developed. ARCHER is a mission the team is proud to stand behind and proud to present. If ever launched, Artemis and Diana would most certainly make a huge impact on the scientific community, return a comprehensive data set which in turn would open up a world of opportunities. It could lay the foundation for safe, ethical deep space exploration missions. It's hard to argue with Oscar Wilde when he said,

> "We are all in the gutter, but some of us are looking at the stars."

Hopefully, with a little bit of luck, ARCHER might help us get there.

Bibliography

[1] California Polytechnic State University, *6U CubeSat Design Specifications*, 4 2016, Provisional.

[2] Ferrari, G., Fradgley, T., Glowacki, M., Hener, J., van t Hof, N. A., Kyle, J. A., Vijverberg, R., Vilella, M., and Rijlaarsdam, D., *ARCHER: Analysis of the Radiation Challenge to Human ExploRation - Baseline Report*, Delft University of Technology, Delft, 2018.

[3] Burian, P., Georgiev, V., Jára, M., Kraus, V., Poláček, L., Pospíšil, S., and Turjafnica, P., "FITPixLite - Compact Particle Detector," *University of West Bohemia - Faculty of Electrical Engineering*, 2018.

[4] Reveles, J., Lawton, M., Fraux, V., Gurusamy, V., and Parry, V., "In-Orbit Performance of AstroTube: AlSat Nano's Low Mass Deployable Composite Boom Payload," *31st Annual AIAA/USU Conference on Small Satellites*, 2017.

[5] Bartington Space and Defence, Oxford, United Kingdom, *Spacemag & Spacemag Lite, three axis magnetometers*.

[6] Busek Co. Inc., "3cm RF Ion Thruster BIT-3 Data Sheet," 2018.

[7] Kaminskiy, M., "CubeSat Data Analysis - Revision," Primary research report, NASA, 11 2015.

[8] Seedhouse, E., "Beyond Suborbital," *Virgin Galactic*, Springer, 2015, pp. 171–180.

[9] Chaikin, A. and Hanks, T., *A man on the Moon: The voyages of the Apollo astronauts*, Author's Republic, 2015.

[10] Seedhouse, E., *Lunar outpost*, Springer, 2009.

[11] Musk, E., "Making humans a multi-planetary species," *New Space*, Vol. 5, No. 2, 2017, pp. 46–61.

[12] Cucinotta, F. A. and Durante, M., "Cancer risk from exposure to galactic cosmic rays: implications for space exploration by human beings," *The lancet oncology*, Vol. 7, No. 5, 2006, pp. 431–435.

[13] Leuraud, K., Richardson, D. B., Cardis, E., Daniels, R. D., Gillies, M., O'hagan, J. A., Hamra, G. B., Haylock, R., Laurier, D., Moissonnier, M., et al., "Ionising radiation and risk of death from leukaemia and lymphoma in radiation-monitored workers (INWORKS): an international cohort study," *The Lancet Haematology*, Vol. 2, No. 7, 2015, pp. e276–e281.

[14] Hassler, D. M., Zeitlin, C., Wimmer-Schweingruber, R. F., Ehresmann, B., Rafkin, S., Eigenbrode, J. L., Brinza, D. E., Weigle, G., Böttcher, S., Böhm, E., et al., "Mars' surface radiation environment measured with the Mars Science Laboratory's Curiosity rover," *science*, 2013, pp. 1244797.

[15] Poghosyan, A. and Golkar, A., "CubeSat evolution: Analyzing CubeSat capabilities for conducting science missions," *Progress in Aerospace Sciences*, Vol. 88, 2017, pp. 59–83.

[16] Ferrari, G., Fradgley, T., Glowacki, M., Hener, J., van t Hof, N. A., Kyle, J. A., Vijverberg, R., Vilella, M., and Rijlaarsdam, D., *ARCHER: Analysis of the Radiation Challenge to Human ExploRation - Project Plan*, Delft University of Technology, Delft, 2018.

[17] Ferrari, G., Fradgley, T., Glowacki, M., Hener, J., van t Hof, N. A., Kyle, J. A., Vijverberg, R., Vilella, M., and Rijlaarsdam, D., *ARCHER: Analysis of the Radiation Challenge to Human ExploRation - Midterm Report*, Delft University of Technology, Delft, 2018.

[18] Gill, E., LaRocca, G., Verhagen, W., and Cervone, A., "AE3211-I Systems Engineering and Aerospace Design Lecture Series," 2018.

[19] Radvanyi, P., "The Discovery of Radioactivity," *Europhysics News*, Vol. 27, No. 2, 1996, pp. 57–59.

[20] Bertolotti, M., "The Discovery: Victor F. Hess and the Balloon Ascents," *Celestial Messengers*, Springer, 2013, pp. 33–44.

[21] Wulf, T., "On the radiation of high penetrating power that exists in the atmosphere," *Phys. Zeit*, Vol. 1, No. 152-157, 1909, pp. 124.

[22] Millikan, R. A. and Cameron, G. H., "The origin of the cosmic rays," *Physical review*, Vol. 32, No. 4, 1928, pp. 533.

[23] McPhee, J. C. and Charles, J. B., *Human health and performance risks of space exploration missions: evidence reviewed by the NASA human research program*, Vol. 3405, Government Printing Office, 2009.

[24] NASA, "Mars Science Laboratory Launch, Press Kit," 2011.

[25] *The Martian Radiation Environment Experiment (MARIE) on the 2001 Mars Odyssey Spacecraft*, Vol. 654, 2003.

[26] Spence, H. E., Case, A., Golightly, M., Heine, T., Larsen, B., Blake, J., Caranza, P., Crain, W., George, J., Lalic, M., et al., "CRaTER: The cosmic ray telescope for the effects of radiation experiment on the lunar reconnaissance orbiter mission," *Space science reviews*, Vol. 150, No. 1-4, 2010, pp. 243–284.

[27] Dachev, T. P., Tomov, B., Matviichuk, Y. N., Dimitrov, P. S., De Angelis, G., Spurny, F., and Vadawale, S., "Monitoring of the Earth and Moon radiation environment by the RADOM instrument on Indian Chandrayyan-1 satellite." *40th Lunar and Planetary Science Conference, The Woodlands, TX, USA*, 2009, pp. 2–27.

[28] Klumpar, D. M., "The on-orbit Performance of HRBE (aka Explorer-1 [Prime] FU2)," 18 april 2012.

[29] *ROBUSTA, a student satellite to serve the radiation effects community*, Vol. 23, Logan, UT, USA, 10-13 Aug 2009, AIAA/USU Conference on Small Satellites.

[30] Lee, S., Lee, J.-K., Kum, K., Lee, H., Seo, J., Shin, Y., Jeong, S., Cheon, J., Kim, H., Lim, J., et al., "Development of SIGMA (KHUSAT-3) CubeSat Mission," *SmallSat Conference, Utah State University*, 2014.

[31] Chavy-Macdonald, M.-A., *Strategies and Geant4 Simulations for Radiation Protection on an EML-2 Mission*, Master's thesis, Lulea University of Technology, 2015.

[32] Durante, M. and Cucinotta, F. A., "Physical basis of radiation protection in space travel," *Reviews of Modern Physics*, Vol. 83, No. 4, 2011, pp. 1245.

[33] Friis-Christensen, E. and Lassen, K., "Length of the solar cycle: an indicator of solar activity closely associated with climate," *Science*, Vol. 254, No. 5032, 1991, pp. 698–700.

[34] Benton, E., *Radiation dosimetry at aviation altitudes and in low-Earth orbit*, Ph.D. thesis, University College Dublin, 2004.

[35] Menicucci, A., *Project Guide Design Synthesis Exercise, Understanding the Radiation Risk of Human Interplanetary Travels*, TU Delft, 2018.

[36] Langer, M. and Bouwmeester, J., "Reliability of CubeSats: Statistical Data, Developers' Beliefs & the Way Forward," *30th Annual AIAA/USU Conference on Small Satellites Proceedings*, 11 2016, pp. 4–20.

[37] NASA, "Mars 2020 Draft Environmental Impact Statement (Draft)," 2014.

[38] Klinkrad, H., *Space debris*, Wiley Online Library, 2010.

[39] United Nations, *United Nations Treaties and Principles on Outer Space*, 2002.

[40] COSPAR, *Planetary Protection Policy*, 10 2002.

[41] Rocket Lab, *Payload User's Guide*, 4th ed., 12 2016.

[42] Folta, D. C., Bosanac, N., Cox, A., and Howell, K. C., "The Lunar IceCube mission design: construction of feasible transfer trajectories with a constrained departure," 2016.

[43] Bosanac, N., Cox, A., Howell, K. C., and Folta, D. C., "Trajectory design for a cislunar CubeSat leveraging dynamical systems techniques: The Lunar IceCube mission," *Acta Astronautica*, Vol. 144, 2018, pp. 283 – 296. doi:10.1016/j.actaastro.2017.12.025.

[44] Folta, D. C., Bosanac, N., Cox, A. D., and Howell, K. C., "The Lunar IceCube Mission Challenge: Attaining Science Orbit Parameters from a Constrained Approach Trajectory," *27th AAS/AIAA Space Flight Mechanics Meeting*, Univelt, Inc., San Antonio, Texas, 2 2017, p. 22.

[45] Folta, D., Dichmann, D. J., Clark, P., Haapala, A., and Howell, K., "Lunar Cube Transfer Trajectory Options," *AAS Space Flight Mechanics Meeting*, 2015.

[46] Fortescue, P., Swinerd, G., and Stark, J., *Spacecraft systems engineering*, John Wiley & Sons, 2011.

[47] Litvak, M., Mitrofanov, I., Sanin, A., Malakhov, A., Boynton, W., Chin, G., Droege, G., Evans, L., Garvin, J., Golovin, D., et al., "Global maps of lunar neutron fluxes from the LEND instrument," *Journal of Geophysical Research: Planets*, Vol. 117, No. E12, 2012.

[48] Bate, R. R., Mueller, D. D., and White, J. E., *Fundamentals of astrodynamics*, Courier Corporation, 1971.

[49] Wertz, J. R., Everett, D. F., and Puschell, J. J., *Space Mission Engineering: The New SMAD*, Microcosm Press, 2011.

[50] European Space Agency, *Margin philosophy for science assessment studies*, 2012.

[51] Ley, W., Wittmann, K., and Hallmann, W., *Handbook of space technology*, John Wiley & Sons, Ltd., 2009.

[52] European Space Agency, *Effective Reliability Prediction for Space Applications*, 2016.

[53] Langer, M., Weisgerber, M., Bouwmeester, J., and Hoehn, A., "A reliability estimation tool for reducing infant mortality in Cubesat missions," *Aerospace Conference, 2017 IEEE*, IEEE, 2017, pp. 1–9.

[54] Swartwout, M., "The first one hundred cubesats: A statistical look," *Journal of Small Satellites*, 2013, pp. 213–233.

[55] Venturini, C. C., *Improving Mission Success of CubeSats*, Space and Missile Systems Center Air Force Space Command, 2017.

[56] Barringer, H., "Availability, Reliability, Maintainability, and Capability," *Triplex Chapter Of The Vibrations Institute*, 02 1997, pp. 1–11.

[57] TU Delft, *On-board computer and data handling for small satellites - AE4-S10 Microsat Engineering*, 2018.

[58] Larson, W. J., *Applied space systems engineering*, McGraw-Hill Learning Solutions, 2009.

[59] Bergmann, B., Caicedo, I., Leroy, C., Pospisil, S., and Vykydal, Z., "ATLAS-TPX: a two-layer pixel detector setup for neutron detection and radiation field characterization," *Journal of Instrumentation*, Vol. 11, No. 10, 2016, pp. P10002.

[60] Jakubek, J., "Semiconductor pixel detectors and their applications in life sciences," *Journal of Instrumentation*, Vol. 4, No. 03, 2009, pp. P03013.

[61] Kraus, V., Holik, M., Jakubek, J., Kroupa, M., Soukup, P., and Vykydal, Z., "FITPix—fast interface for Timepix pixel detectors," *Journal of Instrumentation*, Vol. 6, No. 01, 2011, pp. C01079.

[62] Stoffle, N., Pinsky, L., Kroupa, M., Hoang, S., Idarraga, J., Amberboy, C., Rios, R., Hauss, J., Keller, J., Bahadori, A., et al., "Timepix-based radiation environment monitor measurements aboard the International Space Station," *Nuclear Instruments and Methods in Physics Research Section A: Accelerators, Spectrometers, Detectors and Associated Equipment*, Vol. 782, 2015, pp. 143–148.

[63] Granja, C., Polansky, S., Vykydal, Z., Pospisil, S., Turecek, D., Owens, A., Mellab, K., Nieminen, P., Dvorak, Z., Simcak, M., et al., "Quantum imaging monitoring and directional visualization of space radiation with timepix based SATRAM spacecraft payload in open space on board the ESA Proba-V satellite," *Nuclear*

Science Symposium and Medical Imaging Conference (NSS/MIC), 2014 IEEE, IEEE, 2014, pp. 1–2.

[64] Bouchami, J., Gutiérrez, A., Holỳ, T., Král, V., Lebel, C., Leroy, C., Macana, J., Pospíšil, S., Scallon, O., Suk, M., et al., "Fast neutron detection efficiency of ATLAS-MPX detectors for the evaluation of average neutron energy in mixed radiation fields," *Nuclear Instruments and Methods in Physics Research Section A: Accelerators, Spectrometers, Detectors and Associated Equipment*, Vol. 633, 2011, pp. S226–S230.

[65] Vykydal, Z. and Jakubek, J., "USB Lite—Miniaturized readout interface for Medipix2 detector," *Nuclear Instruments and Methods in Physics Research Section A: Accelerators, Spectrometers, Detectors and Associated Equipment*, Vol. 633, 2011, pp. S48–S49.

[66] Dunn, B. D. and Desplat, P., *Evaluation of conformal coatings for future spacecraft applications*, European Space Agency, 1994.

[67] David Pierce, A. P., "NASA Perspectives on Cubesat Technology and Highlighted Activities," *14th Meeting of the NASA SMall Bodies Assessment Group*, 01 2016.

[68] Tummala, A. R. and Dutta, A., "An Overview of Cube-Satellite Propulsion Technologies and Trends," *Aerospace*, Vol. 4, No. 4, 2017, pp. 58.

[69] Kislov, N., "Variable reflectance/transmittance coatings for solar sail attitude control and three axis stabilization," *AIP Conference Proceedings*, Vol. 699, AIP, 2004, pp. 103–111. doi:10.1063/1.1649563.

[70] Tsay, M., Frongillo, J., Model, J., Zwahlen, J., Barcroft, C., and Feng, C., "Neutralization Demo and Thrust Stand Measurement for BIT-3 RF Ion Thruster," *American Institute of Aeronautics and Astronautics*, 2017.

[71] Tsay, M., Model, J., Barcroft, C., Frongillo, J., Zwahlen, J., and Feng, C., "Integrated Testing of Iodine BIT-3 RF Ion Propulsion System for 6U CubeSat Applications," *35th International Electric Propulsion Conference*, 10 2017.

[72] Tsay, M., "Flight Development of Iodine BIT-3 RF Ion Propulsion System for SLS EM-1 CubeSats," *30th AIAA/USU Conference on Small Satellites*, August 2016.

[73] Tommy Paine, Michael (Sok Chhong) Saing, B. A. H., "AMES Cost Model Ames Micro/NanosatellitES Cost Model," *2015 NASA Cost Symposium*, August 2015.

[74] "Radio frequency and modulation," Standard ECSS-E-ST-50-05C Rev. 2, European Cooperation for Space Standardization, Noordwijk, The Netherlands, October 2011.

[75] Müller, P., *ESA Tracking Stations (Estrack) Facilities Manual (EFM)*, European Space Operations Centre, Robert-Bosch-Strasse 5, 64293 Darmstadt, Germany, 1st ed., September 2008.

[76] Cheung, K.-M., Abraham, D., Arroyo, B., Basilio, E., Babuscia, A., Duncan, C., Lee, D., Oudrhiri, K., Pham, T., Staehle, R., Waldherr, S., Welz, G., Wyatt, J., Lanucara, M., Malphrus, B., Bellardo, J., Puig-Suari, J., and Corpino, S., *Next-Generation Ground Network Architecture for Communications and Tracking of Interplanetary Smallsats*, InterPlanetary Network (IPN), August 2015, Progress Report 42-202.

[77] Funase, R., "EQUULEUS: A 6U CubeSat to Fly to Earth—Moon Lagrange Point onboard SLS EM-1," *12th Low Cost Planetary Missions Conference*, University of Tokyo & JAXA, Pasadena, California, August 2017.

[78] Bell, D., *Iris V2.1 CubeSat Deep Space Transponder*, National Aeronautics and Space Administration Jet Propulsion Laboratory, Pasadena, California, 2016.

[79] Gao, S., Rahmat-Samii, Y., Hodges, R. E., and Yang, X. X., "Advanced Antennas for Small Satellites," *Proceedings of the IEEE*, Vol. 106, No. 3, March 2018, pp. 391–403. doi:10.1109/JPROC.2018.2804664.

[80] Hodges, R. E., Chahat, N. E., Hoppe, D. J., and Vacchione, J. D., "The Mars Cube One deployable high gain antenna," *2016 IEEE International Symposium on Antennas and Propagation (APSURSI)*, June 2016, pp. 1533–1534. doi:10.1109/APS.2016.7696473.

[81] EnduroSat, *X-Band Patch Antenna Type I*, rev 1 ed., May 2018.

[82] Hodges, R. E., Chahat, N., Hoppe, D. J., and Vacchione, J. D., "A Deployable High-Gain Antenna Bound for Mars: Developing a new folded-panel reflectarray for the first CubeSat mission to Mars." *IEEE Antennas and Propagation Magazine*, Vol. 59, No. 2, 2017, pp. 39–49.

[83] O'Dea, A., *Telemetry Data Decoding*, Deep Space Network, 810th ed., 2013.

[84] Kobayashi, M., "Iris Deep-Space Transponder for SLS EM-1 CubeSat Missions," *26th AIAA/USU Small Satellite Conference*, 08 2017.

[85] Babuscia, A., Hardgrove, C., Cheung, K. M., Scowen, P., and Crowell, J., "Telecommunication system design for interplanetary CubeSat missions: LunaH-Map," *2017 IEEE Aerospace Conference*, March 2017, pp. 1–9. doi:10.1109/AERO.2017.7943826.

[86] Popescu, O., "Power Budgets for CubeSat Radios to Support Ground Communications and Inter-Satellite Links," *IEEE Access*, Vol. 5, 2017, pp. 12618–12625.

[87] Planetary Systems Corporation, 2303 Kansas Ave, Silver Spring, MD 20910, United States, *CANISTERIZED SATELLITE DISPENSER (CSD) DATA SHEET*.

[88] Starin, S. R. and Mason., P. A. C., "Propellant slosh analysis for the solar dynamics observatory." Tech. rep., NASA, Goddard Space Flight Center, 2005.

[89] Hyperion Technologies, *Datasheet HT-RW400-V1.01F*, 2016.

[90] GOMspace, *Datasheet High performance reaction wheel for 6U and 12U nano-satellites*, 3 2017.

[91] Blue Canyon Technologies, *Datasheet Reaction Wheels*, 2016.

[92] CubeSpace, *Datasheet CubeWheel High reliability reaction wheel with integrated electronics*, 10 2017.

[93] VACCO Industries, *Datasheet X14029003-0X Standard MiPS*, June 2015.

[94] VACCO Industries, *Datasheet X14029003-1X End-Mounted Standard MiPS*, June 2015.
[95] VACCO Industries, *Datasheet X14102000-01 JPL MarCO - Micro CubeSat Propulsion System*, July 2014.
[96] Accion Systems, *Datasheet Tile Next Generation Ion Propulsion*, 2017.
[97] Mier-Hicks, F. and Lozano, P. C., "Electrospray Thrusters as Precise Attitude Control Actuators for Small Satellites," *Journal of Guidance, Control, and Dynamics*, Vol. 40, No. 3, 2016, pp. 642–649.
[98] Van de Loo, M. D., *CubeSat attitude control using micronewton electrospray thruster actuation*, Ph.D. thesis, Massachusetts Institute of Technology, 2014.
[99] Blue Canyon Technologies, *Datasheet Star trackers*, 2016.
[100] Adcole Maryland Aerospace, *Datasheet Low Cost Miniature Star Tracker*, 10 2017.
[101] Hyperion Technologies, *Datasheet HT-SS200.10-V1.0F*, 2017.
[102] New Space Systems, *Datasheet Sun Sensor*, 2007.
[103] SolarMEMS Technologies, *Datasheet nanoSSOC-D60 Sun Sensor Digital Interface*, 5 2016.
[104] Sensonor, *Datasheet STIM300 Inertia Measurement Unit*, 6 2018.
[105] O-NAVI, *Datasheet ONI 23504 GyroCube*^{3F}, 2003.
[106] Silicon Sensing, *Datasheet Low Cost 6-DOF Precision MEMS Inertial Measurement Unit*, 2018.
[107] Hegel, D., "FlexCore: Low-Cost Attitude Determination & Control Enabling High-Performance Small Spacecraft," *30th AIAA/USU Conference on Small Satellites*, Blue Canyon Technologies, 2016, pp. 1–8.
[108] Staff of Princeton Satellite Systems, I., *Attitude And Orbit Control Using The Spacecraft Control Toolbox V4.6*, Princeton Satellite Systems, Inc., 2000.
[109] Y. Bai, J. D. Biggs, F. B.-Z. and Cui, N., "Adaptive Attitude Tracking with Active Uncertainty Rejection," *Journal of Guidance, Control, and Dynamics*, 8 2017.
[110] E. J. Lefferts, F. L. M. and Shuster., M. D., "Kalman filtering for spacecraft attitude estimation." *Journal of Guidance, Control, and Dynamics 5.5*, 1982, pp. 417–429.
[111] Markley, F. L., "Fast Quaternion Attitude Estimation from Two Vector Measurements," *Journal of Guidance, Control, and Dynamics*, Vol. 25, No. 2, 2002, pp. 411–414.
[112] Shirazi, A. and Mirshams, M., "Pyramidal reaction wheel arrangement optimization of satellite attitude control subsystem for minimizing power consumption." *Int'l J. of Aeronautical & Space Sci.*, 2014, pp. 190–198.
[113] Markley, F. L. and Reynolds, R. G., "Maximum Torque and Momentum Envelopes for Reaction-Wheel Arrays." *Journal of Guidance Control and Dynamics*, 7 2001, pp. 327–334.
[114] GOMspace, *Datasheet On-board CPU and FPGA for space applications*, 8 2017.
[115] Pignède, A., *Detumbling of the NTNU Test Satellite*, Master's thesis, Department of Engineering Cybernetics Norwegian University of Science and Technology, 12 2014.
[116] LaBel, K. A., Gates, M. M., Moran, A. K., Marshall, P. W., Barth, J., Stassinopoulos, E., Seidleck, C. M., and Dale, C. J., "Commercial microelectronics technologies for applications in the satellite radiation environment," *Aerospace Applications Conference Proceedings*, Vol. 1, IEEE, 1996, pp. 375–390.
[117] Sydow, M., *Introduction to Single-Event Upsets*, ALTERA, September 2013.
[118] Kraus, V., "FITPix data preprocessing pipeline for the Timepix single particle pixel detector," *Journal of Instrumentation*, 2012.
[119] Students' space association - the faculty of power & aeronautical engineering - Warsaw university of technology, Nowowiejska 24, 00-001 Warszawa, Poland, *Pw-sat2 preliminary requirements review - OBC.*
[120] Furano, G. and Menicucci, A., *Roadmap for On-Board Processing and Data Handling Systems in Space*, Springer International Publishing, Cham, 2018, pp. 253–281. doi:10.1007/978-3-319-54422-9_10.
[121] for Space Standardisation, E. C., *Space product assurance Radiation hardness assurance - EEE components*, ESA-ESTEC, 2012.
[122] ISIS, *ISIS On board computer Brochure*, 2017.
[123] CubeSpace, *CubeComputer Low-power radiation tolerant flight computer - Spec Sheet*, 2017.
[124] IMT, *Cubesat On-Board Computer IMT - Brochure*, 2016.
[125] Hyperion Technologies, *CP400.85 Processing Platform - Flyer*, 2016.
[126] Cubic Aerospace, *Cubic Radiation Hardened Single Board Computer FACT SHEET*, 2017.
[127] Vorago Technologies, *VA10820 Radiation Hardened OBC / C&DH Board & Reference Design Kit - Flyer*, 2018.
[128] Space Micro, *Proton200k™ DSP Processor Board - Datasheet*, 2017.
[129] Aeroflex, *Datasheet RHD5950 16-Channel Multiplexed 14-Bit Analog-to-Digital Converters*, January 2016.
[130] Texas Instruments, *Datasheet ADS1282-SP Radiation Tolerant High-Resolution Delta Sigma ADC*, 2016.
[131] SolAero, *Datasheet IMM-□Space Solar Cell*, 2018.
[132] Spectrolab, *Datasheet XTJ Prime*, 2016.
[133] Spectrolab, *Datasheet XTJ Prime*, 2016.
[134] SolAero, *Datasheet ZTJ+ Space Solar Cell*, 2018.
[135] Azur, *Datasheet TJ Solar Cell Assembly 3G30A*, 2016.
[136] Li, R., Guo, F., Yu, C., He, Y., Ye, Z., and Yuan, S., "Development and validation of a mechatronic solar array drive assembly for mini/micro-satellites," *Acta Astronautica*, Vol. 134, 2017, pp. 54 – 64.

doi:https://doi.org/10.1016/j.actaastro.2017.01.047.

[137] Lindsay, E. M., Hubner, F., Bailet, G., and Laux, C., *Innovative compact solar and antenna array drive assembly enabling deep space CubeSat missions*, May 2018.

[138] Li, D., Harkness, P., and Walkinshaw, T., "Design of a solar panel deployment and tracking system for Pocketqube pico-satellite," *2017 IEEE Aerospace Conference*, March 2017, pp. 1–19. doi:10.1109/AERO.2017.7943910.

[139] HoneyBee Robotics, *CueSat SADA Datasheet*, November 2013.

[140] EXA, *Datasheet BA0X: 1U High Capacity Battery Arrays*.

[141] GomSpace, *NanoPower BPX Datasheet High-capacity battery pack for nano-satellites*, 2018.

[142] GomSpace, *NanoPower P60 Dock Datasheet Electric Power System for nano satellite*, 2018.

[143] GomSpace, *NanoPower Battery Datasheet Lithium Ion 18650 cells for space flight product*, 2018.

[144] GomSpace, *NanoPower P60 ACU-200 Datasheet Array Conditioning Unit daughterboard for the P60 system*, 2018.

[145] GomSpace, *NanoPower P60 PDU-200 Datasheet Power Distribution Unit daughter board for the P60 system*, 2018.

[146] EESA, *Auxillary Passengers Using Arianespace Systems*, 1st ed., 6 2017.

[147] Espalin, D., Muse, D. W., MacDonald, E., and Wicker, R. B., "3D Printing multifunctionality: structures with electronics," *The International Journal of Advanced Manufacturing Technology*, Vol. 72, No. 5-8, 2014, pp. 963–978.

[148] Shemelya, C., Banuelos-Chacon, L., Melendez, A., Kief, C., Espalin, D., Wicker, R., Krijnen, G., and MacDonald, E., "Multi-functional 3D printed and embedded sensors for satellite qualification structures," *Sensors*, IEEE, 2015, pp. 1–4.

[149] Bhavsar, N. R., Shinde, H., and Bhat, M., "Determination of Mechanical Properties of PCB," *International Journal on Mechanical Engineering and Robotics (IJMER)*, Vol. 2, No. 4, 2014.

[150] Young, W. C. and Budynas, R. G., *Roark's Formulas for Stress and Strain*, McGraw-Hill, 7th ed., 2002.

[151] Oh, S.-J. K. . H.-U., "On-Orbit Thermal Design & Validation of 1U Standardized CubeSat of STEP Cube Lab," *International Journal of Aerospace Engineering*, 2016, pp. 17. doi:10.1155/2016/4213189.

[152] Zhang, J., Qu, L., Wang, Z., Zhao, Z., He, Z., and Yi, S., "Simulation and validation of heat transfer during wood heat treatment process," *Results in physics*, Vol. 7, 2017, pp. 3806–3812. doi:10.1016/2017.09.046.

[153] Salvi, D., Boldor, D., Ortego, J., Aita, G. M., and Sabliov, C. M., "Numerical Modeling of Continuous Flow Microwave Heating: A Critical Comparison of COMSOL and ANSYS," *Journal of Microwave Power and Electromagnetic Energy*, Vol. 44, No. 4, 2010, pp. 187–197. doi:10.1080/08327823.2010.11689787.

[154] Jakovenko, J., Werkhoven, R., Formánek, J., Kunen, J., Bolt, P., and Kulha, P., "Thermal simulation and validation of 8W LED Lamp," *2011 12th Intl. Conf. on Thermal, Mechanical Multi-Physics Simulation and Experiments in Microelectronics and Microsystems*, 4 2011, pp. 1/4–4/4. doi:10.1109/ESIME.2011.5765818.

[155] NASA CubeSat Launch Initiative, *CubeSat101- Basic Concepts & Processes for First-Time CubeSat Developers*, California Polytechnic State University, San Luis Obispo CubeSat Systems Engineer Lab, 2017.

[156] Debes, J., Howard, N., Harrington, R., Cobb, R., and Black, J., "Rapid Build and Space Qualification of CubeSats," *25th Annual AIAA/USU Conference on Small Satellites*, 2011.

[157] Technologist, M. S. C., "Science Mission Directorate Strategic Technology - CubeSats," 2016.

[158] Banerdt, W., Smrekar, S., Lognonné, P., Spohn, T., Asmar, S., Banfield, D., Boschi, L., Christensen, U., Dehant, V., Folkner, W., et al., "InSight: a discovery mission to explore the interior of Mars," *Lunar and Planetary Science Conference*, Vol. 44, 2013, p. 1915.

[159] Sorgenfrei, M. and Lewis, B. S., "BioSentinel: Enabling CubeSat-Scale Biological Research Beyond Low Earth Orbit," *Interplanetary Small Satellite Conference*, Pasadena, CA, United States, 4 2014, p. 29.

[160] Hardgrove, C., Bell, J., Thangavelautham, J., Klesh, A., Starr, R., Colaprete, T., Robinson, M., Drake, D., Johnson, E., Christian, J., et al., "The Lunar Polar Hydrogen Mapper (LunaH-Map) mission: Mapping hydrogen distributions in permanently shadowed regions of the Moon's south pole," *Annual Meeting of the Lunar Exploration Analysis Group*, Vol. 1863, 2015, p. 2035.

[161] Gardiner, J., "Suitability of Nickel Chromium Wire Cutters as Deployable Release Mechanisms on CubeSats in Low Earth Orbit," Report 24, Utah State University, 2015.

[162] Schaire, S., Wong, Y., Bussey, G., Shelton, M., Folta, D., Gramling, C., Celeste, P., Anderson, M., Perrotto, T., and Malphrus, B., "Lunar & Lagrangian Point L1/L2 CubeSat Communication & Navigation Considerations," *31st Anaual AIAA/USU Conference on Small Satellite*, Morehead State University, 2017, p. 20.

[163] ChemWatch, *Hydrazine - Review SDS*, 9th ed., 1 2013.

[164] ChemWatch, *Iodine - Review SDS*, 7th ed., 5 2013.

[165] NASA, *Space Launch System (SLS) Fun Facts*, 2016.